

**THE MECHANICAL PROPERTIES OF
CARBON FIBRE WITH GLASS FIBRE
HYBRID REINFORCED PLASTICS**

by
John Summerscales
B.Sc. (Wales), M.Sc. (C.N.A.A.), A.T.P.

**A thesis submitted to
The Council for National Academic Awards
in partial fulfilment of the requirements
for the degree of Doctor of Philosophy**

**Department of Mechanical Engineering
Plymouth Polytechnic**

May 1983

John Summerscales

Ph.D thesis:

The mechanical properties of carbon fibre with glass fibre hybrid reinforced plastics.

ABSTRACT:

Fibre composite hybrid materials are generally plastics reinforced with two different fibre species. The combination of these three materials (in this thesis they are carbon fibres, glass fibres and polyester resin) allows a balance to be achieved between the properties of the two monofibre composites. Over the fifteen years since the introduction of continuous carbon fibre as a reinforcement, there has been considerable speculation about the "hybrid effect", a synergistic strengthening of reinforced plastics with two fibres when compared with the strength predicted from a weighted average from the component composites.

A new equation is presented which predicts the extent of the hybrid effect. Experiments with a variety of carbon-glass hybrids were undertaken to examine the validity of the theory and the effect of the degree of inter-mixing of the fibres. The classification and quantification of the hybrid microstructures was examined with a view to cross-correlation of the intimacy of mixing and the strength.

Mechanical tests were monitored with acoustic emission counting and acoustic emission amplitude distribution equipment. Some specimens were subjected to one thermal cycle to liquid nitrogen temperature prior to testing. Fracture surfaces were examined in the scanning electron microscope.

Numerical analysis by finite element methods was attempted. A constant strain triangular element was used initially, but in the later analyses the PAFEC anisotropic isoparametric quadrilateral elements were used. The system was adapted so that a \sqrt{r} singularity could be modelled, and post processor software was written to allow nodal averaging of the stresses and the presentation of this data graphically as stress contour maps.

DECLARATION

I hereby certify that this work has not been accepted for any degree, and is not being concurrently submitted in candidature for any degree other than the degree of Doctor of Philosophy of the Council for National Academic Awards.

Candidate



John Summerscales

To the librarians of: a) British Library
b) Plymouth Polytechnic

I give permission for my thesis, entitled THE MECHANICAL PROPERTIES OF CARBON FIBRE WITH GLASS FIBRE HYBRID REINFORCED PLASTICS, to be made available forthwith for consultation by readers in the respective libraries, or to be sent away on temporary loan if requested by other institutions. I also give my permission for the production of a microfiche copy of this thesis by the British Library, as required by the regulations of the Council for National Academic Awards (CNAA).

The thesis is made available on the understanding that the reader will not publish in any form either the whole or any part of it without written permission from both the holding library and the author. Where the regulations of the CNAA and of the holding library allow, I give permission for the thesis to be photocopied in whole or in part, for the purposes of private study.

The copyright of this thesis belongs to the author.

Readers must sign their name below to indicate that they accept these conditions, and give their permanent address.

Author's signature: *John Summerscales*,
Permanent address: 21 Southfield Close,
HORBURY,
Wakefield,
West Yorkshire,
WF4 5AZ
Date : *23rd April 1983.*

Reader's name	Permanent Address	Date
---------------	-------------------	------

ACKNOWLEDGEMENTS

The work described in this thesis was carried out with the support of the School of Engineering Science, latterly the Department of Mechanical Engineering, at the Plymouth Polytechnic. From October 1978 this was heavily supplemented by research grants (GR A8210.9 & B5491.9) awarded by the Polymer Engineering Directorate of the Science (and Engineering) Research Council, and from September 1980 onwards I am grateful to the P.E.D. for the provision of my salary.

My thanks are due especially to Mr. David Short for his valuable guidance and patient support throughout. Much valuable assistance has been contributed by members of the technical staff of the Polytechnic, and Mr. Brian Lord and Mr. Terry Richards are to be especially thanked for their quick, careful and accurate work.

I would also like to thank Mr. John Parry for his introduction to Fortran IV, Messrs. David Lee and Peter Hewson for the introduction to the finite element schemes, and Mr. Brian Lakey for the introduction to the scanning electron microscope. Thanks are also due to all the staff of the computer centre for their help and guidance, and especially to Mr. George Wheeler for his help with the implementation of the graphics for the PAFEC 70+ finite element scheme. Also thanks are due to the staff of the Learning Resources Centre, especially Miss Hilary Burgis and her assistants for inter-library loans, and Miss Hilary Johnson for computer aided information retrieval.

Outside the Polytechnic acknowledgement is due to Mr. Avtar Bhabra for the loan of a ringdown counting acoustic emission system and Professor Bryan Harris and Mr. Mike Phillips at the Bath University for the use of their amplitude sorting acoustic emission rig and their hospitality during these visits. For technical assistance whilst at Bath I would also like to thank Mr. Chris Arnold.

I would also like to thank all those people who discussed the project, whether formally or informally, and especially:

Mr. Peter Rice, Mrs. June Hawkins, Dr. Ian Melville and Mr. Vince Osgood @ P.E.D.

Dr. Jim Batchelor, Messrs. Peter Garrington and Terry Gotch @ British Rail

Mr. Ed Trewin @ Courtaulds

Dr. Les Norwood @ Scott Bader

Dr. Lindsay Ewing @ British Gas

Dr. David Walton @ Wavin Plastics, and

Prof. Bryan Harris and Mr. Mike Phillips @ Bath University

Finally I would like to thank all those secretaries in the School/Department/Faculty offices who have typed reports during the course of the research, and particular thanks for typing this epic are due to Mrs. Carolyn Gray of Macdonald & Evans at Estover.

**"Every being which is not homogeneous and simple,
but complex and composite
must have in it some organising principle"**

Balbus' discourse in Book II, Section 29 of
Cicero: "The Nature of the Gods"

Contents

<i>Section</i>	<i>Title</i>	<i>Page</i>
	Title page	i
	Abstract	ii
	Declaration	iii
	Permission for consultation	iv
	Acknowledgements	v
	Quotation	vi
	Contents	vii
	List of figures	x
	List of tables	xiii
1.	Introduction	1
1.1	The definition of fibre reinforced composites	1
1.1.1	The definition of fibre reinforced composites	2
1.1.2	Microscopy	8
1.1.3	Nearest neighbour analysis	10
1.1.3.1	First nearest neighbour analysis	10
1.1.3.2	Nth nearest neighbour analysis	10
1.1.4	Chi-squared analysis	13
1.1.5	Mean free path and mean random spacing	15
1.1.6	Space auto-correlograms	16
1.1.7	General comments on the concept of size	16
1.2	Mechanical properties of composites	18
1.2.1	Elastic properties of monofibre composites	18
1.2.2	Failure of uniaxial monofibre composites	21
1.2.3	Elastic properties of fibre hybrids	22
1.2.4	Strength of fibre hybrids	23
1.3	Acoustic emission	34
1.3.1	Background	34
1.3.2	Instrumentation	36
1.3.2.1	Acoustic emission transducers	36
1.3.2.1.1	Detection of AE signals	36
1.3.2.1.2	Calibration of acoustic emission transducers	37
1.3.2.2	Analysis of acoustic emission signals	37
1.3.3	Composite materials	38
1.3.3.1	Acoustic emission in composite materials	38
1.3.3.2	Amplitude distribution acoustic emission	39
1.3.3.3	Frequency analysis	40
1.4	Finite element analysis	44
1.4.1	Introduction	44
1.4.2	Commercial orthotropic finite element schemes	45
1.4.3	Crack-tip singularities	50
1.5	Composites at cryogenic temperatures	51
1.5.1	Background	51
1.5.2	Glass fibre reinforced plastics	52
1.5.3	Carbon fibre reinforced plastics	53
1.5.4	Hybrid reinforced plastics	53
2	Theory	55
2.1	Microstructure parameters	55
2.1.1	Nearest neighbour index	55
2.1.2	Chi-squared parameter	55
2.1.3	Contiguity index	55
2.2	Mechanical properties	56
2.2.1	Introduction	56
2.2.2	Constant strain	57
2.2.3	Rule-of-mixtures	58
2.2.4	Rule-of-mixtures for failure strain	59
2.2.5	Summary	60
2.3	Acoustic emission	66

<i>Section</i>	<i>Title</i>	<i>Page</i>
2.3.1	Amplitude distribution analysis	66
2.4	Finite element analysis	67
2.4.1	Triangular element	67
2.4.2	Two-dimensional isoparametric element	70
2.4.3	Anisotropic elasticity theory	72
2.4.4	Crack-tip singularity	76
2.5	Cryogenics	77
3	Experimental	80
3.0	Specimen preparation	80
3.0.1	Mixing "intimate" hybrid tows	80
3.0.2	Composite preparation	80
3.1	Examination of the microstructure	82
3.2	Mechanical property testing	83
3.2.1	Longitudinal flexural strength	83
3.2.2	Longitudinal flexural modulus	88
3.2.3	Shear testing	90
3.2.3.1	Interlaminar shear strength	90
3.2.3.2	Alternatives to the short beam test for shear strength	94
3.3	Acoustic emission	94
3.3.1	Acoustic emission counting	94
3.3.2	Amplitude sorting of AE signals	95
3.4	Finite element analysis	95
3.4.1	The anisotropic constant strain triangular element	95
3.4.2	The anisotropic isoparametric elements	96
3.4.2.1	The PAFEC 8-node anisotropic membrane subroutine	96
3.4.2.2	Software modification for the R36510 element	99
3.4.2.3	The 8-node orthotropic curvilinear flat facet shell element	101
3.5	Cryogenic testing	102
3.6	Scanning electron microscopy	102
4	Results	105
4.2	Results of mechanical tests	105
4.4	Finite element analysis	134
5	Discussion	139
5.0	Development of a fibre mixing technique	139
5.1	Microstructure	139
5.1.1	Classification of hybrid component structures	139
5.1.2	Microstructure parameters	139
5.1.3	Microstructure analysis using an automatic television system	143
5.2	Mechanical properties	143
5.2.1	A new strength theory	143
5.2.2	Strength theories and correlation with experimental results	146
5.3	Acoustic emission	152
5.3.1	Acoustic emission total counts	152
5.3.2	Acoustic emission amplitude distribution	152
5.4	Finite element analysis	156
5.4.1	Results from triangular anisotropic constant strain finite elements	156
5.4.2	Isoparametric finite element analysis	157
5.4.3	Isoparametric quarter-point finite elements for stress singularity modelling	158
5.5	Cryogenic testing	160
5.6	Scanning electron micrographs	162
5.6.1	General views of hybrid fracture surfaces	162
5.6.2	Glass fibres	162
5.6.3	Carbon fibres	166
6	Summary	168
7	References	170

<i>Section</i>	<i>Title</i>	<i>Page</i>
	Appendix Index	A1
A1	Publications, papers and special lectures during the research	A2
A2	Courses, conferences and other training during the research	A4
A3	Publication contracts and permission for microfiches	A5
A4	Major sources of relevant publications	A16
A5	Bibliographies	A16
A6	Suppliers of anisotropic/orthotropic finite element software	A18
A7	Computer software listings	A20
A8	Definitions and specifications for fibrous reinforcement	A22
A9	Derivation of the equations for flexural properties	A27
A10	Scott Bader Crystic 272 polyester resin data sheets	A31
A11	Description of Courtaulds Air Knife	A37

List of figures

	<i>Page</i>
Figure 1: The lay-up nomenclature for hybrids.	7
Figure 2: Alternatives to solving exact fibre bundle/unit cell geometry.	9
Figure 3: The calculated reinforcing strengths of mixtures of glass fibres with HTS-carbon fibres.	25
Figure 4: Load-strain curves for bonded layered hybrid composites with two layers of CFRP and two layers of GRP.	30
Figure 5a: The theoretical and experimental work of fracture of carbon-glass hybrids.	32
Figure 5b: Cumulative probabilities of composite fracture modes in glass fibre/carbon fibre hybrid reinforced plastics.	33
Figure 6: Amplitude distribution acoustic emission characteristics of a CFRP panel.	41
Figure 7: Spectral analysis of acoustic emissions from fracture in 60 v/o CFRP.	43
Figure 8: Hybrid of two composites with equal magnitude moduli exhibit rule-of-mixtures strength for the hybrid-effect curve.	61
Figure 9: Hybrid of two composites with equal magnitude failure strains exhibits rule-of-mixtures strength for the hybrid-effect curve.	62
Figure 10: Similar moduli and failure strains lead to a small hybrid effect.	63
Figure 11: Extreme case where carbon-fibre is expected to carry load at the failure strain of nylon.	64
Figure 12: Traditional predictions of hybrid strength for a hybrid composite with fibres having diverse failure strains.	65
Figure 13: Stress intensity factors for cracks in various loading modes using distorted shape function elements.	78
Figure 14: The Air-Comb used to redistribute the fibres in order to form intimately-mixed composites.	81
Figure 15: The configuration of the Apple II microcomputer and peripherals.	87
Figure 16: The flexure test specimen.	89
Figure 17: Observed flexural failure modes.	89
Figure 18: The interlaminar shear strength (ILSS) test.	91
Figure 19: Dependence of flexural strength (of carbon-fibre composites in three point bending) with span-to-depth ratio.	93
Figure 20: Relief map to illustrate the distribution of the stress field in a rectangular cantilever (inset) specimen of highly anisotropic ($E_{11}:E_{22} = 50:5$) material with a half-width notch at the upper left corner.	97
Figure 21: Contour map to illustrate the distribution of the stress field in a rectangular cantilever specimen of highly anisotropic material (the same data as for figure 20).	98

	Page
Figure 22: Illustration of the chamber developed for mechanical testing at cryogenic temperatures, showing the three-point flexure test rig in position, with the positions of thermocouples A and B marked.	103
Figure 23: Temperature record plotted against time, with volume of liquid nitrogen used, at the base of the chamber (thermocouple A:solid line) and slightly above the chamber base in the approximate position of a test-piece (thermocouple B:dotted line).	104
Figure 24: The displaced shape of the finite element mesh from the 810-element analysis (shown dashed) with the original mesh (solid).	138
Figure 25: Photograph of an idealised carbon-glass hybrid, with the line-transects used for determination of the microstructure parameters.	141
Figure 26: Black and white closed circuit television image of the hybrid microstructure.	142
Figure 27: Colour enhanced digitised image of the above hybrid microstructure	142
Figure 28: The longitudinal elastic modulus of EAS-carbon/glass-fibre hybrids plotted against the volume percentage of carbon fibre composite.	147
Figure 29: The initial longitudinal strength of EAS-carbon/glass-fibre hybrids plotted against the volume percentage of carbon fibre composite.	148
Figure 30: The strength of HT-carbon and E-glass hybrids plotted from data in the thesis by P.W. Manders.	150
Figure 31: The strength of Kevlar 49/E-glass hybrids plotted from data in the thesis by M.B. Gruber.	151
Figure 32: The classical amplitude distribution histograms from three composites during acoustic emission monitoring of flexural tests.	154
Figure 33: The cumulative amplitude distributions from acoustic emission signals during flexural tests on the indicated composites.	155
Figure 34: Typical stress contours from the finite element analysis of a notched anisotropic beam in four-point flexure ($a/w = 1/4$).	159
Figure 35: Typical plot of initial failure strength against calculated elastic failure strain, for EAS-carbon hybrids.	161
Figure 36: Electron micrograph of a hybrid fracture surface (Plate 0001).	163
Figure 37: Electron micrograph of a hybrid fracture surface (Plate 0002).	163
Figure 38: Electron micrograph of a hybrid fracture surface (Plate 0006).	164
Figure 39: Electron micrograph of a hybrid fracture surface (Plate 0010).	164
Figure 40: Electron micrograph of a glass fibre from plate 0002 (Plate 0003).	165
Figure 41: Electron micrograph of a fractured glass fibre (Plate 0005).	165
Figure 42: Electron micrograph of a carbon fibre rich fracture surface (Plate 0008).	166
Figure 43: Electron micrograph of a cluster of carbon fibres in plate 0008 (Plate 0009).	167
Figure 44: Electron micrograph of a possible crack initiation site (Plate 0004).	167

Figure A1: Bending moment diagram for three-point bend.	Page A27
Figure A2: Bending moment diagram for four-point bend.	Page A28
Figure A3: Courtaulds Air-Knife.	Page A37

List of tables

	<i>Page</i>
Table 1: The major techniques of non-destructive testing	35
Table 2: Frequency analysis of acoustic emission from reinforced plastics	42
Table 3: Thermal stresses in carbon-glass hybrids	79
Table 4: Listing of the Apple II computer program to calculate microstructure parameters	84
Table 5: Index to tables of mechanical property experimental results 1	105
Table 6: XAS carbon fibre hybrids, ambient tests	106
Table 7: XAS carbon fibre hybrids, one cycle to 77K	107
Table 8: XAS carbon fibre hybrids, one cycle to 77K, bagged	108
Table 9: XAS carbon fibre hybrids, tested cold	109
Table 10: XAS carbon fibre hybrids, ambient tests	110
Table 11: XAS carbon fibre hybrids, one cycle to 77K	111
Table 12: XAS carbon fibre hybrids, tested cold	112
Table 13: EAS carbon fibre hybrids, ambient tests	113
Table 14: EAS carbon fibre hybrids, one cycle to 77K	114
Table 15: EAS carbon fibre hybrids, tested cold	115
Table 16: EAS carbon fibre hybrids, ambient tests	116
Table 17: EAS carbon fibre hybrids, one cycle to 77K	117
Table 18: EAS carbon fibre hybrids, tested cold	118
Table 19: EHMS carbon fibre hybrids, ambient tests	119
Table 20: EHMS carbon fibre hybrids, one cycle to 77K	120
Table 21: EHMS carbon fibre hybrids, tested cold	121
Table 22: EHMS carbon fibre hybrids, ambient tests	122
Table 23: EHMS carbon fibre hybrids, one cycle to 77K	123
Table 24: EHMS carbon fibre hybrids, tested cold	124
Table 25: Index to tables of mechanical property experimental results 2	125
Table 26: EAS carbon fibre and XRE 23 47 glass fibre results	126
Table 27: EAS carbon fibre fine hybrid results	127
Table 28: EAS carbon fibre fine hybrid results	128
Table 29: EAS carbon fibre coarse hybrid results	129
Table 30: EAS carbon fibre coarse hybrid results	130

	<i>Page</i>
Table 31: EAS carbon fibre coarse hybrid results	131
Table 32: Properties of unidirectional HT-carbon/E-glass hybrid composites (taken from the thesis by P.W. Manders)	132
Table 33: Properties of unidirectional E-glass/Kevlar 49 hybrid composites (taken from the thesis by M.B. Gruber)	133
Table 34: Material properties used in the finite element analysis	134
Table 35: Summary of stresses predicted by 36-element PAFEC analysis	135
Table 36: Stresses at node 129	135
Table 37: Computer time taken for each finite element analysis	136
Table 38: Results from the 810-element analysis	137
Table 39: Calculated microstructure parameters for figure 25	140
Table 40: Computer program for colour-enhanced microstructure images	144
Table A1: The functions of the oxides in glasses	A23
Table A2: Fibre glass compositions and their comparative properties	A24
Table A3: Carbon fibres and their comparative properties	A25
Table A4: Typical composite efficiencies attained in reinforced plastics	A26
Table A5: Range of formulations for Crystic 272	A31
Table A6: Temperature dependance of setting time for Crystic 272	A31
Table A7: Pot-life of Crystic 272	A32
Table A8: Typical properties of liquid Crystic 272	A33
Table A9: Typical properties of cured unfilled Crystic 272 castings	A34
Table A10: Typical properties of a Crystic 272 glass fabric laminate	A34
Table A11: Laminate not post-cured at elevated temperature	A35
Table A12: Typical properties of a Crystic 272 woven rovings laminate	A35
Table A13: Typical properties of a Crystic 272 continuous rovings laminate	A35
Table A14: Typical properties of a Crystic 272 chopped strand mat/woven rovings laminate	A36
Table A15: Typical properties of a Crystic 272 chopped strand mat	A36

1 Introduction

Materials constructed by the reinforcement of a binder matrix with a fibrous reinforcement are commonly called fibre composite materials. These materials have, by virtue of combining complimentary properties, numerous advantages over conventional structural materials, such as

- high strength and stiffness
- low density
- corrosion resistance
- relative ease of forming complex shapes.

The use of two different types of fibre within a single component is known as "*hybridisation*" and results in a "*fibre composite hybrid material*". The advantages to be gained by using composite materials can be further enhanced by such hybrids to give a product with improved properties tailored to a specific requirement, and yet they can often result in enhanced performance parameters (weight, properties) or savings in fabrication costs (man hours/item, reduced no. of inserts or machining operations, lower energy requirements). The use of hybrid reinforced plastics fibre composites is increasing rapidly, and is beginning to move out of the specialist industries such as aerospace and sports goods into mass production industries such as the automotive sector. However, most hybrids which have been produced today are created by gross mixing of the two fibre species and it is therefore the intention of this work to investigate the effect of reducing the scale of mixing in respect of the mechanical properties of the resulting composite.

1.1 The definition of fibre reinforced composites

The term microstructure has outgrown its original meaning, namely that structure which is seen through a microscope (=1). In scientific engineering usage it is advantageous to associate a microstructure with heterogeneities of polycrystalline and polyphase materials. The most general characteristic of a microstructure is the presence of boundaries between the phases which comprise the material.

Composites are complex material systems composed of distinct phases, in which there is generally a continuous medium (the matrix), and a discontinuous medium (the fibres) held together by the matrix. A recent development in composite materials is the use of two different fibres (a hybrid composite), in an attempt to produce a material with a balance between the properties of the individual monofibre materials. Quantitative microscopy of a cross section of any multiphase material has advantages over ordinary chemical analyses, primarily in that it is possible to ascertain the relative position of the individual components, for example: the fibres in a composite.

This section will first review the types of definition which have so far been applied to fibre composites, and will then consider the analyses of point patterns used in such areas as ecology, geography and ceramics with a view to establishing an appropriate quantitative

definition of the patterning in hybrid composites.

1.1.1 The definition of fibre reinforced composites

a) unidirectional composites:

For continuously uniaxially aligned fibres a rule-of-mixtures based on a parallel model has been found to agree well with experimental values for the tensile modulus of specimens tested in the direction of fibre alignment (=2), using only a simple parameter of the microstructure: the volume fraction. This parameter can be obtained either by chemically removing one of the ingredients and determining the volume remaining as a proportion of the original volume, or by polishing a specimen normal to the major axis of the fibres and determining the ratio of the area of the fibres to the area of the specimen examined. The modulus of the composite, E_c , is then derived from the moduli, E_x , and volume fraction, V_x , of the fibre (subscript f) and matrix (m) using the equation:

$$E_c = E_m V_m + E_f V_f \quad (E1.1.1)$$

where:

$$V_m + V_f = 1 \quad (E1.1.2)$$

Benveniste *et al* [=3] point out that the equivalent modulus theory which replaces the fibre reinforced material by a homogeneous anisotropic medium destroys all micro-structure effects and is therefore not suitable for certain problems in composites, and especially dynamic, fracture and flexure situations.

For uniaxially aligned fibres of finite length (=2) the rule of mixtures can be modified by the inclusion of a length correction factor, n_L , such that:

$$E_c = n_L E_f V_f + E_m V_m = n_L E_f V_f + E_m (1 - V_f) \quad (E1.1.3)$$

Cox (=4) developed an expression for n_L of the form:

$$n_L = 1 - \frac{\tanh(\beta L/2)}{(\beta L/2)} \quad (E1.1.4)$$

where:

$$\beta = \frac{G_m \cdot 2\pi}{E_f A_f \ln(R/r_o)} \quad (E1.1.5)$$

where: L is the fibre length

G_m is the shear modulus

A_f is the cross sectional area of the fibre

r_o is the fibre radius, and

R is the mean separation of the fibres, normal to their length.

The effect of the fibre length distribution (FLD) in the Cox (=4) approach will give:

$$E_c = \sum_{j=1}^n E_f V_{fj} \left[1 - \frac{\tanh(\beta L_j/2)}{(\beta L_j/2)} \right] + E_m (1 - V_f) \quad (E1.1.6)$$

where: n is the number of intervals in the FLD, and

V_{fj} is the volume fraction of fibres with length L_j

The coarser that a structure is, and thus the more commensurate the structural scale factors are with the specimen scale factors, the stronger becomes the scale factor effect on strength with all other conditions remaining equal (=5). In composite materials this scale factor is a consequence of the structural inhomogeneity. As structural scale factors for fibrous materials with unidirectional orientation, Bolotin proposes that:

$$h_1 = 2r \text{ and } h_2 = 2r\sqrt{E_f/E_m} \quad (\text{E1.1.7})$$

where: r is the fibre radius

E is the material modulus

h_1 characterises the structure in sections across the fibre, and

h_2 is of the order of the characteristic length associated with the edge effect in the composite.

Hlavacek considers a composite material of infinitely long fibres with a circular cross-section of radius, r , arranged in a hexagonal array throughout the matrix material (=6). If the fibres are parallel to the z-axis and at a distance apart of $2l$ from centre to centre, where l is obviously greater than r , then the hexagonal prisms can be replaced by circular cylinders of the same volume. The radius of the cylinder will then be:

$$r_2 = l \sqrt{\frac{2\sqrt{3}}{\pi}} \approx 1.1l \quad (\text{E1.1.8})$$

The results of finite element numerical analyses by Murakami (=7) *et al.* for several geometries of practical interest indicate that for achievable volume fractions, the "concentric circular cylinder approximation" (using a polar co-ordinate system) provides an adequate indication of the global and local isothermal contours in the temperature-microstructure problem for composites containing circular fibres in a hexagonal array.

Verchery (=8) has reported that the strength of boron fibres reinforcing aluminium decreases sharply when the fibre setting disorder increases, however little.

Guild (=9, 10) has attempted to gain a more quantitative definition of the microstructure of glass reinforced polyester, than volume fraction, using data derived from a Quantimet image analysing computer. The first analysis involved the determination of the variances of the values of fractional area covered for different cell sizes of a contiguous grid. Information regarding the nature of the fibre distribution was sought both from comparing the variance values with those predicted for the null hypothesis, a random distribution, and from examining the shape of a surface defined by a variance matrix. The second method of analysis was based on the concept that a structure may be defined by its relationship to a structuring element, in this case squares and rectangles of empty space. The probability of finding such empty space is estimated and information regarding the nature of the fibre distribution is sought from the probability matrices.

It was found that, although Nomarski interference shows that the fibres do not truly touch, a significant number of groups of two or more fibres were detected as single features during the analysis of a photomicrograph at X 1750 magnification. The shape of the features may be classified by the form factor (non-dimensional) which is the area divided by the square of the perimeter. The form factor of a circle is $1/4\pi$ and that of a group of fibres detected as a single feature will be less than for a circle.

Qualitative analysis suggested that two factors should be considered, the tendency for fibres of the same type to aggregate into clusters, and the tendency for regions of pure resin to occur. There is an additional need to carefully consider the choice of cells before counting. Using the null hypothesis, in which fibres are considered as a random distribution of point particles which may co-exist at any position:

the theoretical variance (fractional area covered) = $\lambda M_2 / A^2$, and

the standard derivation (variance of fractional area covered) =

$$\sqrt{\frac{\lambda M_4 + 2\lambda^2 M_2^2}{A^4}} \quad (\text{E1.1.9})$$

where: λ is the mean number of points per cell

A is the mean cell area, and

M_x is the x th moment of area of distribution of fibres about zero

from which it follows immediately via the standard properties of the Poisson distribution that the probability of an empty cell is given by $e^{-\lambda}$, assuming the approximation of fibres to point particles. The second method of analysis arises from the visual observation that the microstructure includes distinct regions of empty space or resin-rich areas containing less than the equivalent of one-half of a fibre.

b) bidirectional composites

In addition to the length correction factor introduced for unidirectional composites Cox (=4) derived an efficiency factor dependent on the fibre orientation, n_o , to give:

$$E_c = n_o n_L E_f V_f + E_m [1 - V_f], \quad (\text{E1.1.10})$$

and he showed that n_o took values of 1/3 for two dimensional random fibre distributions (and 1/6 in three dimensions).

For the general case of planar fibre orientation distributions (FOD), Krenchel (=11) proposed that n_o be given the simple form:

$$n_o = \sum_{k=1}^m a_k \cos^4 \theta_k \quad (\text{E1.1.11})$$

where: a_k is the fibre fraction at angle θ_k to the reference axis, and

m is the number of angle intervals considered.

Rossmannith (=12) has derived an expression for the random variable volume fraction of fibre reinforced cylindrical shells given by:

$$\delta = \frac{2\pi a}{m} \cos \alpha \quad (m \in N) \quad (E1.1.12)$$

where: a is the radius of the shell,
 α is the wrapping angle,
 m is the number of fibres intersecting a circumferential line,
 δ is the mutual distance of the fibres which obey the restrictive law, and
 V is the volume fraction given by:

$$V = \frac{1}{2} \sum_{i=1}^N m_i \frac{r_i^2}{a_i \cos(\alpha_i + \epsilon_i)} \quad (E1.1.13)$$

where: N is the number of layers in the laminate
 r is the radius of the fibre, and
 ϵ_i are uniformly distributed random variables.

Stroeven (=13) in consideration of fibre reinforced cementitious materials (FRC) treats the fibres as lineal features in space, because of their slenderness. The FRC specimens develop an axis of symmetry which coincides with the direction of the gravity field, and slices in this axial direction show partial orientation after projection. The image is then sampled in two different ways, firstly by counting the number of fibre projections per unit area (N_A), or secondly by the number of intersections with the fibre projections per unit length of a line array covering the image (P_L). The problem considered by Stroeven is the relationship of these two basic dimensional data to the spatial characteristics (L_v , the fibre length per unit volume, V_v the volume fraction of the fibres and w , a measure of the degree of orientation).

Milewski (=14) has considered the efficiencies of packing fibres into a composite in a variety of ways and presents graphs of the relative bulk volume at various component ratios for the systems below:

fibre packing at various length to diameter ratios

fibre packing with various fibre diameters, and short fibres packed with glass beads.

c) hybrid composites

Kanovich *et al.* (=15) have shown that when fibres of different diameters are used, even if the distance between the reinforcing elements increases, the reinforcement content remains high by filling the spaces between the main fibres (D) with fibres of a smaller diameter (d) and cutting down on the "ballast" matrix. In the case of fibres with the same diameter:

$$\alpha_1 = \frac{\pi d n}{\pi d^2 n / 4F} = \frac{4F}{d} \quad (E1.1.14)$$

whereas with interstitial fibres of different diameters:

$$\alpha_2 = \frac{\pi(d + D) n F}{\frac{\pi(d^2 + D^2)n}{4}} = \frac{4F(d + D)}{(d^2 + D^2)} \approx 1.2\alpha_1 \quad (E1.1.15)$$

where: α is the interface density

ie: the total interface perimeter per cross section of composite

F is the relative volume content of the fibres.

The total interface perimeter increases with the number of interstitial fibres present and consequently a greater volume fraction of fibres can be incorporated into the matrix by mixing the fibre diameters.

Kulkarni and Rosen (=16, 17) identify two major types of patterning in hybrids, firstly "intimate" in which each fibre is surrounded by fibres of the second type, and secondly, "zebra" or "discrete" in which fibres of the same type occur in aggregates. These two types may of course be combined in interply-intraply combinations.

A more segmented classification (=18, 19) divides the possibilities for fabrication into six classifications (figure 1):

- A :mixed fibre tows
- B :mixed fibre ply
- C :individual fibre ply
- D :core-shell sandwich
- E :internal ribs, and
- F :external ribs,

followed by a number to denote the directionality of the net composite. Mixtures of the categories are still possible, but are unlikely to be economically viable to produce.

Bader and Manders (=20) have defined the dispersion of a hybrid composite as the reciprocal of the thickness in metres, of the smallest representative repeat unit of the laminate. In the case of simple sandwich laminates the repeat distance, t_r , is the total laminate thickness, otherwise: $D = 1/t_r$, (E1.1.16)

Clearly in a bicomponent composite with a given volume fraction of one component, decreasing the size of one component automatically involves decreasing the size of the other (=21), since pieces of one component separate those of the other. When fibres are aligned in a matrix the separation of the surfaces are on average given by s , which can be written in terms of the fibre diameter, d , for a given volume fraction V_f as the equation:

$$s = d \left[\left(\frac{\beta}{V_f} \right)^{\frac{1}{2}} - 1 \right] \quad (E1.1.17)$$

where β is a constant equal to 0.912 for a hexagonal array and 0.785 for a square array. Clearly s and d will vary in direct proportion, decreasing the fibre diameter also decreases the spacing and the effect of fibre size and of fibre spacing is thus interdependent.

Marshall (=22) reports that in composites formed from a hybrid tape the tows of carbon fibre will adopt a trapezoidal shape, in cross section, in order to interlock more efficiently with the glass fibres.

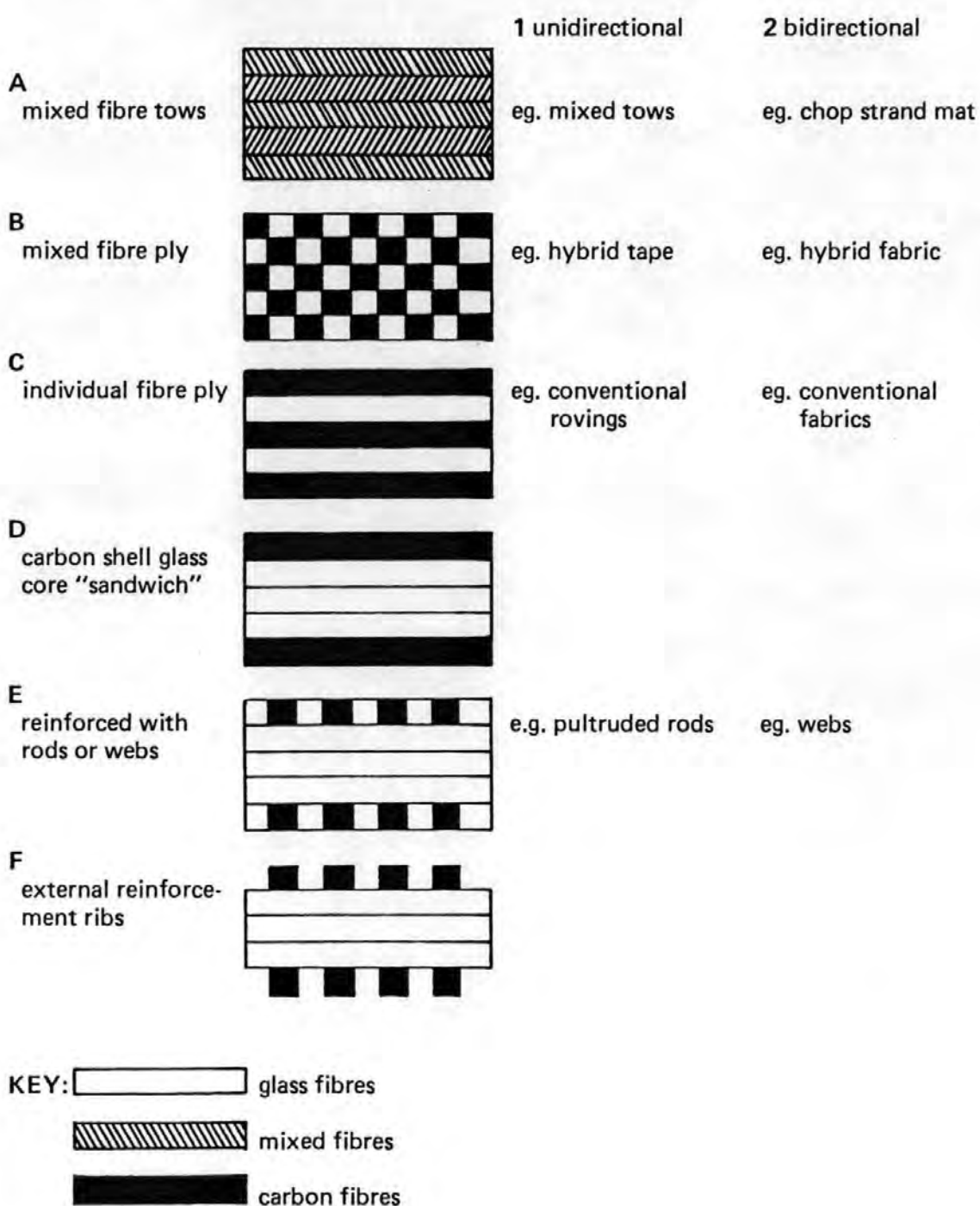


Figure 1. The lay-up nomenclature for hybrids (=18, 19).

1.1.2 Microscopy

The sample to be examined must be selected to accurately represent the overall patterning of the composite. In order to analyse the fibre distribution it is necessary to make the individual fibres contrast with the matrix, and with one another in hybrids, before microscopy is undertaken. Glass fibres may be indistinguishable from the matrix in reflected light, but this can be overcome by careful etching with hydrofluoric acid to remove material along the interface and leave a dark ring (=23).

There are several methods of quantitative microscopic analyses recognised (=24):

- a) estimation: with practice observers can judge to an accuracy of $\pm 10\%$.
- b) counting the individual features using a net-ruled eyepiece: to determine volume percentage the fibre size must be accounted for.
- c) areal analysis: the sum of the areas of any given component relative to the total area of the measured surface is approximately the volume percentage.
- d) linear (Rosiwal) analysis depends on the principle that for any line of adequate length drawn on a plane surface, the ratio of the sum of the linear intercepts on any given component to the total length across the sample will tend to the value for volume fraction of that component.
- e) point counting: the material lying at the intersection of crosshairs at each step movement of the slide is identified and counted. About 1000 to 1500 points should be observed on average.

The mean intercept of a line on a circle is $\pi D/4$. Objective discrimination of those points where the crosshairs coincide with an interface can be obtained by counting all intercepts and deleting all exits (=25). The ideal standard deviation is then:

$$\sigma_{xi} = \sqrt{X} \quad \text{for the Poisson distribution, or} \quad (\text{E1.1.18})$$

$$\sigma_{xi} = \sqrt{pqN} \quad \text{for the binomial distribution} \quad (\text{E1.1.19})$$

where X is the actual number of points counted in one phase, and
 N is the total number of points counted.

If p is the volume fraction of one phase and q the volume fraction of the second phase, then in a binary system: $p + q = 1$. At 50% of each component the binomial expression gives a σ_x value which is smaller by $\sqrt{2}/2$. In either case the percentage standard deviation will be $100\sigma_x/N$. However the two equations above apply to completely ideal sampling cases only, when $p = 0.5$ the real standard deviation of X at equal volume fraction will be:

$$\sigma_x = 0.5k\sqrt{N} \quad (\text{E1.1.20})$$

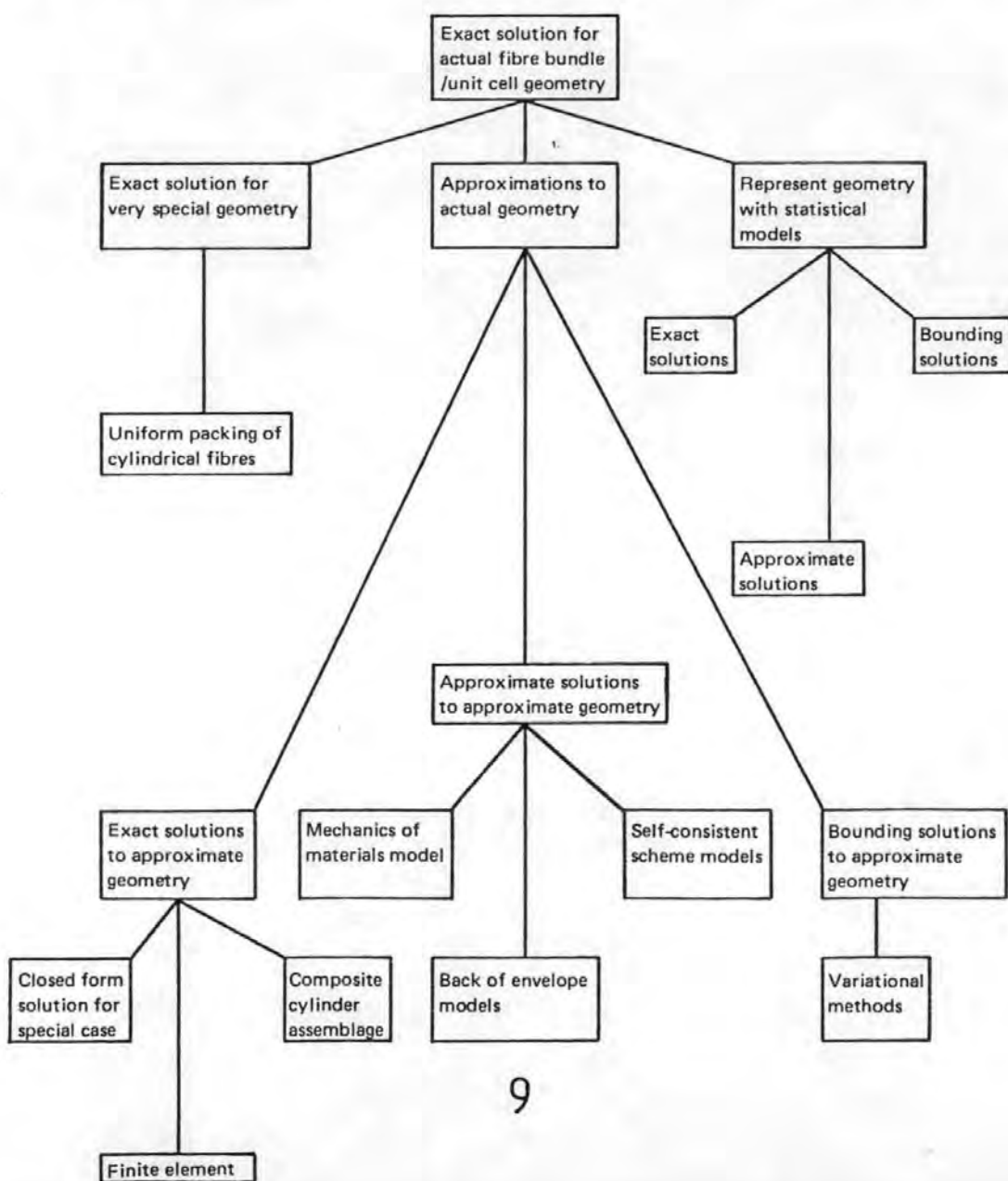
where k is a variable factor, which includes all parameters which cause distortion of the results, and is always greater than 1. A value of $k = 3$ is suggested as an appropriate estimate for results obtained by subsample methods.

Ripley(=26) identifies four classes of statistical test for obtaining the randomness of spatial patterns, and qualifies the first two as the most appropriate for preliminary field-work:

- i) quadrat counts
- ii) distance or nearest neighbour methods
- iii) second order methods, including spectra
- iv) the "test set" approach.

For a schematic presentation of the alternatives to solving exact fibre bundle-unit cell geometrics see Rosen, Chatterjee and Kibler (=27) (figure 2).

Figure 2: Alternatives to solving exact fibre bundle/unit cell geometry from Rosen STP 617



1.1.3 Nearest neighbour analysis (=28, 29)

1.1.3.1 First nearest neighbour analysis

Nearest neighbour analysis was developed by Clark and Evans (=30) and is based on the measurement of the distance from one point to the nearest neighbouring point. In a clustered distribution these distances will obviously be low, while in an ordered pattern relatively high spacings between points will be found. To standardise results the overall density of points is taken into account in the calculation of the index. The method generally employed is:

- * locate the points in the pattern to be analysed
- * measure the distance from each point to the nearest neighbour
- * find the mean observed distance \bar{d}_o
- * calculate the density of points in the area, $p = n/a$
- * calculate the expected mean distance, $\bar{d}_e = 1/(2\sqrt{p})$

The nearest neighbour index compares the observed mean distance with that expected for a random distribution:

$$R_n = \bar{d}_o / \bar{d}_e = 2\bar{d}_o \sqrt{(n/a)} \quad (\text{E1.1.21})$$

If the pattern under consideration is itself random, then the nearest neighbour index should have a value of 1.00. Clustering causes the value of R_n to fall significantly below 1, a value of zero indicating the total coincidence of all the points. A value of R_n greater than 1 indicates a greater degree of uniformity or ordering and R_n has a limiting value of 2.15 which is equivalent to all the points lying at the vertices of a mesh of equilateral triangles.

In general this technique is more rigorous than the chi-squared analysis (covered later) as it deals with individual points rather than grouped data, and the analysis allows simple objective comparison between distributions without the limits of χ^2 , but with a large number of points the calculation is time consuming. The scale of investigation is important, especially when the frame of reference can be enlarged or reduced without altering the number of points.

1.1.3.2 Nth nearest neighbour analysis

If a population of individuals is distributed randomly with density m per unit area, the probability of x individuals falling in any area of unit size is obtained from the Poisson series and is $m^x e^{-m} / x!$, (=31). The number of individuals in a circle of radius, r , will follow a Poisson distribution with a mean of $\pi r^2 m$, written λr^2 , as πm is now denoted λ . Now if a random individual is taken as centre, the probability that no individual occurs inside a circle of radius r_1 , is given by the first term of the Poisson series:

$$P(0 \text{ in } (0, r_1)) = e^{-\lambda r_1^2} \quad (\text{E1.1.22})$$

and the probability of at least one individual then being inside a circle of radius R_1 is given by:

$$P(>1 \text{ in } (r_1, R_1)) = e^{-\lambda(R_1^2 - r_1^2)} \quad (\text{E1.1.23})$$

which will tend to $2\lambda r_1 dr_1$ as R_1 tends to r_1 . Therefore the probability that the nearest neighbour is at distance r_1 from the centre is as obtained by Clark and Evans (=30):

$$P(r_1) = e^{-\lambda r_1^2} \cdot 2\lambda r_1 dr_1 \quad (\text{E1.1.24})$$

If the second individual is at distance r_2 given that the nearest neighbour is at r_1 , the probability is written $P(r_2|r_1)$, and the joint probability is $P(r_1, r_2)$, the latter when not given r_1 . Thus:

$$P(0 \text{ in } (r_1, r_2)) = e^{-\lambda(r_2^2 - r_1^2)} \quad (\text{E1.1.25})$$

$$P(> 0 \text{ in } (r_2, R_2)) = 1 - e^{-\lambda(R_2^2 - r_2^2)} \quad (\text{E1.1.26})$$

which tends to $2\lambda r_2 dr_2$ as R_2 tends to r_2

$$P(r_2|r_1) = e^{-\lambda(r_2^2 - r_1^2)} \cdot 2\lambda r_2 dr_2, \text{ and} \quad (\text{E1.1.27})$$

$$P(r_1, r_2) = P(r_1) \cdot P(r_2|r_1) = e^{-\lambda r_1^2} \cdot (2\lambda)^2 \cdot r_1 r_2 dr_1 dr_2 \quad (\text{E1.1.28})$$

And the general result follows from this:

$$P(r_1, r_2, \dots, r_n) = e^{-\lambda r_n^2} \cdot (2\lambda)^n \cdot r_1 dr_1, r_2 dr_2, \dots, r_n dr_n \quad (\text{E1.1.29})$$

where $0 \leq r_1 \leq r_2 \leq \dots \leq r_n$.

The absolute probability that the n th nearest neighbour is at distance r_n from the centre, $P(r_n)$, is obtained by integrating the general result successively with respect to r_1 from 0 to r_3, \dots and is:

$$P(r_n) = 2\lambda^n \cdot e^{-\lambda r_n^2} \cdot r_n^{(2n-1)} \cdot dr_n / (n-1)! \quad (\text{E1.1.30})$$

showing that $2\lambda r_n^2$ is distributed as χ^2 with $2n$ degrees of freedom. If we put $x_n = 2\lambda r_n^2$ into the above equation:

$$P(x_n) = e^{-\frac{x_n}{\lambda}} \cdot \left(\frac{x_n}{\lambda}\right)^{n-1} \cdot dx_n / (n-1)! \quad (\text{E1.1.31})$$

and it follows that in a sample of size N , the statistic $N\bar{x}_n$ is distributed as χ^2 with $2Nn$ degrees of freedom, where \bar{x}_n is the mean of the N observed values of the mean value of x_n , and so we immediately have a simple test of randomness or otherwise for a given distribution of distances. A probability of χ^2 greater than 0.95 indicates significant overdispersion of individuals, the distances being smaller than expected. A probability less than 0.05 indicates significant underdispersion.

The mean distance to the n th nearest neighbour is:

$$E(r_n) = \int_0^\infty r_n \cdot P(r_n) = \sqrt{\frac{\pi}{\lambda}} \cdot \frac{(2n)! n}{(2^n \cdot n!)^2} = \frac{1}{\sqrt{n}} \cdot \frac{(2n)! n}{(2^n \cdot n!)^2} \quad (\text{E1.1.32})$$

and the second moment is:

$$E(r_n^2) = \int_0^\infty r_n^2 P(r_n) = n/\lambda \quad (E1.1.33)$$

Using the Stirling approximation we obtain:

$$\frac{E(r_n)}{E(r_1)} = \frac{(2n)! 2n}{(2n.n!)^2} \rightarrow 2\sqrt{(n/\pi)} \approx 1.13\sqrt{n}, \quad (E1.1.34)$$

so that the area of the circle containing the nth nearest neighbour on its circumference is expected to be approximately n times as large as the area of the circle with the nearest neighbour on its circumference. In other words, the series of radii, $E(r_n)$, describe concentric circles with annuli of approximately equal area, as would be expected intuitively.

The limits for the expected mean $E(\bar{x}_n)$, if the population is random, can be derived using the normal approximation to the χ^2 distribution, if the number of degrees of freedom is fairly large. The 95% limits for $E(\bar{x}_n)$ are given by:

$$(\sqrt{(4Nn - 1)} \pm 1.96)^2 / 2N \quad (E1.1.35)$$

where 1.96 is the deviate corresponding to a probability of 0.05 in the two tails of the normal distribution. In practice then estimation of $\lambda_o = \pi m_o$ (where m_o is the observed density), and calculation of the mean, $\bar{x}_n = 2\lambda_o \bar{r}_n^2$ allows comparison with the expected limits under the hypothesis of randomness.

An approximate result, applying normal probability theory to the mean and standard deviation gives 95% limits of:

$$E(r_n) \pm 1.96 \sigma(r_n) / \sqrt{N} \quad (E1.1.36)$$

or alternatively the statistic, c, can be taken as a normal deviate and tested against probability levels of the normal distribution:

$$c = \frac{\bar{r}_n - E(r_n)}{\sigma(r_n) / \sqrt{N}} \quad (E1.1.37)$$

but most reliance should be placed on the tests employing the χ^2 distribution.

Eberhardt (=32) has suggested an *index of non-randomness*:

$$I_n = (C[x_n])^2 + 1 = E(x_n^2) / (E(x_n))^2 \quad (E1.1.38)$$

where $C[x_n]$ is the coefficient of variation of x_n , x_n is the distance to the nth nearest point and $E(y)$ is the mean of a random variable, y. This will however require that to define a hybrid composite there will be a value of I_n for each fibre type, if the relative distributions are to be made clear and also that the relative numbers of fibres will vary with the individual fibre volume fractions. The ratio, I_n , is easily calculated from field data and increases with increasing tendency to aggregation, yet it does not require a knowledge of density. A disadvantage is that the sampling distributions of the ratio have not been worked out and an exact test of deviation from randomness is not available.

1.1.4 Chi-squared – (χ^2) analysis

The main application of chi-squared analysis is in the testing of results for statistical significance, but it may be adapted to the description of point patterns (=28). If we have a perfectly ordered distribution of 100 points and superimpose on it a grid of ten squares, we may confidently expect that each square will contain ten points. The basis of χ^2 analysis is the comparison of frequencies expected under precisely defined conditions such as the above, with the frequencies observed in the actual pattern under consideration. The procedure is as follows:

- * count the number of points in the pattern under investigation,
- * completely cover the study area with a grid of equal sized squares,
- * calculate the expected frequency, E, in points/square, for perfect ordering.
- * count the number of points actually located within each grid square, and record each total as an observed frequency, O.

$$* \text{ Then } \chi^2 = \sum \frac{(O - E)^2}{E} \quad (\text{E1.1.39})$$

With perfect ordering, then χ^2 will be zero, and a higher value suggests a greater degree of clustering. A problem arises here in that a random pattern should also have a χ^2 value of zero, although this is unlikely to occur exactly in practice especially with a limited number of points. At the lower end of the range there will be little discrimination between perfect ordering and a random pattern. The maximum value of χ^2 occurs when all the points lie within one grid square, and in this case the value increases with either the total number of points or with the total number of grid squares. In view of this χ^2 is of little value in applying descriptive labels to individual patterns, but is useful for comparing the degree of clustering in different patterns, and is relatively simple in this latter respect. Changes in the size and orientation of individual squares in the grid can have a considerable effect on the value of χ^2 even though the number and pattern of points in the study area is unchanged. If grid square size is reduced the discrimination of clustering is improved, and therefore, the χ^2 value is increased. If a single grid square covers the entire area then perfect ordering is inferred.

Greig-Smith (=33) has described a method of determination of the scales of heterogeneity in the abundance of a species which depends on the analysis of density in a grid of contiguous quadrats, the data from which are associated into successively larger blocks. The mean square plotted against block size shows a peak at the block size corresponding to the mean size of the clump or mosiac unit.

The grid method of analysis as developed by Greig-Smith makes the implicit assumption that the areas of heterogeneity are isodiametric, but Kershaw (=34) suspected that in plant communities which are a result of ploughing and reseeding, the area of any heterogeneity might be elongated in the direction of cultivation. The grid method as it stood would thus be inadequate. This was overcome by associating single grid units into blocks

of 2, 8, 32 etc. in rows and columns and plotting two sets of mean square against block size results. For the majority of species, analysis of the same data in these two ways revealed a shift of the peak in the variance curve to the right when the long axis of the group was at right angles to the contours of the site. The difficulty of testing the significance level of such a peak once non-randomness has been established is discussed and from an analysis of a series of experiments with artificial communities, a subjective approach is proposed for the problem. The experiments indicate the importance of using an optimum sample size and sampling unit for the accurate detection of small scale pattern. A series of sampling experiments give an indication of the sample size required for a given level of percentage cover and it is suggested that the sampling unit be less than one half of the size of the smallest dimension of an area of heterogeneity likely to be encountered in any given community.

The analysis by Usher (=35) of models of basic patterns suggests that the starting point for sampling is important. If the series starts towards the centre of a clump there is a strong possibility that the indicated peak mean square will be one size smaller than the actual value, a shift of the peak in the variance curve to the left, unlike the shift to the right identified by Kershaw.

Miles (=36) has considered the problem of deciding whether or not to include particles truncated by the quadrat boundaries, by the use of a general "associated point" solution. The particle is counted as in the randomly located quadrat *only* if its unique associated point falls in the quadrat. The scheme is identified as similar to, but less restricted than, the Gundersen method (=37) in which the plane is covered by a rectangular or hexagonal tessellation of congruent regions with the same orientation and then a count is taken of the particles associated with a randomly positioned region. A corresponding edge effect problem to consider the specimen boundary has also been reported (=38).

In an attempt to undertake simultaneous testing for pattern at various scales, Mead (=39) has concluded that a set of tests based on randomisation arguments provides a fully valid method. If the grid is in the form of a square, instead of considering pairing or halving of quadrats alternatively horizontally and vertically, it is possible to consider sets of four quadrats in squares. This halves the number of scales of pattern which can be examined, and it may be impractical, but the two within four randomisation test can be easily extended to a 4 within 16 randomisation test. One advantage of this extension is that the number of points in the randomisation distribution is $16!/(4!)^4$ and is quite large enough for one 4 X 4 square grid to give a realistic test on its own.

Tests conducted for data in the form of quadrat counts are based on the standard result that the counts have a Poisson distribution for random cover of the area under consideration. In addition to the "obvious but usually ineffective" χ^2 goodness of fit test various statistics have been suggested. The ineffectiveness is because of the power of the technique relative to particular alternatives. Among the test statistics suggested are the variance, the mean ratio, and the estimated index of dispersion probably first used by Clapham (=40):

$$I = (n - 1) \cdot \text{variance/mean}$$

(E1.1.40)

and the Morisita index (=41):

$$\frac{n \sum x(x - 1)}{\sum x(\sum(x - 1))} \quad (E1.1.41)$$

Tests of the random hypothesis based on these statistics use the result that I has an approximate χ^2_{n-1} distribution. Other tests involving less detailed recording have been suggested (=42, 43) using only the number of quadrats with up to 2 counts and the total number of plants or quadrats.

The distance at which two samples can be considered to be independent of each other can be found by constructing the semivariogram (=44). The procedure involves plotting half of the average variance between pairs of samples against the distance between the pairs. In an ideal case, pairs close together have the lowest semivariance, and there is a distance, h , beyond which semivariance no longer increases with increasing distance between pairs. Two samples separated by a distance that exceeds h , may be considered to be independant. (=45).

1.1.5 Mean free path and mean random spacing (=46)

Cribb has reviewed the relationship of mean free path and mean random spacing with respect to microstructures. The statistically exacts expression for the mean free path, commonly referred to as the mean phase intercept, λ , of individually dispersed particles in a matrix phase is given by:

$$\lambda = 4V_v/S_v \quad (E1.1.42)$$

where V_v is the volume fraction of the dispersed phase and S_v is the interface area relative to the matrix phase. The equation denotes the mean edge-to-edge distance between second phase particles, or alternatively the average distance to surfaces common to matrix and particles.

In the case of three-phase structures consisting of matrix phase, α , with a dispersion of β and γ clusters, the concept of the above equation is expanded to give six relationships. However as frequently occurs in polyphase systems there may be negligible contact between similar particles, and as a result when the secondary phases are not multigrained, the six equations are simplified to yield a complete specification of the mean phase intercepts with only four equations:

$$\lambda^\alpha = 4V_v^\alpha/(S_v^{\alpha\beta} + S_v^{\alpha\gamma}) \quad (E1.1.43)$$

$$\lambda_\beta^\alpha = 4V_v^\alpha/(S_v^{\alpha\beta} + S_v^{\alpha\gamma} + 2S_v^{\alpha\alpha}) \quad (E1.1.44)$$

$$\lambda^\beta = 4V_v^\beta/S_v^{\alpha\gamma} \quad (E1.1.45)$$

$$\lambda^\gamma = 4V_v^\gamma/S_v^{\alpha\gamma} \quad (E1.1.46)$$

where λ^x is the mean free path in the x -phase

λ_g^x is the mean phase intercept between xx boundaries in the x -phase.

The term, λ_g^x , is the “ α -grain size”, and will be the same as λ^α when there are no boundaries within the homogeneous α -phase. An additional parameter, similar to the intercept is the mean random spacing, denoted σ , which is defined:

$$\sigma^x = 1/N_L^x \quad (E1.1.47)$$

where N_L^x are the particle, or cluster, intercept counts. This latter parameter may be interpreted as the mean centre-to-centre distance between dispersed particles or clusters of a phase.

The amount of internal boundary area can be determined with a reasonable degree of accuracy by a simple counting procedure (=17), often intercepts of boundaries with a random line transect across the section. The boundary area per unit volume, S_v , is then given by $S_v = 2P_L$ where P_L is the number of boundaries crossed by a unit of length of the random line.

1.1.6 Space auto-correlograms

Mirza (=47) has identified space auto-correlograms as capable of giving a clear picture of the structure of a mixture (of particulate solids) with the power of showing features, such as periodicity, in any given direction and even slight departures from the optimum random structure. It was possible to analyse the structure of mixtures by means of directional auto-correlograms. As the mixing proceeded, it was shown that changes in the spatial arrangement, which were not detected by the usual statistical methods based on second or higher moments of composition about their mean, were revealed. The space auto-correlograms are more informative than serial correlograms, but the method is limited by the need for exhaustive sampling.

1.1.7 General comments on the concept of size

It has been suggested that the ultimate criteria for evaluating the meaning of such terms as cluster, or similarity, is the value judgement of the user. If using the terms produces an answer of value to the investigator, then that is all that is required (=48).

The conclusions derived from studies made at one scale may not be applicable to problems whose data are expressed at other scales. Every change in scale will bring about the statement of a new problem, (=49), and there is no basis for assuming that associations existing at one scale will exist at any other scale.

Understanding the perceived structure is an important aspect of image analysis, (=50). Schacter discusses several models for generating isotropic *cellular* textures, which tessellate a region into cells and assign grey level probability density to the cells. The models can in principle be used to predict statistical texture properties commonly used for texture classification. The models are intended to describe a variety of natural textures arising from physical processes that create cellular decompositions of a region. Model fitting can yield

useful results as long as the cell size distribution for the model is similar to that of the texture.

In map reading several small compact shapes are much more visually comparable than a few large regular shapes (=51). The average of unweighted small area ratios may well differ from the weighted averages of larger areas, but with regular grids problems arise when the edge of the specimen area under consideration is outside the real area, for example at the coastline.

The separation of observation and explanation problems, and the distinction between macro and micro issues within each, are somewhat artificial. Levels are continuous rather than dichotomous and observations and explanations are but segments of the gestalt of scientific enterprise (=52). Nevertheless, the failure to separate analysis levels results in a host of logical and methodological problems. Ultimately it is required to integrate macro- and micro-observations and explanations. This integration is not achieved by mixing levels between the data and the interpretation: synthesis can only result from preliminary separation of micro- and macro-analysis and their eventual reintegration.

Small scale exceptions to macro-models are inevitable. Although the relationship between areal size and population size is not direct, the population density is specifically affected by areal size. Indeed there is a negative exponential relationship between the size of particular areal units and the population density (=53). Simple ways of reducing the irregularities of areal units are:

- by grouping them into fewer more regular areas,
- by weighting them according to size,
- by eliminating aberrant areas,
- by the use of grid meshes.

Grid squares offer, through aggregation, a broad range of precisely defined scales in a spatial series, to which it is possible to apply quantitative techniques in order to determine the degree of variance at successive levels of aggregation. There can be no clearly defined threshold between the micro- and the macro-population.

Aggregation of squares is, conceptually at least, a simple matter either for larger areal units or for population units of more regular size, but less regular shape. The disadvantages include the greater difficulty of data collection. Absolute counts should not be plotted in relation to areas of variable extent, but division to give a density measure is essential (=54). Squares are more easily compared with regard to size, and are more easily drawn by mechanical machines. In certain statistics it is essential that a distinction be made between "out-of-area" and "missing data" before matrix operations are performed. If the aim is to compare spatial patterns of several variables, then standard deviation units have much to commend them relative to mapping.

Given the definition of a population as an aggregate of the members, it appears superficially that the characteristics of the population are merely derivative from the character-

istics of the individuals by summation. The situation is in fact more complex than that. Just as the properties of the individuals may be used in aggregate form as properties of the population, so the properties of the population can be used as properties of the individuals (=55). The macro-analytic level of inquiry consists of propositions or statements of relationships among the properties of individuals as the unit of reference. In general it is invalid either to transform a proposition about populations into a proposition about individuals or to transform a proposition about individuals into a proposition about populations. The relationships among individual characteristics, expressed as a regression equation linking individual variables, will generally have different parameters from one population to another.

1.2 Mechanical properties of composites

1.2.1 Elastic properties of monofibre composites

The simplest type of composite material consists of continuous unidirectional fibres in a solid matrix. The composition of a composite is normally defined by the volume fraction of a component, i.e. the volume of that component relative to the total volume. Microscopy of such a composite sectioned normal to the major axis of the fibres will yield an image which consists of a set of circles (the fibres) on a continuous background (the matrix). Component x will have a volume fraction V_x , calculated from the area, A_x of that component relative to the total area of image considered. The subscript x will be taken as c for composite, f for fibre and m for matrix. Hence:

$$V_f = A_f / A_c \quad V_m = A_m / A_c \quad A_f + A_m = A_c \quad (E1.2.1)$$

and therefore:

$$V_f + V_m = 1 \quad (E1.2.2)$$

This assumes that the void content, V_v , is zero. If this is not so:

$$V_f + V_m + V_v = 1 \quad (E1.2.3)$$

If the fibres and matrix both act as perfectly elastic solids, then at low tensile stress with the fibres and matrix equally strained, the composite strain will be:

$$\epsilon_c = \frac{\sigma_m}{E_m} = \frac{\sigma_f}{E_f} \quad (E1.2.4)$$

and since the stress, σ , is equal to the load, P , acting on an area, A , and from equilibrium considerations $P_m + P_f = P$, then:

$$\epsilon_c = \frac{P_m}{E_m A_m} = \frac{P_f}{E_f A_f} = \frac{P}{E_m A_m + E_f A_f} = \frac{\sigma_c}{E_m V_m + E_f V_f} \quad (E1.2.5)$$

If the volume fraction of fibres, V_f , is high, and they have a high modulus, E_f , then in equilibrium conditions the composite strain for a given load will be dominated by the

fibre properties and the stiffness can be estimated by:

$$\frac{\sigma_c}{\epsilon_c} = E_f V_f \quad (E1.2.6)$$

The equivalent modulus theory replaces the random multiphase fibre reinforced material with a homogeneous, anisotropic medium, and destroys all microstructure effects. Therefore it is not suitable for describing certain properties in composites, especially in dynamic situations and in fracture behaviour.

The modulus of elasticity along the major axis of the fibres can be derived from the following equation, which is commonly termed the rule of mixtures:

$$E_c = E_f V_f + E_m V_m \quad (E1.2.7)$$

Tsai (=56) derives an expression for the transverse stiffness of the composite, E_{22} , by regarding the filaments as parallel, cylindrical inclusions. The problem is regarded as analogous to Hashin's considerations of spherical and cylindrical inclusions (=57, 58). This assumes that the inclusion is completely enclosed by the matrix and that the amount of resin enclosing each inclusion is the same as the average matrix content of the entire composite. The maximum theoretical volume fraction for a hexagonal array of aligned cylindrical fibres of the same diameter is 90.6 v/o but this is unlikely to be achieved in practice. Tsai considers that, at filament contents as high as 80 v/o, the fibres may come into contact with one another and not be isolated by the matrix. Guild (=9) and Guild and Silverman (=10) have reported that Noymarski interference during microscopy of 30 v/o glass fibre reinforced polyester resin shows that the fibres do not truly touch, although a significant number of groups of two or more fibres were detected as single features in the analysis.

The theoretical prediction of E_{22} , modified for filament contiguity, can be resolved by taking the two extreme cases and using a contiguity factor, C . When all fibres are isolated $C = 0$; when all fibres are contiguous, $C = 1$, and in practice fractional values will probably occur at high volume fractions.

The resulting relationship is:

$$E_{22} = 2[1 - \nu_f + (\nu_f - \nu_m)V_m] \\ \times \left[(1 - C) \frac{K_f(2K_m + G_m) - G_m(K_f - K_m)V_m}{(2K_m + G_m) + 2(K_f - K_m)V_m} \right. \\ \left. + C \frac{K_f(2K_m + G_f) + G_f(K_m - K_f)V_m}{(2K_m + G_f) - 2(K_m - K_f)V_m} \right] \quad (E1.2.8)$$

where:

$$K_x = E_x / 2(1 - \nu_x) \text{ and}$$

$$G_x = E_x / 2(1 + \nu_x). \quad (E1.2.9)$$

The major Poisson's ratio has been obtained by considering the isotropic plane of the unidirectional composite to be in a state of plane stress, ($\sigma_{11} = 0$, where σ_{11} is the normal stress component along the axis of the filaments). The amount of lateral contraction as measured by ϵ_{12} is proportional to ν_{12} , so that:

$$\nu_{12} = -\frac{E_{11}\epsilon_{11}}{\sigma_{22} + \sigma_{33}} \quad (\text{E1.2.10})$$

Again the effect of filament packing must be taken into account, as in the prediction of E_{22} , and the equation is:

$$\nu_{12} = (1 - C) \frac{K_f \nu_f (2K_m + G_m)(1 - V_m) + K_m \nu_m (2K_f + G_m)V_m + C \frac{K_m \nu_m (2K_f + G_f)V_m + K_f \nu_f (2K_m + G_f)(1 - V_m)}{K_f (2K_m + G_m) - G_m (K_f - K_m)V_m}}{K_f (2K_m + G_f) + G_f (K_m - K_f)V_m} \quad (\text{E1.2.11})$$

The shear modulus is similarly derived from consideration of the extremes of contiguity such that:

$$G_{12} = (1 - C)G_m \frac{2G_f - (G_f - G_m)V_m}{2G_m + (G_f - G_m)V_m} + CG_f \frac{(G_f + G_m) - (G_f - G_m)V_m}{(G_f + G_m) + (G_f - G_m)V_m} \quad (\text{E1.2.12})$$

The value of C must be the same for the transverse modulus, shear modulus and Poisson's ratio within any single specimen.

Alternative semi-empirical equations have been developed by Halpin and Tsai (=59) from rigorous elasticity calculations. These are:

$$E_{11} = E_f V_f + E_m V_m \quad (\text{E1.2.13})$$

$$\nu_{12} = \nu_f V_f + \nu_m V_m \quad (\text{E1.2.14})$$

and:

$$\frac{\bar{\rho}}{\rho_m} = \frac{(1 + \xi \eta V_f)}{(1 - \eta V_f)} \quad (\text{E1.2.15})$$

where $\eta = (\rho_f / \rho_m - 1) / (\rho_f / \rho_m + \xi)$,

$\bar{\rho}$ is the composite modulus, E_{22} , G_{12} or G_{23} ,

ρ_f is the corresponding fibre modulus, E_f , G_f , ν_f respectively,

ρ_m is the corresponding matrix modulus, E_m , G_m , ν_m , and

ξ is a measure of reinforcement which depends on the boundary conditions.

Once the ξ factors are known for the geometry of inclusions, packing geometry and loading conditions, the composite elastic moduli for fibre reinforced composites are approximated from the Halpin-Tsai formulae. Reliable estimates for the ξ factor can be

obtained by comparison of the equations with the numerical micro-mechanics solutions employing formal elasticity theory. The only assumption made, Halpin and Kardos (=60), in assigning values for the geometrical factor is that the engineering stiffness expressions for the composite ply are insensitive to the differences in the Poisson's ratios of the constituent phases in the ply.

The effect of the interface, of discontinuous fibres, of lay-ups with multiple orientation of the fibres and of defects in the composite are discussed in reference (=61) which is included in Appendix 1.

1.2.2 Failure of uniaxial monofibre composites

The concept of failure in composite materials requires some qualification. In the discussion of this topic the term failure will indicate the first load drop off in the stress-strain curve, and any other types of failure will be qualified as they arise. Failure is therefore considered to occur when the elastic properties cannot be retrieved completely upon unloading, and not when the specimen has separated into two discrete pieces. A similar equation to that obtained for the elastic modulus parallel to the fibres may be used to predict the tensile strength of a fibrous composite, σ'_c , assuming that the composite fails at the breaking strain of a fibre not embedded in resin:

$$\sigma'_c = \sigma'_f V_f + \sigma_m V_m \quad (\text{E1.2.16})$$

where σ_m is the stress acting on the matrix at the breaking strain of the fibres. If the equal strain concept holds up to the breaking stress of the fibre, σ'_f , then:

$$\sigma'_c = \sigma'_f V_f + \frac{\sigma'_f E_m V_m}{E_f} \quad (\text{E1.2.17})$$

As a result of this assumption that the fibres govern the strength, it can be seen that both the strength and stiffness of a unidirectional composite will vary linearly with the volume fraction of the fibres.

Considering a bundle of fibres not enclosed in a matrix and subjected to a tensile stress, any fibre which breaks will no longer take its share of the load, which is then transferred to the remaining fibres. It can be shown that the strength of a bundle will, therefore, not be as great as the sum of the strengths of the individual fibres. The bundle strength will decrease with an increase of variability in strength of the filaments because of this transfer of load.

When short fibres are embedded in a matrix which is subjected to a tensile stress they will take up the stress to an extent related to the ability of the matrix to sustain shear deformation. The fibre stress will build up from zero at the fibre ends, and if the fibre is long enough will reach a certain constant value. If the fibre is shorter than a critical length the fibre will never carry a stress high enough to cause fibre fracture, as the composite will fail in shear, either in the matrix or at the fibre matrix interface. The critical length, l_c (when there is no debonding) is given by the expression:

$$I_c = \frac{R_f \sigma_{11}}{\sigma'_{12}} \quad (\text{E1.2.18})$$

where R_f is the fibre radius,
 σ_{11} is the tensile stress in the fibre, and
 σ'_{12} is the shear strength of the interface (or matrix).

1.2.3 Elastic properties of fibre hybrids

Hayashi (=62) developed an expression for the elastic modulus of a hybrid laminate, constructed of three kinds of unidirectionally fibre reinforced materials, in tension. If all the materials have brittle properties for the stress strain curve, and the elastic moduli, ultimate strengths and strains are represented by (E_A, E_B, E_C) , $(\sigma'_A, \sigma'_B, \sigma'_C)$ and $(\epsilon'_A, \epsilon'_B, \epsilon'_C)$ respectively, then if the volume fraction of each laminate type is V_x the expression for the total modulus will be:

$$E_i = E_A V_A + E_B V_B + E_C V_C \quad (\text{E1.2.19})$$

up to the failure of the low elongation component, after which it will be independent of the properties of the failed component and, until the medium elongation component fails, will be determined by:

$$E_{ii} = E_B V_B + E_C V_C \quad (\text{E1.2.20})$$

and then until the final failure will be further reduced to:

$$E_{iii} = E_C V_C \quad (\text{E1.2.21})$$

The above equations assume that the fibre failure strain distributions do not overlap. This result is now generally accepted as the rule of mixtures for the initial elastic modulus of hybrid composites at all levels of dispersion, but is more commonly written in terms of the volume fraction of the component fibres, assuming a common matrix:

$$E = E_{Af} V_{Af} + E_{Bf} V_{Bf} + E_{Cf} V_{Cf} + E_m V_m \quad (\text{E1.2.22})$$

According to Chamis and Lark (=63) reasonable agreement between measured and calculated flexural modulus data, using the properties of each of the k plies, is given by:

$$E_H = \frac{1}{3t} \sum_{i=1}^k (z_{i+1}^3 - z_i^3) E_i \quad (\text{E1.2.23})$$

where E_H is the elastic flexural modulus of the hybrid,
 t is the thickness of the complete hybrid,
 z_i is the distance to the bottom of the i th ply, and
 z_{i+1} is the distance to the top of the i th ply.

When thin fibres are used to fill the spaces between thick fibres, (=64) the Young's

modulus of the composite rises by an amount:

$$\Delta E = E_1 (V_{\max} - V_2), \quad (\text{E1.2.24})$$

where E_1 is the elastic modulus of the thin fibres,
 V_2 is the volume fraction of the thick fibres, and
 V_{\max} is the theoretical maximum mixed fibre content.

Skudra *et al.* (=65) have obtained a linear plot of Poisson's ratio against the volume content of glass fibres in a hybrid composite:

all carbon, $\nu = 0.249$,
 all glass, $\nu = 0.263$.

1.2.4 Strength of fibre hybrids

In addition to his proposed equations for elastic modulus Hayashi (=62) derived expressions for the tensile strength of a three fibre brittle elastic composite. Until the failure of the lower elongation component (LEC), the tensile stress, and ultimate strength, will be given by:

$$\sigma_i = E_i \epsilon \quad \sigma'_i = E_i \epsilon'_A \quad (\text{E1.2.25})$$

At the failure of all the LEC fibres there will be a discontinuity in the stress strain curve and for failure of the medium elongation component (MEC):

$$\sigma_{ii} = E_{ii} \epsilon \quad \sigma'_{ii} = E_{ii} \epsilon'_B \quad (\text{E1.2.26})$$

For final failure:

$$\sigma_{iii} = E_{iii} \epsilon \quad \sigma'_{iii} = E_{iii} \epsilon'_C \quad (\text{E1.2.27})$$

and the total elastic strain energy per unit volume up to separation will be given by:

$$U = \frac{1}{2} E_A V_A \epsilon'_A{}^2 + \frac{1}{2} E_B V_B \epsilon'_B{}^2 + \frac{1}{2} E_C V_C \epsilon'_C{}^2 \quad (\text{E1.2.28})$$

This assumes that all fibres of a single type fail at a definite strain and then no longer contribute to the load carrying capability of the composite.

In a mixture of two materials systems, if the failure of the high elongation component (A) occurs with no contribution to the strength from the low elongation component (B) then the strength of the hybrid will be given by:

$$\sigma' = V_A E_A \epsilon'_A \quad (\text{E1.2.29})$$

where V_A is the volume of component A as a proportion of the total volume of the composite.

However, when the low elongation component fails there will be a contribution to the overall strength from the high elongation component which will be given by:

$$\sigma' = (V_A E_A + V_B E_B) \epsilon'_B \quad (\text{E1.2.30})$$

At the volume fraction at which the minimum strength occurs, we can equate the two equations, so that:

$$V_A E_A \epsilon'_A = (V_A E_A + V_B E_B) \epsilon'_B \quad (E1.2.31)$$

and by rearranging and taking $V_A = 1 - V_B$:

$$\frac{(1 - V_B)}{V_B} = \frac{E_B \epsilon'_B}{E_A (\epsilon'_A - \epsilon'_B)} \quad (E1.2.32)$$

and therefore:

$$\frac{1}{V_A} = 1 + \left[\frac{E_A}{E_B} \left(\frac{\epsilon'_A}{\epsilon'_B} - 1 \right) \right] \quad (E1.2.33)$$

hence allowing the determination of point T in figure 3.

Gunyaev (=64) and Chamis (=66, 67) presented equations for the ultimate deformation of hybrid composites and derived a related expression for the critical volume content of low modulus fibre at which the fracture mode changes from being dominated by the low elongation to the high elongation material. The ratio μ_{cr} , of the critical content of low modulus fibre composite to the total amount of composite is given by:

$$\mu_{cr} = \left[1 + \frac{\sigma'_1}{\sigma'_2} - \frac{E_1}{E_2} \right]^{-1} \quad (E1.2.34)$$

where 1 and 2 refer to the low and high modulus fibres respectively, and σ' and E are the tensile strength and modulus.

The minimum strength associated with this critical content of low modulus fibre is:

$$\sigma'_{min} = \epsilon'_1 E_1 V_1 \quad (E1.2.35)$$

$$= \mu_{cr} V \epsilon'_1 E_1 \quad (E1.2.36)$$

where ϵ' is the failure strain, and

$$\mu_{cr} = V_1 / V.$$

The minimum strength of the hybrid is proportional to the critical content of low modulus fibres. If the content of low modulus fibres in the composite is greater than the critical content, a characteristic inflection occurs in the stress-strain diagram, corresponding to the limiting elongation of the high modulus material.

The ultimate failure stress of a hybrid composite when multiple fracture occurs should be that of the high elongation component (HEC) multiplied by the volume fraction of that component, provided that failure of the LEC causes no stress concentration on the HEC.

Kelly (=21) postulates that the failure strain of the high elongation component is invariably reduced by the presence of the low elongation component but that the ultimate strain of the LEC may remain unchanged, or be increased by decreasing the dimensions

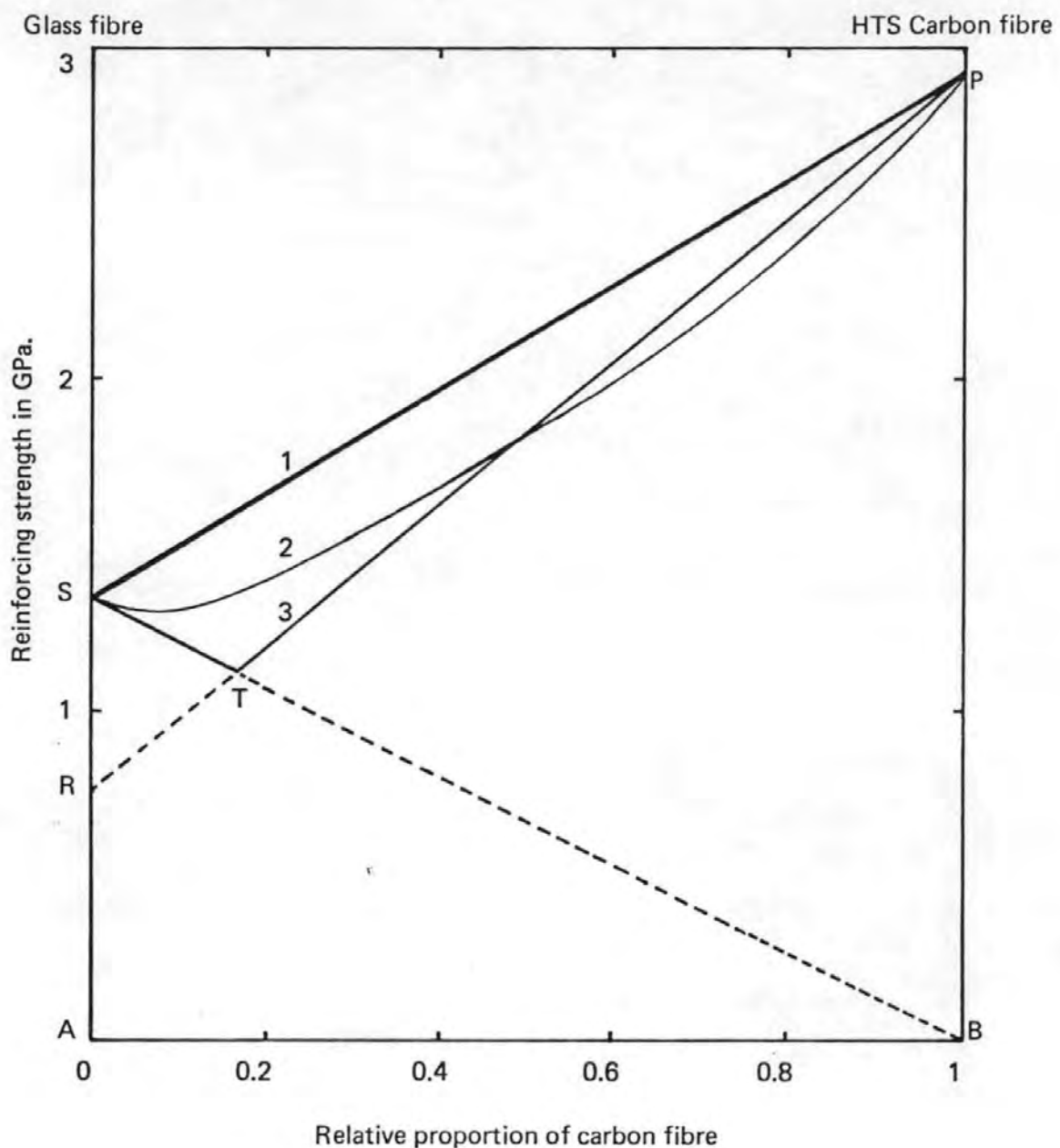


Figure 3: The calculated reinforcing strengths of mixtures of glass fibre with HTS carbon fibres (=72)

- 1 = rule of mixtures
- 2 = bundle theory
- 3 = constant strain

(bundle diameter, individual fibre diameter, or transverse ply thickness in bidirectional laminates). He demonstrated that an earlier theory of multiple cracking and constrained failure can be applied to the prevention of thermal cracking in laminated hybrids. The stress concentrations due to failure in the LEC do not appear to be very important. Irreversible first failure can occur by fracture of one fibre population, cracking of a brittle matrix or cracking in the 90° plies of a cross-plied laminate. Multiple cracking occurs wherever one component of a hybrid system breaks at a smaller strain than the other, and there is sufficient HEC to bear the total load at this first cracking strain, assuming no stress concentrations result on the HEC. The spacing of these multiple cracks depends on the absolute size of the microstructure and results in a relaxation of the material around the broken component. This leads to local extension of the specimen, due to the additional load borne by the HEC.

Failure of the low elongation fibres will lead to an additional strain on the adjacent fibres. If the adjacent fibre is the high elongation component of the hybrid it is probable that this HEC fibre will bridge the crack rather than suffer consecutive failure. In intimately mixed hybrids the area of the HEC/LEC interface per unit volume will be high compared to the interfacial area in composites where each fibre type occurs in large homogeneous groups. Hence there will be only a small distance from the failed fibre to the bridging fibre in an intimate hybrid. It is therefore probable that the full reinforcing strength will be redeveloped within the failed fibre within a short distance of the fracture surface of that fibre (approximately the critical length). In composites which contain large areas of a single fibre species there is likely to be a greater distance between bridging and broken fibres, and therefore a greater distance will be required along the broken fibre before the full reinforcing strength is redeveloped. As a consequence of the greater utilisation of the fibre in the intimate hybrid, there will be a reduced displacement of the specimen ends compared to that in unmixed hybrids. As a result, for a greater dispersion of the two species, the energy required to form the multiple cracks is increased.

The same theory is applicable to both external mechanical and thermal loading. If there is no contribution from mechanisms such as pull-out of the LEC, and provided that no stress concentration on the HEC fibre occurs on failure of the LEC, then the ultimate failure stress when multiple fracture occurs will be that of the HEC multiplied by its volume fraction. The strain however will be less because the HEC is not stretched uniformly along its length and the ultimate tensile strain of the composite will lie between calculable limits, depending on the crack spacing and, hence, on whether the two phases are elastically bonded or debonded. There is a transition from cracked to uncracked matrix with increase in dispersion at approximately constant thermal strain.

Aveston and Sillwood (=68) and Kelly (=69) point out that the matrix cracking strain of a brittle matrix composite can be raised above its normal value, under certain conditions, and extended the work to cover the failure strain of LEC fibres in a hybrid. Assuming the existence of a sliding frictional bond these authors give the following equation for the failure strain of the LEC fibres in a matrix consisting of the HEC fibres and resin:

$$\epsilon_f' = \frac{12\tau\gamma_f E_m V_m^2}{E_c V_f E_f^2 R_f} \quad (E1.2.37)$$

where $2V_f/R_f$ is the area of fibre matrix interface per unit length parallel to the fibres,
 ϵ' is the longitudinal strain at failure,
 V_x is the volume fraction of component x ,
 E_x is the Young's modulus of component x ,
 γ_x is the work of fracture of component x , and
 τ is the shear strength.

Aveston and Sillwood argue that τ is not commonly known but that the stress transfer length, L , between fibre and matrix is, and is related to the fibre stress by:

$$\epsilon_f' E_f = \frac{2\tau L}{R_f} \quad (E1.2.38)$$

Thus by substitution equation E1.2.37 becomes:

$$\epsilon_f'^2 = \frac{6\gamma_f V_m^2 E_m}{L E_c E_f V_f} \quad (E1.2.39)$$

They quote an example of 3.5 v/o type I carbon fibre in 35 v/o glass fibre reinforced plastic (i.e. a brittle fibre in a less brittle matrix). For granular graphite $\gamma_f = 150 \text{ Jm}^{-2}$, and for the composite studied $L = 1 \text{ mm}$. The predicted value of ϵ_f' , the mean LEC fibre breaking strain in the hybrid, was 1.1% compared with an experimentally determined value of $1.08 \pm 0.02\%$. For the plain carbon type I fibre composite the breaking strain was $0.5 \pm 0.06\%$, by experiment.

The enhancement of the strain to failure of brittle matrices is observed in the direction of reinforcement, the increased breaking strain has frequently been demonstrated, and it is most noticeable when the fibres are fine and provide an extended surface to which the matrix adheres thereby preventing the opening of the matrix cracks.

Bader and Manders (=20) define two fundamental constitutional parameters for hybrids—the hybrid ratio or factor and the state of dispersion. The hybrid ratio is the proportion of a given fibre component to the total amount of all fibre components. It is most easily expressed in terms of layer thickness. For the layer by layer lamination considered, the dispersion is defined as the reciprocal of the thickness, t_r , of the smallest representative repeat unit. They confirm the existence of a hybrid effect in glass shell-carbon core laminates. The failure strain of the carbon fibre layer may be enhanced to a degree dependent on the laminate geometry, up to 35% in high tensile carbon and up to 45% in high modulus carbon fibres. The extent of this hybrid effect is greater when the carbon is present at low volume fractions and when the dispersion is high. In certain hybrids it can be up to double the strain of monofibre carbon composites. The absolute thickness of the carbon fibre ply must be small to observe this enhanced failure strain and virtually no effect is

observed when the core thickness exceeds three laminae. The extent of the debonding at the glass carbon interface is decreased as the dispersion is increased and the volume percentage of carbon is reduced. Debonding is inhibited when the core thickness is diminishingly small and is contained in the interface throughout the test until the glass fibres fail. The thermal stresses due to fabrication only account for a minor part of the observed failure strain enhancement and the bulk of the enhancement is attributed to a constraint mechanism (the restriction of carbon relaxation by the glass leads to a higher hybrid strain which increases fracture energy), but only a moderate agreement has been found between the simple model and experiment. Progressive failure occurs in the carbon fibre ply in a multiple fracture mode with matrix cracks appearing more frequently in resin-rich areas. The acoustic emission count rate becomes significant at about 0.005 strain.

Better load distribution is provided by the uniformly distributed interply hybrids than by core shell systems according to Rao and Hofer (=70) and Hofer *et al.* (=71). This also overcomes the modulus mismatch across the core shell interface, which causes high inter-laminar stresses and early failure.

Edwards *et al.* (=72) have studied the mechanical properties of aligned intimately mixed short fibre hybrids. The pre-pregs required to produce composite specimens were created by a convergent fibre flow in a liquid suspension, followed by deposition by either vacuum filtration or centrifugal action. Fibres of nominally brittle behaviour can be isolated sufficiently from fibres of their own type that they attain their full reinforcing efficiency because they are not subject to consecutive cracking or to stress concentrations from adjacent failed brittle fibres. Sets of fibres which have overlapping distributions of elongation at failure can combine to produce a hybrid composite which is stronger than the single component values would predict. In the analysis of the glass-HTS carbon system, using weighted mean of the fibre breaking strains the results show the bridging of the hybrid strength trough expected when fibres behave elastically but have different elongations at failure.

It appears that for two fibres of equal diameter brittle behaviour can be suppressed completely when the brittle fibre is slightly in the minority. When the environment of a single brittle fibre is analysed in terms of the surrounding five fibres characteristic of normal imperfect fibre packing, the suggestion is that if the brittle fibres have the larger diameter, they need only be in a numerical minority to modify composite behaviour. The conscious overlapping of distributions of fibre breaking strain can in principle be tailored to maximise the energy absorbed on a rising load curve and to minimise the deterioration of hybrid strength below the rule of mixtures value. This procedure will be most effective with simple composites which are weak largely because their fibres have a high variance in strength values. Both the coordination and bundle strength arguments ignore local stress concentrations caused by fracture of the other set of fibres and hence represent an upper bound to the strength. If the glass fibre is assumed to adhere to the matrix less strongly than the carbon fibre, then to enable it to develop adequate reinforcing strength the glass fibre must be correspondingly longer.

Bunsell and Harris (=73) reconsidered the Hayashi work using hybrids in which alternate layers were either bonded or not bonded to one another. Initial fracture was similar in both cases but in the bonded hybrid the carbon fibre continued to carry load and contribute to stiffness until final failure, which occurred at a lower strain than in the unbonded or all GRP specimens. It was suggested that extension only takes place in the regions of GRP adjacent to the fractured CFRP.

Bunsell and Harris (=74) report that the fracture of the carbon in a sandwich hybrid in three point bend was heralded by a burst of acoustic emission and began at a strain greater than that expected of monofibre CFRP. The carbon fibre continues to contribute to stiffness because of the good bond between the laminate plies (figure 4). At a critical distance from the fracture the carbon fibre is again able to take load and multiple cracking results at subsequent failures, normal to the fibre direction. On cooling from the cure temperature the fibres attempt to contract in proportion to their individual expansion coefficients and at room temperature the glass will be in tension and the carbon in compression. Failure of the composite in tension will therefore occur at higher strains in a hybrid composite than in a monofibre carbon material, because the loading will first reduce the compressive strain in the fibre to zero and then the tensile strain will build up.

McColl and Morley (=75) report that major advantages can be gained by the design of composite systems using fibres of very different sizes to perform distinct functions. As a consequence of the difference of scale, the action of the second, toughening, fibre phase can be confined to the matrix fracture faces, while the much larger primary fibres influence the fracture process at a distance from the crack front. This was examined experimentally with a 600 µm diameter steel wire/glass fibre tissue/epoxy resin system at low fibre volume fractions. The hybrid system carried about twice the tensile strain before crack growth than did either of the component composites. The values of critical stress observed by McColl and Morley were found to be in reasonable agreement with the theoretical predictions.

Fischer *et al.* (=76) have shown that the hybrid effect depends on the loading configuration, in three point bending, through its dependence on the mode of failure. The results for Young's modulus in interlaminar or translaminar loading indicate that this property is determined by the rule of mixtures and does not depend on the construction of layers in the hybrid. Values of the critical stress intensity factor and work of fracture for the initiation and propagation of failure exhibit similar trends in that they decrease from the values predicted by the rule of mixtures as the plies of the two reinforcements become more segregated. Visual and scanning electron microscope examination reveals that failure under interlaminar loading occurs by delamination. When the fibres are more intimately mixed, failure by delamination will be more difficult because of the greater energy involved in creating the larger amount of new surface in an intimate mix than that required to cause delamination of a layered hybrid. Thus it is clear that under interlaminar loading with failure by delamination, the grouping of like fibres into distinct layers results in a reduced hybrid effect.

OE

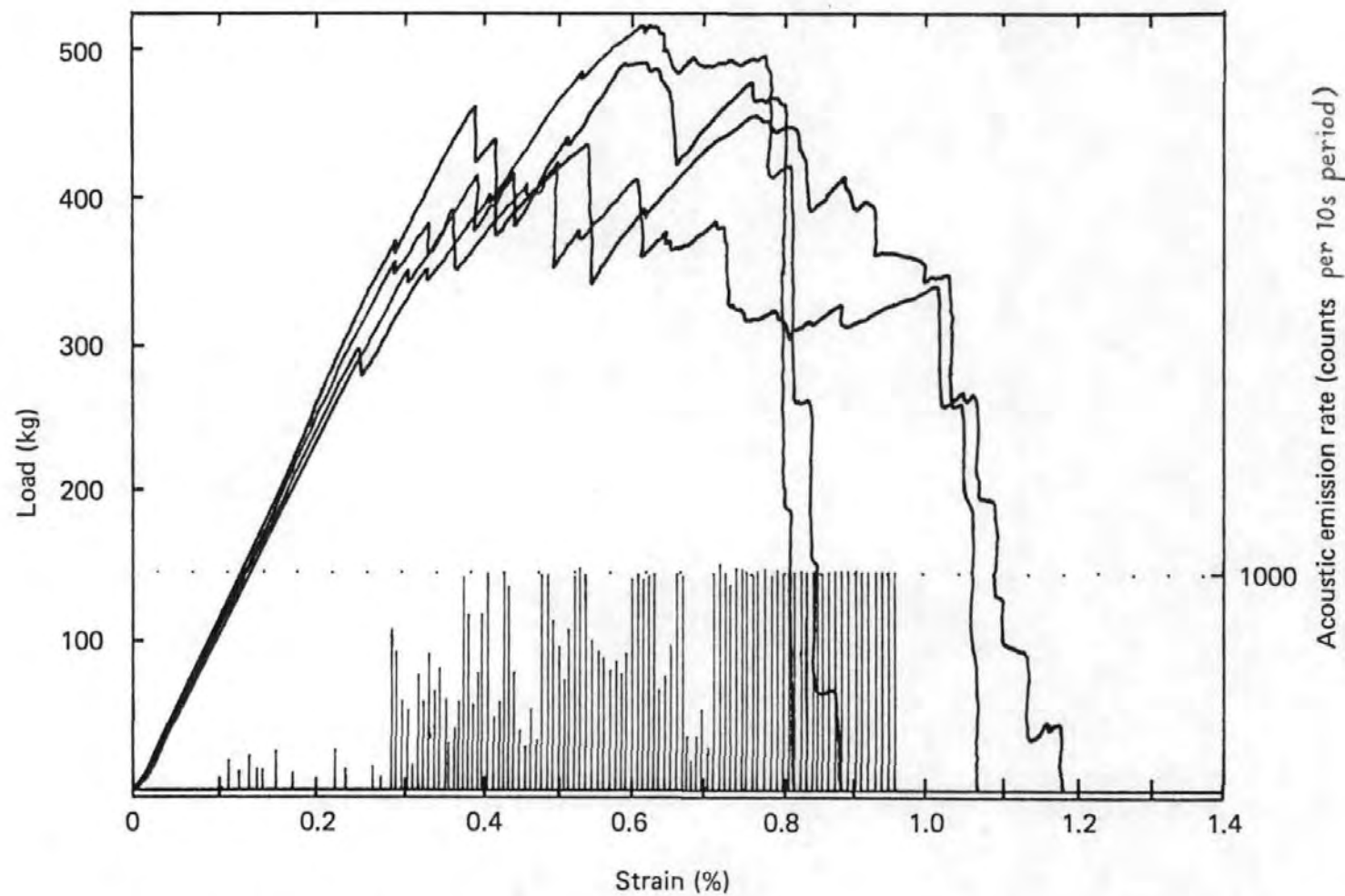


Figure 4: Load-strain curves for bonded layered hybrid composites with two layers of CFRP and two layers of GRP (=73)

Under translaminar loading the prominent failure mechanism is pullout. The work of fracture under interlaminar loading is greater than in the translaminar configuration. The stress deflection curves reflect the different energy dissipation mechanisms in hybrids under the two types of loading. Delamination develops most readily in hybrids with thick layers of a single fibre type and occurs at the HEC/LEC interface. Beaumont (=77, 78) has presented microscopic observations of fibre-matrix debonding, fibre fracture and the pullout of broken fibres from a cracked matrix. Models for the dissipation of the energy in these processes were presented and comparison was made between the theoretical and experimental work of fracture data for a carbon fibre and glass fibre hybrid reinforced plastics (CGHRP) composite. The dominant mechanism of fracture was shown to be dependent on the relative proportions of the components (figure 5). The shape of the fracture energy curve was dominated by the post-debond sliding mechanism of the glass fibres, but in carbon-fibre-rich samples the pullout of the carbon fibres became important. The cumulative probability of each of the pullout lengths and of the glass fibre debond length are shown in the figure.

Manders (=79) has identified three factors which contribute to the hybrid effect:

- residual strains of thermal origin,
- variation of carbon fibre first failure strain with volume in the hybrid,
- thickness dependence of the defect limited strength in the reference material (all-carbon-fibre composite).

The hybrid effect in this case, the enhancement of first failure strain in the low elongation component, has been shown to arise partly from the differential thermal contraction of the components. As a result of the slight expansion of carbon fibres upon cooling being more than balanced by the contraction of the glass fibres and the matrix (the latter supplemented by the volume reduction during curing), a residual compressive strain results in the carbon fibre, but this only accounts for a small proportion of the effect.

A Weibull probability graph (strength vs. discrete volume of cfrp: on logarithmic axes) enabled the strength of specimens with different cfrp volumes to be compared. Good agreement between the experimental strength values and numerical predictions (from a statistical model presented by Harlow and Phoenix (=80, 81)) showed that volume was the parameter of overriding importance limiting the strength of the cfrp component in the hybrid. This strength dependence has "weakest link characteristics", whereby the strength is limited by the catastrophic propagation of a small group of fibre fractures which has exceeded some critical size.

Manders identifies five factors which could further improve the agreement between the experimental and predicted strengths:

- inaccurate extrapolation of single fibre strengths to short gauge lengths where they do not fit a Weibull distribution (see =82, 83),
- a difference in the variability of fibre strength between fibres tested in isolation and when surrounded by other fibres in a composite,
- over simplification of the load redistribution at fibre fractures,
- the two-dimensional nature of the hybrids,

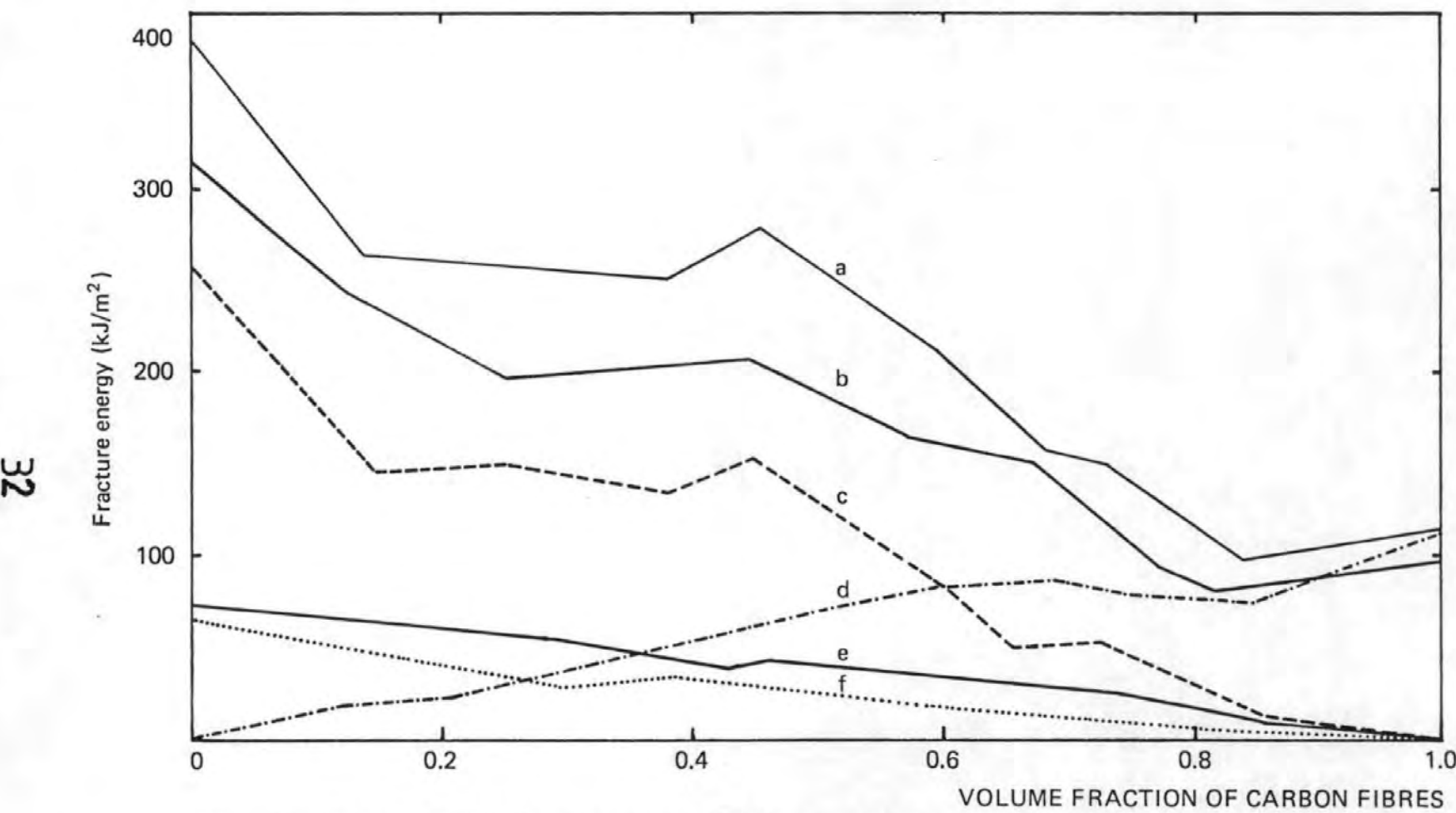
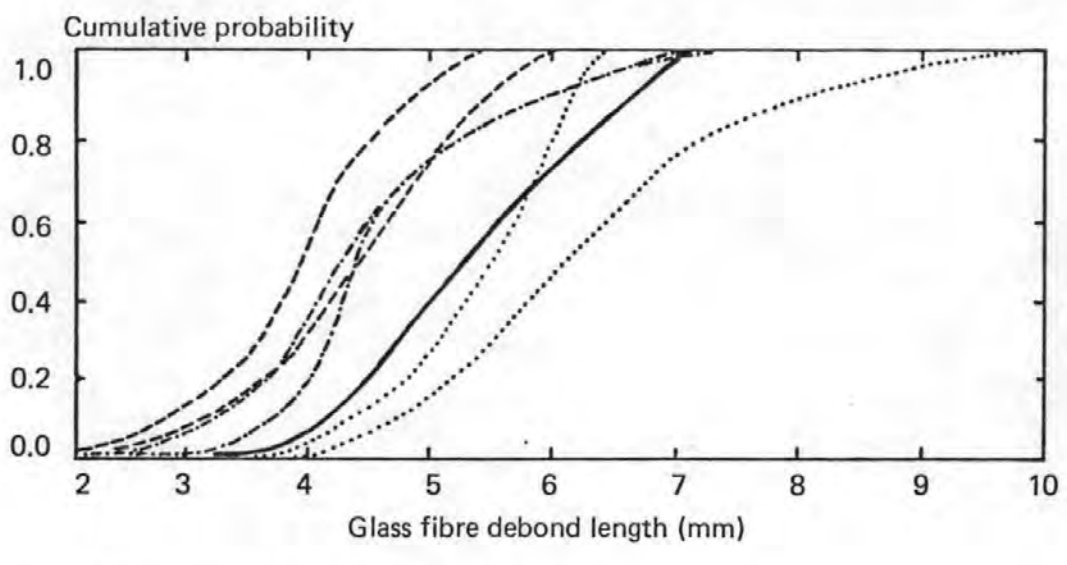
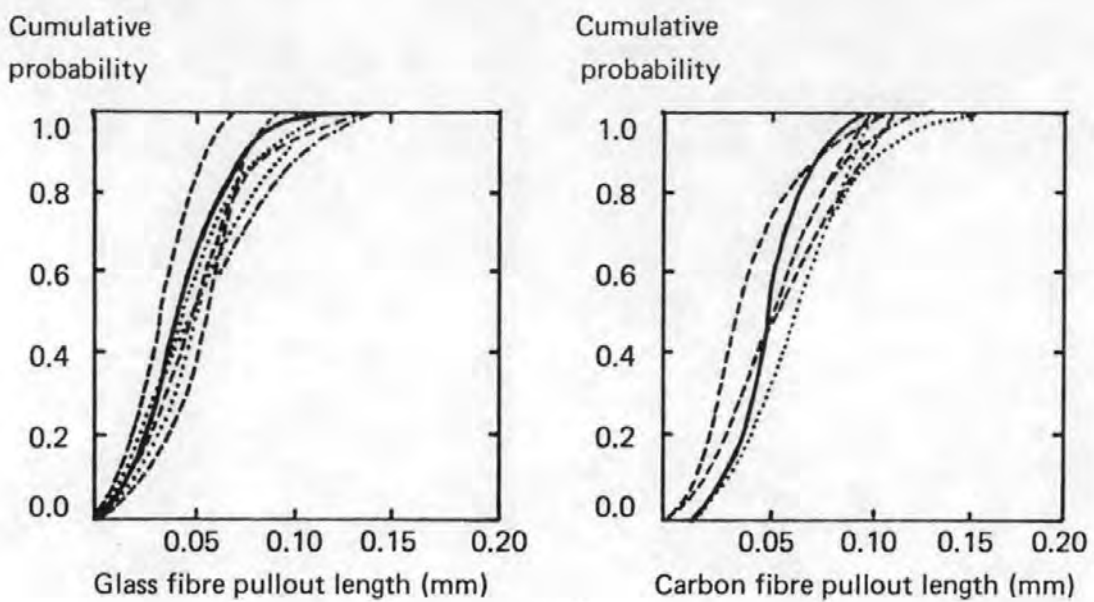


Figure 5a: The theoretical and experimental work of fracture of carbon-glass hybrids (=77)

KEY: Total theoretical fracture energy (a),
 Glass fibre post debond energy (c),
 Glass fibre pull-out energy (e),

Experimental work of fracture (b),
 Carbon fibre pull-out energy (d),
 Glass fibre debond energy (f).



KEY:

- monofibre glass or carbon composite
- - - less than 40% glass fibre
- 50% ± 10% glass fibre
- more than 60% glass fibre.

Figure 5b: Cumulative probabilities of composite fracture modes in glass fibre/carbon fibre hybrid reinforced plastics (=77)

- the increased ineffective length as the number of adjacent fibre fractures increases.

When a single carbon fibre fractures it will briefly overstress the surrounding material (by a maximum factor of 1.27 in a two dimensional case (=84)), which will be more likely to fail, allowing the crack to propagate. If the fracture is partially surrounded with glass fibres, then the temporary overstressing may be reduced, leading to crack arrest. Manders reports that the failure of carbon fibres initially occurred at isolated positions, and then accumulated into small groups on account of the overstressing of adjacent fibres. These groups had a maximum size in the range 2-5 fibres, beyond which there was catastrophic propagation of the crack through all the carbon fibres in the bundle. Regions reinforced with glass fibres were shown to act as barriers to the propagation of cracks between bundles of carbon fibres.

Manders results indicate that there is considerable advantage to be gained by dispersing the low elongation fibre as a number of small bundles, although his composites were fabricated from thin ($\approx 100 \mu\text{m}$) layers of carbon fibre laminate, and not at a fibre-by-fibre level of mixing.

1.3 Acoustic Emission

1.3.1 Background

Non destructive testing (NDT) of materials and structures is a rapidly growing field, of particular application where a structure is liable to fatigue stress, stress corrosion or catastrophic crack growth. The growth of fracture critical analysis in design has increased interest in the improvement of the sensitivity, reliability and ease with which NDT can be carried out. Acoustic emission (AE), also known as stress wave emission (SWE) is a relative newcomer to the field, although it promises to be amongst the most reliable techniques for in-situ determination of structural integrity. The most important techniques in NDT are given in table 1.

It has been known for a considerable time that materials under stress emit sounds prior to, and at, failure, and this phenomenon has been useful in giving warning of impending failure — notably in wooden roof-props used in mining. When a material is deformed, there will be short impulsive stress waves generated at the failure source, which will then propagate through the structure, to be detected at the surface by suitable instrumentation. The terms "acoustic emission" and "stress wave emission" cover the generation, propagation and detection of transient elastic strain waves in materials as they undergo deformation or fracture. The literature on acoustic emission is extensive; Drouillard (=86) has published a bibliography-with-abstracts which contains 1900 references. Two papers have reviewed the acoustic emission from fibre reinforced composites:

Guild <i>et al.</i>	: July 1976	: 43 references (=87), and
Williams and Lee	: October 1978	: 54 references (=88).

The first major systematic approach to the acoustic emission of materials under stress is generally accepted to be the thesis by Kaiser in 1950 (=89). He used electronic equip-

ment capable of detecting sub-audible signals. From single load and repeated rising load tests on a series of metals, Kaiser concluded that the number of emissions increased with the applied stress, and that after unloading there was no acoustic emission upon reloading until the previous maximum load was exceeded.

If a specimen is held *under load until all emissions have stopped*, and is then unloaded and reloaded, emissions will not occur until the previous maximum load is reached. This is known as the *Kaiser effect*, and is observed in both metals and composites.

However if a composite is not held at load for a sufficient duration and is unloaded, emissions will occur at a load lower than the previous maximum load. This phenomenon is known as the *modified Kaiser effect* or the *Felicity effect*. The ratio of the load at which emissions occur and the previous maximum load is known as the *Felicity ratio* or the *Felicity percentage*, and is indicative of the amount of damage (=90, 91). After the work by Kaiser, very few further papers were published until 1964 when the first applications were reported. The same year results from tests using equipment detecting only signals at frequencies higher than the audio range were published. This excluded most of the background noise, but at the cost of increased structural attenuation. Schofield (=92) and Tatro (=93) had developed more sensitive equipment and by now had identified that the emissions from metals could be primarily associated with plastic deformation.

TABLE 1: The major techniques of non-destructive testing

Reproduced from: J.R. Houghton and P.F. Packman, December 1977 (=85).
Supplemented by: I.M. Daniel and T. Liber, April 1979 (=85a).

<u>Techniques</u>	<u>Limitations</u>	<u>Smallest detectable crack</u>
X-ray photography	Grain size of film Defect orientation re: film Absorption of x-rays by material	> 3 mm. — can be enhanced with tetrabromoethane
Dye penetrants	Void length and depth	> 2 mm.
Eddy currents	Diameter of detector field	> 1 mm.
Ultrasonics		> 1 mm.
Magnetised particle		> 1 mm.
Acoustic emission		> 2 nm.
Visual inspection		
Moiré fringe		
Photoelastic coating		
Holographic interferometry		
Liquid crystal thermographic coatings		
Infrared imaging		

Acoustic emission signals can be divided into two basic types, although there is no clear logical transition between them:

- a) white noise — continuous emission with a wide frequency range,
- b) burst type — emissions mainly occurring as single decaying sinusoids (ringdown mode) when detected, because of resonances both in the structure and in the transducer.

1.3.2.1.1 Detection of AE signals

The source of a stress wave may be assumed to be a point and to produce an expanding spherical wave with the energies distributed over a very broad frequency band, identified by Bell (=94) as 0 — 20 MHz. As the wave expands it loses energy at a rate proportional to the reciprocal of the square of the radius. At the boundary of the component the wave is converted into shear waves and either Rayleigh waves, or in thin structures, Lamb waves. These waves move across the surface of the material with an energy that decreases in inverse proportion to the distance.

In order to detect the stress wave at the specimen surface a piezoelectric transducer is normally employed. Piezoelectric materials, for example quartz, respond to a mechanical impulse by emitting an electrical signal with a sharp rise and slower decay of voltage amplitude. The frequency inside the signal envelope is determined by the resonance of the transducer crystal, but may be altered to regions of low background noise by a change in the physical size of the crystal. A wide variety of piezoelectric crystal materials have been employed:

- a) Ammonium dihydrogen phosphate (=95-98)
- b) Barium titanate (=99, 100)
- c) Cadmium sulphide film (=101, 102)
- d) Lead zirconium titanate (PZT) (=98, 103-106)
- e) Lithium niobate (=101, 107-111)
- f) Lithium sulphate (=98, 101)
- g) Quartz (=89, 98, 100, 104, 112, 113)
- h) Rochelle salt (=89, 98)
- i) Zinc oxide and zinc sulphide (=102)

A wide variety of other techniques have also been employed for a variety of reasons, usually with a view to the analysis of the signal output for the amplitude or frequency information:

- a) accelerometers (=94)
- b) capacitive devices (=114)
- c) magnetostrictive (=115-118)
- d) microphones (=119)
- e) passive pressure (=98)
- f) phonograph pickup (=120)

- g) polymeric foil (=121-123)
- h) pure electromagnetic detection (=124)
- i) strain gauge records (=125, 126)
- j) WO_2 or ZrO_2 or SiO_2 dielectric with Ta electrodes (=127)
- k) embedded single-mode optical fibre interferometry (=127a)

1.3.2.1.2 Calibration of acoustic emission transducers

A wide variety of simulated acoustic emission sources have been reported for use as standards for calibration or checking of the system:

- a) breaking a 0.5 mm diameter 2H propelling pencil lead, extended by 3 mm and supported by a guide ring (=128, 129)
- b) fracture of a glass capillary (=130)
- c) electric spark discharge (=94, 131-134)
- d) ultrasonic transducer driven at steady state energy (=98, 102)
- e) highly sensitive capacitive transducer plate as standard (=130, 135)
- f) grinding of glass powder (=135) or silicon carbide (=104, 135)
- g) air abrasive (=102, 136)
- h) white noise energy by helium gas jet against surface (=137, 138)
- i) ball drop (=139-141)
- j) martensitic phase transformation in Au-Cd alloy (=142)
- k) stress corrosion due to tightening a screw in a notched aluminium block exposed to salt solution (=143)
- l) pulsed laser (=134, 144, 144a)

1.3.2.2 Analysis of acoustic emission signals

The simplest form of acoustic emission equipment records the number of times that a signal exceeds a preset threshold level. This is the cumulative *acoustic emission count*. The threshold is generally set to eliminate background signals.

Often the differential of the AE count is recorded to give a record of the *acoustic emission rate*, as this sometimes allows an easier analysis of the time at which events happened most rapidly.

Amplitude sorting is a more sophisticated development in which all the signals detected by the transducer during a test are grouped according to their amplitude. This can be achieved by making an analogue recording of the transducer output during a test and then counting the events above a series of thresholds on each of the successive replays. Commercial digital systems have now emerged which can present the information in the form of a histogram as the test progresses. In the classical mode the number of counts in each amplitude band is plotted, in the cumulative mode *all* the events above each threshold are plotted and the line on the display will run from top left to bottom right if the amplitude increases from left to right. Amplitude distributions may be based on several parameters

(eg. peak value, integral values such as energy or number of threshold crossings). These distributions can be correlated if the detailed shapes of the acoustic emission waveforms are known. It is also necessary to have an understanding of the waveform shape in order to define an event before the amplitude distribution is computed (=145).

Frequency sorting can be similarly carried out to establish a characteristic frequency signature for a test or for a particular failure mode. The scheme is limited by the frequency response of the transducer and the associated electronics, and also by frequency shifts or mode conversions due to the specimen geometry. Both swept-frequency spectrum analysis and autocorrelation analysis have been used. Particular features of the power spectrum may be characteristic of a specific source, but the phase information contained in the signal is destroyed. Fourier transform analysis will preserve phase information and is thus potentially of greater use in source characterisation (=145).

Pulse analysis has been reported by Houghton *et al.* (=85). They examined the signature of single pulses in both the frequency domain and the time domain. The techniques tested included Fourier spectra, Fourier transfer function, shock spectra and shock spectrum ratio. Deconvolution of the first few microseconds of the pulse train was shown to be the region in which the significant signatures of the AE event had occurred.

Other less common techniques include the analysis of the rise time or the decay time of the initial AE burst.

1.3.3.1 Acoustic emission in composite materials

The sources of AE in composite materials include low level emissions such as plastic deformation of the matrix and fibres as well as high level emissions from:

- resin crazing,
- fibre debonding,
- fibre fracture,
- relaxation of fibres when they fracture, and
- fibre pullout against friction.

Because the glass fibre reinforced plastics are viscoelastic and distribute load over time (=146) they do not generally exhibit the classic Kaiser response (=147). Upon initial loading the residual stresses stored in the fibres are released. The emission from these internal stresses, along with the AE resulting from fibre breakage and matrix crazing, will dissipate with time as the stresses are relieved. Once the internal stresses are released the composites display a more normal Kaiser effect. The Kaiser effect is observed during fibre breakage at low and non-critical loads. Repeated loading to a single critical stress level will cause fibre breakage to recur, although this phenomena will dissipate with the number of load cycles applied.

Attempts have been made to correlate the acoustic emission with different failure modes. FitzRandolph *et al.* (=148) combined AE monitoring with compliance and work

of fracture measurements to propose that fibre debonding was the dominant mode in the tensile failure of a boron epoxy composite. The total acoustic emission count was related to the number of broken fibres as measured by an electrical method. Rathburn *et al.* (=149) were unable to locate such a relationship, although they monitored the AE arising from the fracture of a single fibre embedded in resin. Balderston (=150) noted that high level acoustic emissions were associated with fibre fracture. Fuwa, Bunsell and Harris (=151) clearly demonstrated that significant AE was associated with fibre fracture by testing composites with fully and semicured resins and also without a matrix. Similar work to establish a correlation of AE with fibre debonding and pullout (=148, 150/2/3) and resin cracking (=150, 153, 154) has been attempted. This type of work is very susceptible to errors arising from signal attenuation due to fibre misorientation, specimen geometry and transducer attachment.

Arrington and Harris (=155) have reported the results of experiments to examine the acoustic emission of carbon I-carbon II-resin hybrids. The overall numbers of counts were observed to be of the same order for failure either by interlaminar shear or by fracture normal to the fibres. However, as failure at the threshold levels set was expected to be by fibre failure it would seem that the span-to-depth ratio of the interlaminar shear strength (ILSS) test was close to the limit for clearly defined shear failure. The total numbers of counts recorded during both shear and slow bend testing of the hybrids were (sometimes substantially) higher than those recorded from the unmixed composites. This is probably due to the release of the elastic constraints, fabricated into the hybrid, through local cracking. This idea is reinforced by the work of Bunsell and Harris (=73) in which a similar effect was observed in CFRP and GRP layers tested either separately or laminated and bonded together.

1.3.3.2 Amplitude distribution acoustic emission (ADAE)

In the amplitude sorting of acoustic emission signals a parameter "b" is often used. This parameter has a unique value when a single type of emission source predominates. If the energies of the emission events are randomly distributed, then statistical analysis shows that a plot of the number of emissions $n(a)$ exceeding a given amplitude level "a" is generally a smooth curve of the form:

$$n(a) = (a/a_0)^{-b} \quad (E1.3.1)$$

where a_0 is a constant. A logarithmic plot of the cumulative distribution would thus be a straight line of negative slope equal to "b" (=91). Size effects are eliminated in using the "b" parameter because it is not affected by the attenuation of sound in the material, provided that all amplitudes are equally attenuated.

Composite materials are well suited for ADAE analysis. It is well known that in the initial stages of tensile testing, low amplitude emissions are detected, which correspond to matrix crazing. Fibre fracture, which starts later in the test is characterised by higher

amplitude emissions. In some CFRP tensile specimens failure occurs by gross delamination rather than by localised fibre failure, so that the b-value rises as the test proceeds. This situation is easily recognised from the very high rate of low-amplitude emissions accompanying the delamination, so that the failure mode can be predicted while the test is running. A double-peaked or bimodal amplitude distribution would be expected for the normal case of failure by fibre fracture. One such experiment, by three-point bend of an FRP bar, gave a best-fit b-value of 0.65, the bimodal distribution being indicated by a poor fit to the power law. In the case of failure by gross delamination, a high b-value of around 1.7 was observed (=156, 157).

Wadin and Pollock (=158) have identified an ascending order of amplitude spectra running from fibre rubbing through delamination to gross tearing of the fibres. Emissions in the smaller amplitude range recur during successive proof tests of the same magnitude, although their quantities tend to diminish after several cycles. Events with amplitudes greater than 60dB are identified as probably representing fibre fracture, and do not recur at low loads. Hence, changes in the shape of the amplitude histogram between different tests may well indicate changes of failure mode.

Graham (=159) has reported that the average amplitude of emissions, as measured by the ratio N/N_E , during loading of unidirectional graphite epoxy rises to a maximum and then levels off at some lower value. The growth and stabilisation of existing flaws is identified with the maximum average amplitude. The constant amplitude region is then identified with the growth of the cracks, which had formed in the weak areas of matrix, in the remaining stronger matrix. The average values for unaged specimens were always greater than those for moisture aged specimens.

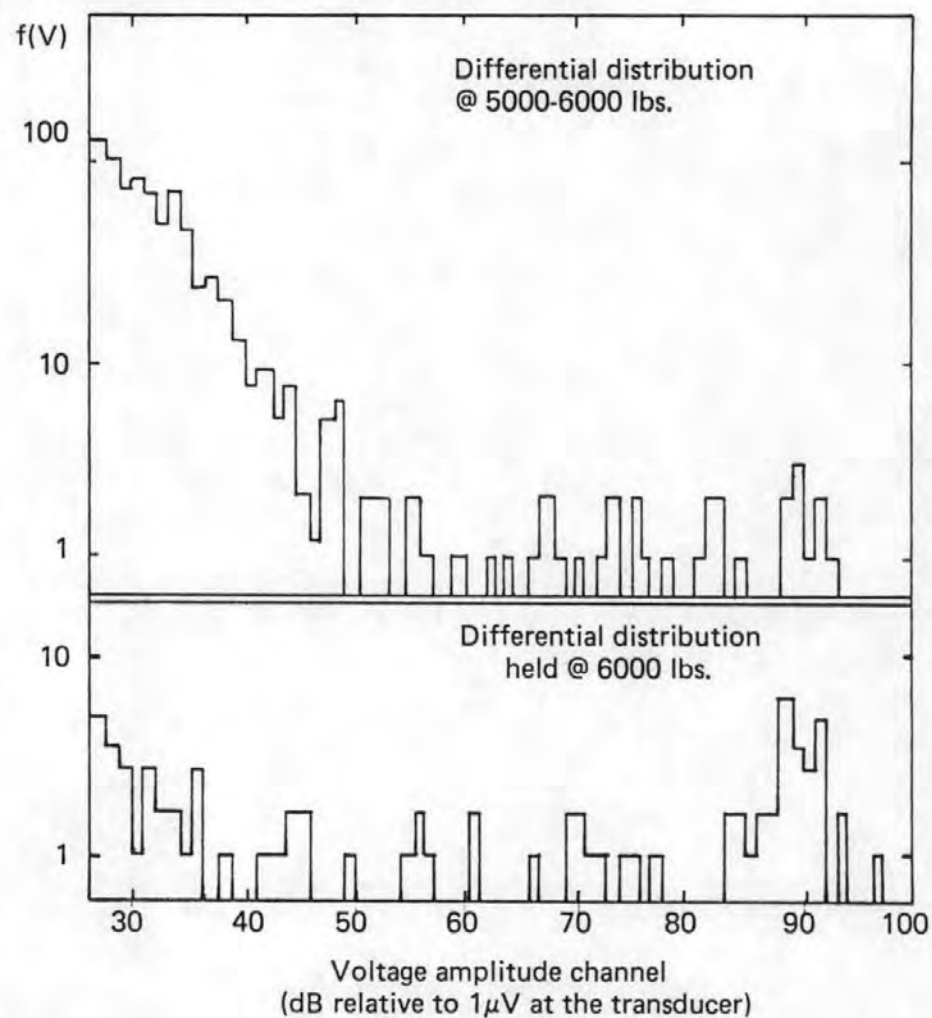
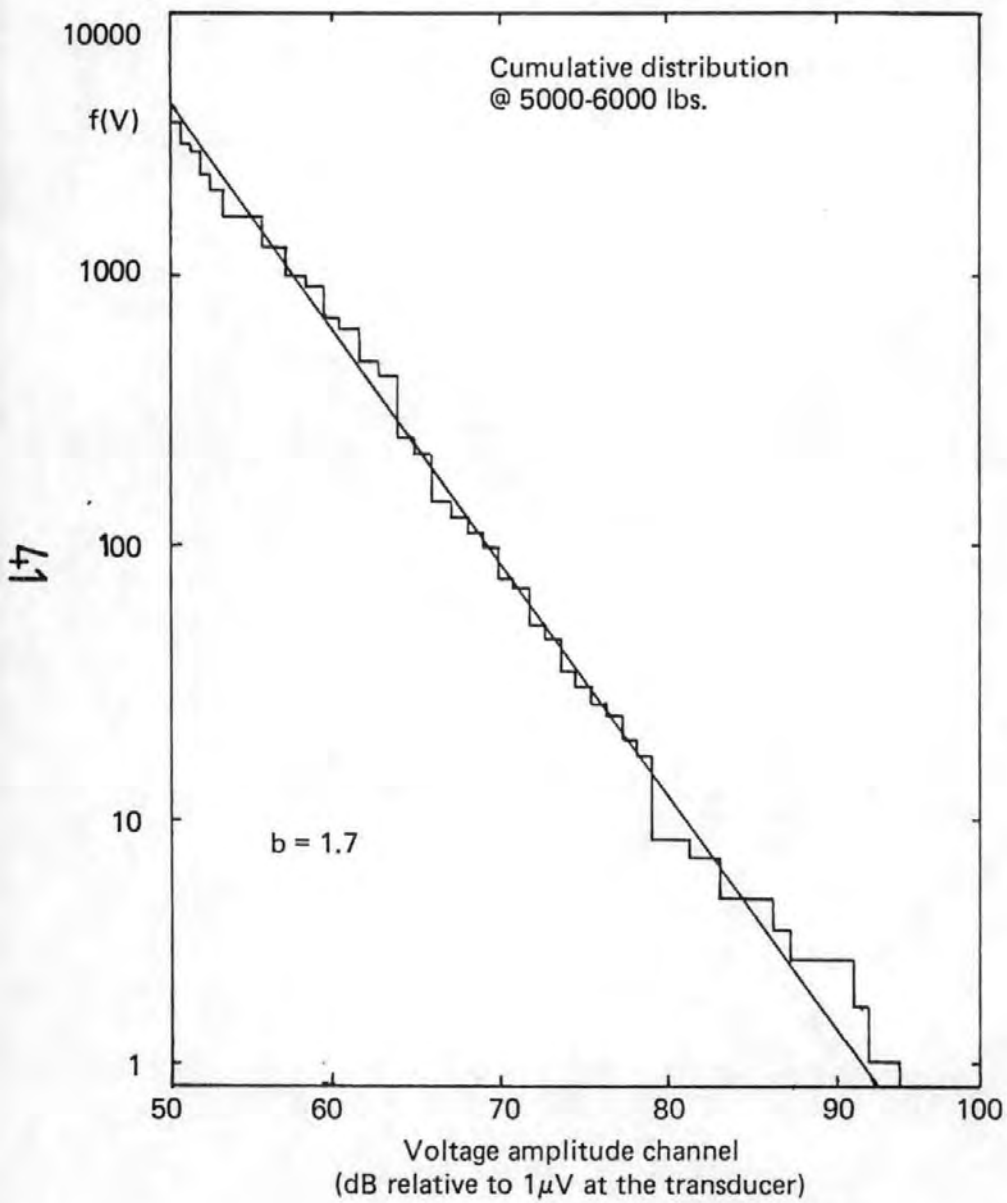
Guild *et al.* (=160) have published results to show that the above simple correlations are unrealistic because the amplitude of a fibre failure event depends sensitively on the condition of the local fibre resin interface, the extent of debonding, the presence of an environment hostile to the glass and probably many of the other parameters not included in this list. In consequence they caution against assigning events to specific AE amplitudes and recommend an identification of such unique features by a statistical approach.

1.3.3.3 Frequency analysis

Acoustic emission has been detected in some materials at frequencies as high as 30MHz. However, ultrasonic damping is high in most materials above 10MHz, and the frequency range from 30kHz to 3MHz is generally regarded as the most suitable for monitoring emissions (=161). Green *et al.* (=162) have described a procedure for the frequency analysis of acoustic emissions by which they claim to distinguish between fibre fracture and inter-laminar shear failure.

Mehan (=152) and Mullin (=163) have stated that acoustic events in carbon, boron and glass reinforced epoxies have a broad frequency band in the audible range with dominant frequencies apparent according to the material (see Table 2). A characteristic signature

Figure 6: Amplitude distribution acoustic emission characteristics of a CFRP panel (=157)



could be assigned to each failure mechanism: fibre fracture, matrix fracture or debonding.

Speake and Curtis (=164) have attempted to correlate the frequency spectrum of acoustic emissions with the fracture mode of carbon-epoxy. Waisted tensile specimens failed by fibre breakage with AE in the range 0(dc)-70kHz. Notched tensile specimens failed in shear with cracking parallel to the fibres with a predominant frequency band from 30-130kHz. The dominant frequencies remained unchanged during these tests, although the frequency bands moved to higher frequencies (figure 7).

When the bundles of carbon fibre were tested in tension a broad band of frequencies was noted (65-135kHz) with a few higher discrete frequencies depending on the fibre type. Polyacrylonitrile fibres (precursor for carbon fibres!) also had the same broad frequency band. Glass rovings produced a frequency band from 0-125kHz with discrete frequencies at 185kHz and 225kHz.

In the torsion tests failure progressed from plastic deformation of the resin through crack propagation parallel to the fibres to eventual fibre breakage. Composites of type I fibres exhibited a broad spectrum up to 500kHz while type II composites had frequencies up to 1MHz. Below 90° of twist the type I composites had frequencies in the range 0-100kHz, while above that angle the spectrum shifted to 100kHz-325kHz, probably because of either changes in the failure mode or in the specimen resonance.

TABLE 2: Frequency analysis of acoustic emission from-reinforced plastics

REFERENCE	FREQUENCY BAND	DOMINANT FREQUENCY	COMPOSITE	FAILURE MODES
178EGAN	125KHZ-	1MHZ	C/POLYIMIDE	TENSION
784GREEN	5 HZ-	40KHZ	FIL.WOUND,GLASS	BURST PRESSURE
71MEHAN	-	20KHZ	GRAPHITE-EPOXY	
75MORAIS	2KHZ-	26KHZ	FIL.WOUND GLASS	BURST PRESSURE
73MULLIN	500 HZ-	16KHZ	BORON-EPOXY HI%	
73MULLIN	600 HZ-	6KHZ	1,2,2,3KHZ	BORON-EPOXY LO%
73MULLIN	-	-	600HZ,3,2KHZ	GLASS-EPOXY HI%
274SPEAKE	ZERO	125KHZ	185,225KHZ	GLASS ROVINGS
274SPEAKE	30KHZ-	130KHZ	GRAPHITE-EPOXY	TENSILE FAILURE
274SPEAKE	ZERO(DC)	70KHZ	GRAPHITE-EPOXY	NOTCHED TENSION*
274SPEAKE	65KHZ-	135KHZ	CARBON 1 BUNDLE	WAISTED TENSION*
274SPEAKE	65KHZ-	135KHZ	PAN FIBRES	
274SPEAKE	65KHZ-	135KHZ	CARBON 2 BUNDLE	
274SPEAKE	-	500KHZ	CARBON 1 EPOXY	TORSION
274SPEAKE	-	1MHZ	CARBON 2 EPOXY	TORSION
274SPEAKE	ZERO	100KHZ	CARBON 1 EPOXY	TORSION <90°
				ANGLE £
274SPEAKE	100KHZ-	325KHZ	CARBON 1 EPOXY	TORSION > 90°
				ANGLE £
164STEELE	5 HZ-	40KHZ	2,1,4,2,6,3KHZ	FIL.WOUND,GLASS
TAKEHA	30 HZ-	20KHZ	DIP NEAR 2KHZ	GLASS POLYESTER
179WILLIAMS	-	-	AS1 C/POLYIMIDE	TENSION

* CHANGE OF FAILURE MODE OR OF SPECIMEN RESONANCE

• HIGHER FREQUENCY COMPONENTS BECOME APPARENT AS SPECIMEN RUPTURE APPROACHED

= EVENT SPECTRAL DENSITIES

Egan and Williams (=165, 166, 167) tested unidirectional and cross-plyed carbon-polyimide composites to attempt to correlate AE spectra with visually identified failure modes, which differed according to the specimen lay up. The mean normalised frequency spectra of individual AE events were obtained in the range 125k-1MHz. Visual inspection

This diagram is labelled as in reference 87,
but the original paper implies that the
frequency spectrum is the Fourier transform
of the time signature.

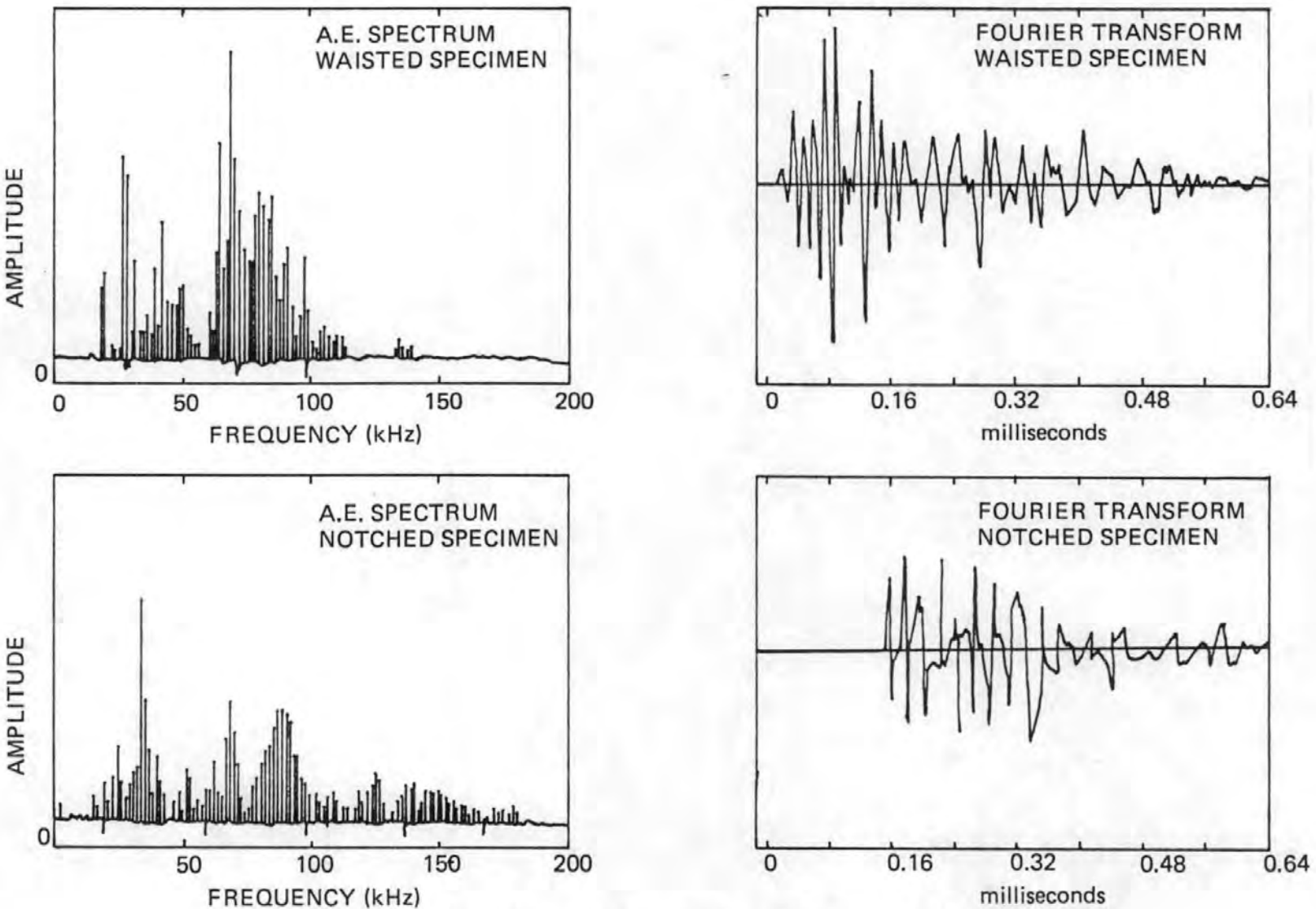


Figure 7: Spectral analysis of acoustic emissions from fracture in 60 v/o CFRP (=164)

of the mean normalised spectral densities (the combined individual AE event spectral densities) of each specimen suggested little with regard to quantitative distinction. Statistical analysis (paired sample t comparison) did however suggest that the spectra within any group of specimens were similar.

1.4 Finite element analysis

1.4.1 Introduction (=171)

The finite element method was originally developed in the aircraft industry, and in 1941 an arrangement of simple elastic bars was used to approximate continuum problems. The use of piecewise continuous functions over a subregion was first considered by Courant (=171) in the context of a torsion analysis. This approach was later formalised and the term "finite element" was adopted in 1960 by Clough (=172). The method subsequently developed rapidly and has now become the general numerical technique for the solution of partial differential equations subject to known boundary and initial conditions. The development of the modern digital computer has ensured that the method now occupies a unique place as a powerful and versatile route to obtaining an insight into the complex advanced engineering problems which exist in many areas of modern technology. The basic steps of a finite element analysis are summarised below:

- a) A mesh of distinct non-overlapping regions, known as "elements", is created to model the structure.
- b) Each of the elements is assigned a distinct number of points, called "nodal points" or more simply "nodes". By assigning the same number to the equivalent node in two separate elements, they will be modelled as if connected at this nodal point in the analysis.
- c) A stiffness matrix is calculated for each element, according to the material properties and geometry assigned.
- d) An applied load vector is calculated for each element.
- e) The element stiffness matrix and the load vector for each element are assembled to give the "global stiffness matrix" and the "global load vector" for the complete structure.
- f) The resulting system of simultaneous equations is solved for the unknown nodal variables, eg. displacements in structural problems.
- g) Stress components are evaluated at the nodal points and element centres.

In addition to the basic software indicated by the above most finite element schemes contain additional programming to fulfill a variety of other requirements, usually preparatory to and subsequent to the main program, eg.

Mesh generation routine,

Data checking routines – warnings and graphics,

Visualisation of results – graphic representation of displaced shapes and stress distributions.

1.4.2 Commercial orthotropic finite element schemes

[Addresses included in Appendix Six]

Mathers and Morman (=173) have surveyed the computational methods available to solve the composite structural response problem for the automotive industry. It was required that three conditions were fulfilled before a system was included. The programs had to be:

- a) Capable of modelling general geometrical configurations, and especially the complexity of automotive structures.
- b) Capable of modelling "anisotropic" laminated shell type structures, without user-written pre- or post-processors. However, instead of truly anisotropic, the models included are:
 - i) orthotropic for continuous fibres, and
 - ii) isotropic or transversely isotropic for chopped fibres.
- c) Available to any user:
 - i) in the public domain
 - ii) for sale or lease through a computer bureau.

However, the special purpose programs with restrictions on geometry (eg. shells of revolution) or analysis type (eg. panel buckling or joint analysis) were not included in the survey. The survey was limited to the large general purpose (finite element) programs which contain a large element library and can perform a variety of analysis tasks.

Seven analysis schemes were found to meet these requirements:

- i) ANSYS: ANalysis SYStem:
 - three node triangular flat shell element.
 - based on Kirchoff plate theory, transverse shear deformation neglected.
 - inplane and bending displacements approximated by linear and cubic polynomials, respectively.
- ii) ARGUS: (after the mythic guardian giant of Io):
 - triangular and quadrilateral flat shell elements.
 - eight-node quadratic isoparametric curved shell element in prospect.
 - based on Kirchoff theory.
 - generalisations of Clough-Felippa element.
- iii) NEPSAP: Nonlinear Elastic-Plastic Structural Analysis Program:
 - comments for ARGUS apply as the two schemes were once incidental, but have developed separately for several years.
- iv) NISA: Numerically Integrated Systems Analysis:
 - family of isoparametric flat and curved quadrilateral shells.
 - between 4 and 12 nodes each.
 - based on shear deformation shell theory.
- v) PATCHES: (from the parametric cubic patches which map structural geometry and materials):

- fundamental element is isoparametric 3D solid with complete tricubic interpolation functions.
- based on the equations of 3D elasticity.
- data generation scheme known as PATRAN.

vii) SPAR: (unofficially attributed to Structural Performance And Resizing,

next release to be EAL: Engineering Analysis Language):

- triangular and quadrilateral elements.
- based on Kirchoff theory and developed to hybrid-stress formulation.
- modular system which communicates through a database.

viii) STAGS: STructural Analysis of General Shells:

- initially developed for analysis of the non-linear behaviour of cylindrical shells with cutouts.
- an energy-based finite difference program, in which the finite difference operators are used to replace derivatives in the energy functional instead of in differential equations (=174). The approach shares many aspects of the finite element method, and a recent modification of the package includes a library of finite elements:
- triangular, quadrilateral and higher-order elements.
- axial rod, torsional spring, nonlinear general beam and triangular plate.
- cylindrical*, conical*, spherical, toroidal, paraboloidal, ellipsoidal, hyperboloidal shells (*with elliptical cross section).
- layered shells, may be anisotropic with respect to the surface coordinates.
- three dimensional brick element and “contact element” in prospect.
- eight node isoparametric shell element in prospect.
- bifurcation buckling analysis.
- options include linear and non-linear static stress analysis, stability vibrations and transient response.
- cubic interpolation functions for both bending and in plane displacements.

In addition to the schemes identified above, there exist further schemes which fulfil the above system requirements. These include:

viii) ADINA: Automatic Dynamic Incremental Nonlinear Analysis (=175):

- two dimensional orthotropic linear elastic quadrilateral elements.
- three dimensional orthotropic linear elastic quadrilateral elements.
- plane stress, plain strain and axisymmetric 2D elements.
- written in standard FORTRAN IV.

ix) APPLE SAP: (by ITALIMPIANTI SpA, Genoa) (=176):

- two and three dimensional isoparametric elements for both structural mechanics and thermal analysis.
- truss, beam, straight or curved pipe, and expansion joint elements.
- improved version of University of California — Berkeley SAP4 structural analysis programme.

- several programmes connected by standard files.
 - automatic data generation for geometry description and loading.
 - written in FORTRAN IV (98%), COBOL (< 2%), and ASSEMBLER.
- x) ASAS-G: Atkins Stress Analysis System; Version G (=177a):
- triangular, quadrilateral, isoparametric, brick and prism elements (17 types).
 - from 3 to 32 nodes dependant on element type.
 - axisymmetric triangular ring element with anisotropic properties (=177b).
 - special crack tip element for isotropic properties only (LEFM/Westergaard).
 - membrane and thin-plate bending and thick-plate bending capability.
 - plane strain behaviour in anisotropic membrane elements.
 - anisotropic heat conduction analysis referred to local elements axes.
 - elements capable of modelling discontinuities of curvature or thickness.
 - based on displacement, strain or stress distribution assumptions.
 - written in a selected subset of FORTRAN IV for UK AWRE.
 - installed at Rutherford and Appleton Laboratories.
- xi) ASKA: (by the Institute for Statics and Dynamics in Aerospace Engineering at Stuttgart University in cooperation with Imperial College, London) (=176):
- beam, flange, triangular, quadrilateral, ring, tetrahedron, prism and brick elements.
 - solution by the displacement method.
 - linear elastic fracture mechanics, crack opening displacement and J-integral.
 - modular structure with dynamic storage allocation.
 - automatic generation of topology and data.
 - written in FORTRAN IV with a few machine dependent routines.
 - can be installed on systems with 64 k words or virtual memory systems.
- xii) BERSAFE: BERkeley Stress Analysis Finite Element system (=178, =179):
- line, beam, triangle, quadrilateral, isoparametric, axisymmetric, brick, prism, tetrahedron and facet shell elements (31 types).
 - line element used for reinforcing effects, typically in concrete.
 - special fracture mechanics elements (triangular and prism only) give displacement variations consistent with true displacement variations.
 - finite element displacement method with front solution of semi-bandwidth symmetric stiffness matrix.
 - parallel program "FLHE" to analyse steady state or thermal transient conditions.
 - dynamics program "BERDYNE" for calculation of natural frequencies and mode shapes, with a variety of forcing functions.
 - degrees of freedom in cartesian and occasionally polar or cylindrical coordinates.
 - automatic mesh generation.
 - fracture mechanics techniques in Phase 2.
 - nonlinear analysis (plasticity/creep) in Phase 3.
 - developed by CEGB Berkeley Nuclear Laboratories Research and Development.
 - installed at Rutherford and Appleton Laboratories.

xiii) CASTOR: CAIcul de STructures sur ORdinateur (=176):

- truss, beam, triangular, quadrilateral, brick, boundary and shell elements.
- plane stress, plane strain and axisymmetric elements.
- thermal analysis and 2D elasto-visco-plasticity.
- perfect contact, perfect sliding or frictional supports as a special contact element.
- automatic mesh generation.
- written in FORTRAN.
- two dimensional analysis: size is 120 000 words although memory is dynamically allocated.
- three dimensional analysis: size is about 85 000 words.

xiv) COMET-PR (=176):

- triangular, curved rectangular, isoparametric, tetrahedral, prism and brick elements.
- symmetric, eccentric and curved stiffeners.
- 2D and 3D elastic fracture mechanics.
- 2D ductile fracture with J-integral and tearing modulus.
- stress contours on surfaces and plane sections.
- written in FORTRAN 77.

xv) DIAL (=176):

- truss, beam, quadrilateral, isoparametric and brick elements.
- ring stiffener, gap and constraint elements in both 2D and 3D libraries.
- lumped non-linear springs and dashpots are provided.
- total Lagrangian formulation used for geometric nonlinearities and finite strains.
- sliding friction capability.
- nonlinear elastic orthotropic materials with different tension and compression properties.
- communicates through a common database.
- written in FORTRAN IV with a few inner loops in assembly language.

xvi) FLASH 2: Finite eLement Analysis of SHells 2 (=176):

- shells, folded plates, ribbed slabs, frames and trusses.
- plates in bending and stretching (plane strain or plane stress).
- uses an improved hybrid stress model.
- buckling analysis.
- automatic mesh generation and node renumbering.
- “clear” modular program structure.
- written in ANSI-standard FORTRAN IV and FORTRAN 77.

xvii) MARC: Marc Analysis Research Corp. (=176):

- beam, truss, quadrilateral, isoparametric and brick elements.
- triangular ring, open or closed section beam, quadrilateral ring, pipe bend elements.
- plane stress rebar, friction and gap element, and heat transfer elements.
- elastic and plastic anisotropic behaviour.
- evaluation of J-integral.

- incremental mesh generators.
- written in FORTRAN IV.

xviii) NASTRAN: NASA STRuctural ANalysis (=180):

- triangular, quadrilateral and three (toroidal, trapezoidal, triangular) ring elements.
- isoparametric, brick and prism elements.
- thin walled cylindrical tube element.
- membrane, bending and transverse shear, buckling and viscous damper elements.
- pressure, temperature, dynamic and static loading.
- orthotropic materials ($E_x, E_y, E_z, \nu_{xy}, \nu_{yz}, \nu_{zx}, G_{xy}, G_{yz}, G_{zx}$)
- anisotropic materials ($G_{11}, G_{12}, G_{13}, G_{22}, G_{23}, G_{33}$).
- written in FORTRAN IV version 13 (> 99%) and assembly language.
- inverse square root singularity element.
- extra-point resequencing subroutine.
- automatic mesh generator – SAIL II: Structural Analysis Input Language.

xix) PAFEC 75: Program for Automatic Finite Element Calculations (=181):

- triangular, quadrilateral, isoparametric, brick and prism elements (19 types).
- from 3 to 30 nodes dependant on element type.
- plane stress, plane strain and bending capability.
- based on Castigliano's theories (=182):

1st: the partial derivative of the total strain energy with respect to the (k)th generalised displacement is equal to the (k)th generalised force.

2nd: the partial derivative of the total complementary strain energy (for linear elasticity) with respect to the (k)th generalised force is equal to the (k)th generalised displacement.

- modular system which communicates through a data base.
- orthotropic capability only available at level 3.1 and above.
- written in FORTRAN IV, for the University of Nottingham.
- installed at Plymouth Polytechnic.
- at least 32K of 24-bit words required to run worthwhile jobs.

xx) SAP 7: (Structural Analysis Program 7) (=176):

- truss, beam, gap, constraint, sandwich, pipe, shell and solid elements.
- automatic generator for geometry and topology.
- program source is entirely in FORTRAN IV.

xxi) SCIA: (=176):

- truss, beam, 2D solid and 3D solid elements.
- anisotropy modelled by a triangular plate together with a beam element.
- geometry and loading preprocessor: menu oriented input.
- written in BASIC to use overlayed programming technique.
- written specifically for WANG 2200 series desktop computer (from 16kb) with secondary storage.

xxii) SUSAN: (=176):

- bar, membrane, plate and thin shell elements.
- part of the GENESYS master system.
- written in GENTRAN.

xxiii) TITUS: (=176):

- beam, bar, triangular, quadrilateral, tetrahedral, prism and brick elements.
- unilateral boundary condition, gap and friction special mechanisms.
- crack elements.
- automatic mesh generation.
- written mostly in FORTRAN IV with some Assembler language.

1.4.3 Crack tip singularities

The use of finite element methods to analyse fracture problems is complicated by the stress field singularity which exists at the crack tip. This problem has recently been reviewed by three separate authors:

Swedlow	:	September 1978	:	38 references (=183)
Fawkes <i>et al.</i>	:	1979	:	42 references (=184)
Akin	:	March 1979	:	35 references (=185)

There are numerous computational methods available to include known singularities in finite elements, and there is ample mathematical proof of the importance of treating these known singularities. The actual improvement in the accuracy of the computed solutions has been demonstrated in most of the references, but relatively few comparisons of the various methods exist. For a linear problem with $p = \frac{1}{2}$ (p is the [unknown] power in $u = O(r^p)$), a brief comparison by Akin and Swany (=186)) showed that the elements could be ranked in order of decreasing accuracy:

hybrid elements,
singularity interpolation elements,
quarter-point elements, and
standard elements (=185)

For a linear problem with $p = 0.6619$, the Yu and Wilson (=187) special interpolation element gave good estimates for the singularity intensity. The use of the same element in a nonlinear problem gave results which were in reasonable agreement with several other solution methods and appear to be more reliable (=185).

Fawkes *et al.* (=184) have assessed the performance of various singularity function elements in the solution of standard test problems of both single and combined mode fracture. These elements were based on the eight node parabolic isoparametric element, in particular using:

- distorted shape functions
- standard shape functions
- analytic functions
- a superposition process
- a hybrid technique.

The study showed that only the analytical element reproduced similar results to the reference values for all the test cases considered, and over a large range of a/w . The analytic approach represents the full crack field over a single element, which allows the crack to be placed anywhere within this element, and consequently crack extension studies can be performed without regenerating new element meshes.

All other elements produced serious discrepancies in at least one test situation, usually in the calculation of K_{II} . The next best group was that using distorted shape functions, but these produced widely varying results for the mixed mode cases and required considerable effort to extrapolate the stress intensity factors from the displacement values. Distorted shape functions are formulated very easily, and work satisfactorily in single mode situations. The failure in the mixed mode case is probably due to the limit of $1/r^{1/2}$ stress modelling only along certain directions in the element.

All other methods produced serious discrepancies, and were highly inaccurate in the mixed mode and pure shear tests. The superposition method did not even adequately represent mode I opening in tension, and generally gave the worst agreement of all the methods considered (=184).

Swedlow (=183) concludes that in the majority of practical circumstances, a straightforward adaptation of the eight node isoparametric quadrilateral would seem to meet engineering requirements for crack tip analysis. The development of further procedures is deemed only necessary under a limited range of conditions, especially in order to smooth out the numerics. Greater value is attached to improvements in the modelling of real materials behaviour and the correlation of analyses with experiment.

1.5 Composites at cryogenic temperatures

1.5.1 Background.

The majority of development work in composites has arisen from a need to reduce the cost of structures designed for use at ambient temperatures or to improve the long term mechanical properties at elevated temperatures. Comparatively little effort has been devoted to the development of composites for use at cryogenic temperatures, with the notable exception of the work sponsored by NASA and the USAF on the characterisation of glass reinforced plastics to 20K. The literature on the mechanical and thermal properties of glass-reinforced and advanced-fibre reinforced composites was extensively reviewed in 1975 (=188, 189), and major conferences on "Non-metallic materials and composites at low temperatures" were held in Munich (=190) and Geneva (=191).

The potential applications of reinforced plastics at low temperatures include superconducting motors and generators, tankers for the transportation of liquified gases and structural frameworks and panels for Arctic/Antarctic/Space applications. It is highly probable that future equipment in these categories will capitalise on composite technology because of the increased reliability, reduced weight and increased efficiency through the increased strength and moduli coupled with the ability to design the material to the application, especially where the very low thermal conductivity will be advantageous compared to the metallic materials used at present. However, at the moment there are three problems in implementing these advances:

- a) most designers lack a feel for the properties available with composites,
- b) the data base on composites at cryogenic temperatures needs to be extended, and
- c) most composites are designed for use at ambient or elevated temperatures and not for cryogenic use.

1.5.2 Glass fibre reinforced plastics

Kasen (=188) concludes that glass-reinforced composites are most useful in applications requiring high tensile strength combined with high toughness and low thermal conductivity, if high stiffness is not required and where cyclic fatigue is not a major problem. The NASA Resin 2 formulation was selected as the most useful of the candidates tested, based on criteria of fibre and composite tensile strength, composite tensile modulus, ultimate tensile strain, interlaminar shear strength, thermal shock resistance, coefficient of linear thermal contraction, and favourable processing characteristics. The available data on the Polaris E-787/58-68R suggest that this resin formulation is capable of producing composite mechanical properties equal to those obtained with Resin 2 at cryogenic temperatures, at least for certain fibre orientations. The absence of experimental data from composite components subjected to dynamic loads or cyclic thermal stresses is identified as an area of ignorance. The glass-polyimidazole composites returned a "surprisingly good overall performance". At 77K this composite ranks second only to the epoxies in tensile and flexural strength, with tensile and flexural moduli superior to those of the epoxies. The compressive properties are average, but the cyclic fatigue response in respect of strength retention is better than in the epoxides.

The composites display an erratic behaviour in their mechanical properties on cooling from 77 to 20K, by which time the strain capability of the matrix had already decreased to a level far below that of the glass reinforcement. It appears from work with unfilled thermoplastics (=192/3) that failure is controlled by a crazing phenomena which is in turn related to the activity of the gas or liquid in contact with the polymer surface. Until such studies have been extended to cross-linked polymers, the possibility that the mechanical properties may be influenced by the ambient media must be considered.

Composites fabricated with a highly flexibilised epoxy matrix are reported to provide better cryogenic properties than those fabricated with nonflexibilised systems (=194, 195), but Kasen (=196) restricts the validity of this statement to laminates containing less than

32v/o of reinforcement. However the intrinsic weakness of highly flexibilised resin systems near room temperature has resulted in the catastrophic failure of several structures designed for cryogenic use but necessarily subjected to moderate stresses at room or slightly elevated temperatures.

1.5.3 Carbon fibre reinforced plastics

Carbon fibre reinforced epoxies (=189) have the highest thermal stability of any class of composites, which is an advantage for many cryogenic applications. However the strength tends to decrease upon cooling to cryogenic temperatures. Kasen reports that mechanical property results are frequently unpredictable and contradictory, although it is unclear to what extent this is due to problems in the testing or due to an inherent characteristic of the material. Larsen and Simon (=197) have reported that the overall performance of carbon fibre composite cryogenic pressure vessels was much better than would have been predicted from their basic test data.

The tensile strengths of graphite-epoxy are reported (=189) to tend to decrease on cooling, such that at 77K the strengths are 138MPa lower than at room temperatures. The compressive strength of graphite epoxy is reported to increase during cooling to 77K. There is insufficient data available to indicate trends in the in-plane shear strength and modulus on cooling graphite-epoxy to 77K, but one reference (=198) indicates that a 14% drop in shear strength is accompanied by an increase in shear modulus of around 50%. The tensile and compressive moduli are reported to be unchanged on cooling from room temperature to 77K. The available data indicates that a decrease of up to 15% in the failure strain of graphite-epoxy occurs on cooling to 77K, although transverse failure strain appears to be independant of temperature.

Carbon fibre reinforced plastics are the most dimensionally stable of the advanced composites and exhibit a very small expansion parallel to the major axis of the fibre on cooling, with a moderate transverse contraction. The thermal conductivity is much lower transverse to the fibres than it is along them. The specific heat appears to be almost linear from 295K to 77K, and to lie below the value for aluminium but above titanium or copper.

1.5.4 Hybrid reinforced plastics

Vasiliev *et al.* (=199) have studied the thermal conductivity, thermal diffusivity and heat capacity of dispersed fibre carbon and glass filled epoxy resin from 10K to 400K to ascertain the applicability of such materials in cryogenic engineering. Because of the anisotropy of the material, conductivity varies with direction but the difference between the values in the hybrid is larger than for either of the single fibre composites. The carbon fibres have most effect in conducting the heat along the composite, because of the covalent bonding. Heat transfer normal to the fibres depends on the weaker van der Waals forces and is governed mainly by the response of the glass fibres. All the composite thermal properties are considerably affected by the fibres, compared to unfilled resin.

Nelson (=200) has reported a design approach tending to minimise the thermally induced distortions and then compensate for residual stresses in the member. Athermalia-

ation, "a technique of controlling the expansivity of an ensemble structure by the use of compensating expansions of individual elements," was rigidly applied in the design of a structurally efficient support truss for the secondary mirror of a Richey-Cretien optical system for the Large Space Telescope. In the absence of a suitable constructional material with "zero" thermal expansivity, graphite-epoxy was selected because it could also fill the requirements for a high natural frequency. Boron and glass cloth are also used in small amounts for property tailoring and to offset the negative coefficient of thermal expansion. A cylindrical truss, constructed using existing composite materials and process controls can be designed to satisfy *micron-level stability* requirements. It requires a sophisticated concern for detail and application of not only the best suited materials but also the judicious development of athermalisation techniques and geometry optimisation.

2 Theory

2.1.1 Nearest neighbour index

The nearest neighbour index is defined as the ratio of the mean observed distance to the mean expected distance and can be calculated from:

$$NNI = \frac{MOD}{1/(2\sqrt{n/a})} = \frac{\text{mean observed distance}}{\text{mean expected distance}} \quad (\text{E2.1.1})$$

In the consideration of areal patterns the values of nearest neighbour index are indicative of the extent of patterning as follows:

<u>NNI</u>	<u>Type of pattern</u>
0	total coincidence of the points
< 1	clustering
1	random
> 1	uniformity or ordering
2.15	(limit) equilateral triangle mesh.

2.1.2 Chi-squared parameter

The chi-squared index is derived by dividing the unit to be considered into smaller equally sized segments and then obtaining an observed and an expected count for the number of occurrences in that segment. The observed count is obtained by visual inspection. However in order to discriminate partial occurrences the centre of the fibre is taken as a point occurrence. Alternatively a method can be adopted which entails counting all entries into the fibre area and discounting all exits.

If the expected count is simply the total number of occurrences in the whole unit divided by the number of segments (n) then the chi-squared parameter will be given by:

$$XCHI = \sum_{i=1}^n \frac{(\text{observed} - \text{expected})^2}{\text{expected}} \quad (\text{E2.1.2})$$

If the value of XCHI is zero then there is perfect ordering or truly random pattern. Clustering will give a greater value of XCHI.

2.1.3 Contiguity index

The contiguity index is a measure of the extent of clustering insofar as the number of changes of fibre along a line transect will be directly related to the patterning of the mixture. If the first half of the transect is all glass fibres and the second half is all carbon fibres there will only be one change of fibre type. Thus if 100 fibres were considered the ratio of the number of changes of interface to the number of interfaces would be 1/99 (there will be one fibre more than there are gaps between them). However, if the fibres are arranged in a strictly alternating pattern the ratio would be 99/99. Thus if x is the number of fibres

on the line transect and y is the number of interfibre spaces bounded by two different fibres then the contiguity index z can be defined as:

$$z = y/(x - 1) \quad (\text{E2.1.3})$$

In a monofibre composite z will be zero.

In a core-shell composite z will be very small.

In a pure randomly mixed composite z will be unity.

2.2.1 Mechanical Properties: introduction

In a single fibre composite the modulus of the composite, E_c , can be calculated from the volume fraction of each component, v_x , and the modulus of that component, E_x . If the subscripts f and m indicate fibre and matrix respectively, then the initial composite modulus will be given by equation (1):

$$E_c = v_f E_f + v_m E_m = v_f E_f + (1 - v_f) E_m \quad (\text{E2.2.1})$$

because the sum of the volume fractions must be unity, as in equation (2):

$$v_f + v_m = 1 \quad (\text{E2.2.2})$$

In a two-fibre composite, commonly known as a hybrid composite, the equations (1) and (2) can be expanded:

$$E_c = v_a E_a + v_b E_b + v_m E_m = v_a E_a + v_b E_b + (1 - v_a - v_b) E_m \quad (\text{E2.2.3})$$

$$v_a + v_b + v_m = 1 \quad (\text{E2.2.4})$$

where a and b indicate each of the fibre species. In practice, the contribution of the matrix to the overall stiffness of the composite is negligible, and is normally ignored:

$$E_c = v_a E_a + v_b E_b \quad (\text{E2.2.5})$$

An alternative method of calculating the initial modulus is to consider the hybrid as an equivalent material fabricated from two composites. If the ratio of the volume fraction of one composite component, V_x , to the total volume of composite is denoted by R_x , then:

$$E_A = v_a E_a + v_m E_m; E_B = v_b E_b + v_m E_m \quad (\text{E2.2.6}; \text{E2.2.7})$$

$$R_A = V_A / (V_A + V_B); R_B = V_B / (V_A + V_B) \quad (\text{E2.2.8}; \text{E2.2.9})$$

$$E_{c_i} = R_A E_A + R_B E_B; R_A + R_B = 1 \quad (\text{E2.2.10}; \text{E2.2.11})$$

$$E_{c_i} = v_a E_a + v_b E_b + v_m E_m \quad (\text{E2.2.12})$$

If both the fibres have brittle properties, then the modulus of the composite after failure of all the low elongation component (A) will be given by:

$$E_{c_{ii}} = R_B E_B = v_b E_b + v_m E_m \quad (\text{E2.2.13})$$

The above equations assume that the matrix remains intact until failure of the composite, and that the fibre failure strain distributions do not overlap. The failed fibres are now assumed to be either completely debonded, or broken into sections which are shorter than the "critical length", so that they now make significant contribution to the modulus. However the presence of the fractured ends of these fibres is also assumed to cause no stress concentration on the adjacent high elongation fibres (species B). Equation (12) is now generally accepted as the "rule of mixtures" for the initial elastic modulus of a hybrid composite.

2.2.2 Constant strain (=201)

In addition to the above equations, Hayashi (=62) derived expressions for the tensile strength of a brittle two-fibre elastic composite. Until the failure of the low elongation component, the tensile stress and the strength of the hybrid at this failure, will be given by:

$$\sigma_i = E_i \epsilon \quad \sigma'_i = E_i \epsilon'_a \quad (\text{E2.2.14})$$

where ϵ'_a is the failure strain of the low elongation fibres.

At the failure of the low elongation component there will be a discontinuity or a gradual change in the slope the stress-strain curve, and until the final failure the stress and strength will be given by:

$$\sigma_{ii} = E_{ii} \epsilon \quad \sigma'_{ii} = E_{ii} \epsilon'_b \quad (\text{E2.2.15})$$

where ϵ'_b is the failure strain of the high elongation fibre. This assumes that all the fibres of a single type fail at a definite strain, and then no longer contribute to the load carrying capability of the composite. The work of fracture (i.e. the total elastic strain energy) up to complete separation will be given by:

$$U = \frac{1}{2} E_A R_A \epsilon'^2_a + \frac{1}{2} E_B R_B \epsilon'^2_b \quad (\text{E2.2.16})$$

In the case where the high elongation component contributes to the load carrying capability of the hybrid throughout the range of compositions the equations (17) and (18) will apply. The strength of the hybrid will be given by the equation which predicts the greatest strength:

$$\sigma' = (R_L E_L + R_H E_H) \epsilon'_L \quad (\text{E2.2.17})$$

$$\sigma' = R_H E_H \epsilon'_H \quad (\text{E2.2.18})$$

The minimum strength of the hybrid will occur at a specific volume fraction which can be derived by equating the two strength equations such that:

$$(R_L E_L + R_H E_H) \epsilon'_L = R_H E_H \epsilon'_H \quad (\text{E2.2.19})$$

which can be rearranged, with $R_H = 1 - R_L$, to give:

$$\frac{1 - R_L}{R_L} = \frac{E_L \epsilon'_L}{E_H (\epsilon'_H - \epsilon'_L)} \quad (\text{E2.2.20})$$

and hence:

$$\frac{1}{R_H} = 1 + \frac{E_H}{E_L} \left[\frac{\epsilon'_H}{\epsilon'_L} - 1 \right] \quad (\text{E2.2.21})$$

which allows the determination of the point T in figure 3.

In this analysis there will be a critical volume content of the high strain fibres (low modulus fibres) above which the fracture mode changes from being dominated by the low elongation fibre, to domination by these high elongation fibres. An identical expression for this critical ratio, expressed in terms of the failure of stress of the fibres, has been derived by both Gunyaev (=64) and Chamis (=66, 67):

$$V_{\text{CRIT}} = \left[1 + \frac{\sigma'_H}{\sigma'_L} - \frac{E_H}{E_L} \right]^{-1} \quad (\text{E2.2.22})$$

The failure strength of this minimum strength hybrid associated with the critical content is given by:

$$\sigma'_{\min} = (1 - V_{\text{CRIT}}) E_L \epsilon'_L \quad (\text{E2.2.23})$$

A characteristic inflection will occur in the stress-strain curve corresponding to the limiting elongation of the low strain fibres.

2.2.3 Rule-of-mixtures

In order to estimate the tensile strength of two-fibre hybrids it is tempting to use the rule of mixtures for hybrid strength:

$$\sigma' = R_L \sigma'_L + R_H \sigma'_H \quad (\text{E2.2.24})$$

However, if the individual components are linear elastic materials until failure, such that $\sigma_s = E_s \epsilon'_s$, then equation (24) can be rearranged to give:

$$\sigma' = R_L E_L \epsilon'_L + R_H E_H \epsilon'_H \quad (\text{E2.2.25})$$

which requires that the individual components of any hybrid composite will fail simultaneously, but at different strains. This is obviously not a very satisfactory representation of the truth.

2.2.4 Rule-of-mixtures for failure strain

In the theoretical model which follows the basic assumptions are that the failure strain of the hybrid composite will follow the rule of mixtures:

$$\epsilon' = V_L \epsilon'_L + V_H \epsilon'_H \quad (E2.2.26)$$

and that the first failure of the fibres will occur at random throughout the complete volume of the composite.

In a hybrid composite in which the brittle low elongation fibres are isolated from one another because of the intimacy with which the two fibre species are interspersed, it is possible that the catastrophic crack propagation which would occur in the brittle mono-fibre composite can be suppressed by the presence of the tough fibres. In an optimised mixture this could allow individual brittle fibres to fail at their own weakest points because they would only rarely be subjected to the dynamic stress concentration due to fracture of an adjacent brittle fibre. The strain energy released would therefore be absorbed by the tough fibres, to result in a small local overstraining of the composite. Provided that the failed brittle fibres are uniformly distributed throughout the composite, and that the frequency of fracture within any single fibre is such that the unbroken lengths are greater than the critical length, it is probable that these brittle fibres will continue to carry load and hence contribute to the hybrid modulus and strength.

Parratt (=202) has reported that 25% HMS carbon – 75% R-glass composites show yielding behaviour as the carbon fibres break up. Although fracture starts very consistently at a strain characteristic of the bundle strength of HMS carbon fibres, these fractured fibres continue to carry load and are broken down to a measured length of 0.8 mm, requiring that three or four fractures must occur in each fibre to accommodate the "final composite breaking strain of 1.9%".

Manders (=79) has reported failure strain enhancement of up to 35% in high tensile strength carbon fibres when incorporated into a hybrid composite with glass fibres, and enhancements of up to 46% in high modulus carbon fibre-glass fibre hybrids.

Based on the expectation that the failure strain of hybrid composites will follow the rule-of-mixtures for fibres with similar elongations to failure, it is proposed to derive a new expression for the upper bound of hybrid strength. The increase in strength due to the enhancement of failure in the low elongation fibre, $\sigma \uparrow$, will thus be given by the expression:

$$\sigma \uparrow = V_L E_L (1 - V_L)(\epsilon'_H - \epsilon'_L) \quad (E2.2.27)$$

and similarly the degradation of strength required in order that the composite fails at a constant strain, $\sigma \downarrow$, will be given by:

$$\sigma \downarrow = V_H E_H (1 - V_H)(\epsilon'_L - \epsilon'_H) \quad (E2.2.28)$$

The factor for strength degradation is of course negative because by definition $\epsilon'_H > \epsilon'_L$, and equation (28) can thus be rewritten:

$$\sigma_f = -V_H E_H (1 - V_H)(\epsilon'_H - \epsilon'_L) \quad (\text{E2.2.29})$$

The total strength of the hybrid composite will therefore be given by the rule-of-mixtures strength expression (equation 24) together with the two expressions for a change to a rule-of-mixtures failure strain (equations 27 and 29):

$$\sigma' = V_L E_L \epsilon'_L + V_H E_H \epsilon'_H + V_L E_L (1 - V_L)(\epsilon'_H - \epsilon'_L) - V_H E_H (1 - V_H)(\epsilon'_H - \epsilon'_L) \quad (\text{E2.2.30})$$

which can be simplified by rearranging and taking $(1 - V_L) = V_H$ to give:

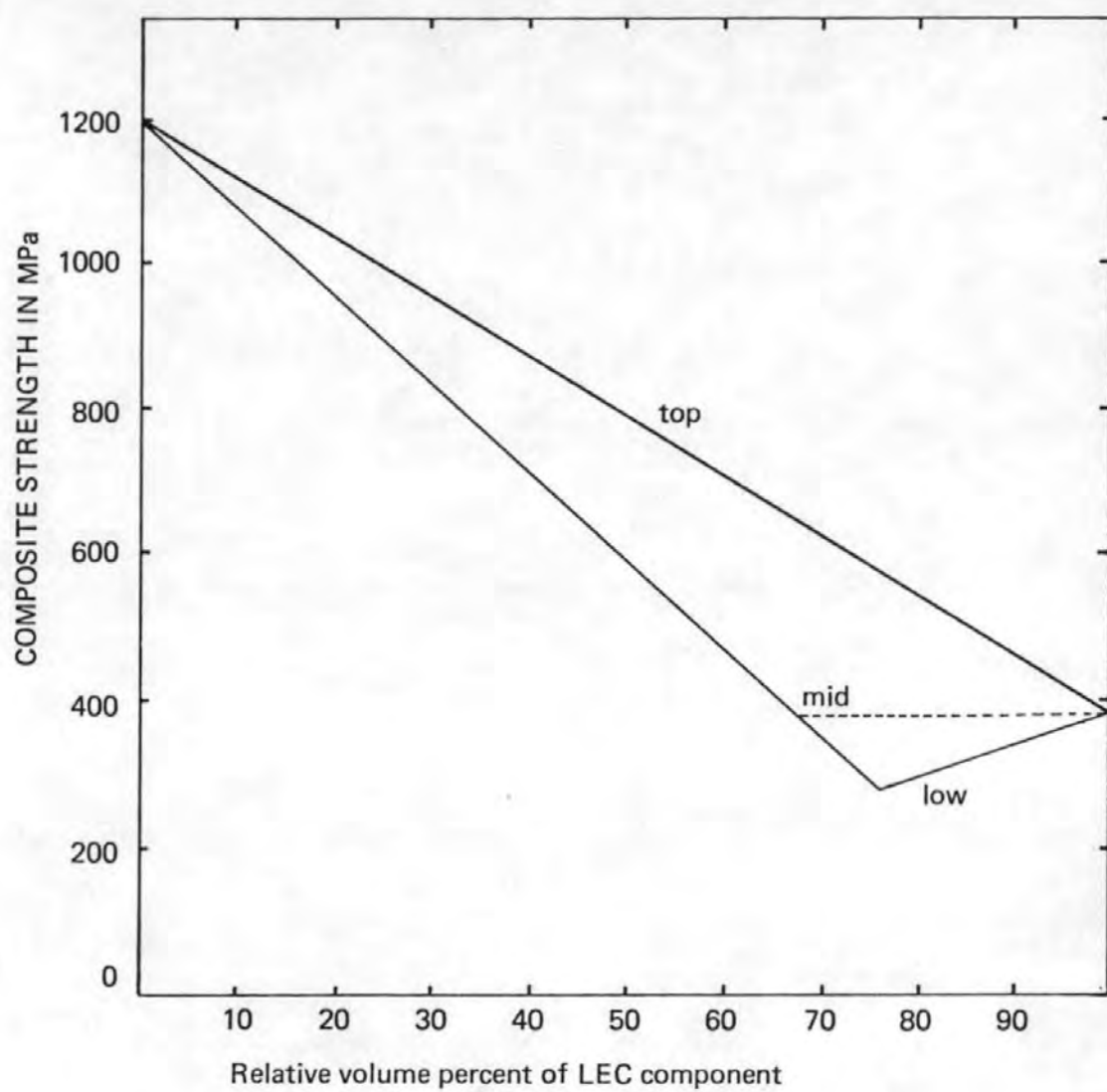
$$\sigma' = V_L E_L \epsilon'_L + V_H E_H \epsilon'_H + V_L V_H (E_L - E_H)(\epsilon'_H - \epsilon'_L). \quad (\text{E2.2.31})$$

The third term of this expression will therefore predict the magnitude of any benefit to be expected in the composite strength through the judicious combination of different fibres. Obviously, when the moduli of the two component composites are equal (figure 8), or when the failure strains of the component composites are equal (figure 9), there will be no benefit to the hybrid strength. Maximum benefit is therefore to be expected by maximising the difference in either (or both) the failure strains or (and) the elastic moduli of the components (figure 10). However, if the difference in failure strains is too great then the assumptions of the model will be broken (figure 11), as the low strain fibres will be multi-fractured, and the interaction of these defects will affect the strength because of the increased stress concentrations on the unfractured fibres.

This theory takes no account of the benefits which may arise because of the thermal residual strains which arise from the differences in the coefficients of thermal expansion between the two fibres. These may be evenly spread throughout the intimate composite rather than concentrated at the laminate interfaces. As an example of the beneficial effect this can lead to, consider a carbon fibre and glass fibre hybrid reinforced plastic. Carbon fibres are unusual in that they undergo a slight longitudinal expansion upon cooling. When constrained by a contracting gfrp matrix during cure and cooling, a net compressive strain in the carbon fibre at no net elongation of the composite could result, with consequent benefits in tensile loading.

2.2.5 Summary

A new equation for the prediction of the strength of hybrid composites is presented, which can be used to indicate the extent of any "hybrid effect". It is assumed that the failure strain of the low elongation component can be linearly increased to the failure strain of the high elongation composite, in line with the strain predicted by the rule-of-mixtures, provided that the difference in these two strains is not extreme. The two species



Steel
40 vol. % fibre

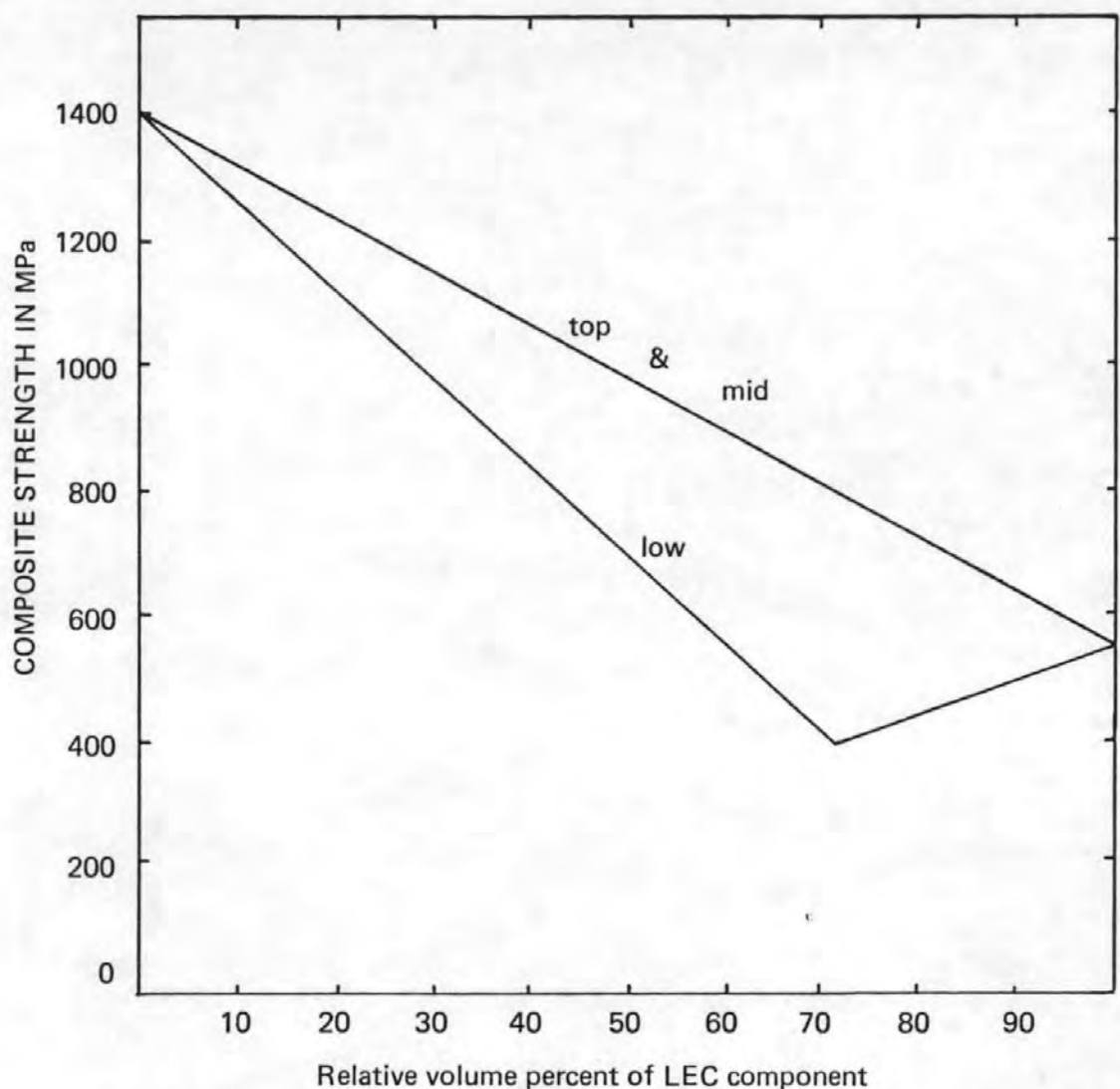
Carbon I (HM)
20 vol. % fibre

TOP LINE: Fibres both fail at r-o-m strain
MID LINE: HEC fail at strain of majority fibres
LOW LINE: Component only effective on one side

The two monofibre composites are:

	Steel 40 Vol. % Fibre	Carbon I (HM) 20 Vol. % Fibre
Strength (GPa)	1.200	0.380
Modulus (GPa)	80.000	80.000
Elongation	0.015	0.005

Figure 8: Hybrid of two composites with equal magnitude moduli exhibit rule-of-mixtures strength for the hybrid effect curve.



Carbon II (HT)
50 vol. % fibre

Carbon II (HT)
20 vol. % fibre

TOP LINE: Fibres both fail at r-o-m strain
MID LINE: HEC fail at strain of majority fibres
LOW LINE: Component only effective on one side

The two monofibre composites are:

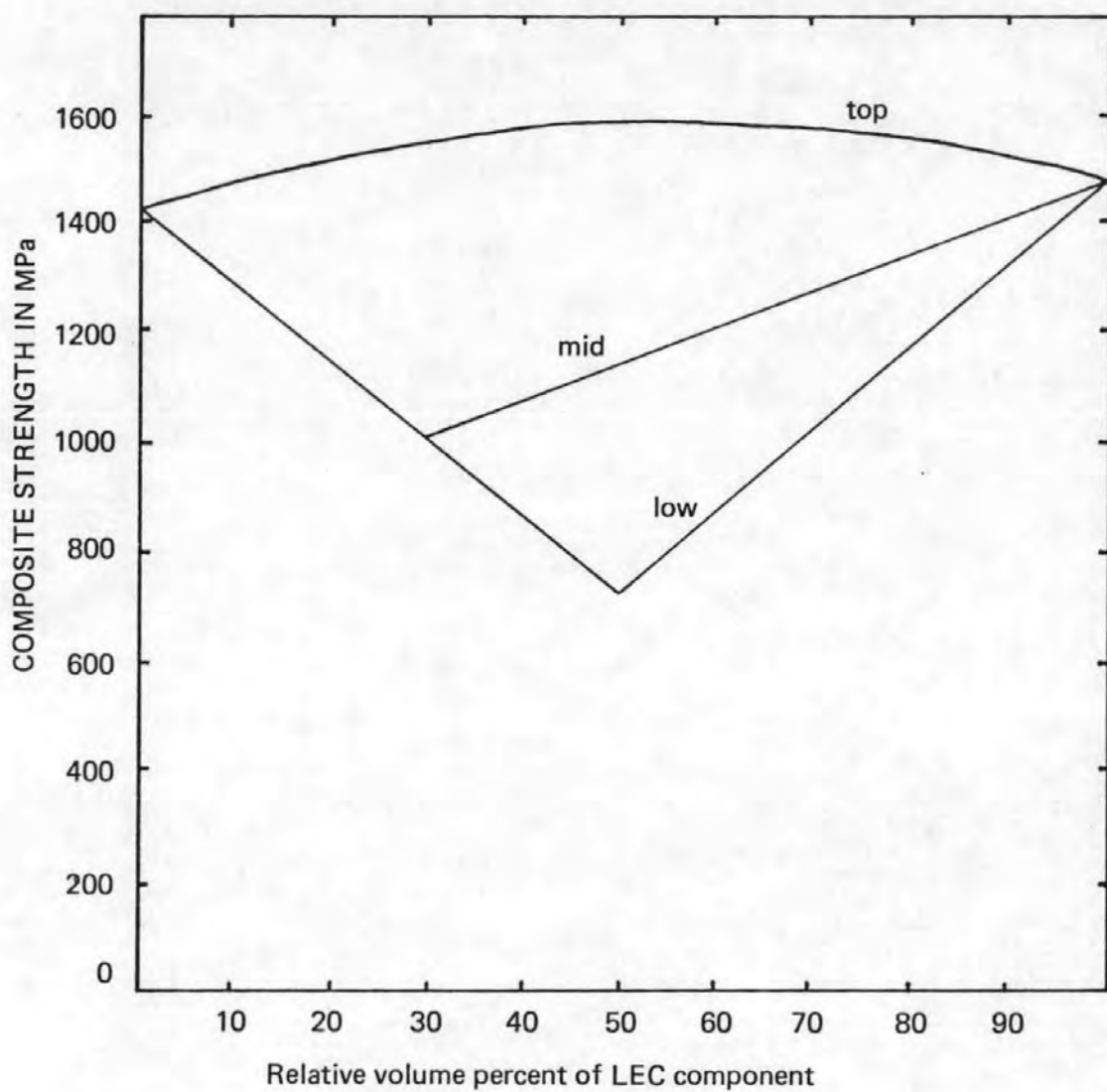
Carbon II (HT)
50 Vol. % Fibre

Carbon II (HT)
20 Vol. % Fibre

Strength (GPa)	1.300
Modulus (GPa)	103.500
Elongation	0.013

0.520
41.400
0.013

Figure 9: Hybrid of two composites with equal magnitude failure strains exhibit rule-of-mixture strength for the hybrid effect curve.



E-Glass
50 vol. % fibre

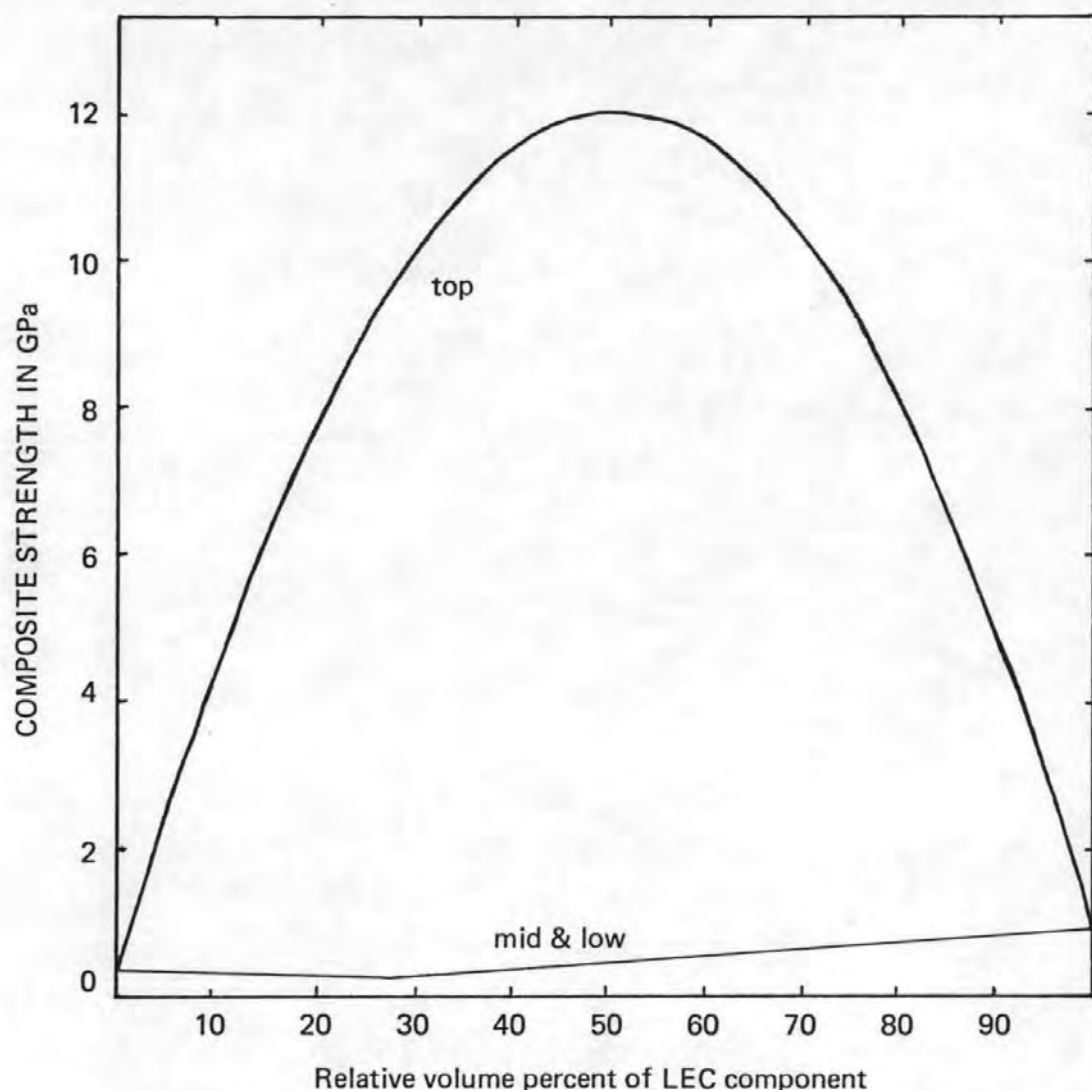
Kevlar 49
50 vol. % fibre

TOP LINE: Fibres both fail at r-o-m strain
MID LINE: HEC fail at strain of majority fibres
LOW LINE: Component only effective on one side

The two monofibre composites are:

	E-Glass 50 Vol. % Fibre	Kevlar-49 50 Vol. % Fibre
Strength (GPa)	1.325	1.380
Modulus (GPa)	36.000	65.500
Elongation	0.037	0.021

Figure 10: Similar moduli and failure strains lead to a small hybrid effect.



Nylon

50 vol. % fibre

Carbon I (HM)

50 vol. % fibre

TOP LINE: Fibres both fail at r-o-m strain

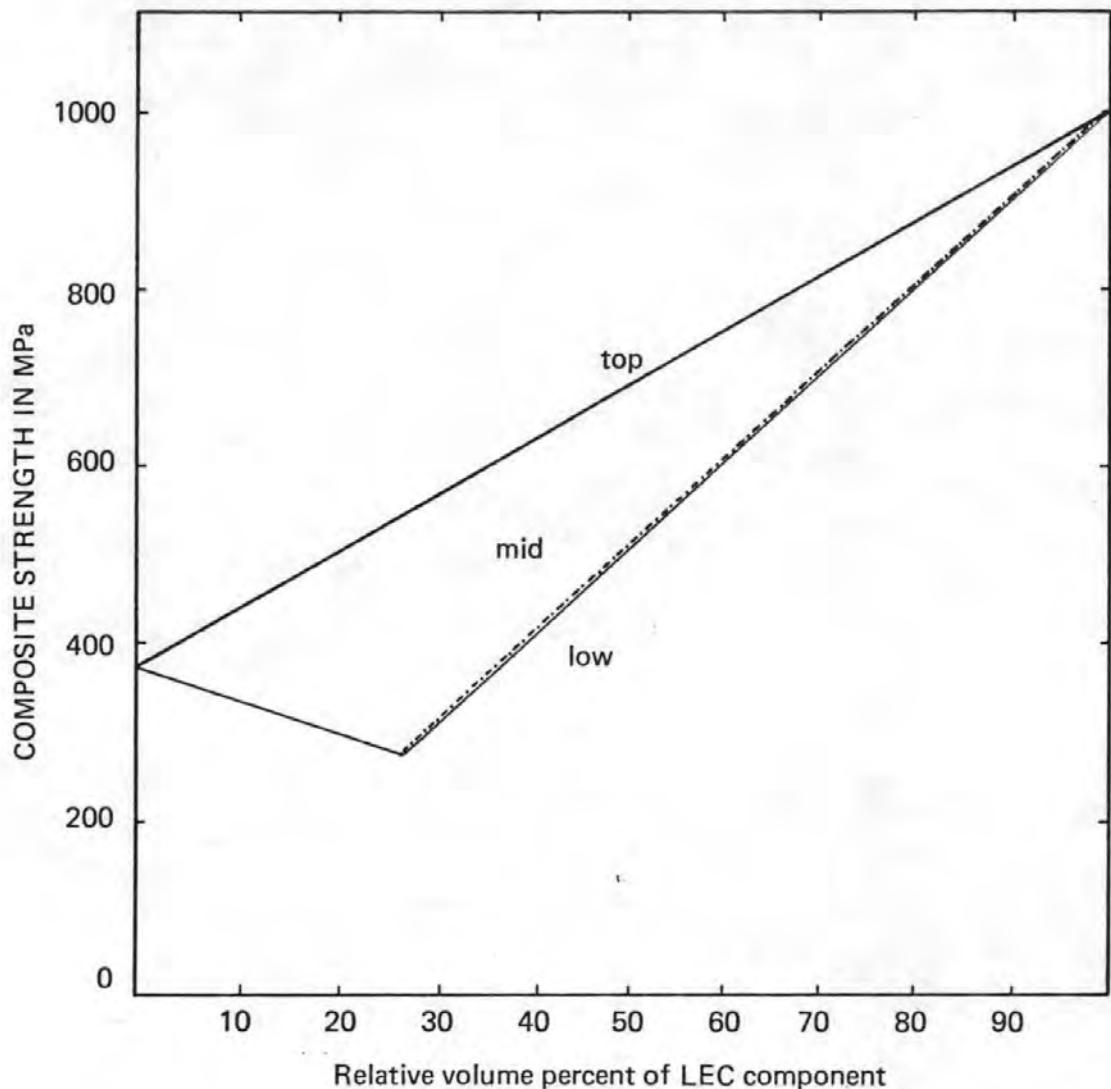
MID LINE: HEC fail at strain of majority fibres

LOW LINE: Component only effective on one side

The two monofibre composites are:

	Nylon 50 Vol. % Fibre	Carbon I (HM) 50 Vol. % Fibre
Strength (GPa)	0.350	0.950
Modulus (GPa)	1.500	200.000
Elongation	0.233	0.005

Figure 11: Extreme case where carbon I ($\epsilon' = 0.48\%$) is expected to carry load at the failure strain of nylon ($\epsilon' = 23.3\%$). In consequence the predicted hybrid effect is very unlikely to be realised in practice.



Nylon
50 vol. % fibre

Carbon I (HM)
50 vol. % fibre

TOP LINE: Traditional rule of mixtures for strength
MID LINE: HEC fail at strain of majority fibres
LOW LINE: Component only effective on one side

The two monofibre composites are:

	<i>Nylon</i> 50 Vol. % Fibre	<i>Carbon I (HM)</i> 50 Vol. % Fibre
Strength (GPa)	0.350	0.950
Modulus (GPa)	1.500	200.000
Elongation	0.233	0.005

Figure 12: Traditional predictions of hybrid strength for a composite with fibres having diverse failure strains. Detail of the lower lines in figure 11.

of fibre should be so intimately mixed that any stress concentration from a broken fibre is sufficiently isolated by the surrounding high elongation fibres. The stress released from the broken fibres is transferred to the matrix and to the high elongation fibres without fracture, to prevent consecutive failure of adjacent low strain fibres. The catastrophic failure which is associated with monolithic brittle fibre composites is thus avoided.

2.3 Acoustic emission

Nomenclature:

- a : measured amplitude level
- a_0 : reference amplitude level
- b : a constant for a specified value of an external variable
- β : no. of events
- β_d : number of detected events
- β_t : total number of events
- $f(V)$: cumulative probability density function
- $F(V)$: cumulative probability function
- $n(a)$: number of emissions
- V_t : time-dependent voltage
- V' : detected voltage (amplitude)
- V : reference voltage (amplitude)
- $V^* \equiv (V'/\beta_t)^{1/b}$

2.3.1 Amplitude distribution analysis (=145)

The amplitude of an event is a variable quantity in most processes. Simple measures of the amplitude of an acoustic emission burst include its peak value or the integral value parameters (such as the energy or the number of crossings of preset threshold). In practice the amplitude parameter selected is usually the peak voltage of an acoustic emission burst (the first "count" of an AE event normally). These studies have shown that the number of detected events, β_d , with peak amplitudes larger than V is given by the equation:

$$\beta_d = (V'/V)^b \quad (\text{E2.3.1})$$

where b and V' are constant, subject to external variables.

If β_t is the total number of events with peak amplitudes in the range $0 < V < \infty$, then the probability that the event amplitude will be larger than V is given by the cumulative probability function, $F(V)$, and is dependent on β_d according to:

$$F(V) = \beta_d / (\beta_t + 1) \quad (\text{E2.3.2})$$

Therefore, when $\beta_t \gg 1$ a substitution for β_d from equation E2.3.1 gives:

$$F(V) = (V^*/V)^b \quad (\text{E2.3.3})$$

where $V^* \equiv (V'/\beta_t^{1/b})$ and should be a constant if external variables are unchanged. The corresponding density function $f(V)$ which describes the probability of an event with a peak amplitude between V and $V + dV$, is given by:

$$f(V) \equiv |dF(V)/dV| \quad (\text{E2.3.4})$$

$$= \frac{b}{V} \left[\frac{V^*}{V} \right]^b \quad (\text{E2.3.5})$$

It is common practice ($=91, =160$) to derive the parameter "b" from the amplitude sorted AE signal. The value of b has a unique value as long as a single type of emission source predominates. If the energies of the events are randomly distributed then statistical analysis yields an equation similar to E2.3.1, but commonly expressed in a different nomenclature:

$$n(a) = \left[\frac{a}{a_0} \right]^{-b} \quad (\text{E2.3.6})$$

A plot of the number of emissions, $n(a)$, exceeding a given amplitude level, a_0 , is generally a smooth curve. A logarithmic plot of the cumulative distribution would therefore be a straight line of negative slope equal to b. A large value of b indicates a predominance of low amplitude events and conversely a small value of b indicates a dominance of energetic events. If the condition that all sound-amplitudes are equally attenuated holds then size effects are eliminated because b will be unaffected by the attenuation.

In reinforced plastics several types of failure can occur simultaneously and a single unique value of b is not obtained. However, critical points of the amplitude spectrum may be identified by discontinuities in the slope of the b-plot.

2.4 Finite Element Analysis ($=181$)

In the numerical analysis used in this project three finite element schemes were used:

- a) Hewson-Lee modification of the Cheung and King triangular element
- b) PAFEC 70+ experimental scheme isoparametric membrane element
- c) PAFEC 75 commercial scheme isoparametric hybrid membrane/bending element.

In this introduction to the theory of the method the following sequence will be followed:

- | | |
|--|-----------------|
| a) triangular three-noded element | (Section 2.4.1) |
| b) two dimensional isoparametric element | (Section 2.4.2) |
| c) anisotropic elasticity theory | (Section 2.4.3) |
| d) crack tip singularity | (Section 2.4.4) |

2.4.1 Triangular element

This element will be an isotropic three-noded plane stress or plane strain triangular

element of constant thickness h , and with straight sides. As the element is to be used for membrane problems, there will be two independent displacements, u_x and u_y , in the plane of the element. They may be written as:

$$u_x = \alpha_1 + \alpha_2 x + \alpha_3 y \quad \text{and} \quad u_y = \alpha_4 + \alpha_5 x + \alpha_6 y \quad (\text{E2.4.1})$$

or in matrix form:

$$\begin{Bmatrix} u_x \\ u_y \end{Bmatrix} = \begin{bmatrix} [1xy] & 0 \\ 0 & [1xy] \end{bmatrix} \{ \alpha \} \quad (\text{E2.4.2})$$

where α contains the constants α_1 through to α_6 .

The (x,y) coordinates of each node in the element are known and hence:

$$\begin{Bmatrix} u_{x1} \\ u_{x2} \\ u_{x3} \end{Bmatrix} = \begin{bmatrix} 1 & x_1 & y_1 \\ 1 & x_2 & y_2 \\ 1 & x_3 & y_3 \end{bmatrix} \begin{Bmatrix} \alpha_1 \\ \alpha_2 \\ \alpha_3 \end{Bmatrix} \quad (\text{E2.4.3})$$

or:

$$\{ \alpha_{xe} \} = [A] \{ \alpha_{1-3} \}$$

and hence, if $[P] = [1xy]$:

$$u_x = [P] [A^{-1}] \{ u_{xe} \} \quad (\text{E2.4.4})$$

On consideration of the u_y displacements at the element nodes we find that the same $[A]^{-1}$ matrix is again required:

$$\begin{Bmatrix} u_x \\ u_y \end{Bmatrix} = \begin{bmatrix} [P] & 0 \\ 0 & [P] \end{bmatrix} \begin{bmatrix} [A]^{-1} & 0 \\ 0 & [A]^{-1} \end{bmatrix} \begin{Bmatrix} \{ u_{xe} \} \\ \{ u_{ye} \} \end{Bmatrix} \quad (\text{E2.4.5})$$

In equation (5) the column $\{ u_{xe} \}, \{ u_{ye} \}$ will be renamed $\{ u_e \}$ which is a complete listing of the element nodal displacements. In subjecting a two dimensional element to membrane loads and hence displacements, the strain energy will be stored in x -, in y - and in shear- extensions. It is convenient to define vectors for both the strains and the corresponding stresses:

$$\{ \epsilon \} = \begin{Bmatrix} \epsilon_{xx} \\ \epsilon_{yy} \\ \epsilon_{xy} \end{Bmatrix}; \quad \{ \sigma \} = \begin{Bmatrix} \sigma_{xx} \\ \sigma_{yy} \\ \sigma_{xy} \end{Bmatrix} \quad (\text{E2.4.6}; \text{E2.4.7})$$

The strain energy of an element is now:

$$SE = \frac{1}{2} \int_{\text{area}} (\epsilon_{xx} \sigma_{xx} + \epsilon_{yy} \sigma_{yy} + \epsilon_{xy} \sigma_{xy}) . h . dA \quad (\text{E2.4.8})$$

or in matrix terms:

$$SE = \frac{1}{2} \int_{\text{area}} \{ \epsilon \}^T \cdot \{ \sigma \} . h . dA \quad (\text{E2.4.9})$$

In two-dimensional analysis an elasticity matrix [D] can be defined although there are important distinctions in different situations:

a) *Plane stress* cases in which the stress in the third direction, corresponding to the thickness of membranes, is zero. There is also no constraint on the through thickness strain derived from the Poisson contraction. These situations are common in practice, and:

$$[D] = \frac{E}{1-\nu^2} \begin{bmatrix} 1 & \nu & 0 \\ \nu & 1 & 0 \\ 0 & 0 & \frac{1}{2}(1-\nu) \end{bmatrix} \quad (\text{E2.4.10})$$

b) *Plane strain* cases in which the strain in the transverse direction is negligible, but the stress perpendicular to the plane of interest is not zero. In practical engineering problems plane strain situations are rare, and:

$$[D] = \frac{E(1-\nu)}{(1+\nu)(1-2\nu)} \begin{bmatrix} 1 & \nu/(1-\nu) & 0 \\ \nu/(1-\nu) & 1 & 0 \\ 0 & 0 & (1-2\nu)(2-2\nu) \end{bmatrix} \quad (\text{E2.4.11})$$

The strains and stresses of equations (6) and (7) can now be connected using the elasticity matrix [D]:

$$\{\sigma\} = [D]\{\epsilon\} \quad (\text{E2.4.12})$$

The strains can be written in terms of derivatives of displacements as:

$$\begin{bmatrix} \epsilon_{xx} \\ \epsilon_{yy} \\ \epsilon_{xy} \end{bmatrix} = \begin{bmatrix} P_x & 0 \\ 0 & P_y \\ P_y & P_x \end{bmatrix} \begin{bmatrix} [A]^{-1} & 0 \\ 0 & [A]^{-1} \end{bmatrix} \{u_e\} \quad (\text{E2.4.13})$$

and by defining new matrices [B] and $[A_1]$:

$$\{\epsilon\} = [B][A_1]^{-1}\{u_e\} \quad (\text{E2.4.14})$$

Using equations (12) and (14) in (9), the element strain energy can be derived in terms of the nodal displacements. By taking the constants outside the integral:

$$SE = \frac{1}{2} \{u_e\}^T [A_1]^{-T} \int_{\text{area}} [B]^T [D] [B] . dA . h . [A_1]^{-1} \{u_e\} \quad (\text{E2.4.15})$$

Because the matrix [B] and its transpose $[B]^T$ are composed of polynomial terms which vary over the area of the element, they have remained within the integral sign. Closer examination of [B] shows that the differentiation in equation (15) leads to a constant [B]:

$$[B] = \begin{bmatrix} 0 & 1 & 0 & 0 & 0 & 0 \\ 0 & 0 & 0 & 0 & 0 & 1 \\ 0 & 0 & 1 & 0 & 1 & 0 \end{bmatrix} \quad (\text{E2.4.16})$$

Normally the stress-strain matrix [D] is constant over the element and the product $[B]^T [D] [B]$ may be written outside the integral to leave only the area of the element, A,

thus:

$$SE = \frac{1}{2} \{u_e\}^T [A_e]^{-T} [B]^T [D] [B] \cdot h \cdot A_e [A_e]^{-1} \{u_e\} \quad (E2.4.17)$$

or:

$$SE = \frac{1}{2} \{u_e\}^T [S_e] \{u_e\} \quad (E2.4.18)$$

The strain energy is differentiated with respect to the $\{u_e\}$ as $[S_e] \{u_e\}$. This concept of nodal forces is fictitious, but this is a convenient way of discretising the force. However internodal forces may only be transferred by the element of which they are part, and the displacement assumption may therefore be said to constrain the element side to remain straight. $[S_e]$ is known as the element stiffness matrix.

2.4.2 Two-dimensional isoparametric element

The isoparametric element family is more powerful than the triangular element and, in general, has curved sides. The stiffness and other element matrices are derived by transforming the element into a very simple shape in the (ξ, η) domain. The eight-noded quadrilateral has a node at each corner and a node positioned part way along each edge. The four vertices can lie anywhere in a plane and the "midside" nodes can also be arbitrarily placed. To give a square of side 2-units in the (ξ, η) plane the following transformation is used:

$$x = \alpha_1 + \alpha_2 \xi + \alpha_3 \eta + \alpha_4 \xi \eta + \alpha_5 \xi^2 + \alpha_6 \eta^2 + \alpha_7 \xi^2 + \alpha_8 \xi \eta^2 \quad (E2.4.19)$$

and similarly y is derived using the arbitrary constants α_9 through to α_{16} .

The transformation can be written in matrix form as:

$$[x, y] = [P] [\{\alpha_1 \text{ to } \alpha_8\}, \{\alpha_9 \text{ to } \alpha_{16}\}] \quad (E2.4.20)$$

where the row matrix $[P]$ contains the polynomial terms in (ξ, η) and the vectors $\{\alpha\}$ contain arbitrary constants. The number of terms in the polynomial $[P]$ is always the same as the number of nodes in the element. In the case of an eight-noded quadrilateral the transformation is to a square $(\pm 1, \pm 1)$ in the (ξ, η) domain.

The x -coordinates $\{x_e\}$ of all the nodes and their corresponding (ξ, η) values are inserted into the equation:

$$\{x_e\} = [A] \{\alpha_1 \text{ to } \alpha_8\} \quad (E2.4.21)$$

where each row of $[A]$ corresponds to the insertion of particular nodal values of (ξ, η) into the row matrix $[P]$. By inverting $[A]$ we find:

$$\begin{aligned} \{\alpha_1 \text{ to } \alpha_8\} &= [A^{-1}] \{x_e\} \\ \{\alpha_9 \text{ to } \alpha_{16}\} &= [A^{-1}] \{y_e\} \end{aligned} \quad (E2.4.22)$$

As displacements are being confined to simple in-plane motion the displacements may be defined u_x and u_y . The displacements are assumed to be variable over the element in a manner corresponding exactly with the transform assumption, where $[P]$ is the usual poly-

nomial row matrix in (ξ, η) :

$$\begin{aligned} u_x &= [P] \{\alpha_{17} \text{ to } \alpha_{24}\} \\ u_y &= [P] \{\alpha_{25} \text{ to } \alpha_{32}\} \end{aligned} \quad (\text{E2.4.23})$$

If the nodal values of u_x and u_y are $\{u_{xe}\}, \{u_{ye}\}$, then:

$$[\{u_{xe}\}, \{u_{ye}\}] = [A] [\{\alpha_{17} \text{ to } \alpha_{24}\}, \{\alpha_{25} \text{ to } \alpha_{32}\}] \quad (\text{E2.4.24})$$

and hence:

$$[u_x, u_y] = [P] [A^{-1}] [\{u_{xe}\}, \{u_{ye}\}] \quad (\text{E2.4.25})$$

and thus an expression exists for the displacements (u_x, u_y) at any point in the element in terms of (ξ, η) and the nodal values of displacement $\{u_{xe}\}$ and $\{u_{ye}\}$. To find the stiffness matrix it is necessary to know the strain energy and the strains. As u_x and u_y are functions of the curvilinear axes (ξ, η) the strains are not immediately available from du_x/dx etc. By differentiating $[P]$ term by term to find $[\delta P/\delta \xi]$, the equation for $\delta x/\delta \xi$ (etc.) can be derived:

$$\frac{\delta x}{\delta \xi} = \left[\frac{\delta P}{\delta \xi} \right] [A^{-1}] \{x_e\} \quad (\text{E2.4.26})$$

A 2×2 matrix $[J]$ and the inverse $[J^{-1}]$ may now be formed:

$$[J] = \begin{bmatrix} \delta x / \delta \xi & \delta y / \delta \xi \\ \delta x / \delta \eta & \delta y / \delta \eta \end{bmatrix} \text{ and } [J^{-1}] = \begin{bmatrix} \delta \xi / \delta x & \delta \eta / \delta x \\ \delta \xi / \delta y & \delta \eta / \delta y \end{bmatrix} \quad (\text{E2.4.27})$$

A polynomial derivative with respect to x and y hence becomes:

$$\begin{Bmatrix} \delta P / \delta x \\ \delta P / \delta y \end{Bmatrix} = [J^{-1}] \begin{Bmatrix} \delta P / \delta \xi \\ \delta P / \delta \eta \end{Bmatrix} \quad (\text{E2.4.28})$$

A strain vector for two-dimensional analysis may be defined:

$$\{\epsilon\} = \{\epsilon_{xx}, \epsilon_{yy}, \epsilon_{xy}\} \quad (\text{E2.4.29})$$

with: $\epsilon_{xx} = \delta u_x / \delta x$ and $\epsilon_{yy} = \delta u_y / \delta y$.

The strains are set up using the polynomial and its derivatives with respect to x and y :

$$\{\epsilon\} = \begin{Bmatrix} \epsilon_{xx} \\ \epsilon_{yy} \\ \epsilon_{xy} \end{Bmatrix} = \begin{bmatrix} \delta P / \delta x & 0 \\ 0 & \delta P / \delta y \\ \delta P / \delta y & \delta P / \delta x \end{bmatrix} \begin{bmatrix} [A^{-1}] & 0 \\ 0 & [A^{-1}] \end{bmatrix} \begin{Bmatrix} \{u_{xe}\} \\ \{u_{ye}\} \end{Bmatrix}$$

or:

$$\{\epsilon\} = [B] [A^*] \{u_e\} \quad (\text{E2.4.30})$$

The element strain energy may now be written as the following integral over the element area multiplied by the thickness, h :

$$SE = \frac{1}{2} \int \{\epsilon\}^T \{\sigma\} dA.h \quad (E2.4.31)$$

substitution for $\{\epsilon\}$ and $\{\sigma\}$ yields:

$$SE = \frac{1}{2} \iint \{u_e\}^T [A^*]^T [B^T] [D] [B] [A^*] \{u_e\} h dx dy \quad (E2.4.32)$$

since $\{u_e\}$ and $[A^*]$ are independent of x and y they may appear outside the integration:

$$SE = \frac{1}{2} \{u_e\}^T [A^*]^T \iint h [B^T] [D] [B] dx dy [A^*] \cdot \{u_e\} \quad (E2.4.33)$$

The kernel $[B^T] [D] [B]$ is a function of ξ, η and is a square symmetric matrix with an integral which could be devised by integrating each term separately to give a similar matrix. It is convenient to change the variables using:

$$dx dy = (\text{determinant of } 2 \times 2 J \text{ matrix}) d\xi d\eta$$

or:

$$dx dy = |[J]| d\xi d\eta \quad (E2.4.34)$$

and the limits of the integration thus become $\pm 1, \pm 1$. The integral does not exist in closed form and numerical integration is necessary. The element strain energy thus becomes:

$$SE = \frac{1}{2} \{u_e^T\} [S_e] \{u_e\} \quad (E2.4.35)$$

where $[S_e]$ is square and symmetric, and is known as the "element stiffness matrix". In two-dimensional cases it is given by:

$$[S_e] = [A^{*T}] \iint_{-1 -1}^{+1 +1} h [B^T] [D] [B] |[J]| d\xi d\eta [A^*] \quad (E2.4.36)$$

The thin shell hybrid element (R44215) used in this project involves superimposing membrane and thin plate bending effects. The analysis for the bending effects will not be included here as such effects are not an integral part of the analysis performed in this project. The element was chosen in the absence of an anisotropic membrane-only element equivalent to the PAFEC 70+ R36510 element in the PAFEC 75 scheme. The hybrid bending and membrane element is derived by combining the element matrices for each of these two configurations.

2.4.3 Anisotropic elasticity theory

Anisotropic materials possess properties which are dependent on the direction in the material. In order to present a generalised Hooke's Law for the various possibilities it will be assumed that the material is homogeneous. The stress and strain, in this case, will be specified by second-rank tensors. All components of the strain will be linearly related to all the components of the applied stresses. Nine stress terms will exist: $\sigma_{xx}, \sigma_{yy}, \sigma_{zz}, \sigma_{xy}, \sigma_{yx}, \sigma_{xz}, \sigma_{zx}, \sigma_{yz}$ and σ_{zy} . If the x, y and z directions are referred to in terms of the inte-

gers 1, 2, 3, then the generalised Hooke's Law may be written as:

$$\epsilon_{ij} = C_{ijkl} \sigma_{kl} \quad (\text{E2.4.37})$$

where i, j, k, l may each be any of the integers from 1 to 3. C_{ijkl} form a fourth-rank tensor, and are termed the material compliances and ϵ_{ij} is a second-rank mathematical strain tensor. Similarly the stress-strain tensor is given by:

$$\sigma_{ij} = E_{ijkl} \cdot \epsilon_{kl} \quad (\text{E2.4.38})$$

where E_{ijkl} are referred to as the material stiffness or the terms of the modulus tensor.

C_{ijkl} contains 81 terms (3^4) and from the definitions of the components of the stress and strain tensors the number of independent terms reduces to 36 because:

$$C_{abcd} = C_{abdc} = C_{badc} \text{ etc.} \quad (\text{E2.4.39})$$

The finite element method is based on matrix algebra and it is therefore necessary to convert C_{ijkl} from tensor to matrix form. The relationship between stress and strain tensors can be defined using matrices, with the 4 tensor suffices reduced to 2 matrix suffices according to:

Tensor: 11 22 33 12 13 21 23 31 32

Matrix: 1 2 3 6 5 6 4 5 4

Factors of 2 are also introduced to cater for the differences between tensorial and engineering strains:

$$C_{ijkl} = C_{mn} \text{ when both } m \text{ and } n \text{ lie between 1 and 3}$$

$$2C_{ijkl} = C_{mn} \text{ when either } m \text{ or } n \text{ lie between 4 and 6}$$

$$4C_{ijkl} = C_{mn} \text{ when both } m \text{ and } n \text{ lie between 4 and 6.}$$

As an example the matrix component C_{45} will be equivalent to tensor component $4C_{2331}$.

The tensor equations may thus be contracted to matrix and vector operations, in engineering rather than in mathematical strains:

$$\epsilon_i = C_{ij} \cdot \sigma_j \quad (i, j = 1, 2, \dots, 6) \quad (\text{E2.4.40})$$

$$\sigma_i = E_{ij} \cdot \epsilon_j \quad (\text{E2.4.41})$$

The C_{ij} matrix still contains 36 terms, but due to symmetry only 21 are independent, and because of Maxwell's reciprocal theorem this number further reduces to 9 independent terms.

Composite materials, such as fibre reinforced plastics are often inaccurately referred to as anisotropic. In practice, these materials usually exhibit planes of symmetry with the principal constants not dependent on position, and are more correctly named "orthotropic". Normally the C_{ij} matrix is referred to the planes of material symmetry so that the components of the matrix are aligned with the principal directions of the material

(the material symmetry axes, x_m , y_m , z_m , also defined as the 1, 2 and 3 axes). A generally orthotropic material has three planes of symmetry and the compliance matrix reduces to 9 independent constants:

$$[C^m] = \begin{bmatrix} C_{11}^m & C_{12}^m & C_{13}^m & 0 & 0 & 0 \\ & C_{22}^m & C_{23}^m & 0 & 0 & 0 \\ & & C_{33}^m & 0 & 0 & 0 \\ & & & C_{44}^m & 0 & 0 \\ \text{Symmetric} & & & & C_{55}^m & 0 \\ & & & & & C_{66}^m \end{bmatrix} \quad (\text{E2.4.42})$$

The zero terms occur when the reference axes coincide with the material symmetry axes, and may otherwise be non-zero due to shear coupling effects. Simple relationships exist between the components of $[C^m]$ and the elastic moduli of the material:

$$\begin{aligned} C_{11}^m &= 1/E_{11} & C_{22}^m &= 1/E_{22} & C_{33}^m &= 1/E_{33} \\ C_{12}^m &= -\nu_{12}/E_{11} & C_{23}^m &= -\nu_{23}/E_{22} & C_{31}^m &= -\nu_{31}/E_{33} \\ C_{66}^m &= 1/G_{12} & C_{55}^m &= 1/G_{13} & C_{44}^m &= 1/G_{23} \end{aligned} \quad (\text{E2.4.43})$$

where E and G are the Young's modulus and shear modulus respectively

11, 22 and 33 refer to the x_m , y_m and z_m directions

12, 13 and 23 are associated with the $(x_m - y_m)$, $(x_m - z_m)$ and $(y_m - z_m)$ planes and ν_{12} etc, are the Poisson's ratio values.

A transversely isotropic material is isotropic about one axis. For example a unidirectional composite has fibres running parallel to the x_m axis (the 1 axis). This additional symmetry causes a reduction in the number of terms in the compliance matrix because:

$$\begin{aligned} C_{22}^m &= C_{33}^m & C_{55}^m &= C_{66}^m \\ C_{12}^m &= C_{13}^m & C_{44}^m &= 2(C_{22}^m - C_{23}^m) \end{aligned} \quad (\text{E2.4.44})$$

A square symmetric material is isotropic in one plane because there are equal amounts of reinforcement in two mutually perpendicular directions, as in a bidirectional laminate. If the reinforcement is in the z_m plane (the 3-plane), then:

$$C_{11}^m = C_{22}^m \quad C_{44}^m = C_{55}^m \quad C_{13}^m = C_{23}^m \quad (\text{E2.4.45})$$

The compliance matrix retains the nine terms but only six of these are now independent.

The formulation of the expressions for the element stiffness matrix of 2-dimensional in-plane finite elements was presented in sections 2.4.1 and 2.4.2. The only matrix affected by the introduction of material anisotropy is the stress-strain matrix $[D]$. This matrix for an orthotropic material is set up by calculating the elements of the compliance matrix $[C^m]$ since these are easily obtained from the relevant material moduli and Poisson's ratio. $[C^m]$ is then inverted to give the stress-strain matrix $[D^m]$ corresponding to $[D]$ for an isotropic case. It is usual to relate the material x_m , y_m planes to the global (struc-

tural) x_g, y_g plane so that the x_m, y_m axes lie in the x_g, y_g plane.

The stress-strain matrix in the finite element stiffness expression is related to the stresses and strains along the element axes (x_e, y_e, z_e). When the material symmetry axes coincide with the element axes, the stress-strain equations in matrix form are:

$$\begin{Bmatrix} \epsilon_{xx}^e \\ \epsilon_{yy}^e \\ \epsilon_{xy}^e \\ \epsilon_{zz}^e \end{Bmatrix} = \begin{bmatrix} C_{11} & C_{12} & 0 & C_{13} \\ C_{12} & C_{22} & 0 & C_{23} \\ 0 & 0 & C_{66} & 0 \\ C_{13} & C_{23} & 0 & C_{33} \end{bmatrix} \begin{Bmatrix} \sigma_{xx} \\ \sigma_{yy} \\ \sigma_{xy} \\ \sigma_{zz} \end{Bmatrix} \quad (E2.4.46)$$

If the element axes are oriented at an angle θ to the material symmetry axes, then the stress-strain matrix must be transformed to give the modified compliances associated with the element axes. The stress-strain equations will also need to be modified if the material $y_m - z_m$ axes are interchanged with the structural $y_g - z_g$ axes so that the y_m axis now coincides with the global $x_g - y_g$ plane. Simplifications arise when the finite element analysis of a composite material is limited to two-dimensional (plane stress or plane strain) models. The general cases in which the element axes (x_e, y_e) are not coincident with the material symmetry axes (x_m, y_m), although they must be in the same plane, will be considered.

a) plane stress

In this case several stresses are interdependent:

$$\sigma_{zz}^e = \sigma_{yz}^e = \sigma_{xz}^e = 0 \quad (E2.4.47)$$

As only two dimensions are being considered the stress-strain relationship simplifies to:

$$\begin{Bmatrix} \epsilon_{xx}^e \\ \epsilon_{yy}^e \\ \epsilon_{xy}^e \end{Bmatrix} = \begin{bmatrix} {}_o C_{11}^e & {}_o C_{12}^e & {}_o C_{16}^e \\ {}_o C_{21}^e & {}_o C_{22}^e & {}_o C_{26}^e \\ \text{Symmetric} & & {}_o C_{66}^e \end{bmatrix} \begin{Bmatrix} \sigma_{xx} \\ \sigma_{yy} \\ \sigma_{xy} \end{Bmatrix} \quad (E2.4.48)$$

and the inverse becomes:

$$\begin{Bmatrix} \sigma_{xx}^e \\ \sigma_{yy}^e \\ \sigma_{xy}^e \end{Bmatrix} = \begin{bmatrix} {}_o D_{11}^e & {}_o D_{12}^e & {}_o D_{16}^e \\ {}_o D_{21}^e & {}_o D_{22}^e & {}_o D_{26}^e \\ \text{Symmetric} & & {}_o D_{66}^e \end{bmatrix} \begin{Bmatrix} \epsilon_{xx} \\ \epsilon_{yy} \\ \epsilon_{xy} \end{Bmatrix} \quad (E2.4.49)$$

where the subscript o indicates plane stress, and where ${}_o D_{ij}^e$ is the reduced stress-strain matrix:

$${}_o D_{ij}^e = D_{ij}^e - \frac{D_{i3}^e - D_{j3}^e}{D_{33}^e} \quad (i, j = 1, 2, 6) \quad (E2.4.50)$$

The elements of the stress-strain matrix are now referred to as ${}_o D$ rather than E . This is because the 3×3 compliance matrix has been inverted rather than the full 6×6 matrix. Plane stress analysis only requires the compliances $C_{11}^m, C_{12}^m, C_{22}^m$ and C_{66}^m .

b) plane strain.

$$\text{By definition: } \epsilon_{xx}^e = \epsilon_{yz}^e = \epsilon_{xz}^e = 0 \text{ and } \sigma_{yz}^e = \sigma_{xz}^e = 0 \quad (\text{E2.4.51})$$

The stress-strain relationship reduces to:

$$\begin{Bmatrix} \sigma_{xx}^e \\ \sigma_{yy}^e \\ \sigma_{xy}^e \end{Bmatrix} = \begin{Bmatrix} \epsilon D_{11}^e & \epsilon D_{12}^e & \epsilon D_{16}^e \\ \epsilon D_{22}^e & \epsilon D_{26}^e & \epsilon D_{66}^e \\ \text{Symmetric} & \epsilon D_{66}^e & \end{Bmatrix} \begin{Bmatrix} \epsilon_{xx}^e \\ \epsilon_{yy}^e \\ \epsilon_{xy}^e \end{Bmatrix} \quad (\text{E2.4.52})$$

and the inverse:

$$\begin{Bmatrix} \epsilon_{xx}^e \\ \epsilon_{yy}^e \\ \epsilon_{xy}^e \end{Bmatrix} = \begin{Bmatrix} \epsilon C_{11}^e & \epsilon C_{12}^e & \epsilon C_{16}^e \\ \epsilon C_{22}^e & \epsilon C_{26}^e & \epsilon C_{66}^e \\ \text{Symmetric} & \epsilon C_{66}^e & \end{Bmatrix} \begin{Bmatrix} \sigma_{xx}^e \\ \sigma_{yy}^e \\ \sigma_{xy}^e \end{Bmatrix} \quad (\text{E2.4.53})$$

where the subscript e indicates plane strain and where ϵC_{ij}^e are the reduced compliances in the element axes:

$$\epsilon C_{ij}^e = C_{ij}^e - \frac{C_{i3}^e - C_{j3}^e}{C_{33}^e} \quad (i, j = 1, 2, 6) \quad (\text{E2.4.54})$$

The D elements of the stress-strain matrix are exactly the same as those from the full 6×6 matrix (the inverse of E2.4.42). To obtain them it is necessary to know seven elements of the compliance matrix: $C_{11}^m, C_{12}^m, C_{13}^m, C_{22}^m, C_{23}^m, C_{33}^m, C_{66}^m$.

2.4.4 Crack tip singularity

Henshell and Shaw (=203) were amongst the first to note that some desired singularities can be generated through the use of distorted shape function elements. Generally, the order of the geometric interpolation functions will govern the order of the singularity. The location of the singular point can be controlled by movement of the nodes in the global coordinates, although the singular point usually lies outside the element, and must be forced to occur on an element boundary or node.

To illustrate this concept (=185), consider a one-dimensional quadratic element of length, l , with the three nodes occurring at $x_1 = 0, x_2 = al$ and $x_3 = l$ (where a is an arbitrary constant between 0 and 1). The coordinate transformation of a standard element, when $0 \geq \eta \geq 1$, will be given by:

$$X(\eta) = (4a - 1)l\eta + 2(1 - 2a)l\eta^2 \quad (\text{E2.4.55})$$

while the dependent variable will be:

$$\tilde{u}(\eta) = u_1 + (4u_3 - 3u_1 - u_2)\eta + (2u_1 + 2u_2 - 4u_3)\eta^2 \quad (\text{E2.4.56})$$

and the Jacobian of the transformation in equation (55) will be:

$$J = \delta x / \delta \eta = (4a - 1)l + 4(1 - 2a)l\eta \quad (\text{E2.4.57})$$

In a standard element the nodes are located at the ends and the mid-point of a side ($a = \frac{1}{2}$), and thus J is a positive constant. As a result no singularity occurs in the element. If a singularity is required at x_1 , then by moving the mid-side node x_2 to a position with $a = \frac{1}{4}$ achieves this, because $x_1 = \eta_1 = 0$ and $J = 0$ has been set at $\eta = 0$. In this case equation (55) will yield:

$$X = O(\eta^2) \quad (\text{E2.4.58})$$

and consequently:

$$\eta = O(X^{\frac{1}{2}}). \quad (\text{E2.4.59})$$

Thus from equation (56) we obtain $\tilde{u} = O(x^{\frac{1}{2}})$ close to node 1, which is a common useful form. Although it appears that the exponent, $p = \frac{1}{2}$, was obtained *accidentally*, it has been shown by Henshell (=181a) that this concept can be extended up to the fifth order.

The movement of the midside nodes adjacent to the singularity to the quarter-points of the element boundary closest to the crack tip ($a = \frac{1}{4}$), produces a stress singularity proportional to $1/r^{\frac{1}{2}}$ without resort to special shape functions or numerical integration formulae. The fault of those elements which employ shape functions to describe the stress field is that the traction-free condition over the crack face is not reproduced. This can lead to incorrect representation of the crack tip field, and hence errors in the K factors (=184).

Henshell and Shaw showed that this erroneous stress quickly reduces over the first element, and can be further reduced by refining the mesh in the crack tip zone. However the latter action is self-defeating, given the intention of the element. The Henshell-Shaw elements have been shown (=184) to be in excellent agreement with experimental results (=204) for a range of stress intensity factors (K_I : crack opening mode) with a/w ratios of 0·1 to 0·6, for both pure bending and pure tension. The finite element results of a calculation of the stress intensity factor (K_{II} : shearing mode) were compared (=184) with the results of a boundary colocation method analysis by Wilson (=205). Both the Henshell-Shaw elements, and those from the Blackburn scheme (=206), underestimate the Wilson results by a practically constant 10%, but it is impossible to say which method is correct.

Swedlow (=183) considers that the Henshell-Shaw element is *altogether appropriate* when:

- a) the material responds in a linear-elastic or Hookean manner
- b) planar or axisymmetric behaviour may safely be presumed
- c) the geometry is that of a crack.

2.5 Cryogenics (=207)

In a hybrid composite the differences between the thermal properties of the components will lead to residual stresses in the material after temperature changes. At the curing temperature it can be assumed that whilst the components are bonding together they are

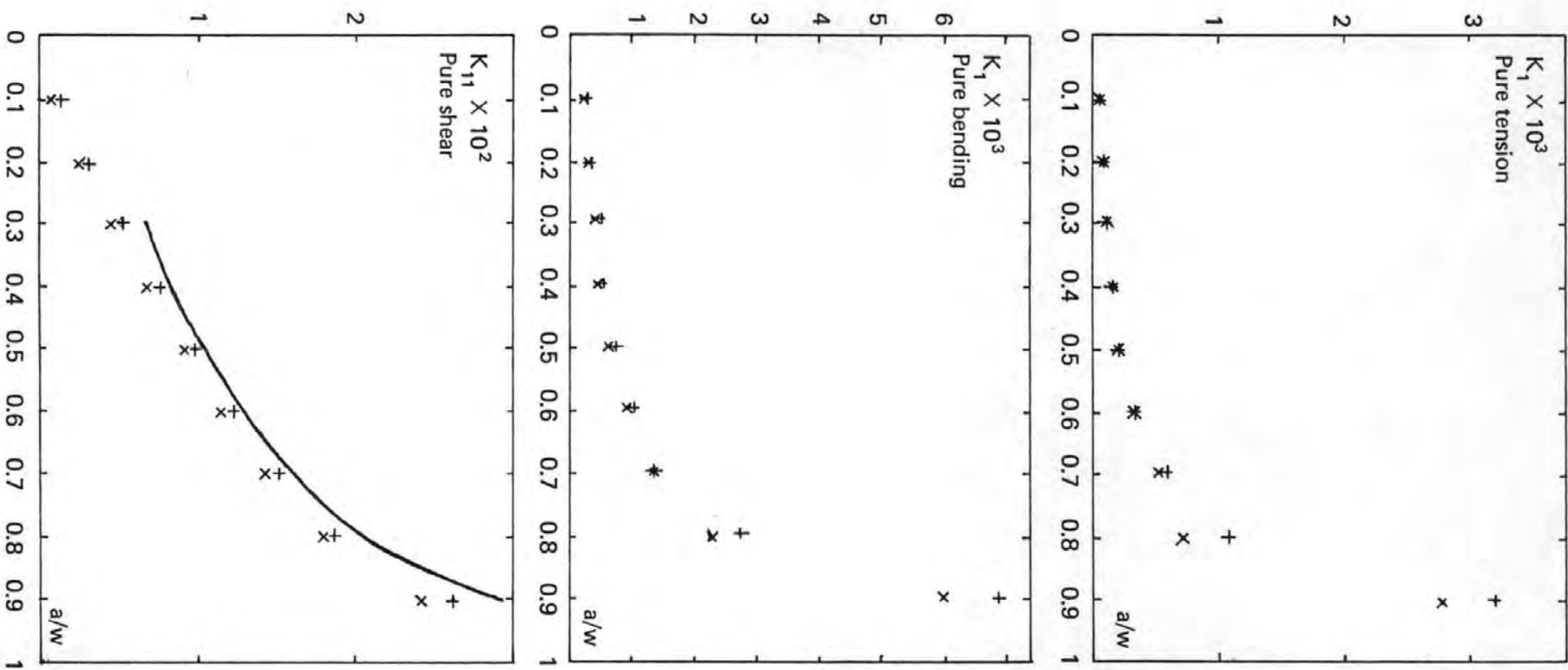


Figure 13: Stress intensity factors for cracks in various loading modes using distorted shape function elements (=184)

Henshall & Shaw elements (+) (=203)

Blackburn elements (x) (=206)

Wilson boundary colocation method (—) (=205)

still stress-free. However as the hybrid cools the glass fibres will contract more than the carbon fibres. The carbon fibres may even expand because of the negative expansion coefficient found in certain types. Using a simple force balance equation gives:

$$\sigma_H A_H + \sigma_L A_L = 0 \quad (\text{E2.5.1})$$

where

- σ is the tensile or compressive stress,
- A is the fractional cross sectional area, and
- H and L subscripts indicate high and low coefficients of expansion.

Equating the strains per unit length yields:

$$\frac{\sigma_H}{E_H} - \frac{\sigma_L}{E_L} = (\alpha_H - \alpha_L) \cdot \Delta T \quad (\text{E2.5.2})$$

where ΔT is the temperature change. However if the composite is continuous and unidirectional the cross-sectional areas in equation E2.5.1 can be replaced by volume fractions, V_x , and by rearrangement and substitution into equation E2.5.2:

$$\frac{-\sigma_L V_L}{V_H E_H} - \frac{\sigma_L}{E_L} = (\alpha_H - \alpha_L) \cdot \Delta T \quad (\text{E2.5.3})$$

Therefore the compressive stress in the low expansivity fibre can be obtained from:

$$\sigma_L = -\frac{(\alpha_H - \alpha_L) \cdot \Delta T \cdot V_H}{\left(\frac{V_L}{E_H} + \frac{V_H}{E_L} \right)} = -\frac{(\alpha_H - \alpha_L) \cdot \Delta T \cdot V_H \cdot E_L}{V_L \left(\frac{E_L}{E_H} - 1 \right) + 1} \quad (\text{E2.5.4})$$

Thus on cooling a room temperature (24°C) cured carbon and glass fibre hybrid composite to liquid nitrogen temperature (-196°C) significant stresses may be obtained because of the 220°C change in temperature. This is indicated below for a variety of carbon-glass hybrids:

V/O	$\alpha(\text{mm/mm}/{}^\circ\text{K})$	$E(\text{GPa})$	$V_L (V_H + V_L = 1)$	$\sigma_{L_{\text{calc}}} (\text{MPa})$	$\sigma_{L_{\text{exptl}}} (\text{MPa})$	$\frac{\sigma_{L_{\text{calc}}}}{\sigma_{L_{\text{exptl}}}} (\%)$
E glass	60×10^{-6}	40	0.5	—	—	—
HMS carbon	-0.5×10^{-6}	210	0.5	26	900	2.8
HTS carbon	0.5×10^{-6}	175	0.5	18	1450	1.2
AS carbon	1.0×10^{-6}	130	0.5	13	1200	1.1

3.0 Specimen preparation

3.0.1 Mixing "intimate" hybrid tows

Initially the intimate fibre tows were created by carefully teasing apart one tow of each fibre species and recombining the two tows by laying the much reduced filament rovings alternately onto a paper backing sheet to create a "Fine mix" hybrid roving. "Coarse mix" hybrids were prepared using a full tow of each fibre species as a structural unit. However some tests were conducted with coarse mix hybrids which had been split and recombined to determine the effect of the mechanical mixing.

A modification of the "Courtaulds air knife" (=208) was subsequently used to create a flat unidirectional ribbon of one fibre species from an individual tow or roving and then to combine one ribbon of each fibre type to produce a finely mixed hybrid ribbon. Details of the Courtaulds air knife are included at Appendix 11.

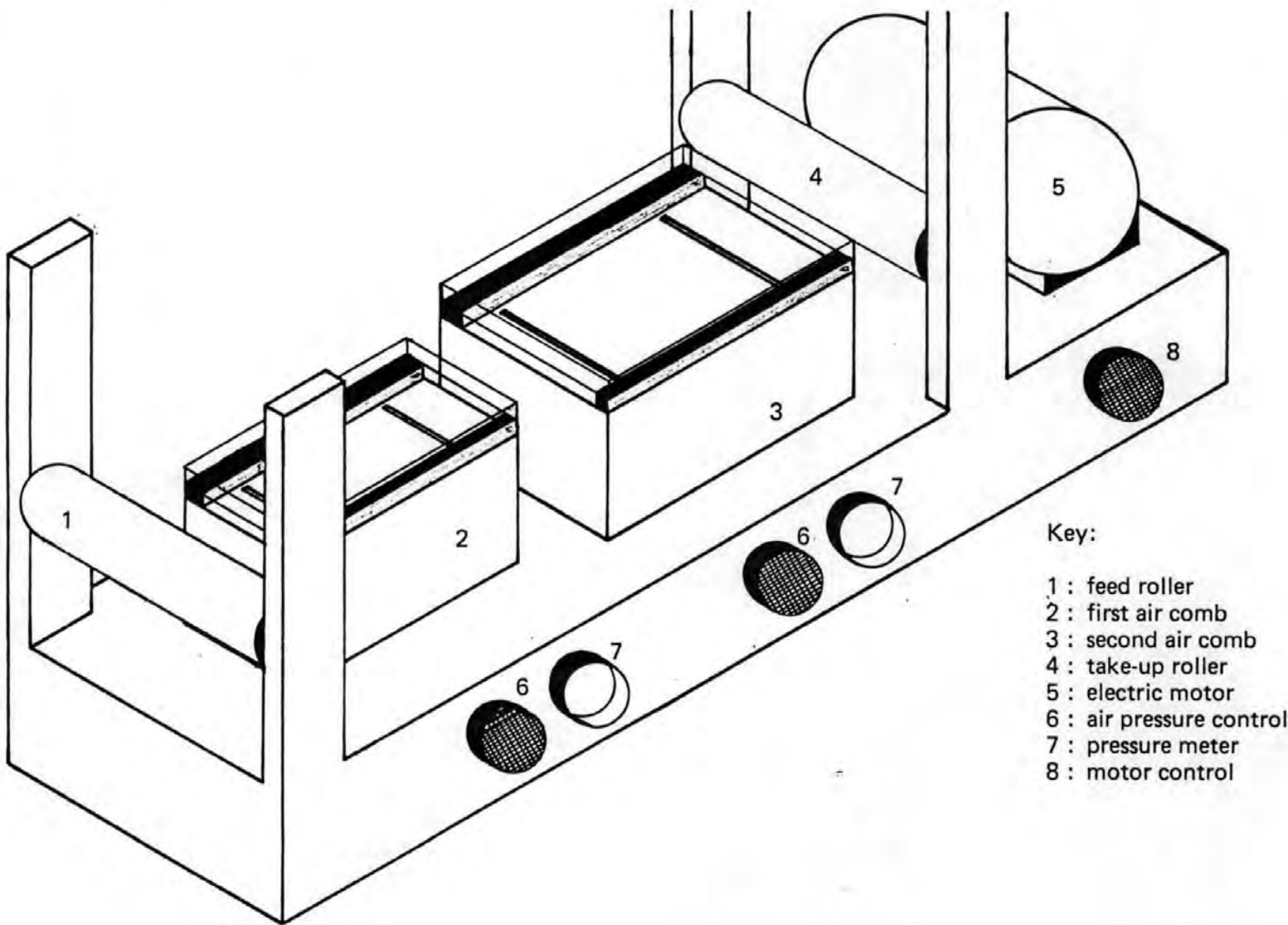
In the modification (known hereinafter as the Aircomb as this is believed to be a more accurate name), the Aircomb has been extended to include two slits in order that fibres are combed both on entry to and on exit from the rig. Also rollers to feed and take up the fibres at equivalent rates have been included. The slots have been widened and the pressure increased to around 700 kPa (100 lbf/in²) using the air line available in the laboratory. The modified Aircomb is illustrated in figure 14.

3.0.2 Composite preparation

The specimens were moulded within open ended moulds, generally referred to as "leaky moulds", with close fitting "plungers", each mould having been prepared to give a specimen of known cross section (nominally 2 mm deep by 5 mm wide). The clean polished mould was first sprayed with release agent (Rocol M.R.S. non-silicone dry film spray mould release agent) after reassembly. Lengths of fibres at least three inches longer than the mould were then cut either direct from the filament rovings or from the mixed fibres prepared in the Aircomb described in the previous section. The resin was then mixed with catalyst and accelerator according to the following formulation,* and allowed to stand until the air bubbles had cleared:

(*)					
Resin	:	100	100	100	100
Catalyst	:	2	2	2	2
Accelerator	:	4	3	2	1
Minutes to cure at 70° C	:	9	12	16	25
		(Scott Bader quoted times)			

The bottom of the mould was first covered with resin and the first fibre tow was lowered into this resin and carefully wetted with resin by the application and release of very slight tension along the fibres, until all air bubbles and dry interfaces were seen to be eliminated. This procedure was repeated with addition of resin and fibres in alternation until the required fibre content was achieved. The resin formulation allows up to 20 minutes before the gelling of the resin makes further work difficult. When all the components of the composite had been loaded the plunger was inserted into the mould and

**Key:**

- 1 : feed roller
- 2 : first air comb
- 3 : second air comb
- 4 : take-up roller
- 5 : electric motor
- 6 : air pressure control
- 7 : pressure meter
- 8 : motor control

Figure 14: The Aircomb used to redistribute the fibres in order to fabricate intimately mixed composites.

pressure was applied to close the mould, taking care to keep the opposing faces of the moulds parallel to avoid net motion of the fibres in respect of the mould. The excess resin is squeezed from the open ends of the mould.

The specimens were then allowed to gel at room temperature so that thermal stresses due to formation of the interface bond followed by cooling are reduced to a minimum. The specimen was removed from the mould when solid, and subsequently post-cured at 70°C for 24 hours. The specimens were then cut using a diamond wheel on a slitting saw to the length required for three flexure specimens, with further segments for interlaminar shear strength tests and optical microscopy being taken where possible.

3.1 Examination of the microstructure

Before it was possible to calculate the microstructure parameters it was necessary to prepare photographs of the optical micrographs. In order to do this the following procedure was undertaken:

i) A section of the unidirectional composite was first mounted in a cylindrical block of casting resin so that the major axis of the cylinder was aligned with the principal axis of the fibres.

ii) Any obvious irregularities on the "flat" surfaces were removed, initially by turning on a lathe and subsequently by polishing on a sequence of "wet and dry" diamond paper at 200, 320, 400 and 600 grade in turn until the surface appeared flat to the unaided eye.

iii) The mounted specimens were then polished to one micron on an "Autopol" automatic metallurgical polishing machine, using 150 mm polishing plates. The edge of the specimen holder was positioned at 6.12 mm from the edge of the polishing plate. After placing the specimen in position the loading springs were allowed to come to rest when unloaded, and they were fastened in position with one division of load added.

The polishing sequence was approximately one hour at 14 μ diamond paste, a thorough washing with hot water to remove any traces of the polishing grit, approximately one hour at 6 μ diamond paste, removal of any traces of the polishing grit, and 30 minutes at 1 μ grit, followed by another thorough washing. By this stage the surface should appear unscratched, with only minimal sign of the presence of the glass fibres.

iv) In those specimens where the glass fibres did not show up in the optical microscope images, the interfaces between the polished resin and the fibres was etched by a 5-10 second exposure to hydrofluoric acid vapour [WITH GREAT CARE!], followed by an extensive washing with water. Overexposure to the acid had to be avoided because the acid can etch the carbon fibres, and also over-etch the glass-resin interface.

v) The specimens were viewed in a Vickers optical projection microscope, using reflected light (hence carbon appears white and resin and glass appear grey). The filters and light intensity were adjusted to obtain sharp images with good contrast, and these were recorded on a Polaroid camera for subsequent analysis.

vi) The images were analysed by recording the position of the fibre-resin interface on line transects and from this data the microstructure parameters were calculated.

vii) In the later stages of the project the analysis of the microstructure was performed by use of an Apple II microcomputer and graphics tablet, (which eliminated the need to record individual data points, and have the data transferred to the mainframe computer) which gave an instant printout of the results (see table 4 & figure 15).

viii) The microstructure parameters:

a) Contiguity percentage

The ratio of the number of changes of fibre species along the line transect, relative to the number of changes of individual fibres.

b) Nearest neighbour index

An index derived from measurement of the individual distances, between the centres of the transect within individual fibres, of the same species.

c) Chi-squared index

An index derived from the deviation of the number of fibres of the species in any single section of one-tenth of the total transect length, to the number of fibres of that type which would be expected if the fibres were uniformly distributed along the transect length.

d) Component volume fraction

The ratio of the total length of the transect which occurs within any individual component to the total length of the transect. This assumes that the cross-section of the material in the photograph is representative of the whole composite.

3.2 Mechanical property testing

3.2.1 Longitudinal flexural strength

This test was designed by Sturgeon (=209) to measure the composite bending strength under three-point loading. The property is of little use in design calculations but is a useful guide to the direct strength properties of a material, provided that it is associated with the mode of failure. It has been shown that the experimental strength and mode of failure (tension, compression, shear or combinations of these) depend on the test span-to-depth ratio and the geometry of the loading anvils (=210). A span-to-depth ratio of 40:1 was chosen by Sturgeon to ensure true flexural failure and to minimise the effects of shear stresses and transverse crushing by the loading anvils. The modified Sturgeon rig and test specimen are shown in figure 16; in the experiments reported in this thesis all test specimens were half the recommended breadth.

Flexural testing was chosen to:

- a) minimise specimen crushing due to tension grips
- b) reduce grip noise for acoustic emission
- c) ensure a small rig with minimal heat paths for later cryogenic tests.

Sturgeon recommends that the rollers should be accurately parallel to each other, with the loading anvil accurately centred between and parallel to them. The outer rollers should be held constant during the test and the load applied at a constant rate which produces failure between 30 and 180 seconds from the start of loading.

<pre>]LOAD A7PRGM]LIST 10 DIM I1(10),J1(10),W\$(40),Z\$(2) 20 Y\$ = "Y":Z\$ = "END" 30 N9 = 5 40 M9 = 6 50 REM DEFINE FILE:DATA 60 REM DEFINE FILE:RESU 70 REM R:G I/F,J7=+1 80 REM G:R I/F,J7=-1 90 REM R:C I/F,J7=+2 100 REM C:R I/F,J7=-2 110 REM START, J7=+3 120 REM FINISH,J7=-3 130 REM OBJECTIVE DISCRIMINATIO N OF THOSE POINTS WHERE THE CROSS HAIRS COINCIDE WITH AN INTERFACE CAN BE OBTAINED 140 REM BY COUNTING ALL ENTRIES AND DISCARDING ALL EXITS 150 INPUT "TABLET(T),KEYBOARD(K) ,DISCFILE(D)";I\$ 152 T\$ = "T" 154 K\$ = "K" 156 X\$ = "D" 158 IF LEFT\$(I\$,1) = X\$ THEN Y \$ = X\$ 160 J2 = 0 170 I2 = 0 180 K1 = 0 190 I3 = 0 200 J3 = 0 210 C4 = 0.0 220 G4 = 0.0 230 C6 = 0.0 240 G6 = 0.0 250 C5 = 0.0 260 G5 = 0.0 270 C8 = 0.0 280 G8 = 0.0 290 G1 = 0.0 300 C1 = 0.0 310 U1 = 0.0 320 U2 = 0.0 330 W1 = 0.0 340 W2 = 0.0 350 Z7 = 0.0 360 V7 = 0.0 370 V9 = 0.0 380 V6 = 0.0 390 V5 = 0.0 400 V4 = 0.0 410 V8 = 0.0 </pre>	<pre> 420 IF LEFT\$(I\$,1) < > X\$ THEN INPUT "W\$? ";W\$ 425 IF LEFT\$(I\$,1) = X\$ THEN GOSUB 6900 430 IF LEFT\$(W\$,3) = Z\$ THEN GOTO 1160 440 IF LEFT\$(I\$,1) = T\$ THEN GOSUB 5100: GOTO 490 450 IF LEFT\$(I\$,1) = K\$ THEN GOTO 480 460 IF LEFT\$(I\$,1) < > X\$ GOTO 150 480 IF LEFT\$(I\$,1) < > X\$ THEN GOTO 487 485 GOSUB 6700 486 GOTO 490 487 INPUT "J7,D7? ";J7,D7: IN# 0 490 IF J7 = - 3 THEN GOTO 570 500 IF J7 = + 3 THEN Z7 = D7 510 IF J7 = 0 THEN V9 = (D7 - Z7) / 10: GOTO 440 520 IF J7 = + 1 THEN X1 = D7 530 IF J7 = + 2 THEN Y1 = D7 540 IF V4 = 0.0 THEN V4 = V9 + Z 7 550 IF D7 < = V4 THEN GOTO 650 570 IF K1 = 11 THEN GOTO 810 580 V4 = V4 + V9 590 I1(K1) = I2 - I3 600 J1(K1) = J2 - J3 610 IF J7 = - 3 THEN GOTO 810 620 I3 = I2 630 J3 = J2 640 K1 = K1 + 1 650 IF J7 < > - 1 THEN GOTO 7 30 660 G1 = (D7 - X1) + G1 670 G6 = (D7 + X1) / 2 680 IF I2 = 0 THEN GOTO 700 690 G5 = G5 + (G6 - G8) 700 G8 = G6 710 I2 = I2 + 1 720 GOTO 800 730 IF J7 < > - 2 THEN GOTO 8 00 740 C1 = (D7 - Y1) + C1 750 C6 = (D7 + Y1) / 2 760 IF J2 = 0 THEN GOTO 780 770 C5 = C5 + (C6 - C8) 780 C8 = C6 790 J2 = J2 + 1 800 GOTO 440 810 PR# 1 </pre>
--	---

TABLE 4: Listing of the Apple II computer program
to calculate microstructure parameters.

<pre> 811 PRINT 812 PRINT W\$ 820 Z7 = D7 - Z7 830 F2 = G1 / Z7 840 F1 = C1 / Z7 850 F3 = 1 - F1 - F2 860 IF I2 = 0 THEN PRINT "***NO GLASS FIBRES***" 870 IF I2 < 2 THEN GOTO 890 880 G4 = (G5 / (I2 - 1)) / (Z7 / I2) 890 IF J2 = 0 THEN PRINT "***NO CARBON FIBRES" 900 IF J2 < 2 THEN GOTO 920 910 C4 = (C5 / (J2 - 1)) / (Z7 / J2) 920 FOR K = 1 TO 10 930 IF I2 = 0 THEN GOTO 980 940 U2 = I1(K) 950 U1 = (I2) / 10. 960 V5 = (U2 - U1) ↑ 2 / U1 970 V6 = V5 + V6 980 IF J2 = 0 THEN GOTO 1030 990 W2 = (J1(K)) 1000 W1 = (J2) / 10. 1010 V8 = (W2 - W1) ↑ 2 / W1 1020 V7 = V7 + V8 1030 I1(K) = 0 1040 J1(K) = 0 1045 PRINT W1,W2 1050 NEXT K 1060 PRINT I2;" GLASS FIBRES" 1070 PRINT "GLASS VOLUME FRACTIO N= ";F2 1080 PRINT "GLASS NEIGHBOUR INDE X= ";G4 1090 PRINT "GLASS CHI-SQUARE VAL UE=";V6 1095 PRINT 1100 PRINT J2;" CARBON FIBRES" 1110 PRINT "CARBON VOLUME FRACTI ON= ";F1 1120 PRINT "CARBON NEIGHBOUR IND EX= ";C4 1130 PRINT "CARBON CHI-SQUARE VA LUE= ";V7 1135 PRINT 1140 PRINT "VOLUME FRACTION OF R ESIN= ";F3 1150 GOTO 150 1160 IF LEFT\$(Y\$,1) = X\$ THEN D\$ = CHR\$(4); PRINT D\$;"CL OSE DATA" 1170 PR# 0 1180 END </pre>	<pre> 5100 PR# 5: PRINT "T1,F,C,Q": PR# 0: REM INITIALISE TABLET 5105 PRINT "CO-ORDINATES" 5110 IN# 5: INPUT X,Y,Z: IN# 0: REM READ TABLET 5112 IF Z < > 2 THEN GOTO 5105 5114 IF Y > 6100 THEN GOTO 5105 5116 IF Y < 1050 THEN GOTO 5105 5118 IF X > 6150 THEN GOTO 5105 5119 IF X < 650 THEN GOTO 5105 5120 GOSUB 6000 5130 XX = X 5140 YY = Y 5150 PR# 1 5160 PRINT "XPOS=";XX; ", YPOS="; YY; 5170 PR# 0 5180 GOTO 5500 5500 PRINT 5520 PRINT "POINT TYPE"; 5530 IN# 5: INPUT X,Y,Z: IN# 0: REM IDENTIFIER 5540 IF Z < > 2 THEN GOTO 5520 5550 IF X < 4430 THEN GOTO 5520 5560 IF X > 6100 THEN GOTO 5520 5570 IF Y > 1000 THEN GOTO 5520 5580 IF Y < 550 THEN GOTO 5520 5600 PR# 1 5610 IF X > 5950 THEN PRINT ", END";J7 = - 3: GOTO 5690 5620 IF X > 5695 THEN PRINT ", C/R";J7 = - 2: GOTO 5690 5630 IF X > 5445 THEN PRINT ", R/C";J7 = + 2: GOTO 5690 5640 IF X > 5175 THEN PRINT ", G/R";J7 = - 1: GOTO 5690 5650 IF X > 4945 THEN PRINT ", R/G";J7 = + 1: GOTO 5690 5660 IF X > 4685 THEN PRINT ", SET END";J7 = 0: GOTO 5690 5670 IF X < 4685 THEN PRINT ", START";J7 = + 3: GOTO 5690 5680 GOTO 5500 5690 PR# 0 5695 D7 = SQR (XX ↑ 2 + YY ↑ 2) 5700 RETURN </pre>
---	---

Table 4 (continued): Microstructure-program listing.

```
6000 REM MAKE NOISE
6005 S = - 16336
6010 FOR I = 1 TO 10
6020 SOUND = PEEK (S) - PEEK (S)
    + PEEK (S) - PEEK (S): NEXT

6030 RETURN
6700 GOSUB 6000
6705 IN# 6
6710 INPUT J7,D7
6720 PRINT J7,D7
6730 IN# 0
6800 RETURN
6900 REM
6910 D$ = CHR$ (4): REM CTRL-D
6920 PRINT D$;"OPEN DATA"
6930 PRINT D$;"READ DATA"
6940 IN# 6
6950 INPUT "W$::::::";W$
6960 PRINT W$
7000 RETURN
```

Table 4 (continued): Microstructure-program listing.

Key:

Slots:

- 0 : Language card
- 1 : Printer
- 2 : Video input
- 3 : (empty)
- 4 : Graphics tablet
- 5 : Clock-calendar
- 6 : Dual disc drives
- 7 : PAL colour video card

Other Input/Output:

- 8 : Loudspeaker
- 9 : Keyboard
- 10 : Graphics cursor control
- 11 : Monitor screen

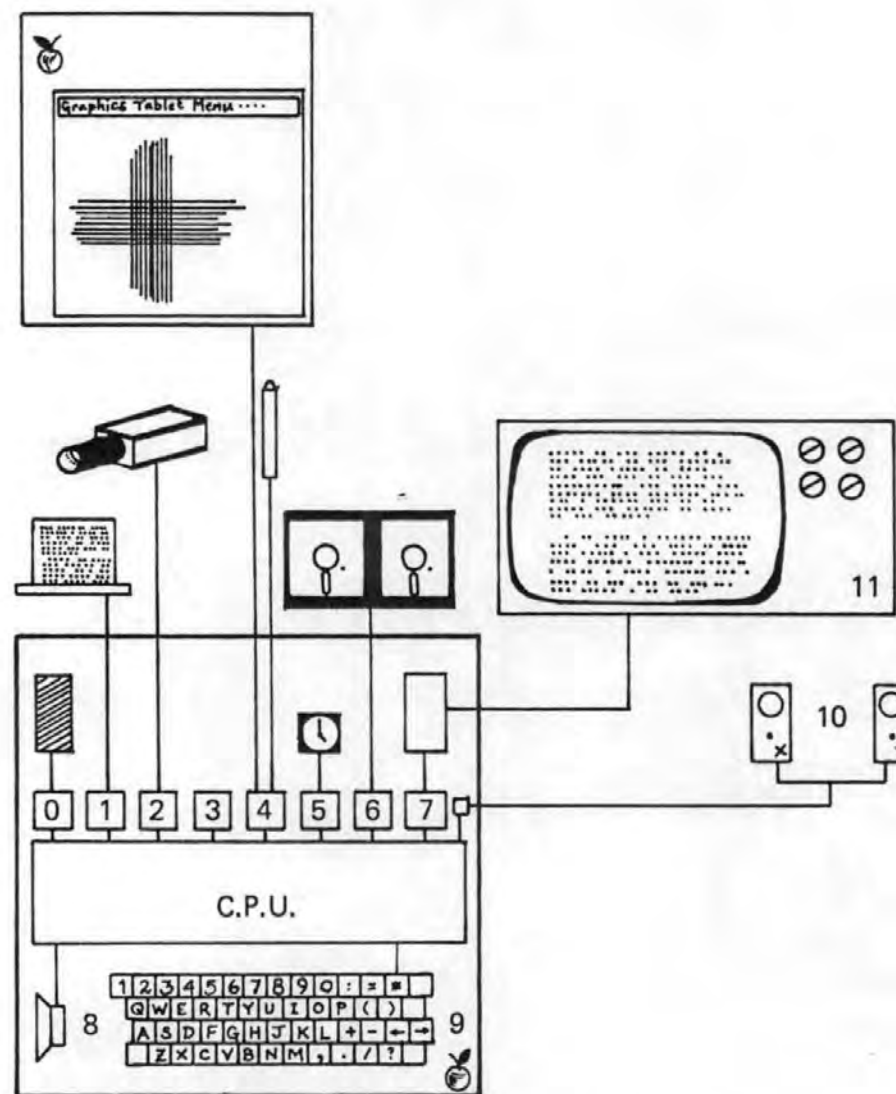


Figure 15: The configuration of the Apple II microcomputer and peripherals.

The longitudinal flexural strength, σ_L' , can be obtained using the following equation:

$$\sigma_L' = \frac{3PL}{2bd^2}$$

where P is the applied load at "failure"

L is the test span between the outer supports

b is the specimen width, and

d is the specimen depth.

Although the test is quick and easy to perform it is limited by the difficulty of determining the mode of failure. Courtaulds (=211a) have identified nine discrete modes of failure, see figure 17. The equation used to obtain the flexural strength is based on simple bending theory and makes use of a number of assumptions which are not realised in practice. In particular, the degree of influence of shear and transverse stresses will depend on the matrix properties and on the volume fraction of fibres. Moreover, there must be an equal distribution of fibres throughout the specimen depth, and the tensile and compressive moduli must be equal for the neutral axis to lie in the central plane.

Sturgeon recommends that the loading anvil be 25 mm diameter and that each of the support rollers has a diameter of 10 mm. However in the Courtaulds test specification the supports have a diameter of 6.35 mm.

3.2.2 Longitudinal flexural modulus

Sturgeon recommends that a similar rig to that for flexural strength be used for determination of the flexural modulus but that the span-to-depth ratio be increased to 100:1, so that the error due to shear deflection imposed by the three-point flexure jig can be reduced (=212). From strain energy considerations it has been estimated that the shear deflection is less than 2% of the deflection due to bending at this span-to-depth ratio, and can therefore be disregarded. The deflection under the central roller should be measured by a means independent of the machine crosshead movement.

In practice for the comparative tests carried out for this thesis the previous flexural strength rig was also used for the determination of flexural modulus. This use of the flexural strength rig is accepted by Courtaulds (=211b) as giving "a reasonable approximation" to the flexural modulus. It has been shown in Appendix 9 that the ratio of bending to shear deflection is 1:0.02 for a representative material at this span-to-depth ratio. Also, after careful cross correlation of measurements derived from linear variable displacement transducers (LVDT's) and from measurement of the crosshead deflection it was decided that the latter was of equivalent accuracy for the determination of specimen deflection, whilst not adding any additional constraint such as would occur with an LVDT.

The longitudinal flexural modulus, E_L , can be obtained using the following equation:

$$E_L = \frac{ML^3}{4bd^3} = \frac{PL^3}{4bd^3\delta}$$

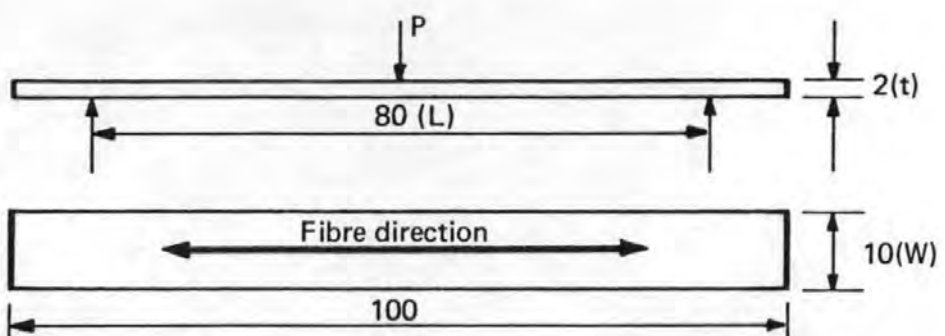


Figure 16: The flexure test specimen (dimensions in millimetres).

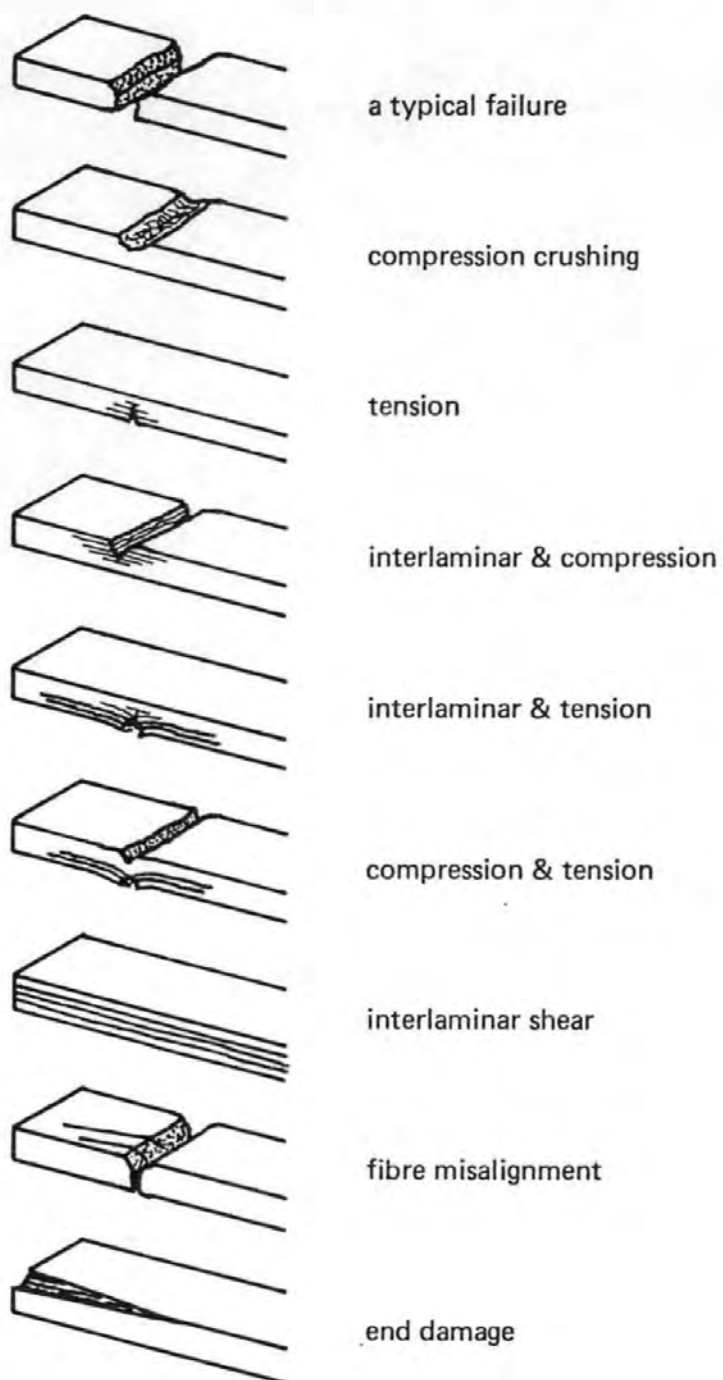


Figure 17: Observed flexural failure modes.

where L is the test span
d is the specimen depth
b is the specimen breadth, and
M is the ratio of the applied load, P, to the deflection produced, δ .

Sturgeon recommends that the maximum load used to calculate the modulus should be about one-fifth of the failure load, Courtaulds suggest that the specimen be taken to two-thirds of the anticipated failure load and the gradient (P/δ) be calculated from two points on the straight line of the load extension graph. The same dimensions as for the strength rig are again individually recommended for the loading anvil and supports. Courtaulds recommend that the loading be at 0.5 mm/min. for the 100 mm span and 1.0 mm/min. for the 80 mm span.

Sturgeon specifically states that the long span test "may only be used for quality control of similar resin-fibre systems". In some resin systems it is expected that creep will be observed at high loads. Once again the equation assumes that the tensile and compressive moduli are equal. Some fibre-resin systems may suffer quite significant indentations (=209, 211c, 213) by the rollers which may contribute large errors to the modulus value which is determined. Sturgeon specifically requires that this indentation error be eliminated if comparisons between different fibre resin systems are undertaken.

3.2.3.1 Interlaminar shear strength (ILSS) (=209, 210, 211d)

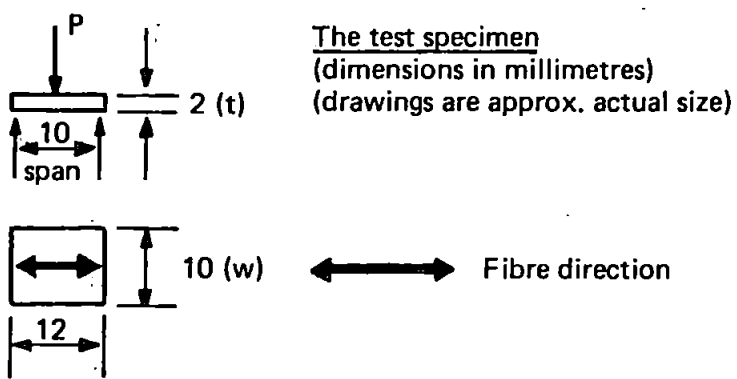
This test was designed to measure the ultimate strength of the composite when subjected to a shear stress in a plane parallel to the fibre direction. The property can be affected both by the properties of the matrix and, more usually, by the fibre-matrix bond. The test is particularly suitable for monitoring the interfacial bond and for assessing the performance of the matrix within the composite. Numerous methods of measuring the ILSS have been used and are compared in a paper by Adams and Thomas (=214). The recommended method consists of applying three-point loading to a specimen whose dimensions are chosen to ensure that shear failure occurs before flexural failure. The recommended roller diameters are 6.35 mm (1/4"). It is recommended that failure should occur in 15-45 seconds. Courtaulds have indicated five modes of failure (figure 18).

The interlaminar shear strength (τ_{12}) can be calculated using the equation:

$$\tau_{12} = \frac{3P}{4bd}$$

where P is the applied load
b is the width of the specimen, and
d is the depth of the specimen.

The recommended span:depth ratio of 5:1 should ensure shear failures in most combinations of carbon fibre and resin, but there will be cases where the ratio of flexural:shear strengths is particularly low and only a minimum value of ILSS can be quoted because of prior flexural failure (=215). In such cases shear failure can be precipitated by reducing



Modes of failure



Single shear



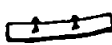
Multiple shear



Shear and tension



Tension



Compression

Figure 18: The interlaminar shear strength (ILSS) test.
ILSS = $3P/4wt$

the span to depth ratio to as low as 3:1 at constant span. However a consequence of this is that direct comparisons with results from the standard rig cannot be obtained. At this reduced span-to-depth ratio the results are liable to errors arising from transverse compressive failure under the rollers. It has been shown (=216, 217) that the specimen width can become significant when fibres of widely differing Youngs moduli are compared. Such comparisons should therefore be made with caution.

It is assumed that the plane cross sections remain plane during the bending and that the specimen shears before failure occurs at either the tensile or the compressive faces of the test piece. Maximum tensile and compressive stresses at the midspan of the specimen are given by the expression:

$$\sigma = \frac{3PL}{2bd^2}$$

where P is the applied load

L is the test span

b is the specimen breadth

d is the specimen depth.

From this elementary beam theory approach it can be shown that the relationship between the maximum flexural stress and the maximum shear stress in a three point loaded beam is given by:

$$\frac{\sigma}{\tau} = \frac{2L}{d}$$

Bader *et al.* (=218) have considered the case of a short beam test with L = 12.7 mm and d = 2 mm, such that the value of 2L/d is 13. In order that the shear strength result be valid it should be not greater than 1/13 of the flexural strength of the material. In a series of tests on beams of various R/d ratios they showed that the recorded flexural strength decreased with reduction of the ratio L/d (figure 19). This has also been reported by Wells *et al.* (=210). The reduction factors for short beam strength/long beam strength amount to 0.9 for the Modmor I (MI) composites and 0.7 for the Modmor II (MII) composites, which increases the effective σ/τ ratios to 14.5 and 18.5 respectively. Therefore those points ringed in figure 19 should be viewed with some caution.

Stinchcomb *et al.* (=219) have shown that the shear failure mode only occurs in those specimens which are of poorer quality in the ASTM short-beam test. The ASTM beam (=220) has measurements of:

	Sturgeon	ASTM
span	10 mm	12.7 mm (0.5")
breadth	10 mm	6.35 mm (0.25")
depth	2 mm	3.2 mm (0.125")
length	12 mm	—
crosshead rate	—	1.3 mm/min (0.05 in/min)

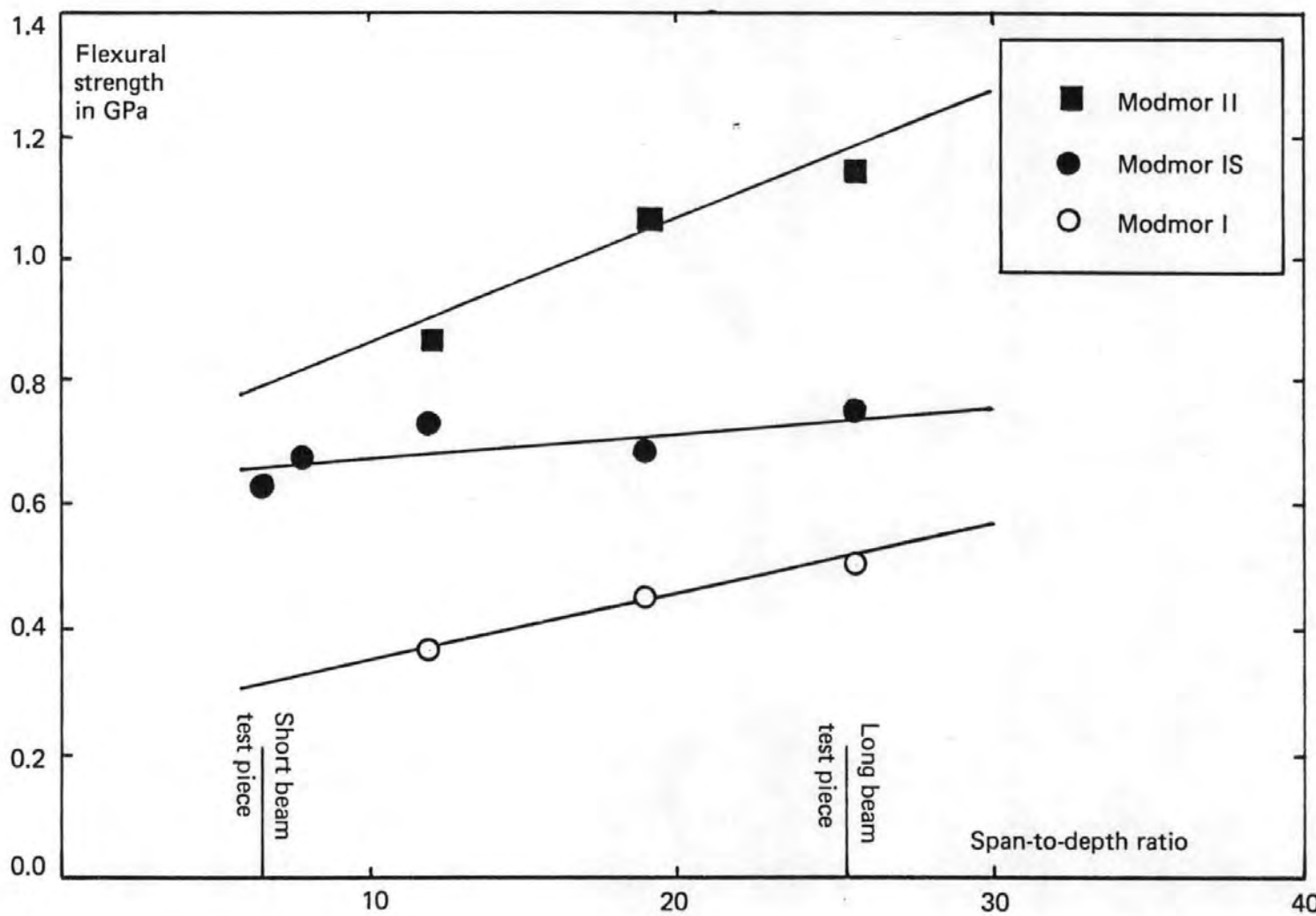


Figure 19: Dependence of the flexural strength (of carbon fibre composites in three-point bending) with span-to-depth ratio (=218)

Two basic but unrealised assumptions occur in the analysis of the data, which used classical Euler-Bernoulli beam theory. They are that

- a) the beam length is large compared to the width and depth, and
- b) the material is isotropic homogeneous and obeys Hooke's law for a simple one-dimensional stress state.

The specimens with less severe defects or good quality bonds failed in microbuckling, or a combination of shear and microbuckling. They suggest that only a minimum value of shear strength can therefore be determined because those specimens which are of good quality failed prematurely because of some other mode of failure.

The short beam shear test has several limitations, some serious enough to imply doubt as to its validity. It is however attractive for the ease and simplicity of testing, the economical specimen size (and especially insofar as it can be fabricated in the same moulds as the flexure specimens), and the direct analysis of the test data.

3.2.3.2 Alternatives to the short beam test for shear strength

A variety of alternatives to the previous test do exist and some are summarised below:

- a) the rail shear test (=221)
- b) torque loading of tubular specimens (=222)
- c) notched cylindrical rod test (=223)
- d) single lap shear test (=224)
- e) balanced double lap shear test (=224)
- f) 10° off-axis tensile test (=225, 226).

3.3 Acoustic emission

3.3.1 Acoustic emission counting

The acoustic emission testing was initially carried out using the systems described by Guild (=9) and Babb (=227).

The major part of the acoustic emission testing at both Plymouth Polytechnic and at Bath University was monitored using an Acoustic Emission Consultants Limited system designated the AECL 109 Stress Wave Emission Processor. The system consists of two major units: a phantom powered 40 dB fixed gain pre-amplifier with a frequency response from 20 kHz to 20 MHz, and a signal processor. There are additionally two auxilliary outputs: a logarithmic amplifier and an audio monitor.

The signal processor supplies the drive current to the preamplifier. In the signal processor the signal path runs through one of four filters, although it may bypass all of these, giving a frequency response from 20 kHz to 2 MHz. In all cases the roll-off is at 18 dB per octave. A variable gain amplifier follows which can apply up to a further 65 dB of gain selectable by push buttons, with a gain repeatability of 0.1%. The signal is then passed directly to a fast comparator and to an envelope detector for event counting. The comparator is referenced from a 1 volt level within the unit. Either the total comparator count

or the total event count can be switched to the six decade counter on the front panel. Any three selected digits from the counter can be displayed at one time, and the three selected digits are available at the rear of the unit in BCD form or as an analogue voltage scaled from 0-10 volts.

In monitoring the experiments in this project a total gain of 60 dB (40 dB preamplifier plus 20 dB from signal processor) and filter A(20 kHz-100 kHz) were used to precondition the signal. The linear analogue output from the system was taken to a chart recorder which was scaled with the zero and full-scale calibration buttons. When an X-X-Y recorder was available load was plotted on the second X-pen. The Y-pen recorded time using a standard timebase. The output from the variable gain amplifier was occasionally examined using a "Datalab" digital transient recorder with 256 bits Y-range and 1024 bits X-range.

3.3.2 Amplitude sorting of AE signals (=160)

The AE test equipment used at Bath University (in conjunction with the AECL 109 total-count rig) was an Acoustic Emission Technology Corporation (AETC) 203 Amplitude Distribution System. This is a multichannel analyser which monitors the number of AE events and sorts the amplitudes of these events into 50 channels, each of 1.2 dB, in the range 10 mV-1 V. The effective signal threshold at the transducer is approximately 20 μ V and the signal amplification is 60 dB (preamplifier type 160A). An AETC FAC-500 PZT transducer is used, which is a flat-response sensor with a nominal resonance in the region of 500 kHz. The system envelopes the transducer ring-down and can distinguish individual events provided that there is a dead-time of 100 μ s between each event. The system is intrinsically capable of registering 2000 counts per second, but if the dead time is not achieved the equipment saturates and the count rate falls to about 20 s^{-1} .

The sorted amplitude information can be displayed on a cathode-ray tube, either as a classical histogram, or as a cumulative display (the low energy channels count all events above the lower threshold rather than only those within the 1.2 dB band) on a linear or logarithmic scale. The classical histogram represents the number of events in a specific amplitude channel (up to a maximum of 1023, i.e. 2^{10}), against the channel within the 60 dB range. The cathode ray tube was photographed using a Polaroid instant camera at intervals during the tests and the time at which the photograph was taken was recorded as a blip on the load-deflection curve.

3.4 Finite element analysis

3.4.1 The anisotropic constant strain triangular element

The initial numerical analysis was carried out using a finite element program for the solution of two-dimensional stress problems. The original program was compiled by Cheung and King (=228), but was adapted to run on the Polytechnic IBM 1130, and subsequently the ICL 1903, and the coverage was extended to include problems involving composite materials by Hewson (=229). The program used the macroscopic (homogeneous rule-of-mixtures) properties of the anisotropic material in a system of constant

strain triangular elements. Provided that sufficient elements were used, satisfactory stress distributions could be determined, but an upper limit to the number of elements was imposed by the available in-core storage on the computer facility.

The stresses at each nodal point on the mesh were calculated as the sum of the stresses in all the elements immediately associated with that node, divided by the number of elements. The symmetry of the specimen was fully exploited to maximise the number of elements at the crack tip. Initially an extended mesh was examined, but it was found that at a finite distance from the crack, the stress values towards the edge remote from the crack were reasonably uniform, and thus those elements were freed to be used at the crack tip.

In order to make the large quantities of numerical data which were output more accessible, the nodal stresses were further processed. A program was written to calculate the stresses corresponding to the integer coordinates of the mesh and present them diagrammatically. Two modes of graphic representation were chosen. In the first the interpolation program also created a "relief map" by plotting the nodal stress values at regular intervals parallel to the crack, against a distorted rectangular frame such that the ends of each line were directly above (tension) or below (compression) the points at which they acted (figure 20). In the second representation, a standard geographic contouring package was used to draw the stress contour maps (figure 21).

3.4.2.1 The PAFEC 8-node anisotropic membrane subroutine (R36510)

This subroutine can analyse plane stress, plane strain or axisymmetric anisotropic problems by setting "ISN" = 0, 1, 2 respectively. If "NA" = 1 the fibre direction is assumed constant across each element. If "NA" = 2 a facility is included for calculating the material direction across elements idealising a portion of a ring where the fibres follow the ring contour. The radius of the ring must have an origin where the global x- and y-axis are zero. If the control integers NA and N are set to 1 and NEI to 9 (the Number of Extra Items stored with the first/every element in the series) the subroutine will solve the case of a single layer orthotropic plate. The data for each element are:

Card 1 — 8 node numbers — density

Card 2 $S_{11}, S_{12}, S_{22}, S_{66}, S_{13}, S_{23}, S_{33}$, thickness, theta.

Card 2 is read in E10.3 format, eight items per card.

S_{13} , S_{23} and S_{33} are only needed for plane strain calculations and should be set to zero if ISN = 0.

S_{11} is the inverse of E_{11} , the Youngs modulus in the major principal direction of the material.

S_{22} and S_{33} are the inverses of E_{22} and E_{33} respectively.

S_{11} and S_{22} are properties in the x-y plane, S_{33} is a property normal to the x-y plane.

Theta is the angle in degrees between the major principal direction (1) of the material and the global x-axis. Theta is measured positive from the global x-axis to the global y-axis. Theta is input as zero if NA = 2, and is recalculated in the element stressing routines.

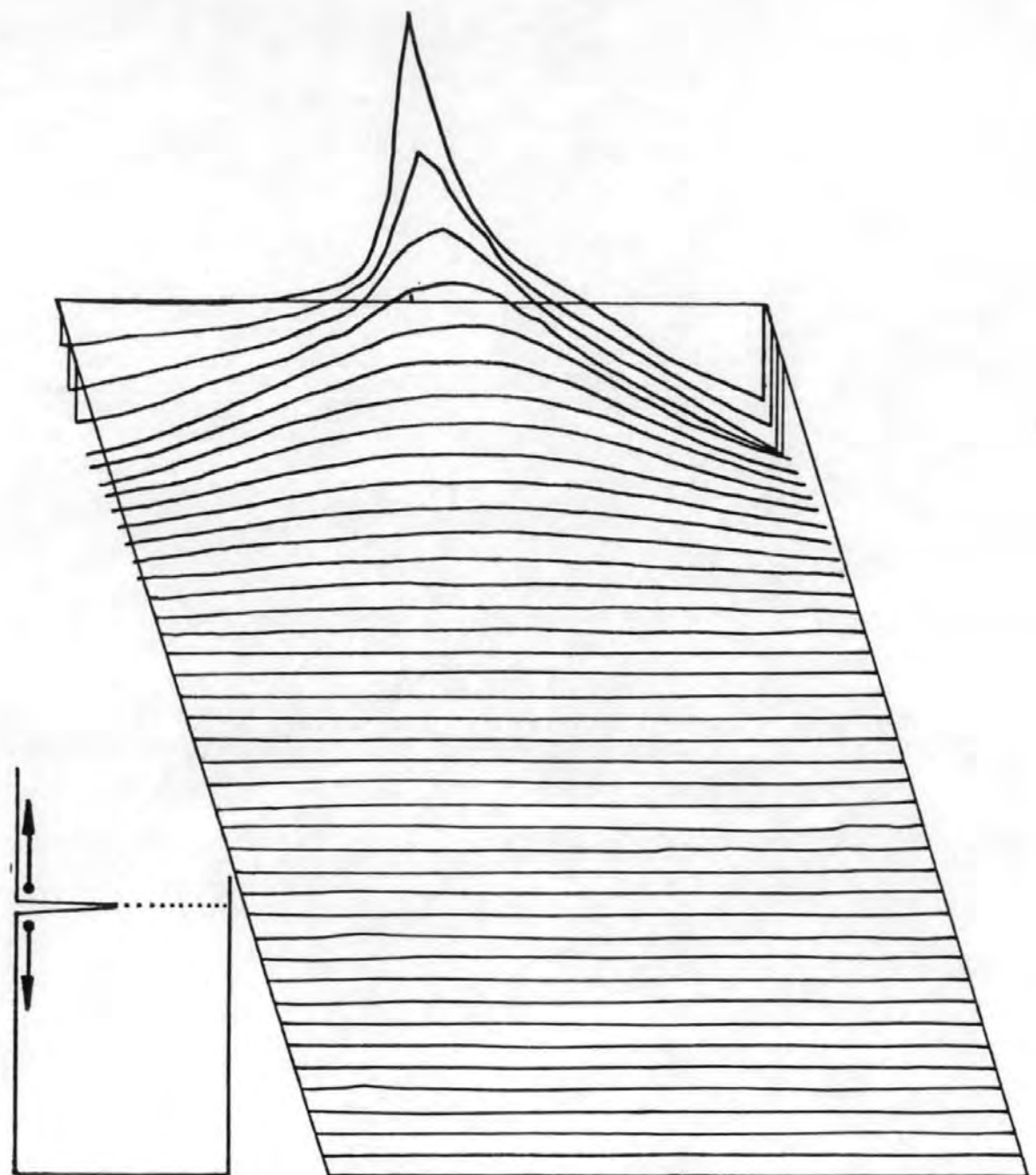


Figure 20: Relief map to illustrate the distribution of the stress field in a rectangular cantilever (inset) specimen of highly anisotropic ($E_{11}:E_{22} = 50:5$) material with a half width notch at the upper left corner.

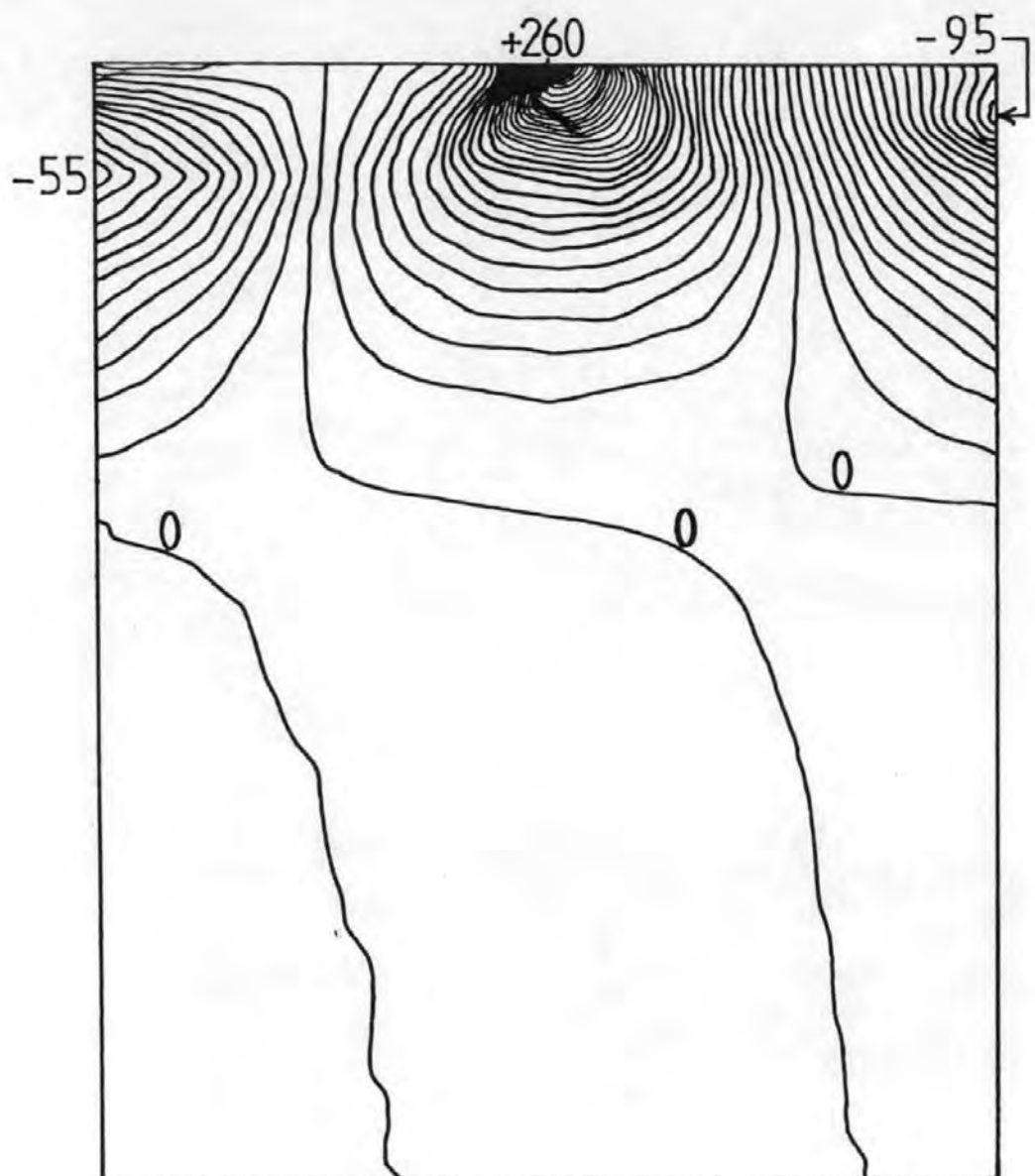


Figure 21: Contour map to illustrate the distribution of the stress field in a rectangular cantilever specimen of highly anisotropic material (the same data as for figure 20).

If the material is laminated, then N is set equal to the number of layers in the laminate and NEI is set to $9 + N$. S_{13} , S_{23} and S_{33} should be set to zero for laminated materials as the plane strain facility is not available. The angles in degrees between the 1 direction of each layer and the major principal direction of the laminate are included on the same card as "THETO", again in E10.3 format. Additional cards will automatically be read if there are nine or more layers. There is no provision in the element/stressing subroutines for more than 20 layers.

Each element is dealt with in turn in the element routine. If the density is -1, then it is assumed that the current element is identical in all respects (shape, size and material properties) to the previous element, although it may have a different position and orientation. There is therefore no need to recalculate the element stiffness matrix (NOTE: the PAFEC 70+ Handbook (page 1.23) simply states that the density must be less than zero). If the density is zero then the compliances, thicknesses and orientations are the same as for the previous element, but the geometry (size and shape) differs in such a manner that the stiffness matrix must be recomputed. This will include the case where the midside nodes are shifted to model a singularity. If the density is greater than zero then new material properties should be read in.

The stressing routine can handle up to five load cases simultaneously. For a larger number of cases certain arrays must be redimensioned. The element principal stresses are given and then transformed to the material principal directions.

3.4.2.2 Software modification for the R36510 element

In order to successfully run the calculations and to obtain plots of the stresses generated in the analysis of a finite element mesh with a discontinuity, a number of corrections and modifications to the PAFEC 70+ scheme were necessary. These are outlined below:

a) Henshell and Shaw (=203) have shown that a singularity occurs in isoparametric finite elements if the midside nodes are moved sufficiently from their normal position. By choosing the midside node positions so that the singularity occurs exactly at the corner of an element it was possible to obtain quite accurate solutions to the problem of determining the stress intensity at the tip of the crack. Henshell (=230) states that the four nodes nearest to the crack tip should be moved from the midside positions, so that they divide the element sides in the ratio 1:3, and were thus closer to the crack tip.

b) For problems with nodes displaced from the midside position, the PAFEC 70+ scheme detected this as an error and replaced them at the midside position in subroutine R25101. The use of a dummy subroutine R25101 in the job which read in the data from cards suppressed this, but immediately before calling R25101, the calling segment (R25100), wrote; "MIDSIDE NODE xx HAS BEEN MOVED TO BE EQUIDISTANT FROM CORNER NODES yy AND zz", on the line printer.

c) It was not uncommon for minor data errors to cause "FAILURE IN CHODET", the Choleski decomposition of the stiffness matrix in the element routine. The known solu-

tions to this are listed below:

- * Check that ID, IDT and IDF are as large as the highest degree of freedom number.
- * Check that no two nodes have the same number, or the same degree of freedom number.
- * Check the material properties, e.g. in R36510:

S_{11}	S_{12}	S_{22}	S_{66}
+0.500E-05	-0.170E-05	+0.100E-03	+0.242E-03
+0.200E-14	-0.540E-15	+0.360E-14	+0.100E-13
will both work while failure results using +.200E-14	-0.360E-14	+0.540E-15	+0.100E-13

d) For stress plotting it was necessary to declare a common array (A) in the element stressing job and in the draw job. The size of A was determined from

$$(IP * ILO * ISTEP + 5) - 1 + ((ISTEP * ILO) + 3) * IE$$

where ISTEP = 3, except when ISN \neq 0 and then ISTEP = 4.

- e) Where stressing was carried out in a separate job to the drawing of stress plots, it was necessary to write matrix A to a magnetic file, and read that file into the draw job. The subroutine R18000 executed rewind and end file when reading or writing data, and hence matrix A had to be written to a separate file.
- f) In order to conserve core in those jobs which did not require averaged nodal stresses, or drawings of the stresses, the extended version of R86510 was allocated a separate subroutine, R86520. This was essentially R86510, modified to include elements of R86004 and a call to R70600.
- g) In R86510 the call to R36505 converted BETA into radians before use but did not make the conversion back and therefore printed out a value of BETA in radians. This was also the angle of the principal stress to the material principal direction. In R86520, BETA was written as defined, and in degrees.
- h) When calculating an average value for BETA the subroutine R86004 altered the sign of BETA if the difference between the current value of BETA and the average of the previous values was greater than 160°. In R86520, when the difference was greater than 160°, the new value of BETA was set to "180 + BETA".
- i) Subroutines R86510 and R86520 work round the nodes of the element in the opposite way to isotropic element subroutine R86210.
- j) It was necessary to "CALL GRBEGIN" before "CALL R19000" in the draw job, otherwise CPU time was wasted and the job would "appear to loop". The libraries (SUBGROUP CCPR) and (SUBPLOTSNPLI) had to be declared in LIST in addition to those required by the handbook.
- k) XLNGTH and BRDTH in the draw data were in metres.
- l) The often repeated statement "CALL TO CRSET (NOSET = 1) MADE BUT IGNORED" can be removed from the printout by use of a dummy SUBROUTINE CRSET (I) without

affecting the output, in any other way.

- m) Because a number of subroutines in the current GHOST plotting routines were dummies, certain information (such as titles) did not appear on the graphic output.
- n) Three of the subroutines must not be overlaid, they are:

R11100; R14801; R18003.

3.4.2.3 The 8-node orthotropic curvilinear flat facet shell element (R44215)

The orthotropic PAFEC 70+ element, R36510, has been replaced in level 3.1 of the PAFEC 75 finite element scheme by the flat facet shell element R44215. The new element has a capability to analyse plane stress, plane strain membrane and bending problems. Two of the principal material planes must be in the plane of the element and the third principal material direction is irrelevant. Within each element the directions and properties are constant.

The data for the element is input in the following modules:

CRACK TIP (this requires use of a dummy routine DMATDI)

ELEMENTS

IN DRAW

LAMINATES

LOADS

NODES

ORTHOTROPIC MATERIAL

OUT DRAW

PLATES AND SHELLS

RESTRAINTS

Each element has five degrees of freedom ($u_x, u_y, u_z, \phi_x, \phi_y$) at the element level, but after transformation to a general shell the extra freedom (ϕ_z) is introduced. In terms of element axes, the matrices relating to the u_x, u_y displacements are exactly analogous to those used for the isotropic isoparametric plane strain element R36210. The bending matrices are based upon thin plate theory using an isoparametric transformation. All loads and the mass matrix are evaluated on a fully consistent basis.

For all the PAFEC 75 orthotropic elements the stresses are output in terms of the principal material directions. For all 2D and plate and shell elements with only one laminate layer the stresses are given on the top, neutral and bottom surfaces of the laminate. When more than one layer of laminate is present only the stresses in the $\sigma_{xx}, \sigma_{yy}, \sigma_{xy}$ directions on material axes are given and these are only output for the centre of each laminate. If stress output is required to show bending stresses in each laminate it is necessary to replace laminates by a number of sub-layers. This plate and shell analysis is not capable of giving interlaminar shear stresses — this requires a full three-dimensional stress analysis.

The graphics software used with the PAFEC 70+ scheme was modified to run on the

PRIME system in order to obtain stress contour plots of the results. The relevant software listings are included in Appendix 5.

3.5 Cryogenic testing

An annular chamber, 170 mm deep with an internal diameter of 180 mm and an external diameter of 200 mm, was constructed in stainless steel, see figure 22. This was enclosed in a jacket of free-foamed polyurethane resin, in order to reduce heat loss to the surroundings and to provide a free-standing support for the chamber. It was intended that a plug of high-elastic-modulus low-thermal-conductivity material would be included between the load cell and test rig. An alumina-filled epoxy resin was found to fulfil these requirements.

The temperature of the chamber was reduced by filling the annular space with liquid nitrogen through a plastic funnel in the polyurethane foam upper closure of the chamber. The internal temperature of the chamber was monitored using a ten-channel Comark 5335 digital thermometer with Cu/CuNi thermocouples. Figure 23 illustrates the dependence of the chamber temperature on the amount of liquid nitrogen consumed. The boiling point of liquid nitrogen at standard pressure is 77K, (-196 °C).

This portion of the test programme was abandoned because of a number of factors:

- change of programme emphasis towards structure/property relationships,
- problems acquiring the necessary quantity of alumina,
- stabilisation of chamber temperature was inadequate, and
- unexplained corrosion of materials in the vicinity of the working cryostat.

There was however an attempt to establish the effect of prior exposure of the materials to extreme cold by total immersion of the specimens in liquid nitrogen. These tests were divided into two main groups. The first group of specimens were immersed in two litres of liquid nitrogen in a polystyrene cylindrical container until the liquid nitrogen had completely evaporated, and were then allowed at least twenty-four hours at room temperature before testing. The second group of specimens were immersed in liquid nitrogen for one minute immediately prior to mechanical testing. A small third group was subjected to the same treatment as the first group except that they were sealed in a plastic bag to prevent contact between the liquid nitrogen and the plastic specimen.

3.6 Scanning electron microscopy

All scanning electron microscopy (SEM) work was done using the JELCO (Japan Electron Optics Laboratory Co, Inc.) JSM-35 unit in the Plymouth Polytechnic Department of Environmental Sciences. The fracture surfaces were vapour-coated with a thin gold layer, of up to 10 nm, in order to provide a conducting surface layer to enhance the image. Focusing was by a combination of the purely visual and by maximising the rise-and fall-slopes and the peaks of the contrast signal provided by the microscope for a single scan-line of the image.

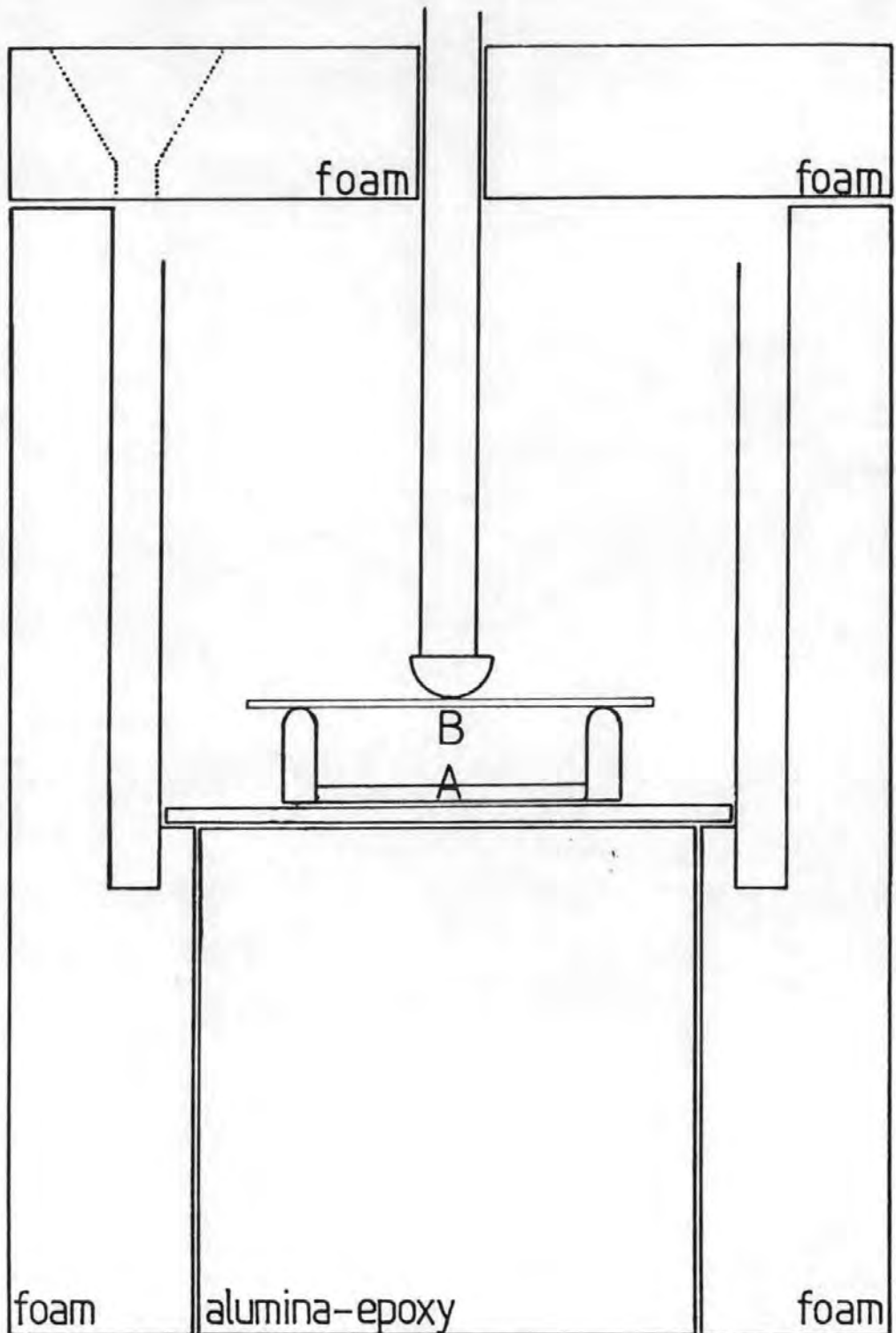


Figure 22: Illustration of the chamber developed for mechanical testing at cryogenic temperatures, showing the three-point flexure test rig in position, with the positions of thermocouples A and B marked.

All photographs were taken on Ilford HP4 film. It should be noted that the " μm " figure at the bottom of the photograph is an integral part of the SEM image and is hence independent of the enlargement of the photographic print. The magnification of the image, where shown, will be dependent on the photograph having been printed at a specific enlargement.

104

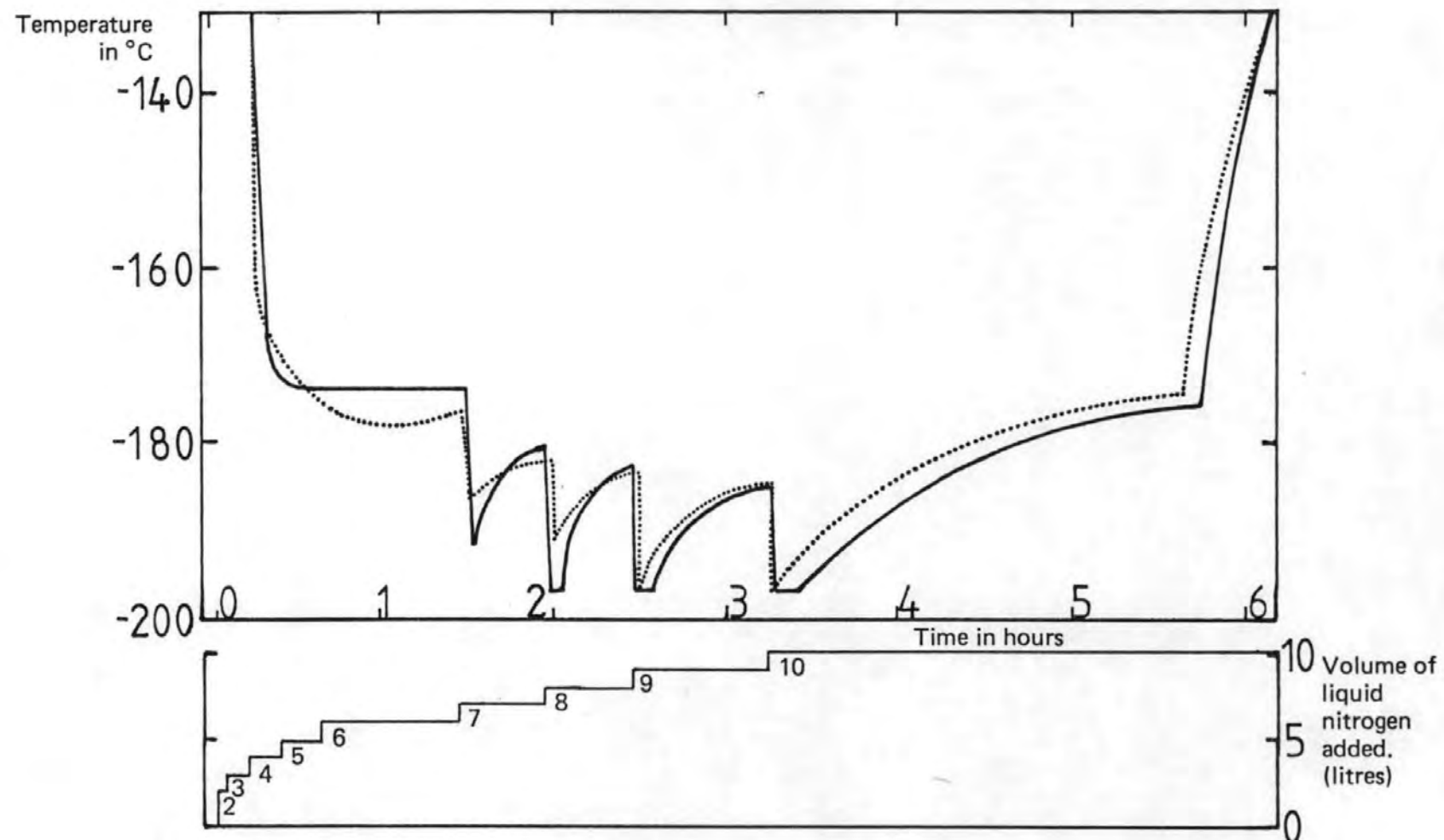


Figure 23: Temperature record plotted against time, with volume of liquid nitrogen used, at the base of the chamber (thermocouple A: solid line) and slightly above the chamber base in the approximate position of a test-piece (thermocouple B: dotted line).

4 Results

4.2 Results of mechanical tests

Table 5: Index to tables of mechanical property experimental results 1

Carbon fibre	XAS		EAS		EHMS	
	Date	Table number	Date	Table number	Date	Table number
Ambient history: ambient test	29.06.81 07.08.81	6 10	17.09.81 27.10.81	13 16	10.11.81 25.11.81	19 22
one cycle down to liquid nitrogen temp. and back to ambient	29.06.81 07.08.81	7 11	18.09.81 30.10.81	14 17	10.11.81 24.11.81	20 23
one cycle to LN2 temp enclosed in plastic bag	29.06.81 ****	8 ****	**** ****	**** ****	**** ****	**** ****
Tested immediately on removal from liquid nitrogen	29.06.81 07.08.81	9 12	18.09.81 30.10.81	15 18	10.11.81 25.11.81	21 24

Table 6: XAS carbon fibre hybrids, ambient tests

Ambient history : ambient test : Plymouth
Date: 29/06/81

Carbon fibres:

XAS Type XAS : 12k tow : batch no. 4LYA 317F 124

Glass fibres:

X Type YRF 23 47 : 2400 tex : product WY 6 41 : quote ref. IR 120 076 012

Resin system:

Scott Bader Crystic 272 : 1t catalyst M : 1x accelerator F

Load cell full scale:

50 kp

Crosshead speed:

0.00 cm/min

Chart speed:

5.00 cm/min

Bryans chart speed:

6.00 cm/min, i.e.: 10.00 sec/cm

Acoustic emission serial:

005 Courtesy of Ranco Controls

Transducer:

175 kHz resonance : model AC175L : serial no.1263 : preamplifier AECL 115

Acoustic emission gain:

60 dB

Acoustic emission full scale:

999

Acoustic emission filter A :

20 kHz - 100 kHz

Acoustic emission mode:

Counts

SJ & DJ are strength and deflection at major load drop

SX & DX are strength and deflection at maximum load

EJ & EX are respective elastic strains at failure

MOD is the flexural elastic modulus

AES & EK are the displacements at 5 and 1000 counts

**** Fine mix hybrid composite

MATERIAL TEST		DEPTH WIDTH						PROPERTIES			ACOUSTIC-EMISSION		
		mm	mm	SJ(MPa)	EJ(%)	DJ(mm)	SX(MPa)	EX(%)	DX(mm)	MOD(GPa)	AES(mm)	AEIK(mm)	
1	3PT-FLEX	2.25	5.07	1008.7	1.676	8.750	1072.9	1.783	9.583	60.2	2.33	5.83	
2	3PT-FLEX	2.29	5.06	948.2	1.326	6.500	945.6	1.479	9.917	63.9	2.25	3.92	
3	3PT-FLEX	2.16	5.09	782.9	1.374	7.083	1124.9	1.902	12.250	57.2	0.58	4.92	
**** Averaged values		879.9		1.492		7.444		1047.8		1.721		10.583	

**** Coarse mix hybrid composite

MATERIAL TEST		DEPTH WIDTH						PROPERTIES			ACOUSTIC-EMISSION		
		mm	mm	SJ(MPa)	EJ(%)	DJ(mm)	SX(MPa)	EX(%)	DX(mm)	MOD(GPa)	AES(mm)	AEIK(mm)	
1	3PT-FLEX	2.06	5.05	906.1	1.404	8.750	906.1	1.404	8.750	64.5	1.00	4.00	
2	3PT-FLEX	2.04	5.02	890.0	1.259	9.583	1008.3	1.426	10.917	70.7	0.75	2.92	
3	3PT-FLEX	2.04	5.01	1010.3	1.400	8.667	1010.3	1.400	8.667	72.1	0.42	2.81	
**** Averaged values		935.5		1.355		9.000		974.9		1.410		69.1	

**** Glass monofibre composite

MATERIAL TEST		DEPTH WIDTH						PROPERTIES			ACOUSTIC-EMISSION		
		mm	mm	SJ(MPa)	EJ(%)	DJ(mm)	SX(MPa)	EX(%)	DX(mm)	MOD(GPa)	AES(mm)	AEIK(mm)	
1	3PT-FLEX	2.54	5.05	1607.3	3.228	14.833	1618.2	3.249	15.917	47.8	1.33	7.17	
2	3PT-FLEX	2.25	5.05	1742.5	2.752	14.917	2020.7	2.872	16.167	70.6	0.50	9.24	
3	3PT-FLEX	2.44	5.17	1479.6	3.210	13.833	1544.6	3.351	14.917	46.1	1.75	9.71	
**** Averaged values		1476.5		3.063		14.361		1727.6		3.154		55.5	

**** Carbon monofibre composite

MATERIAL TEST		DEPTH WIDTH						PROPERTIES			ACOUSTIC-EMISSION		
		mm	mm	SJ(MPa)	EJ(%)	DJ(mm)	SX(MPa)	EX(%)	DX(mm)	MOD(GPa)	AES(mm)	AEIK(mm)	
1	3PT-FLEX	2.16	4.98	1130.6	1.714	8.750	1157.8	1.744	9.417	64.5	0.00	8.67	
2	3PT-FLEX	2.13	4.98	1140.7	1.676	8.917	1140.7	1.698	8.917	71.0	5.50	8.51	
3	3PT-FLEX	2.12	4.99	1296.1	1.868	7.667	1296.1	1.868	7.667	69.4	7.00	9.81	
**** Averaged values		1192.1		1.729		8.944		1178.9		1.739		67.0	

Table 7: XAS carbon fibre hybrids, one cycle to 77K

One cycle down to liquid nitrogen temperature : ambient temperature : Plymouth
 Date: 29/06/81

Carbon fibres: XAS Type XAS : 12k tow : batch no. 4LXA 317F 124
 Glass fibres: X Type YRF 23.47 : 2400 tex : product UK 6741 : quote ref 'P 120 072 012
 Resin system: Scott Bader Crystic 272 : 1% catalyst E : 1% accelerator E

Load cell full scale: 50 kN
 Crosshead speed: 0.50 cm/min
 Chart speed: 5.00 cm/min
 Bryans chart speed: 6.00 cm/min, i.e. 10.00 sec/cm

Acoustic emission serial: 015 Courtesy of Ranco Controls
 Transducer: 175 kHz resonance : model AC175L : serial no.1263 : preamplifier AEC' 115
 Acoustic emission gain: 60 dB
 Acoustic emission full scale: 999
 Acoustic emission filter A : 20 kHz - 100 kHz
 Acoustic emission mode: Counts

SJ & DJ are strength and deflection at major load drop
 SX & DX are strength and deflection at maximum load
 EJ & EX are respective elastic strains at failure
 MOD is the flexural elastic modulus
 AES & AEK are the displacements at 5 and 1000 counts

**** Fine mix hybrid composite

MATERIAL TEST	DEPTH	WIDTH	PROPERTIES						ACOUSTIC-EMISSION		
	mm	mm	SJ(MPa)	EJ(%)	DJ(mm)	SX(MPa)	EX(%)	DX(mm)	MOD(GPa)	AES(mm)	AE1K(mm)
1 SPT-FLEX	2.16	5.02	919.5	1.398	7.750	917.5	1.308	7.833	66.2	1.75	3.67
2 SPT-FLEX	2.11	5.02	889.9	1.393	7.503	926.7	1.451	8.250	63.9	0.75	3.52
3 SPT-FLEX	2.04	5.00	978.4	1.767	8.167	1006.7	1.819	11.167	56.4	2.42	7.01
**** Averaged values ****			929.2	1.516	8.167	951.0	1.552	9.083	61.8	1.47	4.71

**** Coarse mix hybrid composite

MATERIAL TEST	DEPTH	WIDTH	PROPERTIES						ACOUSTIC-EMISSION		
	mm	mm	SJ(MPa)	EJ(%)	DJ(mm)	SX(MPa)	EX(%)	DX(mm)	MOD(GPa)	AES(mm)	AE1K(mm)
1 SPT-FLEX	2.04	5.03	714.0	1.043	5.750	1079.4	1.576	11.333	64.5	1.50	3.77
2 SPT-FLEX	2.07	5.03	748.0	1.068	5.500	1075.6	1.536	11.500	70.0	0.33	3.00
3 SPT-FLEX	2.05	5.03	601.2	0.970	5.167	857.3	1.383	12.083	62.0	4.00	4.83
**** Averaged values ****			487.7	1.027	5.472	1004.1	1.400	11.630	66.8	1.94	3.87

**** Glass eight-tow monofibre composite

MATERIAL TEST	DEPTH	WIDTH	PROPERTIES						ACOUSTIC-EMISSION		
	mm	mm	SJ(MPa)	EJ(%)	DJ(mm)	SX(MPa)	EX(%)	DX(mm)	MOD(GPa)	AES(mm)	AE1K(mm)
1 SPT-FLEX	2.03	5.02	1410.0	2.645	16.667	1410.0	2.645	17.167	53.3	0.92	1.07
2 SPT-FLEX	2.05	5.02	1467.1	2.773	18.250	1461.5	2.762	18.917	52.9	0.67	10.31
3 SPT-FLEX	2.03	5.03	1408.0	2.691	18.167	1408.0	2.671	18.167	52.3	1.58	7.81
**** Averaged values ****			1428.6	2.703	17.604	1426.7	2.699	18.083	52.0	1.06	7.01

**** Carbon monofibre composite

MATERIAL TEST	DEPTH	WIDTH	PROPERTIES						ACOUSTIC-EMISSION		
	mm	mm	SJ(MPa)	EJ(%)	DJ(mm)	SX(MPa)	EX(%)	DX(mm)	MOD(GPa)	AES(mm)	AE1K(mm)
1 SPT-FLEX	2.08	4.97	722.4	1.023	5.167	733.4	1.030	5.750	71.6	3.29	4.92
2 SPT-FLEX	2.12	4.93	1136.6	1.541	7.833	1242.8	1.645	9.023	71.0	7.17	10.01
3 SPT-FLEX	2.07	4.97	963.7	1.245	6.667	963.7	1.246	6.667	77.4	3.08	5.01
**** Averaged values ****			940.0	1.270	6.556	980.0	1.323	7.167	73.4	4.44	6.97

One cycle down to liquid nitrogen temperature : bagged : ambient temperature : Plymouth
 Date: 29/06/81

Carbon fibres: XAS Type XAS : 12k tow : batch no. 41XA 317F 124
 Glass fibres: X Type XRE 23 47 : 2400 tex : product WX 641 : quote ref. IP 120 079 G12
 Resin system: Scott Bader Crystic 772 : 1% catalyst M : 1% accelerator E

Load cell full scale: 50 kg
 Crosshead speed: 0.50 cm/min
 Chart speed: 0.00 cm/min
 Bryans chart speed: 6.00 cm/min, i.e.: 10.00 sec/cm

Acoustic emission serial: 005 Courtesy of Ranco Controls
 Transducer: 175 kHz resonance : model AC175L : serial no.1263 : preamplifier AECL 105
 Acoustic emission gain: 60 dB
 Acoustic emission full scale: 999
 Acoustic emission filter A : 20 kHz - 100 kHz
 Acoustic emission mode: Counts

SJ & DJ are strength and deflection at major load drop
 SY & DY are strength and deflection at maximum load
 EJ & EX are respective elastic strains at failure
 MOD is the flexural elastic modulus
 AFS & AK are the displacements at 5 and 1000 counts

**** Fine mix hybrid composite

MATERIAL TEST		DEPTH WIDTH						PROPERTIES				ACOUSTIC-EMISSION			
		mm	mm SJ(MPa)	EJ(%)	DJ(mm)	SY(MPa)	LX(x)	DX(mm)	MOD(GPa)	AFS(mm)	AE5(mm)	AE1K(mm)			
1	3PT-FLEX	2.07	5.00	977.7	1.896	10.667	1021.7	1.982	12.750	51.6	3.58	7.05			
2	3PT-FLEX	2.17	5.01	783.1	1.106	6.003	848.0	1.197	8.917	70.8	1.33	3.92			
3	3PT-FLEX	2.06	5.02	922.5	1.743	9.667	1016.4	1.920	14.917	52.9	2.33	4.25			
**** Averaged values			894.5	1.582	8.806	962.0	1.700	12.194	50.4	2.42	5.0				

**** Coarse mix hybrid composite

MATERIAL TEST		DEPTH WIDTH						PROPERTIES				ACOUSTIC-EMISSION			
		mm	mm SJ(MPa)	EJ(%)	DJ(mm)	SY(MPa)	LX(x)	DX(mm)	MOD(GPa)	AFS(mm)	AE5(mm)	AE1K(mm)			
1	3PT-FLEX	2.13	4.94	918.9	1.448	9.917	1197.2	1.886	17.500	63.5	2.33	3.04			
2	3PT-FLEX	2.18	4.93	693.1	1.037	5.250	894.1	1.328	7.750	66.8	2.00	3.83			
3	3PT-FLEX	2.19	4.93	1035.2	1.503	7.250	1124.8	1.633	15.167	60.9	4.42	6.04			
**** Averaged values			882.4	1.329	7.472	1072.0	1.619	13.472	66.4	2.92	4.31				

**** Glass monofibre composite

MATERIAL TEST		DEPTH WIDTH						PROPERTIES				ACOUSTIC-EMISSION			
		mm	mm SJ(MPa)	EJ(%)	DJ(mm)	SY(MPa)	LX(x)	DX(mm)	MOD(GPa)	AFS(mm)	AE5(mm)	AE1K(mm)			
1	3PT-FLEX	2.02	5.03	1402.2	2.533	12.250	1466.1	2.649	14.917	55.3	0.42	8.07			
2	3PT-FLEX	2.45	5.04	1237.0	2.399	11.083	1345.7	2.610	13.167	51.6	0.17	6.83			
3	3PT-FLEX	2.41	5.04	1185.9	2.198	9.917	1318.6	2.444	13.000	54.0	0.25	7.24			
**** Averaged values			1275.0	2.377	11.083	1376.4	2.568	13.694	53.6	0.28	7.31				

**** Glass eight-tow monofibre composite

MATERIAL TEST		DEPTH WIDTH						PROPERTIES				ACOUSTIC-EMISSION			
		mm	mm SJ(MPa)	EJ(%)	DJ(mm)	SY(MPa)	LX(x)	DX(mm)	MOD(GPa)	AFS(mm)	AE5(mm)	AE1K(mm)			
1	3PT-FLEX	2.77	4.95	1233.2	3.577	16.500	1233.2	3.577	16.500	34.5	2.08	4.67			
2	3PT-FLEX	2.74	4.97	1204.0	3.097	13.500	1204.8	3.097	13.500	38.9	6.17	10.17			
3	3PT-FLEX	2.73	4.96	1273.4	3.424	15.417	1273.4	3.424	15.417	31.2	3.42	13.83			
**** Averaged values			1237.1	3.366	15.137	1237.1	3.366	15.137	36.9	3.89	9.57				

Table 8: XAS carbon fibre hybrids, one cycle to 77K, bagged

Tested immediately on removal from liquid nitrogen : Plymouth
 Immersion for 12 seconds(first) ; for 24 seconds(second) ; for 48 seconds(third)
 Date: 27/06/81

Carbon fibres: XAS Type XAS : 12k tow : batch no. 4LXA 317F 124
 Glass fibres: X Type XRE 23.47 : 2400 tex : product VX 6741 : quote ref 1A 120 076 012
 Resin system: Scott Bader Crystic 272 : 1% catalyst M : 1% accelerator L

Load cell full scale: 50 kg
 Crosshead speed: 0.50 cm/min
 Chart speed: 5.00 cm/min
 Myron chart speed: 6.00 cm/min; 1 in = 10.00 sec/cm

Acoustic emission serial: 005 Courtesy of Ranco Controls
 Transducer: 175 kHz resonance : model AC175L : serial no.1263 : preamplifier AEC' 150
 Acoustic emission gain: 60 dB
 Acoustic emission full scale: 799
 Acoustic emission filter A : 20 kHz - 100 kHz
 Acoustic emission mode: Counts

SJ & DJ are strength and deflection at major load drop
 SX & DX are strength and deflection at maximum load
 FJ & FX are respective elastic strains at failure
 MOD is the flexural elastic modulus
 AES & AEK are the displacements at 5 and 1000 counts

**** Fine mix hybrid composite

MATERIAL TEST		DEPTH WIDTH						PROPERTIES				ACOUSTIC-EMISSION				
		mm	mm	SJ(MPa)	EJ(t)	DJ(mm)	SX(MPa)	FJ(%)	DX(mm)	MOD(GPa)	AES(mm)	AEK(mm)				
1	3PT-FLEX	2.14	5.08	718.3	1.355	8.583	976.3	1.815	17.167	53.8	1.37	4.12				
2	3PT-FLEX	2.07	5.17	966.8	1.598	9.167	998.7	1.650	10.667	60.5	1.47	5.00				
3	3PT-FLEX	2.05	5.08	975.7	1.372	9.833	975.7	1.372	10.500	71.1	0.42	2.92				
**** Averaged values		886.7		1.435	9.194	983.5	1.612	12.778	61.8	1.07	4.04					

**** Coarse mix hybrid composite

MATERIAL TEST		DEPTH WIDTH						PROPERTIES				ACOUSTIC-EMISSION				
		mm	mm	SJ(MPa)	EJ(t)	DJ(mm)	SX(MPa)	FJ(%)	DX(mm)	MOD(GPa)	AES(mm)	AEK(mm)				
1	3PT-FLEX	2.13	5.12	1028.4	1.753	10.017	977.9	1.666	14.333	58.7	0.83	5.41				
2	3PT-FLEX	2.15	5.05	907.4	1.462	8.333	11n9.7	1.917	12.667	62.0	1.00	5.67				
3	3PT-FLEX	2.02	5.07	621.7	1.002	5.333	834.3	1.344	11.500	62.1	0.92	5.17				
**** Averaged values		852.5		1.406	8.104	1000.6	1.643	12.833	60.7	0.92	5.42					

**** Glass monofibre composite

MATERIAL TEST		DEPTH WIDTH						PROPERTIES				ACOUSTIC-EMISSION				
		mm	mm	SJ(MPa)	EJ(t)	DJ(mm)	SX(MPa)	FJ(%)	DX(mm)	MOD(GPa)	AES(mm)	AEK(mm)				
1	3PT-FLEX	2.44	5.19	1496.7	3.021	15.333	1485.3	2.998	16.583	42.5	1.33	8.01				
2	3PT-FLEX	2.43	5.15	1451.2	3.012	14.833	1474.4	3.000	16.583	46.2	0.75	6.51				
3	3PT-FLEX	2.41	5.17	799.5	1.607	7.417	791.6	1.571	7.833	40.8	0.92	5.71				
**** Averaged values		1249.1		2.547	12.528	1250.4	2.550	13.667	40.2	1.00	6.71					

**** Carbon monofibre composite

MATERIAL TEST		DEPTH WIDTH						PROPERTIES				ACOUSTIC-EMISSION				
		mm	mm	SJ(MPa)	EJ(t)	DJ(mm)	SX(MPa)	FJ(%)	DX(mm)	MOD(GPa)	AES(mm)	AEK(mm)				
1	3PT-FLEX	2.07	4.97	970.0	1.301	7.833	1020.7	1.464	9.833	60.7	2.75	4.31				
2	3PT-FLEX	2.13	5.00	928.6	1.429	7.417	1032.3	1.599	9.083	65.0	1.67	6.51				
3	3PT-FLEX	2.15	4.97	824.7	1.271	6.250	824.7	1.271	6.250	64.9	3.92	5.67				
**** Averaged values		907.0		1.363	7.167	959.3	1.441	8.307	66.5	2.78	5.5					

Table 9: XAS carbon fibre hybrids, tested cold

Ambient history : ambient test : Plymouth
 Date: 07/08/81

Carbon fibres: XAS Type XAS : 12k tow : batch no. 4LKA 317F 124
 Glass fibres: X Type XRE 23 47 : 2400 tex : product WY 6741 : quote ref 1A 120 D70 012
 Resin system: Scott Bader Cryslic 272 : 1% catalyst H : 1% accelerator U

Load cell full scale: 50 kN
 Crosshead speed: 0.10 cm/min
 Chart speed: 5.00 cm/min
 Dryans chart speed: 6.00 cm/min, i.e.: 10.00 sec/cm

Acoustic emission serial: 045 Courtesy of Ranco Controls
 Transducer: 175 kHz resonance : model AC175L : serial no.1263 : preamplifier AEC 105
 Acoustic emission gain: 60 dB
 Acoustic emission full scale: 999
 Acoustic emission filter A : 20 kHz - 100 kHz
 Acoustic emission mode: Counts

SJ & DJ are strength and deflection at major load drop
 SX & DX are strength and deflection at maximum load
 RJ & EX are respective elastic strains at failure
 HOD is the flexural elastic modulus
 AES & IK are the displacements at 5 and 1000 counts

**** Fine mix hybrid composite

MATERIAL TEST DEPTH WIDTH PROPERTIES								ACOUSTIC-EMISSION			
	mm	mm	SJ(MPa)	EJ(x)	DJ(mm)	SX(MPa)	EX(x)	DX(mm)	HOD(GPa)	AES(mm)	AE1K(mm)
1 SPT-FLEX	2.13	5.36	783.0	1.577	10.667	783.0	1.577	10.667	47.6	1.67	4.7
2 SPT-FLEX	2.15	5.13	908.2	1.529	8.417	908.2	1.529	8.417	50.4	0.58	4.67
3 SPT-FLEX	2.26	5.03	774.1	1.274	7.983	774.1	1.274	7.583	60.8	3.17	4.37
**** Averaged values ****		821.8	1.460	8.889	821.8	1.460	8.889	8.889	56.6	1.81	4.59

**** Coarse mix hybrid composite

MATERIAL TEST DEPTH WIDTH PROPERTIES								ACOUSTIC-EMISSION			
	mm	mm	SJ(MPa)	EJ(x)	DJ(mm)	SX(MPa)	EX(x)	DX(mm)	HOD(GPa)	AES(mm)	AE1K(mm)
1 SPT-FLEX	2.09	5.26	476.1	1.461	7.167	665.8	1.439	11.167	46.3	2.42	6.75
2 SPT-FLEX	2.10	5.25	889.5	1.940	13.667	874.2	1.907	14.000	45.8	2.08	8.97
3 SPT-FLEX	2.12	5.25	857.0	1.485	11.500	872.0	1.489	13.750	46.0	3.08	8.51
**** Averaged values ****		807.0	1.755	11.444	804.3	1.749	12.972	46.0	2.69	8.06	

**** Glass monofibre composite

MATERIAL TEST DEPTH WIDTH PROPERTIES								ACOUSTIC-EMISSION			
	mm	mm	SJ(MPa)	EJ(x)	DJ(mm)	SX(MPa)	EX(x)	DX(mm)	HOD(GPa)	AES(mm)	AE1K(mm)
1 SPT-FLEX	2.27	5.30	1465.1	3.053	16.750	1486.6	3.098	18.917	48.0	1.75	11.0
2 SPT-FLEX	2.32	5.35	1046.2	3.128	20.417	1046.2	3.128	20.417	33.4	3.25	7.67
3 SPT-FLEX	2.28	5.16	1623.2	3.042	14.000	1623.2	3.042	18.000	53.4	0.00	8.20
**** Averaged values ****		1378.2	3.074	18.387	1385.3	3.089	19.111	44.9	1.67	8.97	

**** Carbon monofibre composite

MATERIAL TEST DEPTH WIDTH PROPERTIES								ACOUSTIC-EMISSION			
	mm	mm	SJ(MPa)	EJ(x)	DJ(mm)	SX(MPa)	EX(x)	DX(mm)	HOD(GPa)	AES(mm)	AE1K(mm)
1 SPT-FLEX	2.04	5.12	266.5	1.664	7.750	828.4	1.426	10.003	57.1	4.42	8.5
2 SPT-FLEX	2.06	5.19	745.0	1.504	8.750	726.7	1.547	9.003	46.9	7.33	8.70
3 SPT-FLEX	2.00	5.10	921.5	1.777	10.333	921.5	1.779	10.333	51.8	2.50	8.47
**** Averaged values ****		878.7	1.679	9.611	825.5	1.584	9.833	57.3	4.75	8.56	

**** Extra-fine mix hybrid composite

MATERIAL TEST DEPTH WIDTH PROPERTIES								ACOUSTIC EMISSION			
	mm	mm	SJ(MPa)	EJ(x)	DJ(mm)	SX(MPa)	EX(x)	DX(mm)	HOD(GPa)	AES(mm)	AE1K(mm)
1 SPT-FLEX	2.06	5.17	745.6	1.240	5.917	729.5	1.147	6.917	61.7	0.90	5.21
2 SPT-FLEX	2.07	5.17	695.0	1.058	5.583	892.4	1.332	9.750	67.0	0.33	4.87
3 SPT-FLEX	2.07	5.19	644.2	0.765	5.000	700.0	1.166	4.750	61.9	0.17	5.0
**** Averaged values ****		695.0	1.071	5.510	805.0	1.227	7.472	7.472	5.17	0.17	5.0

Table 10: XAS carbon fibre hybrids, ambient tests

Table 11: XAS carbon fibre hybrids, one cycle to 77K

One cycle down to liquid nitrogen temperature : ambient temperature : Plymouth
 Date: 07:08:81

Carbon fibres: XAS Type XAS : 12k tow : batch no. ALXA 317F 129
 Glass fibres: X Type XRF 23.47 : 2400 tex : product UX 6541 : quote ref :B 120 0/2 D12
 Resin system: Scott Rader Cryslic 272 : 1% catalyst M : 1% accelerator C

Load cell full scale: 50 kg
 Crosshead speed: 0.50 cm/min
 Chart speed: 5.00 cm/min
 Bryans chart speed: 6.00 cm/min, i.e. 10.00 sec/cm

Acoustic emission serial: 005 Courtesy of Ranco Controls
 Transducer: 175 kHz resonance : model AC175L : serial no.1263 : preamplifier AECL 105
 Acoustic emission gain: 60 dB
 Acoustic emission full scale: 999
 Acoustic emission filter A : 20 kHz - 100 kHz
 Acoustic emission mode: Counts

SJ & DJ are strength and deflection at major load drop
 SX & DX are strength and deflection at maximum load
 EJ & EX are respective elastic strains at failure
 MOD is the flexural elastic modulus
 AES & AE1K are the displacements at 5 and 1000 counts

**** Fine mix hybrid composite

MATERIAL TEST	DEPTH	WIDTH	PROPERTIES						ACOUSTIC-EMISSION		
	mm	mm	SJ(MPa)	EJ(%)	DJ(mm)	SX(MPa)	EX(%)	DX(mm)	MOD(GPa)	AES(cm)	AE1K(cm)
1 SPT-FLEX	2.23	5.05	970.0	1.546	8.167	965.3	1.538	9.333	62.8	2.00	4.77
2 SPT-FLEX	2.22	5.15	811.4	1.418	7.667	811.4	1.418	7.667	57.2	1.92	5.17
3 SPT-FLEX	2.21	5.07	684.3	1.119	5.750	765.1	1.251	7.583	61.2	2.25	4.57
**** Averaged values ****			821.9	1.361	7.194	847.3	1.402	8.194	60.4	2.06	4.81

**** Coarse mix hybrid composite

MATERIAL TEST	DEPTH	WIDTH	PROPERTIES						ACOUSTIC-EMISSION		
	mm	mm	SJ(MPa)	EJ(%)	DJ(mm)	SX(MPa)	EX(%)	DX(mm)	MOD(GPa)	AES(cm)	AE1K(cm)
1 SPT-FLEX	2.25	5.07	596.0	0.765	4.667	596.0	0.765	5.833	77.9	0.33	1.97
2 SPT-FLEX	2.26	5.04	1243.4	1.606	9.750	1083.4	1.400	11.833	77.4	1.50	2.67
3 SPT-FLEX	2.29	5.02	1019.2	1.364	8.000	1148.0	1.538	16.667	74.7	1.50	2.57
**** Averaged values ****			952.9	1.245	7.472	942.8	1.234	11.444	76.7	1.11	2.37

**** Glass monofibre composite

MATERIAL TEST	DEPTH	WIDTH	PROPERTIES						ACOUSTIC-EMISSION		
	mm	mm	SJ(MPa)	EJ(%)	DJ(mm)	SX(MPa)	EX(%)	DX(mm)	MOD(GPa)	AES(cm)	AE1K(cm)
1 SPT-FLEX	2.45	5.30	1324.3	2.810	14.583	1320.6	2.811	14.917	47.0	0.67	6.97
2 SPT-FLEX	2.35	5.22	1369.6	2.025	15.250	1369.6	2.025	15.250	48.5	0.92	6.67
3 SPT-FLEX	2.39	5.25	1373.5	2.837	14.593	1400.9	2.896	17.083	48.4	0.42	1.77
**** Averaged values ****			1355.8	2.820	14.806	1363.7	2.844	15.750	47.9	0.67	6.11

**** Carbon monofibre composite

MATERIAL TEST	DEPTH	WIDTH	PROPERTIES						ACOUSTIC-EMISSION		
	mm	mm	SJ(MPa)	EJ(%)	DJ(mm)	SX(MPa)	EX(%)	DX(mm)	MOD(GPa)	AES(cm)	AE1K(cm)
1 SPT-FLEX	2.15	5.15	395.5	0.610	3.043	578.4	0.802	5.333	64.0	3.08	4.50
2 SPT-FLEX	2.21	5.16	647.1	0.975	5.667	621.0	0.952	6.167	65.2	3.50	5.20
3 SPT-FLEX	2.17	5.20	860.3	1.482	7.917	860.3	1.482	7.917	59.1	3.42	7.07
**** Averaged values ****			634.7	1.020	5.556	646.6	1.100	6.472	62.7	3.33	5.61

Table 12: XAS carbon fibre hybrids, tested cold

Tested immediately on removal from Liquid nitrogen : Plymouth
 Immersion for 60 seconds
 Date: 07:08:81

Carbon fibres: XAS Type XAS : 12k tow : batch no. 9LXA 317F 124
 Glass fibres: X Type XRE 23 47 : 2400 tex : product UX 6:41 : quote ref IR 120 070 012
 Resin system: Scott Bader Cryslic 272 : 1% catalyst M : 1% accelerator E

Load cell full scale: 50 kN
 Crosshead speed: 0.50 cm/min
 Chart speed: 5.00 cm/min
 Prysans chart speed: 6.00 cm/min, i.e.: 10.00 sec/cm

Acoustic emission serial: 005 Courtesy of Renco Controls
 Transducer: 175 kHz resonance : model AC175L : serial no.1263 : preamplifier AECL 105
 Acoustic emission gain: 60 dB
 Acoustic emission full scale: 799
 Acoustic emission filter A : 20 kHz - 100 kHz
 Acoustic emission mode: Counts

SJ & DJ are strength and deflection at major load drop
 SX & DX are strength and deflection at maximum load
 EJ & EX are respective elastic strains at failure
 MOD is the flexural elastic modulus
 AES & AEI are the displacements at 5 and 1000 counts

**** Fine mix hybrid composite
 MATERIAL TEST DEPTH WIDTH ***** PROPERTIES ***** ACOUSTIC-EMISSION
 mm mm SJ(MPa) EJ(%) DJ(mm) SX(MPa) EX(%) DX(mm) MOD(GPa) AES(mm) AEI(mm)
 1 SPT-FLEX 2.13 5.32 629.0 1.073 6.167 707.0 1.206 7.750 50.6 2.17 3.81
 2 SPT-FLEX 2.09 5.38 731.1 1.278 8.000 796.2 1.392 11.917 57.2 1.00 4.33
 3 SPT-FLEX 2.23 5.25 743.7 1.205 6.503 770.8 1.249 7.750 61.7 0.75 3.51
 **** Averaged values **** 701.3 1.186 6.917 750.0 1.282 9.139 50.2 1.31 3.81

**** Coarse mix hybrid composite
 MATERIAL TEST DEPTH WIDTH ***** PROPERTIES ***** ACOUSTIC-EMISSION
 mm mm SJ(MPa) EJ(%) DJ(mm) SX(MPa) EX(%) DX(mm) MOD(GPa) AES(mm) AEI(mm)
 1 SPT-FLEX 1.99 5.17 804.7 1.183 9.417 862.2 1.267 12.083 60.0 0.92 2.67
 2 SPT-FLEX 2.05 5.27 717.3 1.185 9.000 763.1 1.264 11.290 60.5 3.17 3.71
 3 SPT-FLEX 2.03 5.27 625.2 1.143 6.333 823.7 1.511 13.250 54.5 3.00 6.17
 **** Averaged values **** 715.1 1.170 8.250 817.0 1.347 12.174 61.0 2.36 4.11

**** Glass monofibre composite
 MATERIAL TEST DEPTH WIDTH ***** PROPERTIES ***** ACOUSTIC-EMISSION
 mm mm SJ(MPa) EJ(%) DJ(mm) SX(MPa) EX(%) DX(mm) MOD(GPa) AES(mm) AEI(mm)
 1 SPT-FLEX 2.45 5.15 1465.6 2.670 13.333 1484.7 2.705 14.083 50.0 5.58 10.17
 2 SPT-FLEX 2.35 5.25 1363.8 2.717 14.167 1355.7 2.708 14.417 50.2 1.08 7.31
 3 SPT-FLEX 2.33 5.25 1515.3 2.813 15.250 1523.6 2.820 16.000 53.0 2.58 10.67
 **** Averaged values **** 1448.2 2.733 14.250 1454.6 2.744 14.833 53.0 3.08 8.31

**** Carbon monofibre composite
 MATERIAL TEST DEPTH WIDTH ***** PROPERTIES ***** ACOUSTIC-EMISSION
 mm mm SJ(MPa) EJ(%) DJ(mm) SX(MPa) EX(%) DX(mm) MOD(GPa) AES(mm) AEI(mm)
 1 SPT-FLEX 2.20 5.15 982.0 1.503 8.333 982.0 1.502 8.333 65.3 2.00 5.67
 2 SPT-FLEX 2.15 5.06 955.9 1.267 6.333 955.0 1.267 6.333 75.4 3.25 7.31
 3 SPT-FLEX 2.23 5.20 896.5 1.645 8.917 896.5 1.645 8.917 50.5 4.83 6.17
 **** Averaged values **** 944.8 1.472 7.694 944.0 1.472 7.694 65.3 3.38 6.31

Table 13: EAS carbon fibre hybrids, ambient tests

Ambient history : Ambient test : Plymouth
 Date: 17/09/81

Carbon fibres: EAS Type EAS : 15k tow : batch no. EEA 105C : end no. 1445
 Glass fibres: Y Type XRE 23 47 : 2400 tex : product UX 6 41 : quote ref. IAB 120 675 012
 Resin system: Scott Bader Crystic 272 : 1% catalyst M : 1% accelerator C

Load cell full scale: 50 kN
 Crosshead speed: 0.50 mm/min
 Chart speed: 3.00 cm/min
 "Ryans chart speed: 6.00 cm/min, i.e. 10.00 sec/cm

Acoustic emission serial: 605 Courtesy of Ranco Controls
 Transducer: 175 kHz resonance : model AC175L : serial no. 1263 : preamplifier AECL 105
 Acoustic emission gain: 60 dB
 Acoustic emission full scale: 999
 Acoustic emission filter A : 20 kHz - 100 kHz
 Acoustic emission mode: Counts

SJ & DJ are strength and deflection at major load drop
 SX & DX are strength and deflection at maximum load
 FJ & EX are respective elastic strains at failure
 MOD is the flexural elastic modulus
 AES & 1K are the displacements at 5 and 1000 counts

*** Fine mix hybrid composite

MATERIAL TEST	DEPTH	WIDTH	PROPERTIES						ACOUSTIC-EMISSION		
	mm	mm SJ(MPa)	EJ(%)	DJ(mm)	SX(MPa)	EX(%)	DX(mm)	MOD(GPa)	AES(mm)	AE1K(mm)	
1 SPT-FLEX	2.23	4.75	1123.5	1.555	7.917	1123.5	1.555	7.917	72.2	0.17	5.57
2 SPT-FLEX	2.19	4.96	816.2	1.201	6.500	969.6	1.426	11.417	68.0	0.17	3.97
3 SPT-FLEX	2.23	5.02	867.4	1.219	6.167	1041.8	1.464	8.583	71.2	0.25	4.41
*** Averaged values	****	4.735.7	1.325	6.861	1044.9	1.482	9.306	72.5	0.19	4.61	

*** Coarse mix hybrid composite

MATERIAL TEST	DEPTH	WIDTH	PROPERTIES						ACOUSTIC-EMISSION		
	mm	mm SJ(MPa)	EJ(%)	DJ(mm)	SX(MPa)	FX(%)	DX(mm)	MOD(GPa)	AES(mm)	AE1K(mm)	
1 SPT-FLEX	2.06	5.10	1239.7	1.700	9.250	1359.4	1.864	11.083	72.9	1.25	6.82
2 SPT-FLEX	2.04	5.21	852.1	1.340	7.667	977.0	1.536	9.333	63.6	0.42	6.39
3 SPT-FLEX	2.02	5.16	1151.4	1.743	10.333	1196.1	1.811	15.250	66.1	0.50	6.03
*** Averaged values	****	1081.1	1.594	9.083	1177.5	1.737	11.889	67.5	0.72	6.39	

*** Glass monofibre composite

MATERIAL TEST	DEPTH	WIDTH	PROPERTIES						ACOUSTIC-EMISSION		
	mm	mm SJ(MPa)	EJ(%)	DJ(mm)	SX(MPa)	FX(%)	DX(mm)	MOD(GPa)	AES(mm)	AE1K(mm)	
1 SPT-FLEX	2.47	5.02	1613.8	3.017	15.750	1613.8	3.017	15.750	53.5	1.00	7.40
2 SPT-FLEX	2.51	4.98	1706.6	3.005	14.500	1714.1	3.010	15.917	56.8	0.17	7.47
3 SPT-FLEX	2.45	5.05	1688.8	3.059	15.167	1688.8	3.055	15.167	55.2	0.58	7.17
*** Averaged values	****	1669.7	3.027	15.139	1672.2	3.031	15.444	55.2	0.58	7.34	

*** Carbon monofibre composite

MATERIAL TEST	DEPTH	WIDTH	PROPERTIES						ACOUSTIC-EMISSION		
	mm	mm SJ(MPa)	EJ(%)	DJ(mm)	SX(MPa)	FX(%)	DX(mm)	MOD(GPa)	AES(mm)	AE1K(mm)	
1 SPT-FLEX	2.07	5.03	1525.3	1.753	10.003	1523.3	1.753	10.003	84.9	5.42	6.17
2 SPT-FLEX	2.04	5.01	1140.1	1.312	7.000	1456.2	1.676	10.003	86.9	5.92	6.01
3 SPT-FLEX	2.00	5.03	1292.6	1.423	7.500	1292.6	1.423	7.500	90.8	0.75	7.59
*** Averaged values	****	1318.7	1.496	8.194	1424.1	1.618	9.222	88.2	4.03	7.59	

One cycle down to liquid nitrogen temperature : ambient test : Plymouth
 Date: 1A:09:81

Carbon fibres: EAS Type EAS : 10k tow : batch no. EJA 105C : end no. 144R
 Glass fibres: X Type XRF 23 47 : 2400 tex : product VX 6'41 : quote ref 1P 120 076 012
 Resin system: Scott Dader Crysic 272 : 1% catalyst M : 1% accelerator E

Load cell full scale: 50 kg
 Crosshead speed: 0.50 cm/min
 Chart speed: 3.00 cm/min
 Pryans chart speed: 6.00 cm/min, i.e.: 10.00 sec/cm

Acoustic emission serial: 005 Courtesy of Ranco Controls
 Transducer: 175 kHz resonance : model AC175L : serial no.1263 : preamplifier AECL 105
 Acoustic emission gain: 60 dB
 Acoustic emission full scale: 900
 Acoustic emission filter A : 20 kHz - 100 kHz
 Acoustic emission mode: Counts

SJ & DJ are strength and deflection at major load drop
 SX & DX are strength and deflection at maximum load
 EJ & EX are respective elastic strains at failure
 MOD is the flexural elastic modulus
 AES & AEK are the displacements at 5 and 1000 counts

**** Fine mix hybrid composite

MATERIAL TEST		DEPTH WIDTH						PROPERTIES				ACOUSTIC-EMISSION			
		mm	mm	SJ(MPa)	EJ(%)	DJ(mm)	SX(MPa)	EX(%)	DX(mm)	MOD(GPa)	AES(mm)	AE1K(mm)			
1	3PT-FLEX	2.16	5.03	702.0	1.164	6.750	832.4	1.381	9.083	60.3	0.25	3.5%			
2	3PT-FLEX	2.20	5.03	942.6	1.555	7.667	1034.4	1.707	15.500	60.6	1.92	4.5%			
3	3PT-FLEX	2.13	5.06	753.5	1.126	5.750	917.6	1.372	12.500	64.9	1.83	5.2%			
**** Averaged values		799.4	1.282	7.389	928.1	1.486	12.361	62.6	1.33	4.4%					

**** Coarse mix hybrid composite

MATERIAL TEST		DEPTH WIDTH						PROPERTIES				ACOUSTIC-EMISSION			
		mm	mm	SJ(MPa)	EJ(%)	DJ(mm)	SX(MPa)	EX(%)	DX(mm)	MOD(GPa)	AES(mm)	AE1K(mm)			
1	3PT-FLEX	2.07	4.00	1238.3	1.720	7.583	1458.5	2.035	12.250	71.7	0.33	2.9%			
2	3PT-FLEX	2.07	5.05	1544.5	2.173	12.250	1544.5	2.172	12.503	71.1	0.17	9.0%			
3	3PT-FLEX	2.04	5.03	1321.1	1.899	10.250	1523.5	2.086	13.083	73.0	0.33	3.0%			
**** Averaged values		1368.0	1.903	10.604	1508.8	2.099	12.639	71.9	0.28	5.0%					

**** Glass monofibre composite

MATERIAL TEST		DEPTH WIDTH						PROPERTIES				ACOUSTIC-EMISSION			
		mm	mm	SJ(MPa)	EJ(%)	DJ(mm)	SX(MPa)	EX(%)	DX(mm)	MOD(GPa)	AES(mm)	AE1K(mm)			
1	3PT-FLEX	2.75	5.06	1528.4	2.966	11.917	1583.8	3.073	13.503	51.5	0.50	3.0%			
2	3PT-FLEX	2.75	5.04	1503.6	2.901	11.750	1630.2	3.146	14.167	51.8	0.67	4.7%			
3	3PT-FLEX	2.72	5.15	1318.8	2.775	11.500	1454.7	3.061	14.417	47.5	0.33	1.5%			
**** Averaged values		1450.3	2.881	11.722	1556.2	3.073	14.056	50.3	0.50	3.1%					

**** Carbon monofibre composite

MATERIAL TEST		DEPTH WIDTH						PROPERTIES				ACOUSTIC-EMISSION			
		mm	mm	SJ(MPa)	EJ(%)	DJ(mm)	SX(MPa)	EX(%)	DX(mm)	MOD(GPa)	AES(mm)	AE1K(mm)			
1	3PT-FLEX	2.10	4.05	1336.9	1.677	8.917	1336.7	1.677	8.917	70.7	5.0%	6.9%			
2	3PT-FLEX	2.17	4.06	1461.2	1.860	9.833	1461.2	1.960	9.833	74.5	5.0%	8.5%			
3	3PT-FLEX	2.18	4.04	1388.5	1.774	9.250	1388.5	1.774	9.250	70.3	0.83	0.9%			
**** Averaged values		1305.5	1.770	9.333	1395.6	1.770	9.333	70.8	5.67	6.1%					

Table 14: EAS carbon fibre hybrids, one cycle to 77K

Tested immediately on removal from liquid nitrogen : Plymouth
 Immersion for 60 seconds
 Date: 1P:09:81
 Carbon fibres: EAS Type EAS : 10k tow : batch no. LJA 1050 : end no. 1448
 Glass fibres: X Type XRC 23 47 : 2400 tex : product XH 641 : quote ref. IR 120 070 012
 Resin system: Scott Bader Crystic 272 : 1% catalyst F : 1% accelerator E

Load cell full scale: 50 kg
 Crosshead speed: 0.50 cm/min
 Chart speed: 3.00 cm/min
 Bryans chart speed: 6.00 cm/min, i.e.: 10.00 sec/cm
 Acoustic emission serial: 005 Courtesy of Ranco Controls
 Transducer: 175 kHz resonance : model AC175L : serial no.1263 : preamplifier ALCI 100
 Acoustic emission gain: 60 dB
 Acoustic emission full scale: 999
 Acoustic emission filter A : 20 kHz - 100 kHz
 Acoustic emission mode: Counts

SJ & DJ are strength and deflection at major load drop
 SX & DX are strength and deflection at maximum load
 EJ & EX are respective elastic strains at failure
 MOD is the flexural elastic modulus
 AES & AEK are the displacements at 5 and 1000 counts

**** Fine mix hybrid composite

MATERIAL TEST DEPTH WIDTH		PROPERTIES						ACOUSTIC-EMISSION			
mm	mm	SJ(MPa)	EJ(%)	DJ(mm)	SX(MPa)	EX(%)	CX(mm)	MOD(GPa)	AES(mm)	AE1K(mm)	
1 3PT-FLEX	2.35	5.00	862.7	1.462	7.667	984.1	1.667	9.667	50.0	0.92	4.31
2 3PT-FLEX	2.24	5.01	1189.4	1.684	9.083	1161.0	1.651	11.500	70.3	0.17	3.42
3 3PT-FLEX	2.27	4.97	909.8	1.341	6.917	1240.7	1.828	11.750	67.9	2.08	3.87
**** Averaged values	*****	985.6	1.495	7.722	1128.6	1.715	10.972	65.7	1.06	3.84	

**** Coarse mix hybrid composite

MATERIAL TEST DEPTH WIDTH		PROPERTIES						ACOUSTIC-EMISSION			
mm	mm	SJ(MPa)	EJ(%)	DJ(mm)	SX(MPa)	EX(%)	CX(mm)	MOD(GPa)	AES(mm)	AE1K(mm)	
1 3PT-FLEX	2.18	5.05	730.6	1.105	5.003	1039.5	1.572	9.167	66.1	4.00	5.17
2 3PT-FLEX	2.18	5.23	847.5	1.442	7.593	928.0	1.579	10.833	58.8	0.42	4.51
3 3PT-FLEX	2.15	5.15	1008.4	1.664	9.750	1028.2	1.697	11.417	60.6	1.08	4.92
**** Averaged values	*****	862.2	1.404	7.472	998.6	1.616	10.472	61.8	1.03	4.86	

**** Glass monofibre composite

MATERIAL TEST DEPTH WIDTH		PROPERTIES						ACOUSTIC-EMISSION			
mm	mm	SJ(MPa)	EJ(%)	DJ(mm)	SX(MPa)	EX(%)	CX(mm)	MOD(GPa)	AES(mm)	AE1K(mm)	
1 3PT-FLEX	2.53	5.05	1623.7	3.003	14.750	1623.7	3.003	14.750	54.1	0.25	10.5*
2 3PT-FLEX	2.59	4.95	1754.3	3.322	16.083	1754.3	3.522	16.083	52.8	0.17	6.5
3 3PT-FLEX	2.51	5.00	1565.3	2.973	13.917	1584.0	3.008	16.000	52.7	1.42	9.7*
**** Averaged values	*****	1647.8	3.079	14.917	1654.0	3.111	15.611	53.2	0.61	8.94	

**** Carbon monofibre composite

MATERIAL TEST DEPTH WIDTH		PROPERTIES						ACOUSTIC-EMISSION			
mm	mm	SJ(MPa)	EJ(%)	DJ(mm)	SX(MPa)	EX(%)	CX(mm)	MOD(GPa)	AES(mm)	AE1K(mm)	
1 3PT-FLEX	2.15	5.05	1295.7	1.827	9.833	1336.2	1.994	10.250	70.7	5.25	8.3*
2 3PT-FLEX	2.05	4.99	1386.1	1.803	10.083	1386.1	1.803	10.083	76.9	1.67	8.5
3 3PT-FLEX	2.12	4.97	1527.8	1.909	17.667	1527.8	1.907	16.667	80.0	3.50	9.0*
**** Averaged values	*****	1403.2	1.846	10.194	1416.7	1.805	10.333	74.0	2.47	8.61	

**** Carbon five-low monofibre composite

MATERIAL TEST DEPTH WIDTH		PROPERTIES						ACOUSTIC-EMISSION			
mm	mm	SJ(MPa)	EJ(%)	DJ(mm)	SX(MPa)	EX(%)	CX(mm)	MOD(GPa)	AES(mm)	AE1K(mm)	
1 3PT-FLEX	2.02	5.02	721.0	1.937	10.667	721.0	1.977	10.667	57.2	6.08	11.9*
2 3PT-FLEX	2.05	4.99	571.4	1.703	9.250	571.4	1.703	9.250	55.5	5.50	9.5
3 3PT-FLEX	2.07	4.94	745.0	2.023	11.250	745.0	2.033	11.250	56.7	7.50	10.8
**** Averaged values	*****	679.1	1.891	10.309	679.1	1.851	10.384	57.8	6.39	10.7*	

Table 15: EAS carbon fibre hybrids, tested cold

Table 16: EAS carbon fibre hybrids, ambient tests

Ambient history : ambient test : Plymouth
Date: 27/10/81

Carbon fibres: EAS Type EAS : 10k tow : batch no. EEA 105C : end no. 144P
Glass fibres: X Type XRE 23 47 : 2400 tex : product WY 6041 : quote ref. IA 120 070 012
Resin system: Scott Bader Crysic 272 : ix catalyst M : 1% accelerator C

Load cell full scale: 50 kN
Crosshead speed: 0.50 cm/min
Chart speed: 5.00 cm/min
Pryans chart speed: 6.00 cm/min, i.e.: 10.00 sec/cm

Acoustic emission serial: 005 Courtesy of Ranco Controls
Transducer: 175 kHz resonance : model AC175L : serial no.1263 : preamplifier AECL 100
Acoustic emission gain: 60 dB
Acoustic emission full scale: 999
Acoustic emission filter A : 20 kHz - 100 kHz
Acoustic emission mode: Counts

SJ & DJ are strength and deflection at major load drop
SX & DX are strength and deflection at maximum load
FJ & FX are respective elastic strains at failure
MOD is the flexural plastic modulus
AE5 & AE1K are the displacements at 5 and 1000 counts

**** Fine mix hybrid composite

MATERIAL TEST	DEPTH	WIDTH	PROPERTIES						ACOUSTIC-EMISSION		
	mm	mm	SJ(MPa)	EJ(%)	DJ(mm)	SX(MPa)	EX(%)	DX(mm)	MOD(GPa)	AE5(mm)	AE1K(mm)
1 SPT-FLEX	2.15	4.97	1055.2	1.493	8.417	1085.0	1.516	10.500	70.7	0.33	4.83
2 SPT-FLEX	2.18	4.96	1068.4	1.526	8.500	1098.3	1.545	11.000	70.0	0.33	4.75
3 SPT-FLEX	2.21	4.96	1156.1	1.654	8.583	1161.0	1.661	9.500	69.9	3.17	5.01
**** Averaged values	****	1093.2	1.558	8.500	1115.1	1.589	10.333	70.2	1.28	4.85	

**** Coarse mix hybrid composite

MATERIAL TEST	DEPTH	WIDTH	PROPERTIES						ACOUSTIC-EMISSION		
	mm	mm	SJ(MPa)	EJ(%)	DJ(mm)	SX(MPa)	EX(%)	DX(mm)	MOD(GPa)	AE5(mm)	AE1K(mm)
1 SPT-FLEX	2.16	4.95	1207.6	1.914	11.333	1207.6	1.914	11.333	63.1	1.92	4.83
2 SPT-FLEX	2.20	4.94	1353.5	1.989	10.333	1353.5	1.989	10.333	69.0	0.33	7.67
3 SPT-FLEX	2.17	4.95	1070.3	1.553	8.250	1252.1	1.816	10.250	64.7	0.83	7.02
**** Averaged values	****	1210.5	1.819	9.972	1271.1	1.907	10.639	66.7	1.03	6.51	

**** Glass monofibre composite

MATERIAL TEST	DEPTH	WIDTH	PROPERTIES						ACOUSTIC-EMISSION		
	mm	mm	SJ(MPa)	EJ(%)	DJ(mm)	SX(MPa)	EX(%)	DX(mm)	MOD(GPa)	AE5(mm)	AE1K(mm)
1 SPT-FLEX	2.42	5.06	1402.9	2.542	11.667	1474.2	2.671	13.667	55.2	0.83	9.51
2 SPT-FLEX	2.52	5.12	1429.6	2.679	12.417	1429.6	2.679	12.417	53.4	1.42	6.71
3 SPT-FLEX	2.53	5.06	1453.4	2.802	12.750	1533.1	2.956	15.250	51.9	0.67	8.91
**** Averaged values	****	1428.6	2.675	12.278	1477.0	2.769	13.778	53.5	0.97	8.39	

**** Carbon monofibre composite

MATERIAL TEST	DEPTH	WIDTH	PROPERTIES						ACOUSTIC-EMISSION		
	mm	mm	SJ(MPa)	FJ(%)	DJ(mm)	SX(MPa)	FX(%)	DX(mm)	MOD(GPa)	AE5(mm)	AE1K(mm)
1	2.05	4.74	1394.4	1.520	8.417	1394.4	1.520	8.417	91.2	***	***
2 SPT-FLEX	2.04	4.77	1246.0	1.324	7.167	1246.0	1.324	7.167	94.1	0.75	8.35
3 SPT-FLEX	2.03	4.76	1335.7	1.476	7.833	1335.7	1.476	7.833	93.7	1.00	7.01
**** Averaged values	****	1325.4	1.426	7.806	1325.4	1.426	7.806	93.0	0.88	8.17	

Table 17: EAS carbon fibre hybrids, one cycle to 77K

One cycle down to liquid nitrogen temperature : ambient test : Plymouth																				
Date:	30/10/81																			
Carbon fibres:	EAS Type CAS : 10k tow : batch no. E74 105C : end no. 144R																			
Glass fibres:	X Type TRE 23 47 : 2400 tex : product UX 6441 : quote ref 1A 120 070 012																			
Resin system:	Scott Bader Crysic 272 : 1% catalyst M : 1% accelerator F																			
Load cell full scale:	50 kg																			
Crosshead speed:	0.50 cm/min																			
Chart speed:	5.00 cm/min																			
Bryans chart speed:	6.00 cm/min, ie: 10.00 sec/cm																			
Acoustic emission serial:	005 Courtesy of Ranco Controls																			
Transducer:	175 kHz resonance : model AC175L : serial no.1263 : preamplifier AECL 105																			
Acoustic emission gain:	60 dB																			
Acoustic emission full scale:	920																			
Acoustic emission filter A :	20 kHz - 100 kHz																			
Acoustic emission mode:	Counts																			
SJ & DJ are strength and deflection at major load drop																				
SX & DX are strength and deflection at maximum load																				
RJ & EX are respective elastic strains at failure																				
MOD is the flexural elastic modulus																				
AES & EK are the displacements at 5 and 1000 counts																				
**** Fine mix hybrid composite																				
MATERIAL TEST DEPTH WIDTH PROPERTIES ACOUSTIC-EMISSION																				
mm mm SJ(MPa)	EJ(%)	DJ(mm)	SX(MPa)	LX(%)	DX(mm)	MOD(GPa)	AES(mm)	AEIK(mm)												
1 3PT-FLEX 2.24 5.03	490.1	0.756	5.167	704.1	0.976	5.750	72.2	0.08	2.70											
2 3PT-FLEX 2.25 5.03	725.6	1.008	5.167	739.4	1.027	5.917	72.0	0.08	3.17											
3 3PT-FLEX 2.25 5.03	781.0	1.050	5.417	781.0	1.050	5.417	74.4	0.17	3.00											
**** Averaged values ****	732.2	1.005	5.250	741.5	1.018	5.694	72.8	0.11	3.00											
**** Coarse mix hybrid composite																				
MATERIAL TEST DEPTH WIDTH PROPERTIES ACOUSTIC-EMISSION																				
mm mm SJ(MPa)	EJ(%)	DJ(mm)	SX(MPa)	LX(%)	DX(mm)	MOD(GPa)	AES(mm)	AEIK(mm)												
1 3PT-FLEX 2.05 4.99	1214.6	1.505	9.667	1214.6	1.505	8.667	80.7	0.17	4.00											
2 3PT-FLEX 2.08 4.97	1198.6	1.389	7.333	1198.6	1.389	13.500	86.3	0.25	5.42											
3 3PT-FLEX 2.06 4.97	1283.3	1.515	8.667	1394.9	1.647	10.833	84.7	0.25	6.83											
**** Averaged values ****	1232.2	1.470	8.222	1269.4	1.514	11.000	P3.9	0.22	5.44											
**** Glass monofibre composite																				
MATERIAL TEST DEPTH WIDTH PROPERTIES ACOUSTIC-EMISSION																				
mm mm SJ(MPa)	EJ(%)	DJ(mm)	SX(MPa)	LX(%)	DX(mm)	MOD(GPa)	AES(mm)	AEIK(mm)												
1 3PT-FLEX 2.27 5.30	1516.4	2.473	13.083	1584.9	2.585	15.043	61.3	0.08	2.00											
2 3PT-FLEX 2.33 4.98	1553.0	2.539	13.333	1553.0	2.539	13.333	61.2	0.33	5.42											
3 3PT-FLEX 2.27 4.77	1626.7	2.702	15.917	1626.7	2.702	15.917	60.2	0.23	9.24											
**** Averaged values ****	1565.7	2.571	14.111	1508.5	2.610	14.778	60.9	0.25	5.50											
**** Carbon monofibre composite																				
MATERIAL TEST DEPTH WIDTH PROPERTIES ACOUSTIC-EMISSION																				
mm mm SJ(MPa)	FJ(%)	DJ(mm)	SX(MPa)	LX(%)	DX(mm)	MOD(GPa)	AES(mm)	AEIK(mm)												
1 3PT-FLEX 2.00 4.06	1720.1	1.648	9.750	1720.1	1.648	9.750	104.4	4.23	8.00											
2 3PT-FLEX 2.00 4.97	1474.0	1.456	8.250	1474.0	1.456	8.250	101.2	4.33	8.17											
3 3PT-FLEX 2.01 4.27	1629.3	1.647	9.250	1629.3	1.647	8.250	97.0	0.42	8.97											
**** Averaged values ****	1607.8	1.589	9.003	1607.8	1.589	9.003	101.5	3.19	8.72											

Table 18: EAS carbon fibre hybrids, tested cold

Tested immediately on removal from liquid nitrogen : Plymouth
Immersion for 60 seconds
Date: 30/10/81

Carbon fibres: EAS Type EAS : 15k tow : batch no. E3A 105C : end no. 1440
Glass fibres: X Type XRE 23 47 : 2400 tex : product UX 6741 : quote ref. 18 120 0/0 012
Resin system: Scott Bader Crystic 272 : 1% catalyst M : 1% accelerator F

Load cell full scale: 50 kg
Crosshead speed: 0.50 cm/min
Chart speed: 5.00 cm/min
Bryans chart speed: 6.00 cm/min, i.e.: 10.00 sec/cm

Acoustic emission serial: 005 Courtesy of Ranco Controls
Transducer: 175 kHz resonance : model AC175L : serial no.1263 : preamplifier AFCI 100
Acoustic emission gain: 60 dB
Acoustic emission full scale: 000
Acoustic emission filter A: 20 kHz - 100 kHz
Acoustic emission mode: Counts

SJ & DJ are strength and deflection at major load drop
SX & DX are strength and deflection at maximum load
EJ & EX are respective elastic strains at failure
MOD is the flexural elastic modulus
AES & AEK are the displacements at 5 and 1000 counts

*** Fine mix hybrid composite

MATERIAL TEST	DEPTH	WIDTH	PROPERTIES						ACOUSTIC-EMISSION		
	mm	mm	SJ(MPa)	EJ(%)	DJ(mm)	SX(MPa)	EX(%)	DX(mm)	MOD(GPa)	AES(mm)	AE1K(mm)
1 SPT-FLEX	2.13	5.07	782.0	1.152	6.000	1033.4	1.921	10.000	67.9	0.17	2.5%
2 SPT-FLEX	2.20	4.09	1223.0	1.797	10.000	1291.2	1.882	11.167	66.2	0.75	4.0%
3 SPT-FLEX	2.17	5.04	1145.4	1.570	8.417	1145.4	1.570	8.417	73.0	0.17	4.5%
**** Averaged values	****	1050.4	1.505	R.13 ^a	1156.7	1.661	R.861	R.97	69.7	0.36	3.67

*** Coarse mix hybrid composite

MATERIAL TEST	DEPTH	WIDTH	PROPERTIES						ACOUSTIC-EMISSION		
	mm	mm	SJ(MPa)	EJ(%)	DJ(mm)	SX(MPa)	EX(%)	DX(mm)	MOD(GPa)	AES(mm)	AE1K(mm)
1 SPT-FLEX	2.03	5.10	761.5	1.141	6.500	1063.9	1.593	16.917	66.8	1.42	6.7%
2 SPT-FLEX	2.04	5.22	1059.9	1.648	9.750	1072.6	1.682	10.250	67.8	0.75	6.67
3 SPT-FLEX	2.05	5.17	942.4	1.314	7.417	1077.8	1.503	9.250	71.7	1.75	5.00
**** Averaged values	****	918.3	1.368	R.889	1071.9	1.593	R.13 ^a	R.74	67.4	1.31	6.1%

*** Glass monofibre composite

MATERIAL TEST	DEPTH	WIDTH	PROPERTIES						ACOUSTIC-EMISSION		
	mm	mm	SJ(MPa)	EJ(%)	DJ(mm)	SX(MPa)	EX(%)	DX(mm)	MOD(GPa)	AES(mm)	AE1K(mm)
1 SPT-FLEX	2.49	5.32	1731.7	3.004	14.750	1743.0	3.023	15.333	57.6	0.25	12.3%
2 SPT-FLEX	2.50	5.02	1597.0	2.806	15.167	1642.0	2.885	14.750	50.9	0.50	10.7%
3 SPT-FLEX	2.47	5.01	1405.1	2.604	11.833	1629.0	2.856	14.750	57.0	1.50	10.5%
**** Averaged values	****	1604.7	2.804	R.25 ^a	1671.6	2.921	R.944	R.72	57.2	0.75	11.2%

*** Carbon monofibre composite

MATERIAL TEST	DEPTH	WIDTH	PROPERTIES						ACOUSTIC-EMISSION		
	mm	mm	SJ(MPa)	EJ(%)	DJ(mm)	SX(MPa)	EX(%)	DX(mm)	MOD(GPa)	AES(mm)	AE1K(mm)
1 SPT-FLEX	2.02	4.03	1576.0	1.638	9.250	1648.0	1.713	10.093	96.2	0.33	7.0%
2 SPT-FLEX	2.06	4.05	1538.1	1.757	9.750	1538.1	1.757	9.740	87.6	0.75	8.3%
3 SPT-FLEX	2.05	4.05	1405.1	1.723	9.667	1651.3	1.773	10.250	93.1	1.25	9.5%
**** Averaged values	****	1573.2	1.706	R.556	1617.5	1.749	R.028	R.23	97.0	0.70	8.0%

Ambient history : ambient test : Plymouth
 Date: 10/11/81

Carbon fibres: EHMS Type EHMS : 1.0k tow : batch no. E2M 2570 : end no. 284
 Glass fibres: X Tyne XRE 23 47 : 2400 tex : product WX 6741 : quote ref. IR 120 070 012
 Resin system: Scott Bader Crystic 272 : 1% catalyst H : 1% accelerator E

Load cell full scale: 50 kg
 Crosshead speed: 0.50 cm/min
 Chart speed: 5.00 cm/min
 Oryans chart speed: 6.00 cm/min, i.e. 10.00 sec/cm

Acoustic emission serial: 005 Courtesy of Ranco Controls
 Transducer: 175 kHz resonance : model AC175L : serial no. 1263 : preamplifier AEC 110
 Acoustic emission gain: 60 dB
 Acoustic emission full scale: 999
 Acoustic emission filter A : 20 kHz - 100 kHz
 Acoustic emission mode: Counts

SJ & DJ are strength and deflection at major load drop

SX & DX are strength and deflection at maximum load

FJ & EX are respective elastic strains at failure

MOD is the flexural elastic modulus

AES & AE1K are the displacements at 5 and 1000 counts

**** Fine mix hybrid composite

MATERIAL TEST DEPTH WIDTH		PROPERTIES						ACOUSTIC-EMISSION			
mm	mm	SJ(MPa)	EJ(%)	DJ(mm)	SX(MPa)	EX(%)	DX(mm)	MOD(GPa)	AES(mm)	AE1K(mm)	
1 SPT-FLEX	2.25	5.02	574.2	0.677	3.583	597.3	0.704	3.833	84.9	0.92	2.25
2 SPT-FLEX	2.21	4.97	659.3	0.771	4.500	673.9	0.788	4.833	85.6	1.42	2.67
3 SPT-FLEX	2.21	4.97	649.6	0.724	3.917	703.0	0.784	5.167	69.7	0.08	2.33
**** Averaged values	*****	627.7	0.724	4.000	658.1	0.758	4.611	86.7	0.81	2.42	

**** Coarse mix hybrid composite

MATERIAL TEST DEPTH WIDTH		PROPERTIES						ACOUSTIC-EMISSION			
mm	mm	SJ(MPa)	EJ(%)	DJ(mm)	SX(MPa)	EX(%)	DX(mm)	MOD(GPa)	AES(mm)	AE1K(mm)	
1 SPT-FLEX	2.41	4.97	721.6	1.160	5.667	811.3	1.315	8.333	62.2	2.83	4.91
2 SPT-FLEX	2.15	4.97	901.5	1.076	5.917	886.2	1.058	8.083	83.8	1.25	5.21
3 SPT-FLEX	2.17	4.97	698.9	0.829	4.250	849.8	1.008	5.750	84.3	0.17	3.89
**** Averaged values	*****	774.0	1.022	5.278	849.1	1.123	7.389	76.8	1.42	4.31	

**** Glass monofibre composite

MATERIAL TEST DEPTH WIDTH		PROPERTIES						ACOUSTIC-EMISSION			
mm	mm	SJ(MPa)	EJ(%)	DJ(mm)	SX(MPa)	EX(%)	DX(mm)	MOD(GPa)	AES(mm)	AE1K(mm)	
1 SPT-FLEX	2.50	5.00	1634.3	2.862	13.917	1715.4	3.000	15.417	57.1	1.17	9.01
2 SPT-FLEX	2.51	4.99	1587.2	2.759	13.417	1677.0	2.915	16.083	57.5	0.67	7.17
3 SPT-FLEX	2.51	5.00	1867.7	3.253	16.917	1867.7	3.252	16.917	57.4	0.42	10.42
**** Averaged values	*****	1696.5	2.950	14.750	1752.8	3.056	16.139	57.4	0.75	8.81	

**** Carbon monofibre composite

MATERIAL TEST DEPTH WIDTH		PROPERTIES						ACOUSTIC-EMISSION			
mm	mm	SJ(MPa)	EJ(%)	DJ(mm)	SX(MPa)	EX(%)	DX(mm)	MOD(GPa)	AES(mm)	AE1K(mm)	
1 SPT-FLEX	2.27	4.94	966.2	0.618	4.500	966.2	0.918	4.500	105.3	2.67	4.51
2 SPT-FLEX	2.14	4.95	695.6	0.732	3.833	695.6	0.732	3.833	95.0	2.33	3.41
3 SPT-FLEX	1.90	4.96	828.1	0.663	3.833	828.1	0.663	3.833	124.9	1.58	3.81
**** Averaged values	*****	830.2	0.771	4.056	830.0	0.771	4.056	105.4	2.19	3.94	

Table 19: EHMS carbon fibre hybrids, ambient tests

One cycle down to liquid nitrogen temperature : ambient test : Plymouth
 Date: 10:11:81

Carbon fibres: EHMS Type EHMS : 10k tow : batch no. F2M 257D : end no. 2RA
 Glass fibres: X Type XRE 23 97 : 2900 tex : product UX 6/41 : quote ref IR 126 07C 012
 Resin system: Scott Bader Crystic 272 : 1% catalyst H : 1% accelerator E

Load cell full scale: 50 kN
 Crosshead speed: 0.50 cm/min
 Chart speed: 5.00 cm/min
 Bryans chart speed: 6.00 cm/min, i.e.: 10.00 sec/cm

Acoustic emission serial: 005 Courtesy of Ranco Controls
 Transducer: 175 kHz resonance : model AC175L : serial no.1263 : preamplifier AECL 105
 Acoustic emission gain: 60 dB
 Acoustic emission full scale: 999
 Acoustic emission filter A : 20 kHz - 100 kHz
 Acoustic emission mode: Counts

SJ & DJ are strength and deflection at major load drop
 SX & DX are strength and deflection at maximum load
 EJ & EX are respective elastic strains at failure
 MOD is the flexural elastic modulus
 AES & AEK are the displacements at 5 and 1000 counts

**** Fine mix hybrid composite
 MATERIAL TEST DEPTH WIDTH PROPERTIES ACOUSTIC-EMISSION

	mm	mm	SJ(MPa)	EJ(%)	DJ(mm)	SX(MPa)	EX(%)	DX(mm)	MOD(GPa)	AES(mm)	AE1K(mm)	
1	SPT-FLEX	2.25	5.03	665.5	0.865	5.417	665.5	0.865	5.417	76.9	0.92	3.08
2	SPT-FLEX	2.18	5.02	453.8	0.577	3.167	665.9	0.847	6.250	78.6	0.42	2.21
3	SPT-FLEX	2.21	5.00	576.5	0.737	3.917	483.6	0.871	9.167	78.5	0.25	2.47
**** Averaged values			565.9	0.726	4.167	671.7	0.861	6.944	78.0	0.53	2.50	

**** Coarse mix hybrid composite
 MATERIAL TEST DEPTH WIDTH PROPERTIES ACOUSTIC-EMISSION

	mm	mm	SJ(MPa)	EJ(%)	DJ(mm)	SX(MPa)	EX(%)	DX(mm)	MOD(GPa)	AES(mm)	AE1K(mm)	
1	SPT-FLEX	2.16	4.70	734.4	0.806	4.500	810.4	0.889	7.573	91.1	0.17	2.57
2	SPT-FLEX	2.08	4.75	494.6	0.532	3.500	906.7	0.989	9.750	91.7	0.42	1.51
3	SPT-FLEX	2.15	4.74	618.4	0.745	4.583	850.3	1.025	8.917	83.0	0.25	2.33
**** Averaged values			615.8	0.697	4.194	855.8	0.968	8.750	88.6	0.28	2.13	

**** Glass monofibre composite
 MATERIAL TEST DEPTH WIDTH PROPERTIES ACOUSTIC-EMISSION

	mm	mm	SJ(MPa)	EJ(%)	DJ(mm)	SX(MPa)	EX(%)	DX(mm)	MOD(GPa)	AES(mm)	AE1K(mm)	
1	SPT-FLEX	2.54	4.79	1593.8	2.945	14.093	1659.5	3.067	15.750	54.1	0.50	3.5
2	SPT-FLEX	2.50	4.77	1715.5	3.237	15.917	1715.5	3.237	15.917	53.0	0.25	3.33
3	SPT-FLEX	2.60	4.77	1660.3	3.171	14.917	1705.8	3.258	15.417	52.4	1.58	2.33
**** Averaged values			1656.5	3.118	14.972	1673.6	3.187	15.674	52.2	0.78	3.31	

**** Carbon monofibre composite
 MATERIAL TEST DEPTH WIDTH PROPERTIES ACOUSTIC-EMISSION

	mm	mm	SJ(MPa)	EJ(%)	DJ(mm)	SX(MPa)	EX(%)	DX(mm)	MOD(GPa)	AES(mm)	AE1K(mm)	
1	SPT-FLEX	1.96	4.05	1113.9	0.712	5.003	1113.9	0.912	5.083	122.1	3.33	5.67
2	SPT-FLEX	2.00	4.05	1242.2	0.998	6.167	1242.2	0.998	6.167	124.5	0.25	6.17
3	SPT-FLEX	2.21	4.96	966.7	0.880	4.417	966.7	0.898	4.417	108.6	0.25	4.67
**** Averaged values			1107.6	2.933	5.222	1107.6	0.933	5.222	118.4	1.28	5.5	

Table 20: EHMS carbon fibre hybrids, one cycle to 77K

Table 21: EHMS carbon fibre hybrids, tested cold

Tested immediately on removal from liquid nitrogen : Plymouth
Immersion for 60 seconds
Date: 17/11/81

Carbon fibres: EHMS Type EHMS : 16k tow : batch no. F2M 2570 : end no. 284
Glass fibres: X Type YRE 23 47 : 2400 tex : product UX 6741 : quote ref 18 120 070 012
Resin system: Scott Bader Crystic 272 : 1% catalyst M : 1% accelerator F

Load cell full scale: 50 kN
Crosshead speed: 0.50 cm/min
Chart speed: 5.00 cm/min
Bryans chart speed: 6.00 cm/min, ie: 10.00 sec/cm

Acoustic emission serial: 005 Courtesy of Ranco Controls
Transducer: 175 kHz resonance : model AC175L : serial no.1263 : preamplifier AECL 105
Acoustic emission gain: 60 dB
Acoustic emission full scale: 999
Acoustic emission filter A : 20 kHz - 100 kHz
Acoustic emission mode: Counts

SJ & DJ are strength and deflection at major load drop
Sx & Dx are strength and deflection at maximum load
FJ & FX are respective elastic strains at failure
MOD is the flexural elastic modulus
AES & AE1 are the displacements at 5 and 1000 counts

**** Fine mix hybrid composite

MATERIAL TEST DEPTH WIDTH		PROPERTIES						ACOUSTIC-EMISSION		
mm	mm	SJ(MPa)	FJ(%)	DJ(mm)	SX(MPa)	FX(%)	Dx(mm)	MOD(GPa)	AES(mm)	AE1(mm)
1 3PT-FLEX	2.25	4.97	743.7	0.876	4.250	743.7	0.876	4.500	84.9	0.93
2 3PT-FLEX	2.25	5.00	716.0	0.831	4.417	767.1	0.890	4.917	86.2	2.08
3 3PT-FLEX	2.20	4.99	629.8	0.747	4.250	771.4	0.915	6.333	84.3	0.75
**** Averaged values	****	626.5	0.818	4.306	760.7	0.894	5.250	85.1	1.22	3.1

**** Coarse mix hybrid composite

MATERIAL TEST DEPTH WIDTH		PROPERTIES						ACOUSTIC-EMISSION		
mm	mm	SJ(MPa)	FJ(%)	DJ(mm)	SX(MPa)	FX(%)	Dx(mm)	MOD(GPa)	AES(mm)	AE1(mm)
1 3PT-FLEX	2.07	4.96	808.4	0.796	4.417	1096.3	1.079	9.833	101.6	1.42
2 3PT-FLEX	2.06	4.97	853.7	0.852	4.750	1015.5	1.025	7.750	99.1	0.17
3 3PT-FLEX	2.10	4.97	837.6	0.915	4.750	998.7	1.092	8.500	91.5	0.50
**** Averaged values	****	833.2	0.858	4.639	1036.8	1.065	8.694	97.4	0.69	3.2

**** Glass monofibre composite

MATERIAL TEST DEPTH WIDTH		PROPERTIES						ACOUSTIC-EMISSION		
mm	mm	SJ(MPa)	FJ(%)	DJ(mm)	SX(MPa)	FX(%)	Dx(mm)	MOD(GPa)	AES(mm)	AE1(mm)
1 3PT-FLEX	2.50	5.25	1542.2	2.81%	13.250	1689.2	3.083	16.250	54.8	0.50
2 3PT-FLEX	2.50	5.02	1725.3	3.11%	15.833	1729.1	3.12%	16.003	55.3	0.75
3 3PT-FLEX	2.47	5.00	1766.0	3.12%	16.167	1766.0	3.12%	16.167	56.5	0.17
**** Averaged values	****	1678.1	3.021	15.083	1728.4	3.11%	16.167	51.5	0.47	0.0

**** Carbon monofibre composite

MATERIAL TEST DEPTH WIDTH		PROPERTIES						ACOUSTIC-EMISSION		
mm	mm	SJ(MPa)	FJ(%)	DJ(mm)	SX(MPa)	FX(%)	Dx(mm)	MOD(GPa)	AES(mm)	AE1(mm)
1 3PT-FLEX	2.06	4.93	1091.2	0.927	5.000	1091.2	0.927	5.000	117.7	0.58
2 3PT-FLEX	2.17	4.93	1094.9	0.936	4.750	1094.9	0.936	4.750	117.0	1.22
3 3PT-FLEX	2.02	4.94	AB7.4	0.736	4.000	945.0	0.784	4.250	120.6	2.25
**** Averaged values	****	1024.5	0.866	4.593	1044.0	0.882	4.667	116.4	1.59	4.81

Ambient history : ambient test : Plymouth
Date: 25/11/81

Carbon fibres: EHMS Type EHMS : 1fk tow : batch no. F2M 2570 : end no. 2NA
Glass fibres: X Type XRE 23 47 : 2400 tex : product UX 6'41 : quote ref 18 120 07n 012
Resin system: Scott Bader Crystic 272 : 1% catalyst H : 1% accelerator F

Load cell full scale: 50 kg
Crosshead speed: 0.50 cm/min
Chart speed: 5.00 cm/min
Dyans chart speed: 6.00 cm/min, i.e.: 10.00 sec/cm

Acoustic emission serial: 005 Courtesy of Ranco Controls
Transducer: 175 kHz resonance : model AC175L : serial no.1263 : preamplifier AECI 100
Acoustic emission gain: 6.9 dB
Acoustic emission full scale: 999
Acoustic emission filter A: 20 kHz - 100 kHz
Acoustic emission mode: Counts

SJ & DJ are strength and deflection at major load drop
SX & DX are strength and deflection at maximum load
EJ & EX are respective elastic strains at failure
MOD is the flexural elastic modulus
AES & AEK are the displacements at S and 1000 counts

**** Fine mix hybrid composite

MATERIAL TEST	DEPTH	WIDTH	PROPERTIES						ACOUSTIC-EMISSION		
	mm	mm SJ(MPa)	EJ(%)	DJ(mm)	SX(MPa)	EX(%)	DX(mm)	MOD(GPa)	AES(mm)	AE1K(mm)	
1 SPT-FLEX	2.30	4.99	713.9	1.037	5.583	713.9	1.037	5.593	88.2	1.00	3.17
2 SPT-FLEX	2.33	4.99	864.5	1.025	5.500	842.7	1.000	6.500	84.3	0.92	3.42
3 SPT-FLEX	2.32	5.00	804.6	1.026	5.417	804.6	1.026	7.500	78.4	0.92	2.54
**** Averaged values	****	861.0	1.029	5.500	853.7	1.021	6.528	83.6	0.94	3.04	

**** Coarse mix hybrid composite

MATERIAL TEST	DEPTH	WIDTH	PROPERTIES						ACOUSTIC-EMISSION		
	mm	mm SJ(MPa)	EJ(%)	DJ(mm)	SX(MPa)	EX(%)	DX(mm)	MOD(GPa)	AES(mm)	AE1K(mm)	
1 SPT-FLEX	2.15	4.94	896.7	1.077	5.583	932.8	1.120	6.833	85.3	1.00	5.57
2 SPT-FLEX	2.17	4.95	843.1	1.076	6.000	959.2	1.247	7.833	76.9	0.75	2.67
3 SPT-FLEX	2.16	4.97	933.8	1.119	5.583	898.3	1.078	6.043	83.5	0.17	5.67
**** Averaged values	****	891.2	1.097	5.722	930.1	1.148	6.917	81.2	0.64	4.64	

**** Glass monofibre composite

MATERIAL TEST	DEPTH	WIDTH	PROPERTIES						ACOUSTIC-EMISSION		
	mm	mm SJ(MPa)	EJ(%)	DJ(mm)	SX(MPa)	EX(%)	DX(mm)	MOD(GPa)	AES(mm)	AE1K(mm)	
1 SPT-FLEX	2.52	5.09	1219.6	2.391	10.667	1219.6	2.371	10.667	51.0	1.23	7.47
2 SPT-FLEX	2.59	5.06	1584.4	3.084	16.000	1584.4	3.184	16.000	44.8	0.25	10.71
3 SPT-FLEX	2.57	5.06	1404.9	2.789	14.417	1404.9	2.782	14.417	50.4	0.08	5.67
**** Averaged values	****	1403.0	2.788	13.694	1403.0	2.788	13.694	50.4	0.72	7.94	

**** Carbon monofibre composite

MATERIAL TEST	DEPTH	WIDTH	PROPERTIES						ACOUSTIC-EMISSION		
	mm	mm SJ(MPa)	EJ(%)	DJ(mm)	SX(MPa)	EX(%)	DX(mm)	MOD(GPa)	AES(mm)	AE1K(mm)	
1 SPT-FLEX	2.05	5.01	1201.7	1.009	5.353	1201.7	1.029	5.333	117.1	1.33	5.4
2 SPT-FLEX	2.09	5.02	831.0	0.717	3.750	831.0	0.717	3.750	116.1	3.08	3.81
3 SPT-FLEX	2.01	4.99	1138.3	0.912	5.000	1138.3	0.912	5.000	124.0	5.00	4.0
**** Averaged values	****	1057.3	0.879	4.699	1057.3	0.879	4.694	120.0	3.14	4.71	

Table 22: EHMS carbon fibre hybrids, ambient tests

Table 23: EHMS carbon fibre hybrids, one cycle to 77K

One cycle down to liquid nitrogen temperature : ambient test : Plymouth
 Date: 24/11/81

Carbon fibres: EHMS Type EHMS : 10k tow : batch no. F2M 257D : end no. 2RA
 Glass fibres: X Type XRE 23 47 : 2400 tex : product VX 6741 : quote ref 18 126 070 012
 Resin system: Scott Bader Crysic 272 : IX catalyst N : IX accelerator E

Load cell full scale: 50 kg
 Crosshead speed: 0.50 cm/min
 Chart speed: 5.00 cm/min
 Bryans chart speed: 6.00 cm/min, i.e.: 10.00 sec/cm

Acoustic emission serial: 009 Courtesy of Renco Controls
 Transducer: 175 kHz resonance : model AC17SL : serial no.1263 : preamplifier AECL 1P7
 Acoustic emission gain: 60 dB
 Acoustic emission full scale: 999
 Acoustic emission filter A : 20 kHz - 100 kHz
 Acoustic emission mode: Counts

SJ & DJ are strength and deflection at major load drop

SX & DX are strength and deflection at maximum load

EJ & EX are respective elastic strains at failure

MOD is the flexural elastic modulus

AES & AEK are the displacements at 5 and 1000 counts

**** Fine mix hybrid composite

MATERIAL TEST		DEPTH WIDTH						PROPERTIES			ACOUSTIC-EMISSION		
		mm	mm	SJ(MPa)	EJ(%)	DJ(mm)	SX(MPa)	EX(%)	DX(mm)	MOD(GPa)	AES(mm)	AE1K(mm)	
1	SPT-FLEX	2.34	4.05	846.6	0.955	4.500	846.6	0.955	4.500	88.7	1.75	4.01	
2	SPT-FLEX	2.36	4.93	792.9	0.911	4.250	810.0	0.931	4.750	87.0	0.42	4.04	
3	SPT-FLEX	2.36	4.07	756.7	0.936	4.417	778.0	0.963	6.417	80.8	0.17	3.77	
**** Averaged values		798.7	0.934	4.389	811.5	0.949	5.222	85.5	0.78	3.92			

**** Coarse mix hybrid composite

MATERIAL TEST		DEPTH WIDTH						PROPERTIES			ACOUSTIC-EMISSION		
		mm	mm	SJ(MPa)	EJ(%)	DJ(mm)	SX(MPa)	EX(%)	DX(mm)	MOD(GPa)	AES(mm)	AE1K(mm)	
1	SPT-FLEX	2.12	4.97	763.0	0.806	5.250	779.7	0.823	8.167	94.8	1.00	2.67	
2	SPT-FLEX	2.17	4.98	818.0	0.885	4.500	963.5	1.043	6.417	92.4	1.08	2.50	
3	SPT-FLEX	2.10	4.98	739.5	0.795	5.667	798.4	0.815	7.043	92.0	0.67	2.01	
**** Averaged values		773.8	0.815	5.139	847.2	0.894	7.222	95.0	0.92	2.31			

**** Glass monofibre composite

MATERIAL TEST		DEPTH WIDTH						PROPERTIES			ACOUSTIC-EMISSION		
		mm	mm	SJ(MPa)	EJ(%)	DJ(mm)	SX(MPa)	EX(%)	DX(mm)	MOD(GPa)	AES(mm)	AE1K(mm)	
1	SPT-FLEX	2.50	4.97	1754.1	3.109	16.800	1754.1	3.109	16.500	56.4	0.58	5.17	
2	SPT-FLEX	2.54	5.01	1572.8	3.071	15.917	1565.5	3.057	17.250	51.2	0.58	5.54	
3	SPT-FLEX	2.54	5.01	1652.7	3.170	15.983	1652.9	3.170	16.003	57.1	0.75	10.54	
**** Averaged values		1657.4	3.116	16.000	1657.5	3.112	16.611	53.3	0.64	8.44			

**** Carbon monofibre composite

MATERIAL TEST		DEPTH WIDTH						PROPERTIES			ACOUSTIC-EMISSION		
		mm	mm	SJ(MPa)	EJ(%)	DJ(mm)	SX(MPa)	EX(%)	DX(mm)	MOD(GPa)	AES(mm)	AE1K(mm)	
1	SPT-FLEX	2.05	4.97	1019.8	0.862	4.583	1019.8	0.862	4.583	118.3	1.00	4.27	
2	SPT-FLEX	2.00	4.96	990.6	0.857	4.667	990.6	0.857	4.667	115.6	1.33	4.67	
3	SPT-FLEX	2.06	4.97	797.9	0.695	3.667	797.9	0.695	3.667	114.0	3.67	3.67	
**** Averaged values		936.1	0.874	4.306	936.1	0.884	4.306	116.3	2.00	4.1			

Tested immediately on removal from liquid nitrogen : Plymouth
Immersion for 60 seconds
Date: 25/11/81

Carbon fibres: EHMS Type EHMS : 10k tow : batch no. E2H 2570 : end no. 2RA.
Glass fibres: X Type XRE 23 47 : 2400 tex : product VX 6/41 : quote ref. IR 120 070 012
Resin system: Scott Bader Cryslic 272 : 1% catalyst % : 1% accelerator %
Load cell full scale: 50 kg
Crosshead speed: 0.00 cm/min
Chart speed: 5.00 cm/min
Fryans chart speed: 6.00 cm/min, i.e.: 10.00 sec/cm

Acoustic emission serial: 005 Courtesy of Ranco Controls
Transducer: 175 kHz resonance : model AC175L : serial no. 1263 : preamplifier AECL 100
Acoustic emission gain: 60 dB
Acoustic emission full scale: 1000
Acoustic emission filter A : 20 kHz - 100 kHz
Acoustic emission mode: Counts

SJ & DJ are strength and deflection at major load drop
SX & DX are strength and deflection at maximum load
FJ & EX are respective plastic strains at failure
MOD is the flexural elastic modulus
AE5 & AE1K are the displacements at 5 and 1000 counts

**** Fine mix hybrid composite

MATERIAL TEST	DEPTH	WIDTH	PROPERTIES						ACOUSTIC-EMISSION		
	mm	mm	SJ(MPa)	FJ(%)	DJ(mm)	SX(MPa)	EX(%)	DX(mm)	MOD(GPa)	AE5(mm)	AE1K(mm)
1 SPT-FLEX	2.21	5.01	913.8	1.048	5.250	884.2	1.015	7.500	87.2	0.92	3.94
2 SPT-FLEX	2.22	5.02	756.3	0.936	4.500	780.1	0.965	5.417	80.8	0.92	4.40
3 SPT-FLEX	2.23	5.02	843.0	1.183	6.000	801.4	1.123	7.667	71.4	0.08	4.09
**** Averaged values ****			838.0	1.055	5.250	822.1	1.034	6.861	77.8	0.64	3.97

**** Coarse mix hybrid composite

MATERIAL TEST	DEPTH	WIDTH	PROPERTIES						ACOUSTIC-EMISSION		
	mm	mm	SJ(MPa)	FJ(%)	DJ(mm)	SX(MPa)	EX(%)	DX(mm)	MOD(GPa)	AE5(mm)	AE1K(mm)
1 SPT-FLEX	2.72	4.97	760.1	1.223	4.833	960.1	1.223	4.833	78.5	3.58	4.92
2 SPT-FLEX	2.75	4.94	866.2	1.172	4.500	866.2	1.172	4.500	73.9	3.58	4.50
3 SPT-FLEX	2.76	4.74	838.1	1.221	4.917	831.8	1.212	5.167	68.6	2.58	4.67
**** Averaged values ****			888.2	1.206	4.750	886.1	1.203	4.833	73.7	3.25	4.71

**** Glass monofibre composite

MATERIAL TEST	DEPTH	WIDTH	PROPERTIES						ACOUSTIC-EMISSION		
	mm	mm	SJ(MPa)	FJ(%)	DJ(mm)	SX(MPa)	EX(%)	DX(mm)	MOD(GPa)	AE5(mm)	AE1K(mm)
1 SPT-FLEX	2.72	5.11	1363.4	3.087	13.417	1422.5	3.221	14.750	44.2	5.92	10.67
2 SPT-FLEX	2.78	5.11	1349.9	2.837	11.667	1534.6	3.225	14.667	47.6	1.42	10.0
3 SPT-FLEX	2.68	5.06	1505.7	3.184	15.583	1512.2	3.197	16.167	47.3	0.58	6.92
**** Averaged values ****			1406.3	3.036	13.556	1489.8	3.215	15.194	46.3	2.64	8.19

**** Carbon monofibre composite

MATERIAL TEST	DEPTH	WIDTH	PROPERTIES						ACOUSTIC EMISSION		
	mm	mm	SJ(MPa)	FJ(%)	DJ(mm)	SX(MPa)	EX(%)	DX(mm)	MOD(GPa)	AE5(mm)	AE1K(mm)
1 SPT-FLEX	2.13	5.03	959.2	3.918	4.750	959.2	0.918	4.750	108.4	2.00	4.7
2 SPT-FLEX	2.06	5.01	946.5	0.956	4.500	946.5	0.856	4.500	110.6	2.33	4.67
3 SPT-FLEX	2.14	5.00	978.8	0.806	4.167	878.8	0.806	4.167	109.1	4.17	4.17
**** Averaged values ****			929.2	0.867	4.472	928.2	0.860	4.472	109.0	2.83	4.5

Table 24: EHMS carbon fibre hybrids, tested cold

Table 25: Index to tables of mechanical property experimental results 2

Plymouth tests on 22 September 1982
 EAS carbon fibre: XRE 23 47 glass fibres.

<i>Composite</i>	<i>Table</i>	<i>Block</i>	<i>Page</i>
All glass fibre reinforced plastic	26	1	126
All glass fibre reinforced plastic	26	2	126
All carbon fibre reinforced plastic	26	3	126
All carbon fibre reinforced plastic	26	4	126
90 carbon:10 glass fine hybrid	27	1	127
90 carbon:10 glass fine hybrid	27	2	127
80 carbon:20 glass fine hybrid	27	3	127
80 carbon:20 glass fine hybrid	27	4	127
80 carbon:20 glass fine hybrid	27	5	127
70 carbon:30 glass fine hybrid	28	1	128
50 carbon:50 glass fine hybrid	28	2	128
50 carbon:50 glass fine hybrid	28	3	128
50 carbon:50 glass fine hybrid	28	4	128
90 carbon:10 glass coarse hybrid	29	1	129
90 carbon:10 glass coarse hybrid	29	2	129
80 carbon:20 glass coarse hybrid	29	3	129
80 carbon:20 glass coarse hybrid	29	4	129
80 carbon:20 glass coarse hybrid	30	1	130
80 carbon:20 glass coarse hybrid	30	2	130
70 carbon:30 glass coarse hybrid	30	3	130
70 carbon:30 glass coarse hybrid	30	4	130
60 carbon:40 glass coarse hybrid	31	1	131
50 carbon:50 glass coarse hybrid	31	2	131
50 carbon:50 glass coarse hybrid	31	3	131

Plymouth tests

Date: 22.09.82

Carbon fibres:

EAS Type EAS : 101 tow : batch no. E3A 103C : end no. 144R

Glass fibres:

X Type XRE 23 47 : 2400 tow : product MZ 6041 : quote ref 18 120 070 012

Resin system:

Scott Bader Cragic 272 : IX catalyst H : 1% accelerator E

Load cell full scale:

50 kg

Crosshead speed:

5.00 cm/min

Chart speed:

5.00 cm/min

Bryans chart speed:

6.00 cm/min, i.e.: 10.00 sec/cm

Acoustic emission serial:

009 Courtesy of Renco Controls

Transducer:

175 kHz : model AC175L : serial no. 1263 : preamplifier AECL 103

Acoustic emission gain:

60 dB

Acoustic emission full scale:

999

Acoustic emission filter A :

20 kHz - 100 kHz

Acoustic emission mode:

Counts

BJ & DJ are strength and deflection at major load drop

BX & DX are strength and deflection at maximum load

EJ & EX are respective elastic strains at failure

E & G are the flexural and shear moduli respectively

AE5 & AE10 are the displacements at 5 and 1000 Counts

**** All glass fibre reinforced plastic composite

MATERIAL TEST		DEPTH	WIDTH	PROPERTIES						ACOUSTIC-EMISSION VFC VGO Type			Failure modes	
		mm	mm	BJ(MPa)	EJ(%)	DJ(mm)	BX(MPa)	EX(%)	DX(mm)	MOD(GPa)	AE5(mm)	AE10(mm)		
1	JPT-FLEX	2.50	4.98	1629.6	2.854	14.417	1637.1	2.867	14.750	37.1	0.17	1.50	0	100 Glass Delamination & tensile
2	JPT-FLEX	2.60	4.96	1429.0	2.852	12.917	1470.6	2.715	13.717	30.3	0.17	4.17	0	100 Glass Tension
3	JPT-FLEX	2.56	4.98	1356.7	2.886	13.333	1396.5	2.960	14.300	33.7	0.08	5.33	0	100 Glass Tension & comp
Averaged values		*****		1341.8	2.864	13.556	1566.1	2.914	14.387	33.8	0.14	3.67		

**** All glass fibre reinforced plastic composite

MATERIAL TEST		DEPTH	WIDTH	PROPERTIES						ACOUSTIC-EMISSION VFC VGO Type			Failure modes	
		mm	mm	BJ(MPa)	EJ(%)	DJ(mm)	BX(MPa)	EX(%)	DX(mm)	MOD(GPa)	AE5(mm)	AE10(mm)		
1	JPT-FLEX	2.60	5.02	1474.6	2.815	13.063	1508.5	2.841	13.333	33.1	0.50	8.42	0	100 Glass Tension
2	JPT-FLEX	2.66	5.02	1427.9	2.862	13.063	1520.7	3.047	14.750	49.9	0.08	6.90	0	100 Glass Tension
3	JPT-FLEX	2.66	5.02	1235.8	2.484	10.583	1331.7	2.718	12.083	49.7	0.83	7.33	0	100 Glass Tension & comp
Averaged values		*****		1386.1	2.780	12.230	1460.3	2.869	13.387	30.9	0.47	7.44		

**** All carbon fibre reinforced plastic composite

MATERIAL TEST		DEPTH	WIDTH	PROPERTIES						ACOUSTIC-EMISSION VFC VGO Type			Failure modes	
		mm	mm	BJ(MPa)	EJ(%)	DJ(mm)	BX(MPa)	EX(%)	DX(mm)	MOD(GPa)	AE5(mm)	AE10(mm)		
1	JPT-FLEX	2.12	4.92	1027.1	1.268	6.983	1027.1	1.268	6.983	81.0	0.17	6.67	100	0 Carbon Compression
2	JPT-FLEX	2.14	4.94	972.7	1.216	6.417	983.1	1.230	6.500	80.0	0.67	6.63	100	0 Carbon Comp & tension
3	JPT-FLEX	2.08	4.94	892.0	1.061	5.667	1068.2	1.271	7.000	84.0	0.38	6.67	100	0 Carbon Comp & tension
Averaged values		*****		963.9	1.182	6.222	1026.1	1.256	6.694	81.7	2.47	6.72		

**** All carbon fibre reinforced plastic composite

MATERIAL TEST		DEPTH	WIDTH	PROPERTIES						ACOUSTIC-EMISSION VFC VGO Type			Failure modes	
		mm	mm	BJ(MPa)	EJ(%)	DJ(mm)	BX(MPa)	EX(%)	DX(mm)	MOD(GPa)	AE5(mm)	AE10(mm)		
1	JPT-FLEX	2.00	4.98	1222.9	1.457	8.333	1222.7	1.457	8.333	83.9	1.00	7.17	100	0 Carbon Comp & tension
2	JPT-FLEX	2.04	4.96	1117.4	1.324	7.333	1174.4	1.391	7.833	84.4	0.83	7.08	100	0 Carbon Comp & tension
3	JPT-FLEX	2.10	4.94	1361.2	1.509	8.250	1361.2	1.509	8.250	90.2	1.42	8.25	100	0 Carbon Comp & tension
Averaged values		*****		1233.8	1.430	7.972	1252.7	1.452	84.3	1.00				

Table 26: EAS carbon fibre XRE 23 47/glass fibre results

Table 27: EAS carbon fibre fine hybrid results

Plymouth tests

Date: 22.09.82

Carbon fibres:

EAS Type EAS : 10k tow : batch no. E3A 109C : end no. 164R
 X Type XRE 23 47 : 2400 tex : product MX 6041 : quote ref 18 120 070 012
 Scott Bader Crysic 872 : 1% catalyst H : 1% accelerator E

Resin system:

Load cell full scale: 50 kg
 Crosshead speed: 5.00 cm/min
 Chart speed: 5.00 cm/min
 Bargraph chart speed: 6.00 cm/min, i.e.: 10.00 sec/cm

Acoustic emission serial:

003 Courtesy of Renco Controls
 Transducer: 175 kHz : model AC175L : serial no. 1063 : preamplifier AECL 105
 Acoustic emission gain: 60 dB
 Acoustic emission full scale: 999
 Acoustic emission filter A : 20 kHz - 100 kHz
 Acoustic emission mode: Counts

BJ & DJ are strength and deflection at major load drop

BX & DX are strength and deflection at maximum load

EJ & EX are respective elastic strains at failure

E & G are the flexural and shear moduli respectively

AES & AEK are the displacements at 5 and 1000 Counts

eeee Fine VOC:100 hybrid

	mm	mm	BJ(MPa)	EJ(X)	DJ(mm)	BX(MPa)	EX(X)	DX(mm)	MOD(GPa)	AES(mm)	AEK(mm)	VFC	VGO	Type	Failure modes	
1	3PT-FLEX	2.06	4.78	907.7	1.273	6.917	907.7	1.273	6.917	71.3	4.17	8.08	90	10	Fine	Comp & tension
2	3PT-FLEX	2.04	5.00	904.1	1.437	7.917	909.7	1.445	8.167	68.9	0.23	8.08	90	10	Fine	Comp & tension
3	3PT-FLEX	2.04	5.00	797.4	1.198	6.333	798.4	1.421	8.417	68.8	3.42	8.08	90	10	Fine	Comp & tension
eeee	Averaged values	eeee	896.4	1.290	7.056	938.6	1.290	7.033	69.9	3.29	8.08					

eeee Fine VOC:100 hybrid

	mm	mm	BJ(MPa)	EJ(X)	DJ(mm)	BX(MPa)	EX(X)	DX(mm)	MOD(GPa)	AES(mm)	AEK(mm)	VFC	VGO	Type	Failure modes	
1	3PT-FLEX	2.24	4.92	819.1	1.312	6.953	819.1	1.312	6.953	62.1	1.73	6.67	90	10	Fine	Compression
2	3PT-FLEX	2.00	4.94	1239.7	1.675	9.667	1239.7	1.675	9.667	73.9	2.50	9.92	90	10	Fine	Comp & tension
3	3PT-FLEX	1.96	4.92	721.3	1.212	6.917	721.3	1.212	6.917	76.0	0.17	7.50	90	10	Fine	Comp & tension
eeee	Averaged values	eeee	991.8	1.400	7.722	991.8	1.400	7.722	70.7	1.47	8.03					

eeee Fine VOC:200 hybrid

	mm	mm	BJ(MPa)	EJ(X)	DJ(mm)	BX(MPa)	EX(X)	DX(mm)	MOD(GPa)	AES(mm)	AEK(mm)	VFC	VGO	Type	Failure modes	
1	3PT-FLEX	2.20	5.00	1026.1	1.711	6.667	1137.3	1.930	10.000	60.0	0.42	7.29	80	20	Fine	Shear
2	3PT-FLEX	2.24	5.00	820.9	1.355	6.667	820.9	1.355	6.667	60.6	2.75	9.67	80	20	Fine	Shear
3	3PT-FLEX	2.26	5.00	870.7	1.408	6.633	1072.1	1.766	7.083	61.7	1.73	6.75	80	20	Fine	Shear
eeee	Averaged values	eeee	703.7	1.471	7.389	1023.4	1.663	8.883	60.8	3.31	7.87					

eeee Fine VOC:200 hybrid

	mm	mm	BJ(MPa)	EJ(X)	DJ(mm)	BX(MPa)	EX(X)	DX(mm)	MOD(GPa)	AES(mm)	AEK(mm)	VFC	VGO	Type	Failure modes	
1	3PT-FLEX	2.00	5.00	729.7	1.241	7.333	947.3	1.264	7.667	74.9	1.17	4.00	80	20	Fine	Comp & tension
2	3PT-FLEX	2.02	4.96	721.0	0.969	9.667	721.0	0.969	9.667	74.4	1.67	3.83	80	20	Fine	Tension & bctng
3	3PT-FLEX	2.01	4.96	898.9	1.213	6.750	939.6	1.267	6.333	74.0	0.50	6.50	80	20	Fine	Tension & comp
eeee	Averaged values	eeee	849.7	1.141	6.983	869.3	1.167	7.222	74.5	1.11	4.78					

eeee Fine VOC:200 hybrid

	mm	mm	BJ(MPa)	EJ(X)	DJ(mm)	BX(MPa)	EX(X)	DX(mm)	MOD(GPa)	AES(mm)	AEK(mm)	VFC	VGO	Type	Failure modes	
1	3PT-FLEX	2.10	5.00	1046.0	1.482	8.333	1027.2	1.320	8.833	70.6	0.08	5.17	80	20	Fine	Compression
2	3PT-FLEX	2.06	5.00	1114.8	1.578	9.333	1209.1	1.711	10.833	70.6	1.17	4.83	80	20	Fine	Tension & comp
3	3PT-FLEX	2.06	5.00	948.4	1.369	7.300	1231.3	1.778	11.500	69.3	4.50	6.42	80	20	Fine	Complex
eeee	Averaged values	eeee	1036.4	1.476	8.389	1171.0	1.670	10.389	70.2	1.92	5.47					

Plymouth tests

Date: 22.07.82

Carbon fibres:

EAB Type EAB : 10k tow : batch no. EJA 103C : end no. 144R
 Glass fibres:
 X Type XRE 23.47 : 2400 tow : product WX 6041 : quote ref 1B 120 070 012
 Resin system:
 Scott Bader Crystic 272 : 1% catalyst H : 1% accelerator E

Load cell full scale:

50 kg

Crosshead speed:

5.00 cm/min

Chart speed:

5.00 cm/min

Bragg chart speed:

6.00 cm/min, i.e.: 10.00 sec/cm

Acoustic emission serial:

005 Courtesy of Ranco Controls

Transducer:

175 kHz : model AC175L : serial no. 1263 : preamplifier AECL 105

Acoustic emission gain:

60 dB

Acoustic emission full scale:

999

Acoustic emission filter A:

20 kHz - 100 kHz

Acoustic emission mode:

Counts

BJ & DJ are strength and deflection at major load drop

SX & DX are strength and deflection at maximum load

EJ & EX are respective elastic strains at failure

E & G are the flexural and shear moduli, respectively

AE5 & AE1K are the displacements at 5 and 1000 Counts

**** Fine 70C:300 hybrid

MATERIAL TEST		DEPTH	WIDTH	PROPERTIES						ACOUSTIC-EMISSION				VXC	VZO	Type	Failure modes
		mm	mm	BJ(MPa)	EJ(%)	DJ(mm)	BX(MPa)	EX(%)	DX(mm)	MOD(GPa)	AE5(mm)	AE1K(mm)					
1	JPT-FLEX	2.92	4.92	312.6	0.764	3.750	271.2	0.662	6.030	40.9	0.83	3.98	70	30	Fine	Buckling	
2	JPT-FLEX	2.12	4.92	718.5	0.913	4.893	824.9	1.048	6.667	78.7	0.08	3.75	70	30	Fine	Compression	
3	JPT-FLEX	2.10	4.96	371.2	0.360	3.089	392.7	0.593	8.333	66.2	1.92	3.92	70	30	Fine	Buckling & tens	
**** Averaged values ****		467.4	0.746	3.889	4.96	3	0.768	7.278	62.0	0.94	3.75						

**** Fine 50C:300 hybrid

MATERIAL TEST		DEPTH	WIDTH	PROPERTIES						ACOUSTIC-EMISSION				VXC	VZO	Type	Failure modes
		mm	mm	BJ(MPa)	EJ(%)	DJ(mm)	BX(MPa)	EX(%)	DX(mm)	MOD(GPa)	AE5(mm)	AE1K(mm)					
1	JPT-FLEX	2.20	9.00	627.3	0.972	6.167	603.0	0.935	7.917	64.3	0.25	4.33	50	30	Fine	Compression	
2	JPT-FLEX	2.20	9.08	950.4	0.907	6.250	641.4	1.056	10.917	60.7	0.17	4.08	50	30	Fine	Comp & tension	
3	JPT-FLEX	2.16	5.04	485.4	4.831	5.363	535.3	0.917	5.833	58.4	1.25	4.38	50	30	Fine	Compression	
**** Averaged values ****		554.4	0.903	5.667	593.3	0.969	6.222	61.2	0.56	4.33							

**** Fine 50C:500 hybrid

MATERIAL TEST		DEPTH	WIDTH	PROPERTIES						ACOUSTIC-EMISSION				VXC	VZO	Type	Failure modes
		mm	mm	BJ(MPa)	EJ(%)	DJ(mm)	BX(MPa)	EX(%)	DX(mm)	MOD(GPa)	AE5(mm)	AE1K(mm)					
1	JPT-FLEX	2.30	9.04	737.1	1.310	6.417	860.7	1.930	10.083	56.3	2.50	6.33	50	30	Fine	Comp & delamination	
2	JPT-FLEX	2.26	9.04	850.3	1.506	9.500	850.3	1.506	9.500	56.4	1.00	3.67	50	30	Fine	Buckling & tens	
3	JPT-FLEX	2.28	9.04	662.4	1.613	8.833	716.3	1.714	10.417	53.5	1.00	4.17	50	30	Fine	Tension & comp	
**** Averaged values ****		816.6	1.477	8.230	875.8	1.584	10.000	53.4	1.50	5.39							

**** Fine 50C:300 hybrid

MATERIAL TEST		DEPTH	WIDTH	PROPERTIES						ACOUSTIC-EMISSION				VXC	VZO	Type	Failure modes
		mm	mm	BJ(MPa)	EJ(%)	DJ(mm)	BX(MPa)	EX(%)	DX(mm)	MOD(GPa)	AE5(mm)	AE1K(mm)					
1	JPT-FLEX	2.20	4.96	691.2	1.049	3.730	691.2	1.049	3.730	65.9	0.33	3.30	50	30	Fine	Tension	
2	JPT-FLEX	2.14	4.94	665.8	1.000	3.917	723.0	1.086	7.333	66.6	0.42	4.92	50	30	Fine	B,C,S modes	
3	JPT-FLEX	2.36	4.96	451.5	0.788	3.833	634.7	1.108	6.083	57.3	1.30	2.42	50	30	Fine	Comp & tension	
**** Averaged values ****		602.9	0.946	3.167	683.0	1.081	6.389	63.3	0.73	3.61							

Table 28: EAS carbon fibre fine hybrid results

Plymouth tests
Date:

22.09.82

Carbon fibres:
EAS Type EAS : 10k tow : batch no. E3A 103C : end no. 144R
Glass fibres:
K Type KRE 23 47 : 2400 tow : product MX 6041 : quota ref 18 120 070 012
Resin system:
Scott Bader Crysic 272 : 1% catalyst M : 1% accelerator E

Load cell full scale: 50-kN
Crosshead speed: 5.00 cm/min
Chart speed: 5.00 cm/min
Bryans chart speed: 6.00 cm/min, i.e.: 10.00 sec/cm

Acoustic emission serial: 005 Courtesy of Renco Controls
Transducer: 175 kHz : model AC175L : serial no. 1263 : preamplifier AECL 105
Acoustic emission gain: 60 dB
Acoustic emission full scale: 999
Acoustic emission filter A : 20 kHz - 100 kHz
Acoustic emission mode: Counts

δJ & δX are strength and deflection at major load drop
 δX & δK are strength and deflection at maximum load
 ϵJ & ϵX are respective elastic strains at failure
 E & G are the flexural and shear moduli respectively
AE3K IK are the displacements at 3 and 1000 Counts

**** Coarse 90G:100 hybrid

MATERIAL TEST	DEPTH	WIDTH	PROPERTIES						ACOUSTIC-EMISSION						VXC	VXG	Type	Failure modes
			mm	mm	BJ(MPa)	EJ(X)	DJ(mm)	BK(MPa)	EX(X)	DX(mm)	MOD(GPa)	AES(mm)	AEIK(mm)					
1 3PT-FLEX	2.00	5.00	1000.3	1.208	7.500	1006.2	1.316	7.447	76.4	2.30	6.83	90	10	Coarse	Comp & shear			
2 3PT-FLEX	1.98	4.96	980.4	1.171	6.500	1270.9	1.318	9.000	83.7	0.92	6.80	90	10	Coarse	Compression & shear			
3 3PT-FLEX	1.98	5.00	882.5	1.093	6.083	1140.7	1.413	8.417	80.7	0.83	6.42	90	10	Coarse	Comp & shear			
**** Averaged values	****	****	984.4	1.191	6.694	1139.2	1.416	8.361	80.3	1.42	6.88							

**** Coarse 90G:100 hybrid

MATERIAL TEST	DEPTH	WIDTH	PROPERTIES						ACOUSTIC-EMISSION						VXC	VXG	Type	Failure modes
			mm	mm	BJ(MPa)	EJ(X)	DJ(mm)	BK(MPa)	EX(X)	DX(mm)	MOD(GPa)	AES(mm)	AEIK(mm)					
1 3PT-FLEX	2.10	4.94	848.1	1.091	8.730	848.1	1.091	8.730	77.7	1.06	5.92	90	10	Coarse	Compression			
2 3PT-FLEX	2.03	4.94	788.1	0.996	6.500	803.7	1.018	8.917	79.2	3.50	5.30	90	10	Coarse	Comp & brittle			
3 3PT-FLEX	2.00	4.94	863.3	1.122	6.500	863.3	1.122	6.500	77.0	0.37	9.00	90	10	Coarse	Comp & brittle			
**** Averaged values	****	****	833.3	1.070	8.917	839.1	1.077	8.056	78.0	1.38	5.47							

**** Coarse 80G:200 hybrid

MATERIAL TEST	DEPTH	WIDTH	PROPERTIES						ACOUSTIC-EMISSION						VXC	VXG	Type	Failure modes
			mm	mm	BJ(MPa)	EJ(X)	DJ(mm)	BK(MPa)	EX(X)	DX(mm)	MOD(GPa)	AES(mm)	AEIK(mm)					
1 3PT-FLEX	2.06	4.94	1035.4	1.483	8.000	1212.3	1.704	9.983	71.3	2.42	9.33	90	20	Coarse	Compression & shear			
2 3PT-FLEX	2.00	4.94	1073.6	1.304	8.730	1121.0	1.571	9.230	71.4	3.20	7.75	90	20	Coarse	Comp & shear			
3 3PT-FLEX	2.00	4.94	964.8	1.346	7.900	1298.3	1.812	10.750	71.7	0.25	7.67	90	20	Coarse	Comp & shear			
**** Averaged values	****	****	1031.2	1.445	8.083	1210.6	1.696	9.861	71.4	1.97	8.25							

**** Coarse 80G:200 hybrid

MATERIAL TEST	DEPTH	WIDTH	PROPERTIES						ACOUSTIC-EMISSION						VXC	VXG	Type	Failure modes
			mm	mm	BJ(MPa)	EJ(X)	DJ(mm)	BK(MPa)	EX(X)	DX(mm)	MOD(GPa)	AES(mm)	AEIK(mm)					
1 3PT-FLEX	2.14	4.92	1295.3	1.993	10.750	1295.3	1.993	10.750	65.0	0.17	11.42	90	20	Coarse	Comp & shear			
2 3PT-FLEX	2.00	4.92	1184.0	1.611	9.167	1164.0	1.611	9.167	73.0	0.06	9.23	90	20	Coarse	Comp & shear			
3 3PT-FLEX	2.06	4.92	1341.3	1.923	11.000	1341.3	1.923	11.000	69.7	3.63	10.17	90	20	Coarse	Comp & shear			
**** Averaged values	****	****	1273.4	1.843	10.304	1273.4	1.843	10.304	69.4	1.36	10.26							

Table 29: EAS carbon fibre coarse hybrid results

Table 30: EAS carbon fibre coarse hybrid results

Plymouth tests
Date:

22.09.82

Carbon fibres:
EAS Type EAS : 10t tow : batch no. E3A 105C : end no. 144R
Glass fibres:
X Type XRE 23 47 : 2400 tow : product MX 604L : quote ref 18 120 070 012
Resin system:
Scott Bader Crysic 272 : 1% catalyst M : 1% accelerator E

Load cell full scale: 50 kg
Crosshead speed: 5.00 cm/min
Chart speed: 5.00 cm/min
Bryans chart speed: 6.00 cm/min, i.e.: 10.00 sec/cm

Acoustic emission serial: 005 Courtesy of Ranco Controls
Transducer: 175 kHz : model AC175L : serial no. 1263 : preamplifier AECL 109
Acoustic emission gain: 60 dB
Acoustic emission full scale: 999
Acoustic emission filter A: 20 kHz - 100 kHz
Acoustic emission mode: Counts

B_J & D_J are strength and deflection at major load drop
B_X & D_X are strength and deflection at maximum load
E_J & E_X are respective elastic strains at failure
E & G are the flexural and shear moduli respectively
AE₅ & IK are the displacements at 5 and 1000 Counts

**** Coarse BOC:200 hybrid

MATERIAL TEST	DEPTH	WIDTH	PROPERTIES						ACOUSTIC-EMISSION				V _{XC}	V _{XG}	Type	Failure modes
mm	mm	mm	B _J (MPa)	E _J (%)	D _J (mm)	B _X (MPa)	E _X (%)	D _X (mm)	MOD(GPa)	AES(mm)	AEIK(mm)					
1 3PT-FLEX	2.28	4.96	899.1	1.360	7.667	899.1	1.360	7.667	57.7	0.67	3.75	80	20	Coarse	Bandwidth shear	
2 3PT-FLEX	2.34	4.96	1100.6	1.976	9.667	1100.6	1.976	9.667	55.7	0.33	7.00	80	20	Coarse	Bandwidth shear	
3 3PT-FLEX	2.30	4.96	1475.6	2.393	13.230	1475.6	2.393	13.230	56.7	1.92	12.06	80	20	Coarse	Double shear	
**** Averaged values ****	1198.4	2.043	10.194	1198.4	2.043	10.194	1198.4	2.043	10.194	56.8	0.97	8.28				

**** Coarse BOC:200 hybrid

MATERIAL TEST	DEPTH	WIDTH	PROPERTIES						ACOUSTIC-EMISSION				V _{XC}	V _{XG}	Type	Failure modes
mm	mm	mm	B _J (MPa)	E _J (%)	D _J (mm)	B _X (MPa)	E _X (%)	D _X (mm)	MOD(GPa)	AES(mm)	AEIK(mm)					
1 3PT-FLEX	2.40	4.96	1466.4	2.853	14.000	1466.4	2.853	14.000	51.4	0.23	12.38	80	20	Coarse	Shear	
2 3PT-FLEX	2.24	5.06	1232.9	2.155	10.917	1237.6	2.163	11.167	57.2	0.00	9.08	80	20	Coarse	Shear	
3 3PT-FLEX	2.24	5.04	1358.8	3.366	12.417	1358.8	3.366	12.417	57.4	2.83	7.92	80	20	Coarse	Shear	
**** Averaged values ****	1352.7	2.498	12.444	1354.3	2.460	12.320	1354.3	2.460	12.320	53.4	1.03	9.84				

**** Coarse 70C:300 hybrid

MATERIAL TEST	DEPTH	WIDTH	PROPERTIES						ACOUSTIC-EMISSION				V _{XC}	V _{XG}	Type	Failure modes
mm	mm	mm	B _J (MPa)	E _J (%)	D _J (mm)	B _X (MPa)	E _X (%)	D _X (mm)	MOD(GPa)	AES(mm)	AEIK(mm)					
1 3PT-FLEX	2.00	5.00	841.6	1.248	6.917	876.7	1.301	7.417	67.4	1.30	6.33	70	30	Coarse	Bending & shear	
2 3PT-FLEX	2.00	4.96	925.3	1.339	7.250	1115.1	1.614	9.250	69.1	1.33	6.67	70	30	Coarse	Comp & shear	
3 3PT-FLEX	1.98	5.00	756.4	1.054	5.917	864.9	1.204	7.167	71.8	5.83	7.17	70	30	Coarse	Comp & shear	
**** Averaged values ****	841.1	1.214	6.694	932.1	1.373	7.944	841.1	1.214	7.944	69.4	2.89	6.72				

**** Coarse 70C:300 hybrid

MATERIAL TEST	DEPTH	WIDTH	PROPERTIES						ACOUSTIC-EMISSION				V _{XC}	V _{XG}	Type	Failure modes
mm	mm	mm	B _J (MPa)	E _J (%)	D _J (mm)	B _X (MPa)	E _X (%)	D _X (mm)	MOD(GPa)	AES(mm)	AEIK(mm)					
1 3PT-FLEX	2.10	4.92	1133.6	1.673	9.167	1133.6	1.673	9.167	67.8	2.30	9.92	70	30	Coarse	Comp & shear	
2 3PT-FLEX	2.06	4.96	922.3	1.247	6.667	922.3	1.247	6.667	74.0	0.30	6.73	70	30	Coarse	Compression &	
3 3PT-FLEX	2.10	4.96	1076.0	1.919	8.333	1076.0	1.919	8.333	70.8	0.73	7.17	70	30	Coarse	Comp & shear	
**** Averaged values ****	1044.0	1.479	8.056	1044.0	1.479	8.056	1044.0	1.479	8.056	70.9	1.23	6.61				

Table 31: EAS carbon fibre coarse hybrid results

Plymouth tests
Date:

22.09.82

Carbon fibres: EAS Type EAS : 10k tow : batch no. E3A 103C : end no. 144R
Glass Fibres: X Type XRE 23 47 : 2400 tex : product WX 6041 : quote ref 1B 120 070 012
Resin system: Scott Bader Cragic 272 : IX catalyst M : IX accelerator E

Load cell full scale: 50 kg
Crosshead speed: 5.00 cm/min
Chart speed: 5.00 cm/min
Bryant chart speed: 6.00 cm/min, ie: 10.00 sec/cm

Acoustic emission serial: 003 Courtesy of Ranco Controls
Transducer: 175 kHz : model AC175L : serial no. 1263 : preamplifier AECL 105
Acoustic emission gain: 60 dB
Acoustic emission full scale: 999
Acoustic emission filter A: 20 kHz - 100 kHz
Acoustic emission mode: Counts

E_J & D_J are strength and deflection at major load drop
 E_Y & D_Y are strength and deflection at maximum load
 E_J & E_X are respective elastic strains at failure
 E & G are the flexural and shear moduli respectively
AE9 IR are the displacements at 9 and 1000 Counts

**** Coarse 60C:40G hybrid

MATERIAL TEST	DEPTH	WIDTH	PROPERTIES						ACOUSTIC-EMISSION VXC VZO				Type	Failure modes
mm	mm	mm	B_J (MPa)	E_J (%)	D_J (mm)	B_X (MPa)	E_X (%)	D_X (mm)	MOD (GPa)	$AE9$ (mm)	$AE1K$ (mm)			
1	3PT-FLEX	2.10	4.92	992.5	1.630	8.667	1149.8	1.911	15.417	60.2	2.25	7.75	60	40 Coarse Comp & shear
2	3PT-FLEX	2.06	4.92	1285.1	1.931	11.083	1249.6	1.872	14.250	66.3	0.75	6.75	60	40 Coarse Classic failure
3	3PT-FLEX	2.12	4.92	808.7	1.265	6.383	1043.1	1.631	8.833	63.9	1.17	6.30	60	40 Coarse Comp & shear
	Averaged values	1028.9	4.615	8.778	1146.2	1.805	12.633			63.6	1.39	7.00		

**** Coarse 50C:50G hybrid

MATERIAL TEST	DEPTH	WIDTH	PROPERTIES						ACOUSTIC-EMISSION VXC VZO				Type	Failure modes
mm	mm	mm	B_J (MPa)	E_J (%)	D_J (mm)	B_X (MPa)	E_X (%)	D_X (mm)	MOD (GPa)	$AE9$ (mm)	$AE1K$ (mm)			
1	3PT-FLEX	2.16	4.96	1235.7	1.716	9.417	1240.6	1.723	9.500	72.0	1.33	7.33	50	50 Coarse Complex
2	3PT-FLEX	2.14	5.02	220.1	0.372	1.917	460.7	0.780	19.750	59.1	0.33	2.25	50	50 Coarse Btng & delamination
	Averaged values	343.3	4.98	174.2	0.337	1.667	419.9	0.812	18.000	51.7	0.30	1.75	50	50 Coarse Buckling

**** Coarse 50C:50G hybrid

MATERIAL TEST	DEPTH	WIDTH	PROPERTIES						ACOUSTIC-EMISSION VXC VZO				Type	Failure modes
mm	mm	mm	B_J (MPa)	E_J (%)	D_J (mm)	B_X (MPa)	E_X (%)	D_X (mm)	MOD (GPa)	$AE9$ (mm)	$AE1K$ (mm)			
1	3PT-FLEX	2.04	4.94	967.4	1.374	7.300	1033.3	1.476	8.333	70.4	3.00	9.67	50	50 Coarse Comp & shear
2	3PT-FLEX	2.04	4.96	1436.7	1.976	11.750	1539.3	2.120	13.167	72.6	1.25	5.83	50	50 Coarse Complex
3	3PT-FLEX	2.06	5.00	937.3	1.327	7.083	1175.8	1.644	9.917	70.6	0.17	6.75	50	50 Coarse Comp & shear
	Averaged values	1113.8	4.96	8.778	1256.1	1.760	10.472			71.2	1.47	6.08		

**Table 32: Properties of unidirectional HT-carbon/E-glass hybrid composites
(taken from the thesis by P.W. Manders (=79), Table 4, page 131)**

<i>Composition</i>	<i>Elastic modulus (GPa)</i>		<i>Failure stress (MPa)</i>		<i>Failure strain %</i>	
GFRP (E-glass)	45	(44.5)	1200	(1205)	2.70	(2.75)
	44	(44.5)	1210	(1205)	2.80	(2.75)
5% carbon	49	(49.0)	760	(1210)	1.55	(2.66)
8% carbon	55	(51.7)	820	(1212)	1.50	(2.61)
11% carbon	60	(54.3)	900	(1215)	1.49	(2.55)
14% carbon	59	(57.0)	870	(1218)	1.48	(2.50)
16% carbon	58	(58.8)	820	(1220)	1.41	(2.46)
20% carbon	65	(62.4)	920	(1224)	1.42	(2.39)
25% carbon	72	(66.9)	970	(1228)	1.35	(2.30)
33% carbon	83	(74.0)	1040	(1236)	1.25	(2.16)
33% carbon	76	(74.0)	1030	(1236)	1.35	(2.16)
33% carbon	77	(74.0)	1040	(1236)	1.36	(2.16)
36% carbon	81	(76.7)	1030	(1238)	1.27	(2.11)
50% carbon	93	(89.3)	1200	(1252)	1.29	(1.86)
50% carbon	90	(89.3)	1230	(1252)	1.36	(1.86)
57% carbon	102	(95.5)	1380	(1258)	1.36	(1.73)
60% carbon	104	(98.2)	1430	(1261)	1.37	(1.68)
82% carbon	109	(118)	1400	(1281)	1.29	(1.28)
CFRP	126	(134)	970	(1298)	0.77	(0.96)
CFRP	128	(134)	1130	(1298)	0.88	(0.96)
CFRP (HT-carbon)	143	(134)	1480	(1298)	1.03	(0.96)
CFRP	129	(134)	1250	(1298)	0.97	(0.96)
CFRP	144	(134)	1660	(1298)	1.15	(0.96)

Numbers in brackets are averages (monofibre composites) or rule-of-mixture predictions (hybrid composites).

The prepreg sheets used were designed to give a lamina thickness of 0.125 mm at 60 volume percent of fibres.

*Table 33: Properties of unidirectional E-glass/Kevlar 49 hybrid composites
(taken from the thesis by M.B. Gruber (=246) and converted to SI units)*

<i>Composition</i>	<i>Longitudinal elastic modulus (GPa)</i>	<i>Longitudinal strength (MPa)</i>	<i>Calculated strain %</i>
GFRP (E-glass)	37.7 34.6 36.5	620 724 615	1.66 2.09 1.68
Mean	36.3 (36.3)	653 (653)	1.81 (1.81)
80% Glass: 20% Kevlar	50.3 50.1 51.2	938 869 945	1.86 1.74 1.85
Mean	50.5 (42.6)	917 (710)	1.82 (1.72)
60% Glass: 40% Kevlar	56.3 59.4 54.9	855 862 —	1.52 1.45 —
Mean	56.9 (49.0)	858 (767)	1.49 (1.69)
40% Glass: 60% Kevlar	57.6 57.7 60.3	883 890 834	1.53 1.54 1.38
Mean	58.5 (55.3)	869 (824)	1.48 (1.55)
20% Glass: 80% Kevlar	67.8 64.7 64.1	1083 1034 1041	1.60 1.60 1.63
Mean	65.5 (61.7)	1053 (881)	1.61 (1.47)
AFRP (Kevlar 49)	69.0 65.5 69.6	958 869 986	1.39 1.33 1.42
Mean	68.0 (68.0)	938 (938)	1.38 (1.38)

Numbers in brackets are the rule-of-mixtures predictions using the averages given above for monofibre composites.

Volume fraction of resin was constant at 50%.

4.4 Finite element analysis

Description of finite element mesh model

Element used: PAFEC 75 level 3.1, element R44215.

For the majority of the numerical analyses the model consisted of

36 elements forming a 4 X 9 rectangular mesh, with

135 nodes (four corner nodes and four midside nodes per element)

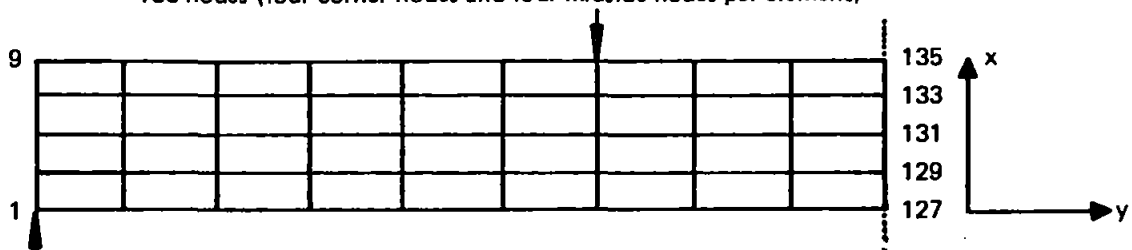


Diagram shows node numbers used in table.

The y-freedom of all nodes on the line shown dotted was constrained, except for nodes 127 and 128 in the notched analysis.

All models had the same topology and node numbering sequences, only the constraints and material properties were changed.

All notched models were assumed to contain a crack running from node 127 to a cracktip at node 129.

An equal magnitude load of 510 kN was applied in all cases.

Model A: no notch
standard PAFEC software used throughout

Model B: cracktip at node 129
standard PAFEC software used throughout

Model C: cracktip at node 129
matrix divide subroutine replaced to model the singularity
(see Appendix 7: microfiche 1: sectors D7 to D9).

Zero stresses in the following tables may be positive or negative, to indicate whether the stress is between (0 and +0.05 kNmm⁻²) or (0 and -0.05 kNmm⁻²) respectively.

Table 34: Material properties (units are mm²/kN) used in the finite element analysis

Material Ref. No.	S _{xx}	S _{yy}	S _{xy}	Material type	Source reference
17	6	16	0.121	GFRP	F.J. Guild
18	30	49	10	GFRP	I.L. Kalnin
19	6	287	5	CFRP	I.L. Kalnin
20	face material as 19: core material as 18.				

Table 35: Summary of stresses predicted by 36-element PAFEC analysis

- A: unnotched beam: all PAFEC subroutines
 B: notched beam: all PAFEC subroutines
 C: notched beam: singularity capability in DMATDIV subroutine: Factor = 1E-20.

<i>Model:</i>	<i>A</i>			<i>B</i>			<i>C</i>			
<i>Node</i>	<i>x-</i>	<i>y-</i>	<i>shear</i>	<i>x-</i>	<i>y-</i>	<i>shear</i>	<i>x-</i>	<i>y-</i>	<i>shear</i>	<i>Material</i>
1	-33.8	2.2	-0.8	-33.8	1.9	-0.8	-33.8	3.0	-0.8	
9	-0.8	1.1	-0.3	-0.8	1.5	-0.2	-0.8	0.5	-0.3	
127	-0.0	238.0	-0.0	3.1	-37.5	-6.1	0.8	-11.4	3.9	
129	-0.0	117.0	-0.0	19.8	434.0	20.0	20.7	1630.0	14.0	17
131	-0.1	-0.0	-0.0	20.5	33.4	-6.6	17.6	59.3	-8.4	
133	-0.1	-117.0	-0.0	4.6	-242.0	-6.3	12.3	-118.0	-8.0	
135	-0.1	-238.0	-0.0	2.9	-388.0	-6.3	4.2	-357.0	-8.0	
<i>Node</i>	<i>x-</i>	<i>y</i>	<i>shear</i>	<i>x-</i>	<i>y-</i>	<i>shear</i>	<i>x-</i>	<i>y-</i>	<i>shear</i>	<i>Material</i>
1	-32.5	8.4	-3.2	-32.4	8.3	-3.2	-32.4	8.4	-3.2	
9	-0.0	0.8	-1.2	0.0	0.8	-1.2	0.1	0.8	-1.2	
127	0.1	217.0	-0.2	20.1	33.6	36.5	14.0	-5.7	23.5	
129	0.0	109.0	-0.2	48.6	225.0	45.5	70.6	640.0	126.0	18
131	-0.0	0.0	-0.2	45.6	27.6	-24.9	46.0	62.4	-46.1	
133	-0.1	-109.0	-0.1	17.7	-121.0	-16.7	33.7	-99.6	-29.4	
135	-0.1	-217.0	-0.1	5.2	-280.0	-14.6	11.6	-259.0	-24.9	
<i>Node</i>	<i>x-</i>	<i>y-</i>	<i>shear</i>	<i>x-</i>	<i>y-</i>	<i>shear</i>	<i>x-</i>	<i>y-</i>	<i>shear</i>	<i>Material</i>
1	-29.2	37.7	-7.7	-29.2	37.7	-7.7	-29.2	37.8	-7.7	
9	0.7	9.4	1.0	0.7	9.5	1.0	0.7	9.5	1.0	
127	-0.0	232.0	-0.0	1.7	-85.4	-7.9	-0.9	-42.7	-0.5	
129	+0.0	116.0	-0.0	17.6	380.0	17.8	17.6	1500.0	-18.9	19
131	-0.0	-0.1	-0.0	14.5	26.2	-7.3	13.3	62.5	-9.9	
133	-0.0	-116.0	0.0	4.5	-125.0	-3.5	6.0	-131.0	-4.6	
135	+0.0	-232.0	-0.0	0.5	-342.0	-2.7	0.8	-357.0	-3.4	
<i>Node</i>	<i>x-</i>	<i>y-</i>	<i>shear</i>	<i>x-</i>	<i>y-</i>	<i>shear</i>	<i>x-</i>	<i>y-</i>	<i>shear</i>	<i>Material</i>
1	-29.7	34.0	-7.2	-29.7	34.0	-7.2	-29.7	34.0	-7.2	
9	0.1	5.5	0.4	0.1	5.5	0.4	0.1	5.5	0.4	
127	-0.0	257.0	-0.0	5.7	-138.0	-9.0	1.1	-98.8	-2.3	
129	-0.0	75.5	-0.0	30.7	388.5	31.9	54.7	2049.0	21.3	20
131	0.0	0.0	-0.0	28.2	33.4	-16.4	33.9	71.9	-33.0	
133	-0.0	-75.5	0.0	9.3	-70.9	-9.2	18.2	-52.4	-18.3	
135	0.0	-257.0	-0.0	1.4	-381.0	-4.3	3.6	-423.0	-8.1	

Table 36: Stresses at node 129

<i>Material</i>	Stresses (kNm^{-2})			Stress concentration factor			<i>Material</i>
	<i>A: Unnotched</i>	<i>B: Notched</i>	<i>C: Singularity</i>	<i>B/A</i>	<i>C/B</i>	<i>C/A</i>	
17	117	434	1630	3.71	3.76	13.93	17
18	109	225	640	2.06	2.84	5.87	18
19	116	380	1500	3.28	3.95	12.93	19
Sandwich	75.5	388.5	2049	5.19	5.27	27.32	Sandwich

*Table 37: Computer time taken for each finite element analysis
(in CPU seconds)*

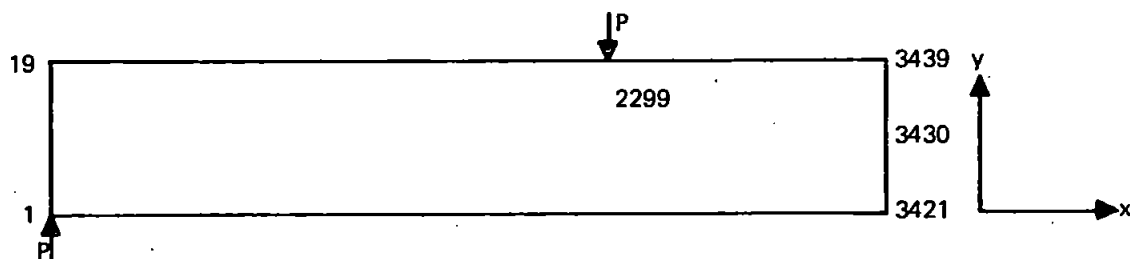
Material	Model		
	A Unnotched	B Notched	C Singularity
17	1292	1226	1309
18	1296	1226	1286
19	1244	1232	1289
Sandwich	1309	1245	1292

Finite element analysis with an unnotched 810-element mesh

Element used: PAFEC level 3.1, element R44215

Each element was one unit square forming a 90 X 9 element mesh (x by y).

Material properties: as material 17 in previous section.



The x-freedom of all nodes on the line shown dotted was constrained.

The magnitude of the load was 510 kN.

Total number of elements: 810

Total number of nodes: 3439

Total number of degrees of freedom: 5239

Size of BASE matrix in phase 9: 71767

Standard PAFEC software.

Start of run: 1545 on 4 February 1981.

End of run: 0134 on 5 February 1981.

Phase 1 end:	1608	cumulative CPU seconds:	647	:Read data
Phase 4 end:	1648		1379	:Pre-solution housekeeping
Phase 6 end:	2259		17081	:Element stiffness matrices
Phase 7 end:	2342		19336	:Displacement solution
Phase 8 end:	0004		20542	:Displacement drawing
Phase 9 end:	0132		25361	:Generate stresses
Macro end:	0134		25416	

Total CPU time was: 7 hours 4 minutes

Run time was: 9 hours 49 minutes

Table 38: Results from the 810 element analysis

Translations of the corner nodes (x1E3)

<i>Node</i>	<i>x-coordinate</i>	<i>y-coordinate</i>	<i>x-translation</i>	<i>y-translation</i>
1	0.0	0.0	272	-577
19	0.0	9.0	-58	-562
3421	90.0	0.0	constrained	229
3439	90.0	9.0	constrained	229

See figure 24, constrained edge at left of diagram,
maximum deflection scaled to two inches.

Stresses at major corner and edge nodes

<i>Node number, elements per node</i>	<i>x-stress</i>	<i>y-stress</i>	<i>tau 12</i>	<i>x-coord.</i>	<i>y-coord.</i>
1.1 (corner)	40.9	-277	-26.2	0.0	0.0
19.1 (corner)	-1.26	-0.69	-0.41	0.0	9.0
3421.1 (corner)	0.025	-6.61	0.003	90.0	0.0
3424.1 (element midside)	0.015	-4.97	0.003	90.0	1.5
3427.2 (element corners)	0.022	-2.90	0.002	90.0	3.0
3430.1 (element midside)	0.031	-0.45	0.002	90.0	4.5
3433.2 (element corners)	0.004	2.39	0.002	90.0	6.0
3436.1 (element midside)	-0.012	5.38	0.001	90.0	7.5
3439.1 (corner)	-0.014	7.57	0.000	90.0	9.0

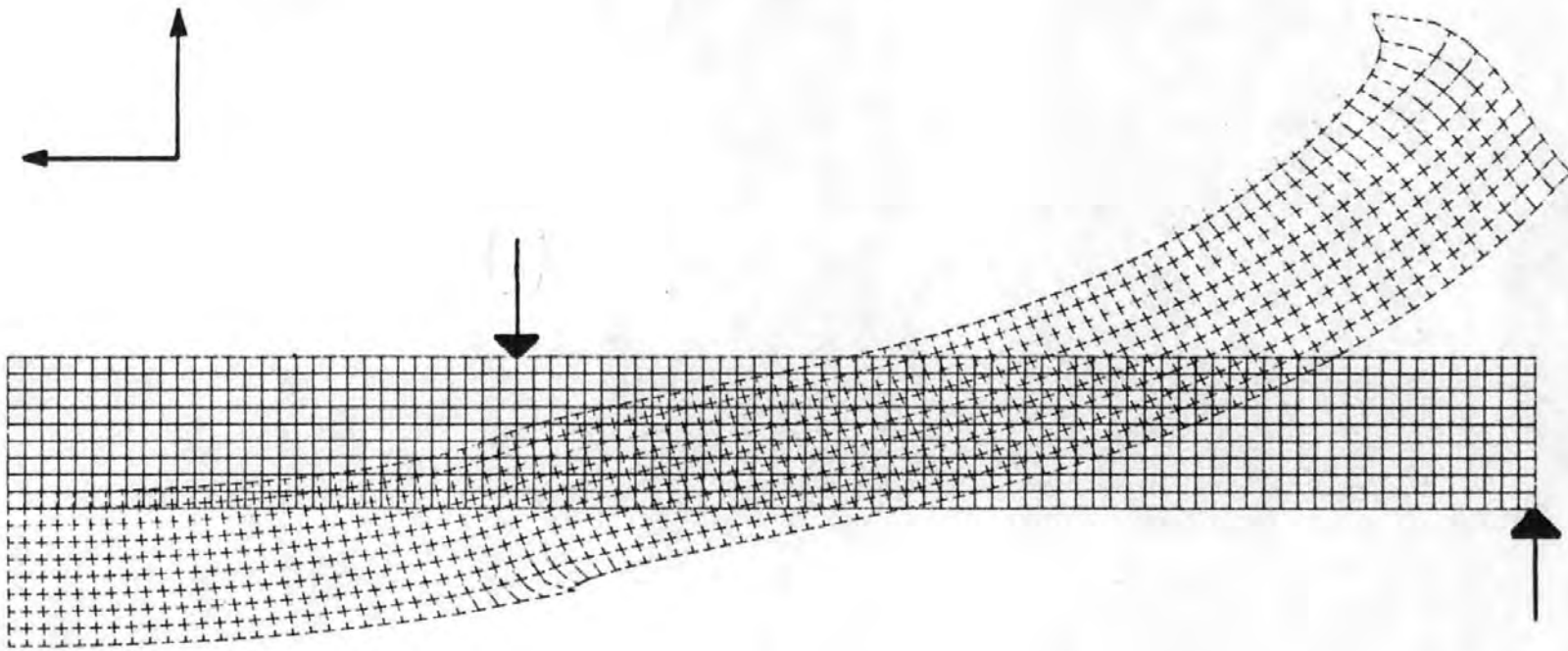


Figure 24: The displaced shape of the finite element mesh from the 810-element analysis (shown dashed) with the original mesh (solid).

5 Discussion

5.0 Development of a fibre mixing technique

A modification of the Courtaulds air knife was developed to create a very flat ribbon of fibre, up to 10 cm (4") wide from a single tow or roving. The original air knife was developed to spread carbon fibre tows into a randomly oriented tape. In the modification, more accurately termed "an Aircomb", it was possible to obtain a very flat continuous ribbon of fibre by the use of two aircombs in series, first spreading the tow to about 5 cm (2") and subsequently expanding this to 10 cm (4"). In order to do this the supply of air pressure to each of the aircombs could be adjusted separately. Full details of the design and operation are given in section 3.0.1 (page 80).

5.1 Microstructure

5.1.1 Classification of hybrid component structures

Because of the diversity of the component materials used in fibre composite hybrid materials, a scheme for the classification of these materials has been proposed (see figure 1, page 7). For example, a hybrid composed of unidirectional hybrid fibre tapes all aligned parallel to one axis would be classified "B1", while the same materials with crossplied tapes would be classified "B2", as would a woven hybrid fabric. A full specification of a hybrid composite should include:

- a) a clear concise indication of the lay-up sequence,
 - b) the volume fraction and weight fraction of each component relative to both the entire hybrid and the individual ply,
 - c) an indication of the components: carbon fibre

glass fibre

resin

together with the relevant properties and trade names of each,

- d) the filament diameter, density and length (in the case of short fibre composites), tow and tex figures and details of the surface treatments,
 - e) resin density, additives and the cure history of the matrix,
 - f) the extent and nature of any voidage or quality defects, and
 - g) the relevant properties of each of the single fibre composites when laid-up in a manner equivalent to that in the hybrid.

5.1.2 Microstructure parameters

A trio of microstructure parameters were examined as possible ways of quantifying the extent of mixing of the two fibre species within a fibre composite hybrid material. The three parameters were:

nearest neighbour index,
chi-squared index, and
contiguity index.

These indices were selected because of the ease with which they could be adapted to line transect analysis, in order to simplify data processing. In the initial analysis these parameters were determined by simple measurement of the photographs from the optical microscope. This involved recording individual data points and then transferring the data to a computer for processing which proved to be a tedious job.

In order to automate the generation of microstructure parameters, an Apple II micro-computer and peripherals were acquired. The system is illustrated in figure 15 and described in section 3.1. The use of the graphics tablet and stylus allowed the data points to be transferred direct to the computer memory, and the parameters were automatically printed out at the end of each line transect. Sample results of line transects of the micro-structure photograph (figure 25) overleaf are summarised in table 39.

Table 39: Calculated microstructure parameters for figure 25

	<u>Nearest neighbour</u> <u>index</u>	<u>Chi-squared</u> <u>index</u>	<u>Volume fraction</u> <u>%</u>			
<u>Glass</u>						
Transect 1	0.77	45	19			
2	1.10	40	26			
3	1.01	40	40			
4	0.78	41	22			
5	1.04	40	33			
6	1.05	40	38			
Average	0.96	41	30			
Range	0.33	5	21			
<u>Carbon</u>						
Transect 1	1.08	12	15			
2	0.90	9.9	22			
3	0.62	12	15			
4	0.78	6.3	30			
5	0.93	7.3	13			
6	1.04	7.8	25			
Average	0.89	9.2	20			
Range	0.46	5.7	17			
<u>Contiguity index</u>	1 0.43	2 0.42	3 0.39	4 0.44	5 0.53	6 0.43
Average	0.44					
Range	0.14					

The microstructure photograph in figure 25 was however an idealised hybrid, an experimental material from PERME Waltham Abbey utilising chopped fibres. In practice with the continuous unidirectional composites used in this project there was a far greater tendency for fibres to cluster into groups of a single fibre species, see for example figure 26. Under these circumstances the microstructure parameters were found to be even less consistent because of the scale of the microstructure and the difficulty of selecting a single representative image.

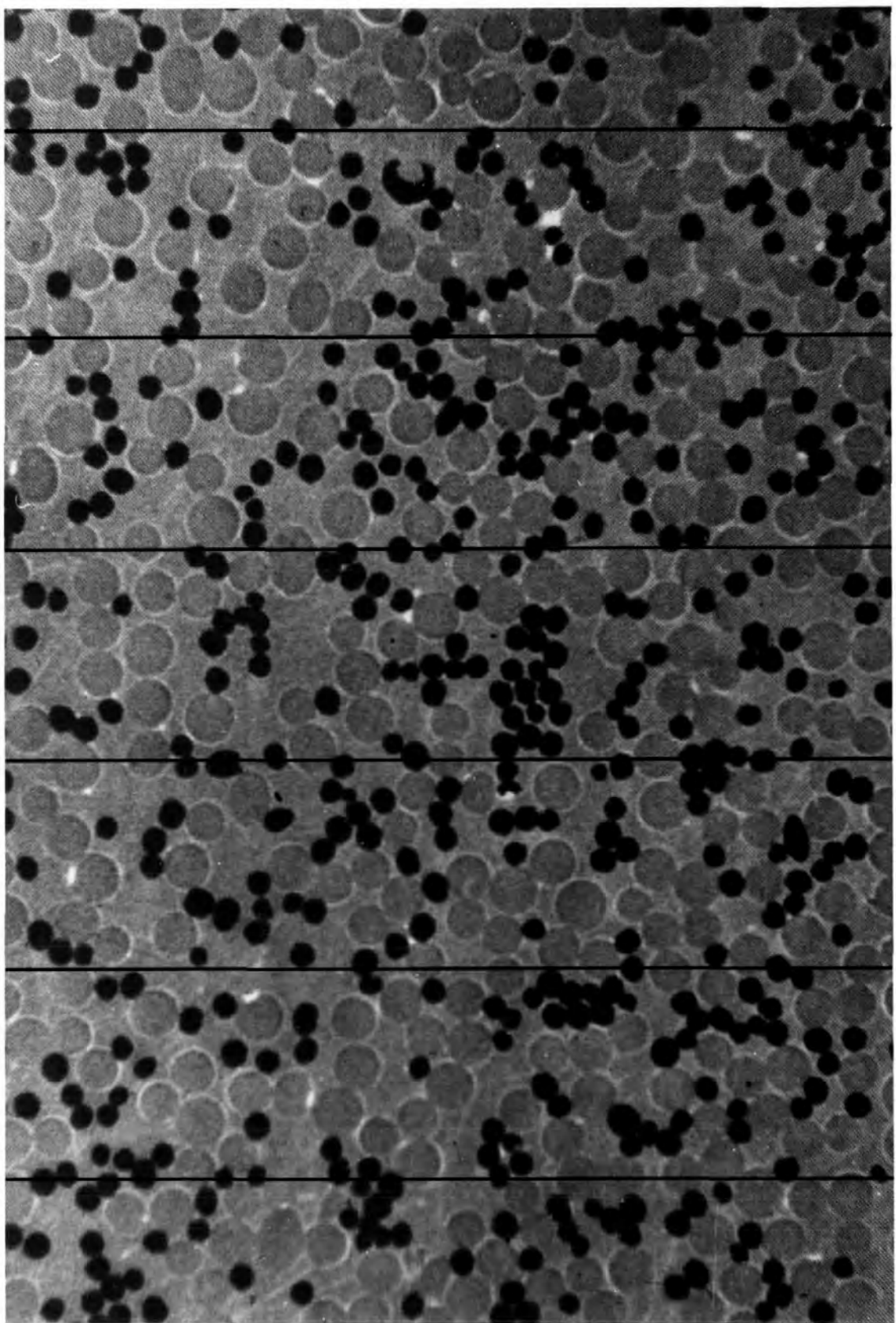


Figure 25: Photograph of an idealised carbon-glass hybrid, with the line-transects used for determination of the microstructure parameters shown. (1 at top, 6 at bottom.)

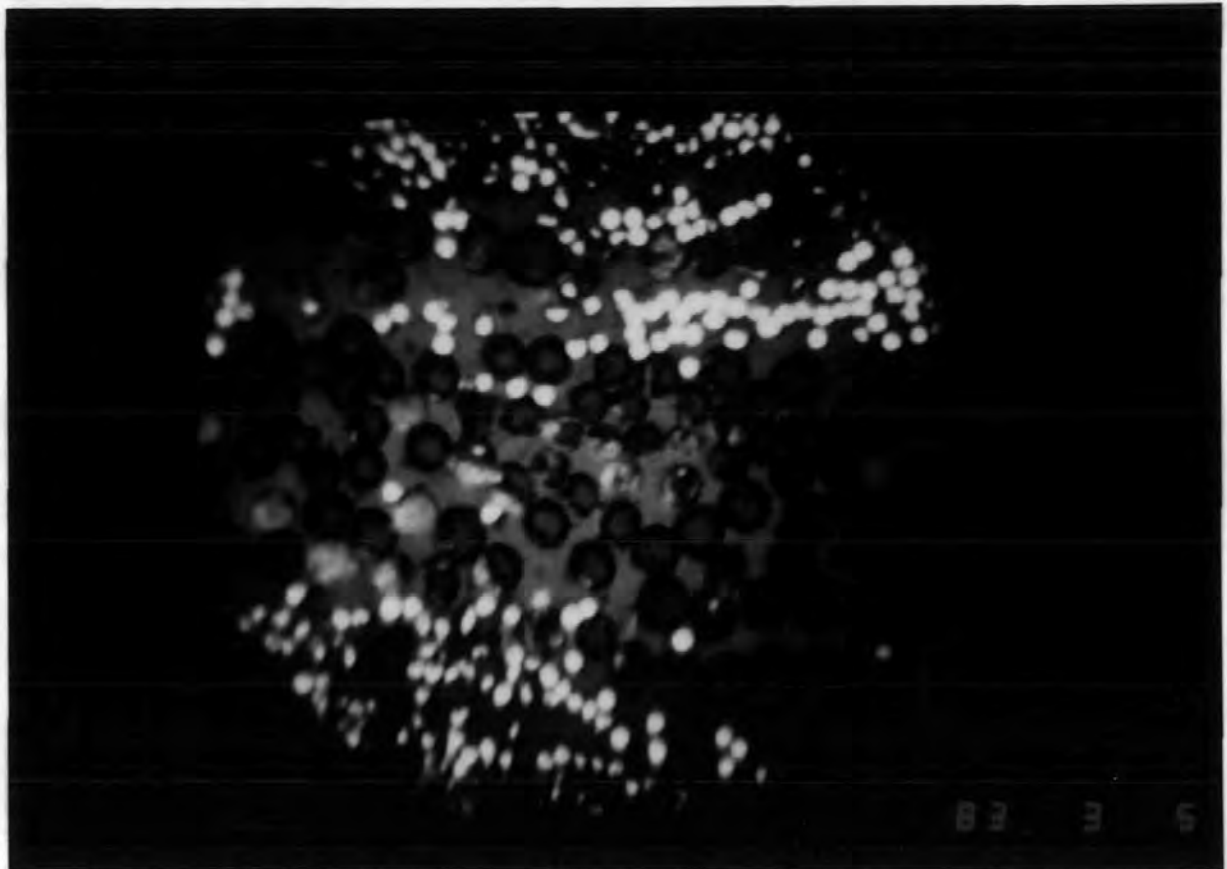


Figure 26: Black and white closed-circuit television image of the hybrid microstructure.



Figure 27: Colour enhanced digitised image of the above hybrid microstructure.

5.1.3 Microstructure analysis using an automatic television system

In order to eliminate the subjectivity in the choice of positioning the line transect on the microstructure photograph, an attempt was made to implement a system for the automatic analysis of this data. A black and white television camera (National CCTV system WV401) was focused on a polished composite specimen in an Olympus optical microscope fitted with a National microscope adaptor (model WV9005N). The video signal was immediately displayed on a monochrome CCTV monitor screen. The video signal was also taken through a Microworks DS65 Digisector card into slot 2 of an Apple II 48K microcomputer, see figure 15 on page 87. The digisector card converts the video signal into a high resolution Apple graphics image. A 256 X 256 picture element (pixel) representation is stored in specific memory locations on a 64-level grey intensity scale. The Apple high resolution graphics screen has only 5 grey levels and cannot therefore adequately represent the information which is held in-core.

Initial tests indicated that there was significant geometrical distortion. In tests with a fine square calibrated microgrid, the resulting screen displayed diamond shapes with curved edges. In order to assess the time required for data analysis of these images a computer program was written to examine every point of the graphics screen image and assign a colour according to the grey intensity value associated with that point. The intention was to produce a colour enhanced image of the microstructure with a different colour assigned to each type of area (resin, fibre or interface). Using a simple program written in Basic this took approximately 100 minutes. The program is listed in table 40, the monitor screen image is illustrated in figure 26, and the colour-enhanced image appears in figure 27. Although this was partially successful, there was considerable spreading of the interface, and a noticeable variation in light levels across the screen. The latter factor, due primarily to the uneven nature of the illumination of the specimen in the microscope, resulted in colour enhanced images in which only a section of the screen was correctly colour coded. This effect of the lighting can be partially corrected by eye on the monitor screen, but is very difficult to completely avoid because of the ability of the human eye to interpret pictures with nonuniform illumination.

This part of the work was terminated because of the problems with illumination, distortion, and the unclear separation between the results from fine and coarse hybrids in the mechanical tests. The speed of image analysis could be significantly improved by programming in machine language, which could offer significant scope for development. A similar system for the analysis of immunoelectrophoresis images has recently been reported by the Rutherford and Appleton Laboratories (=245).

5.2 Mechanical properties

5.2.1 A new strength theory

A new theory for the prediction of the strength of hybrid composites has been derived, which may predict the extent of any hybrid effect. The major assumption is that the failure strain of a hybrid composite will follow the rule-of-mixtures prediction based on

```

1 DIM Z(64)
2 FOR I = 1 TO 64
3 Z(I) = 0
4 NEXT I
10 PRINT "MICROWORKS DS65 DIGISE
        CTOR"
20 PRINT "*****PROGRAM*****"
30 PR# 2
40 PRINT "!*"
45 PR# 0
50 PRINT "ORIGINAL IMAGE SHOWN"
61 GET A$
62 I1 = 1
63 I2 = 254
64 J1 = 31
65 J2 = 191
70 IF A$ < > "S" THEN GOTO 75
71 I1 = 100
72 I2 = 150
73 J1 = 75
74 J2 = 125
75 HCR : PR# 2
80 FOR I = I1 TO I2
90 FOR J = J1 TO J2
100 POKE 64,I
110 POKE 65,J
120 PRINT ","
130 B = PEEK (66)
133 Z(B + 1) = Z(B + 1) + 1
135 PR# 0: PRINT I,J,B: PR# 2
140 IF B > 14 THEN GOTO 170
150 HCOLOR= 3
160 GOTO 210
170 IF B < 50 THEN GOTO 200
180 HCOLOR= 1
190 GOTO 210
200 HCOLOR= 0
210 HPLOT I,(J - 31)
220 NEXT J
230 NEXT I
240 PR# 0
250 PRINT "SAVE PICTURE TO DISC?"
260 GET A$
270 IF A$ < > "Y" THEN GOTO 33
280 PRINT "ENTER FILENAME":
290 INPUT N$
300 D$ = CHR$(4)
310 PRINT D$;"BSAVE P$";N$;"A$1
        92+L8192"
320 TEXT
330 PR# 1
340 PRINT "B"      N"
350 FOR B = 1 TO 64
360 PRINT B,Z(B)
370 NEXT B
380 PR# 0
390 D$ = CHR$(4)
400 PRINT D$;"CATALOG"
410 END

```

Table 40: Computer program for colour-enhanced microstructure images.

the failure strains of the monofibre composites. It is implicit in this assumption that the failure strain of the low elongation component will be enhanced by the presence of tougher high elongation fibres. Both Manders (=79) and Parratt (=202) have observed carbon fibres in hybrid composites continuing to carry load beyond a strain characteristic of the bundle strength of monofibre composites.

In a monofibre carbon composite failure tends to occur catastrophically, with the first fibre fracture leading to crack propagation throughout the composite. If each carbon fibre is surrounded by sufficient glass fibre to allow the complete absorption of the dynamic stress concentration at carbon fibre failure, then a sequence of failed carbon fibres may occur at random positions throughout the testpiece before the stress concentrations interact. Each carbon fibre is thus expected to fail at its own weakest point, rather than at the stress concentration from an adjacent fractured fibre. When the fractured carbon fibres are scattered randomly throughout the composite, each fibre can contribute fully to the strength of the hybrid except in the short distance, the critical length, either side of the fracture where the stress builds up to that in the bulk of the composite.

The new equation for the strength of a hybrid composite in which the failure strain follows the rule-of-mixtures with respect to the volume fraction of the components is derived in section 2.2.4. The equation is:

$$\sigma' = V_L E_L \epsilon'_L + V_H E_H \epsilon'_H + V_H V_L (E_L - E_H)(\epsilon'_H - \epsilon'_L).$$

By definition, $(\epsilon'_H - \epsilon'_L)$ will be a positive term, and in general, $(E_L - E_H)$ will also be a positive term, as there would be little advantage to be expected from a hybrid of a high-elongation-high-modulus fibre with a low-elongation-low-modulus fibre. The first two terms of the equation are those to predict the rule-of-mixtures strength. The third term predicts the extent of any "hybrid effect". Of course when either both of the moduli or both of the failure strains are numerically equivalent there will be no "hybrid effect" predicted.

Maximum benefit is therefore to be expected when the differences in moduli and failure strains are large. However, the assumptions of the model will be broken if the differences require that the fibres are fractured in numerous places, because the failure strains are radically different.

The prediction of the elastic failure strength of hybrid composites using the simple rule-of-mixtures is very unsatisfactory because it assumes that the two fibre components are each strained to their respective elongation-at-break at the moment when failure occurs. This is obviously very unsatisfactory as the probability of this happening must be low either because of the absence of strain compatibility, or because of the complex load-sharing mechanism which would bring this about.

The constant strain theories for hybrid strength require that there will be a step discontinuity in the failure strain of the composite at a specific volume fraction of each component. It is unlikely that an addition of a very few additional fibres will lead to such a radical change in the failure strain of the composite. The theory, even in the later ver-

sions makes no allowance for the contributions of the (fractured) carbon fibres to the modulus of glass-rich composites.

Unlike the existing theories, the new theory assumes that both elongation-at-break and elastic modulus vary linearly with volume fraction. As a consequence of this, the predicted strength of the hybrid composite follows a smooth curve with respect to volume fraction. If the moduli and elongation of both high and low failure strain monofibre composites are assumed to be the same, then the equation will simplify to predict the strength normally associated with a monofibre composite. Similarly, if either the two elastic moduli or the two failure strains are numerically equivalent, then the term to predict "hybrid effect" will disappear and no enhancement of the strength will be expected. A discussion of the experimental results is given in the next section.

The new theory takes no account of the benefits which may arise because of the thermal residual strains which arise from the differences in the coefficients of the thermal expansion in the two types of fibres. Carbon and Kevlar fibres are unusual in that they undergo a small longitudinal expansion upon cooling. In a carbon fibre with glass fibre hybrid reinforced plastic which is fabricated at high temperature, there will be a differential contraction of the components on cooling to room temperature. When expanding carbon fibres are constrained by contracting glass fibres during cure and cooling, an equilibrium is likely in which the carbon fibres have a net compressive strain and the glass fibres have a net tensile strain. As the carbon fibres are the low elongation species, they may now be stressed in tension to a strain equivalent to the sum of the natural elongation-at-break and the net residual compressive strain, with the consequent benefits in tensile loading. This may be further enhanced by the volume contraction of the matrix upon crosslinking during cure, although the relatively low modulus of the resin is unlikely to allow significant residual stress to be achieved. This paragraph assumes that the fibre-matrix interfacial bond is made at the higher temperature and all subsequent contractions occur together because of this. If the interfacial bond is actually formed during curing the residual stress situation will change as a consequence. All hybrid composites in the experimental programme were fabricated using room-temperature curing polyester resin to minimise thermal residual strains, although a minor contribution may arise because of the cure exotherm.

5.2.2 Strength theories and correlation with experimental results

Graphs of typical results obtained from experimental work in this project are presented in figure 28 (longitudinal elastic modulus) and figure 29 (longitudinal strength based on the earliest significant load-drop, ie. not necessarily the peak load). In general, the elastic modulus was found to vary in a linear manner with changing volume fraction as is to be expected from composites in which there is reasonable intermixing of the components.

The carbon fibre composites failed catastrophically from the tensile or compressive surface, and the glass fibre composites failed by massive delamination through the depth of the beam. In the case of longitudinal flexural strength, the failure mode of the hybrid

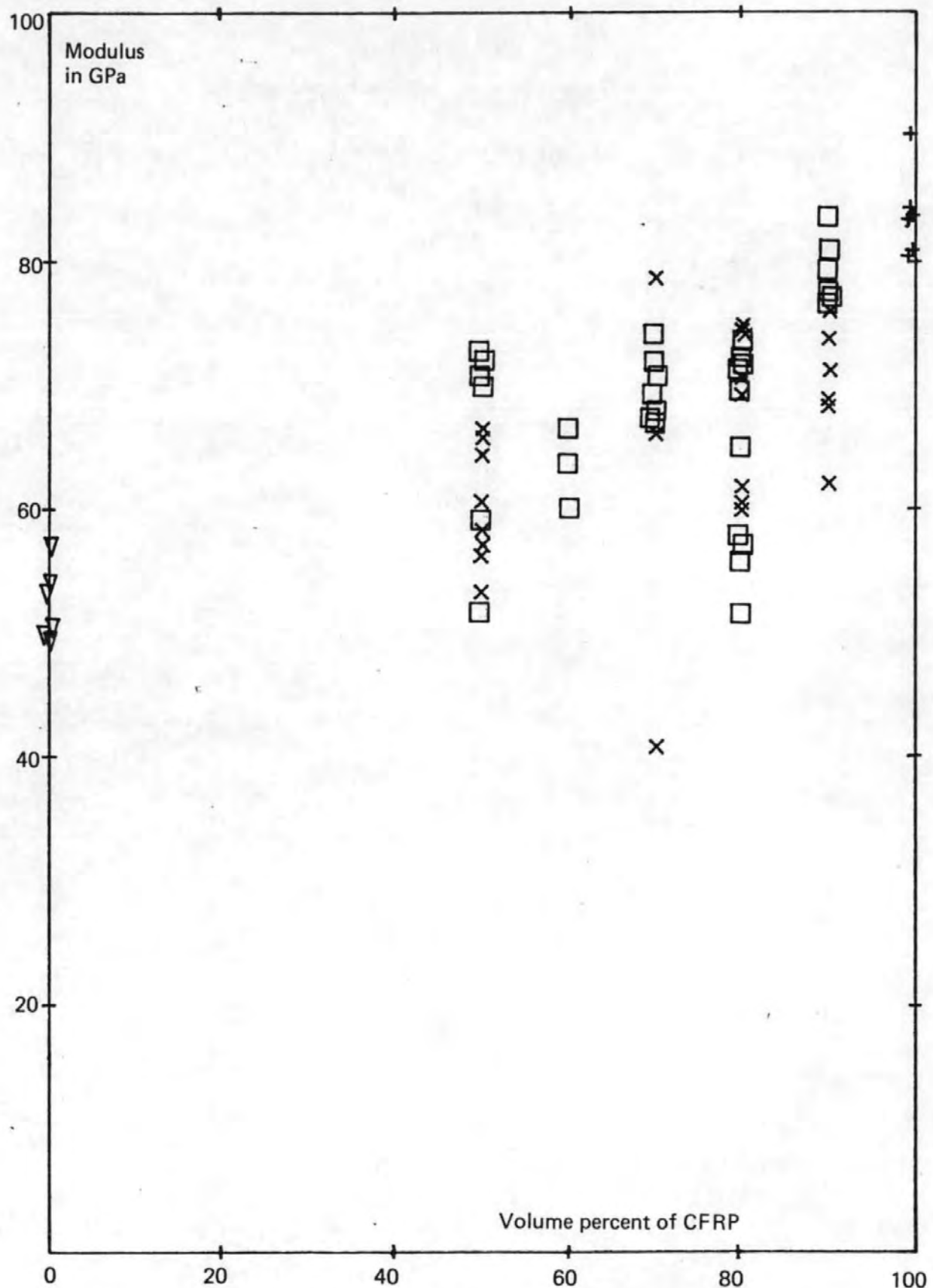


Figure 28: The longitudinal elastic modulus of EAS carbon/glass-fibre hybrids plotted against the volume percentage of carbon fibre composite: fine hybrids (X), coarse hybrids (□), glass (▽), carbon (+).

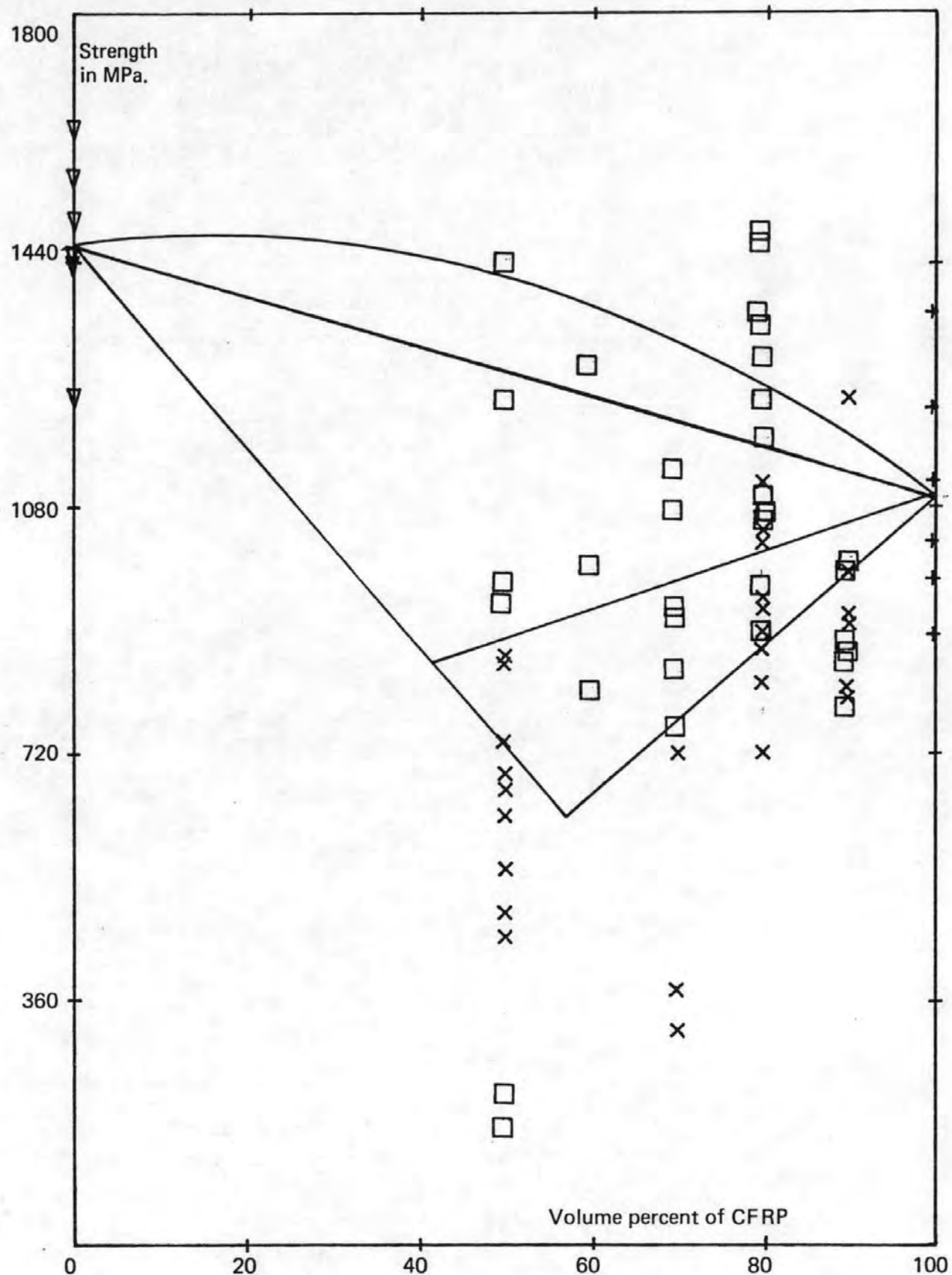


Figure 29: The initial longitudinal strength of EAS carbon/glass-fibre hybrids plotted against the volume percentage of carbon fibre composite: fine hybrids (X), coarse hybrids (□), glass (▽), carbon (+).

composites was generally by a buckling of fibres on the compression side of the beam out of the surface of the specimen. The buckling of the hybrid composites suggests that the true strength of the material is not being achieved, because of the changed failure mode.

On those rare occasions where the tensile, compression, or delamination failure modes were observed in hybrid composites, the strength of the material was found to exceed the rule-of-mixtures prediction. The other hybrid composites did not perform as well as predicted, either by the rule-of-mixtures or by the constant strain theory. The finely-mixed hybrids did not exhibit such high values for failure strength as the coarse hybrids. This may well be that the carbon fibres were damaged by the air comb used to separate individual fibre tows before recombination into the hybrid-tow. In earlier tests there did not appear to be much difference in the performance of coarsely- and finely-mixed hybrids (see for example figure 35). There was little evidence from scanning electron micrographs of damage to the carbon fibres, though the simultaneous failure of the two fibres in Plate 4 (figure 44) may be as a result of the damage or malformation of the left hand fibre, and this damage may be a result of the mixing technique.

The results in the thesis by Manders (=79) are presented in graphical form in figure 30, with the lines for the various predictions superimposed. Once again the strengths of the hybrids do not follow any single prediction, but the carbon-fibre rich composites perform better than the glass-fibre rich composites. It would seem that a small addition of glass fibre to carbon fibre composites can bring about a significant improvement in the strength of the composite. It should however be emphasised that the addition of a small portion of carbon fibres to glass fibre composites generally causes a severe degradation of the composite strength, and this was observed both in Manders results, and in very early tests for this thesis.

Figure 31 presents results for the Kevlar 49/E-glass hybrids from data in the thesis by Gruber (=246). The failure strain of Kevlar 49 is generally accepted as around 2.5% and that for E-glass as 3.37%, and as such these are closer than the elongations of carbon fibres and glass fibres. The assumptions of the new rule-of-mixtures-failure-strain theory are thus more closely adhered to with Kevlar/glass composites than with the carbon/glass composites. The figure shows that all but one of the experimental results fall above the strengths predicted by the new theory based on the average component values of the monofibre composites. However, the thermal stresses imposed by the cure cycle (maximum temperature 163 °C) could be a significant contributory factor in this as the longitudinal coefficient of the components differ widely (Kevlar 49: $-2 \times 10^{-6} \text{ K}^{-1}$, E-glass: $+5 \times 10^{-6} \text{ K}^{-1}$).

In summary, it has not been possible to fully confirm that the new theoretical approach to the strength of fibre composite hybrid materials is valid. There are indications that well fabricated and balanced mixed fibre composites can attain higher strengths than would be predicted by the usual rule-of-mixtures approach. This may be further improved by careful design of the thermal aspects of the fabrication cycle. It should however be noted that the addition of a small portion of carbon fibres to a glass fibre composite

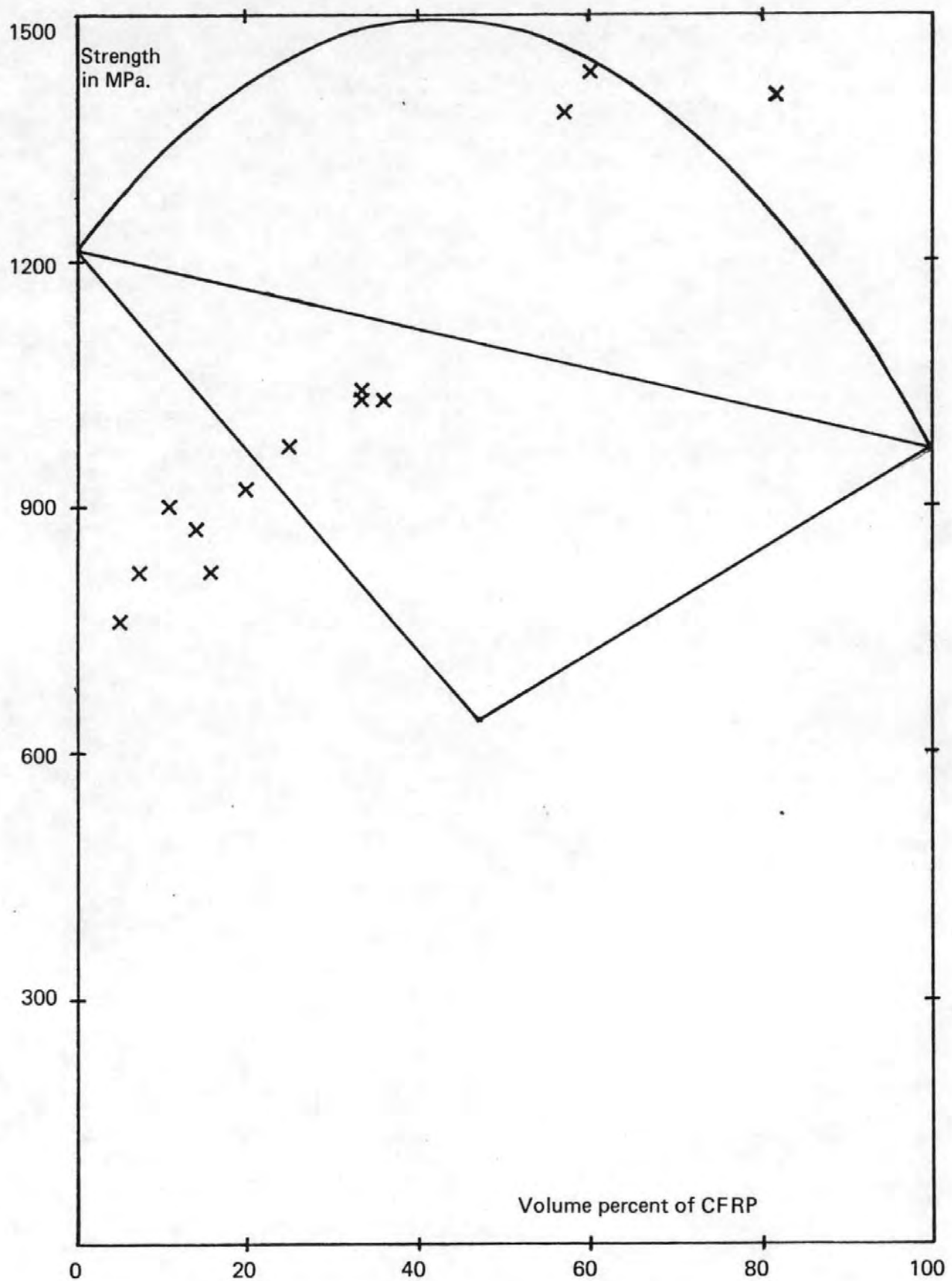


Figure 30: The strength of HT carbon and E glass hybrids plotted from data in the thesis by P.W. Manders (=79).

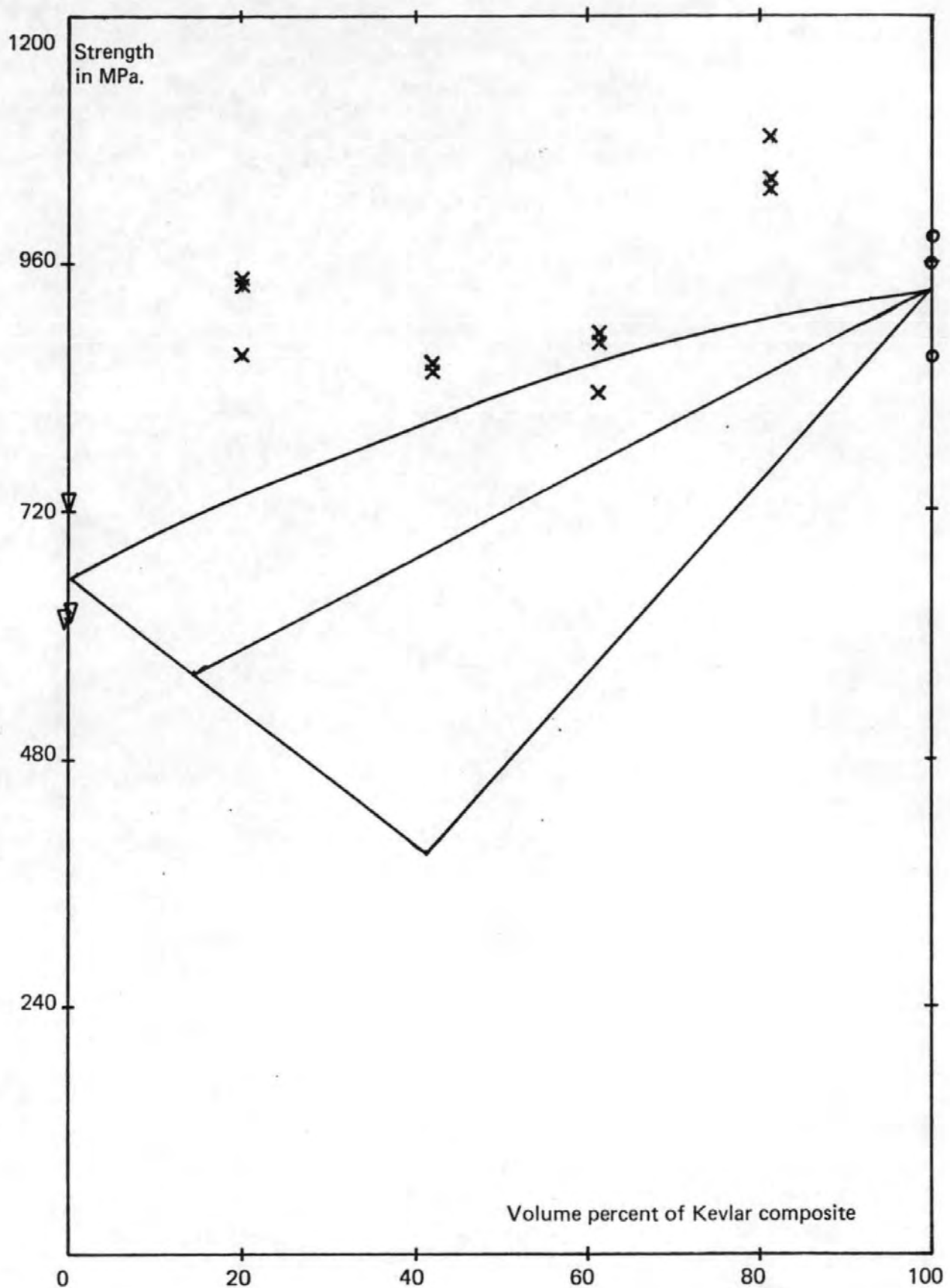


Figure 31: The strength of Kevlar 49/E-glass hybrids plotted from data in the thesis by M.B. Gruber (=246).

generally causes a significant depression of the composite strength. If the buckling failure mode can be suppressed then the potential for hybrid composites will be greatly improved.

5.3 Acoustic emission

5.3.1 Acoustic emission total counts

The acoustic emission counts observed during the flexural testing of composites increase in number, and also in the rate at which they occur, as the test progresses. The acoustic emission event counts for carbon fibre reinforced plastics occur almost entirely during the period immediately before failure of the specimen. The initial few counts in CFRP occur over a wide range of deflections and are probably due to stress relief of minor defects in the sample. At 1000 counts, the deflections are more consistent between different samples of the same material than at 5 counts.

In glass fibre reinforced plastics, the deflection at which the first emissions occur is considerably more consistent. The graph of cumulated counts against deflection for GFRP approximately forms a rising exponential curve. The range of deflections at 1000 counts is however greater than that which occurs in CFRP.

The hybrid composites are generally initially far noisier than either of the monofibre composites. Furthermore, the finely mixed hybrids are noisier than the coarse hybrids. This is further exaggerated by the extremely fine mix hybrid XAS carbon/glass composites in which initial emissions occur almost immediately the test is started. Two major possibilities exist, either the fibres are more damaged during the fabrication of the specimens, or the different properties of the materials contribute to the acoustic emissions.

There is little evidence from the scanning electron micrographs that any obvious damage occurs to the fibres during passage through the air knife. It is not possible to say whether any damage observed in fractured composite is due to damage during moulding or due to the fracture of the specimen under the load applied in testing.

The increased noise in finely mixed hybrids may therefore be due to the physical positioning of the fibres relative to one another. This may be an effect which is overridden in practice by undetected damage inflicted whilst mixing the fibres. However the extremely-fine-mix hybrid XAS carbon/glass composites, which were unlikely to be more severely damaged than the fine-mix hybrids, were noticeably noisier. It would therefore appear that the reduction of the scale on which carbon:glass interfaces occur leads to additional residual stresses in the hybrid composite. The application of small stresses to these composites allow stress relief to occur with the resulting acoustic emissions detected at the specimen surface.

5.3.2 Acoustic emission amplitude distribution

In the major sequence of mechanical property tests, and in all the tests carried out at Bath University using the amplitude sorting acoustic emission rig, the monofibre composites each consisted of ten tows of fibre and the hybrid composites each consisted of five tows of glass fibre and five tows of carbon fibre. Because of the small size of the test specimens in comparison to the face of the acoustic emission transducer it was necessary

to mount the transducer on the support roller of the flexure jig. It must be assumed in the discussion which follows that there are no complications arising from the transfer of the stress wave from the specimen to the jig and thence to the transducer. As the discussion is concerned simply with the relative acoustic emission signatures of related composites, it seems probable that any such attenuation will occur in some proportion related to the composition of the composites.

Figures 32 and 33 are diagrams of acoustic emission amplitude distribution signatures for the various composites at failure. The signatures for coarse and fine hybrids are sensibly the same at either level of mixing. Each of the monofibre signatures is an average of two distributions. The hybrid signature is the mean of two coarse and two fine mix hybrids. The hump in the centre of the hybrid signature only begins to appear in the final stages of the flexure test.

All specimens failed below the roller on the tension face. The hybrids also exhibited some buckling below the loading anvil on the compression face. Delamination in the glass fibre composites was concentrated around the layer where the crack was arrested from propagating normal to the major axis of the fibre. In general the carbon fibre composites failed by crack propagation instantaneously across the specimen, although in some cases there was sufficient "brushing" to hold the two fractured halves together.

The cumulative amplitude distribution has a distinctive shape for each type of specimen. In this mode the equipment displays a trace in which each channel displays all events greater than that energy. The trace must therefore, of necessity, constantly rise from right to left. The alternative mode of display shows the individual counts occurring within the 1.2 dB limits defined for that channel.

The events in channels 16-32 (the centre third of the 50 channels) of the hybrid signature occur in the latter part of the test suggesting that they are probably a result of load transfer from the carbon fibres to the lower modulus, higher strain-to-failure glass fibres. If the events in this centre portion of the amplitude signature could be ascribed solely to failure mechanisms associated with the glass fibres, then the broader spread of events in this region may suggest that the presence of the failed carbon fibres causes weakening of the glass fibres. In the absence of more statistically meaningful quantities of data this can only be speculative. It should be noted that there are a significantly greater number of events in this region on the hybrid trace than in the glass-only composite trace. This would suggest that the glass-resin delamination or glass-fibre fracture has occurred to a greater extent in the hybrid than in the glass composite. It also should be pointed out that failure of the hybrid is deemed to have occurred at a lower crosshead displacement than in the glass fibre composite.

The occurrence of the second peak in recorded events on the individual events distribution would suggest that this is a glass fibre only phenomena. If this is so then the spreading of the group of events could be due to a number of causes, most noticeably:

increased delamination due to increased residual stress,
stress concentrations arising from fractured carbon fibres.

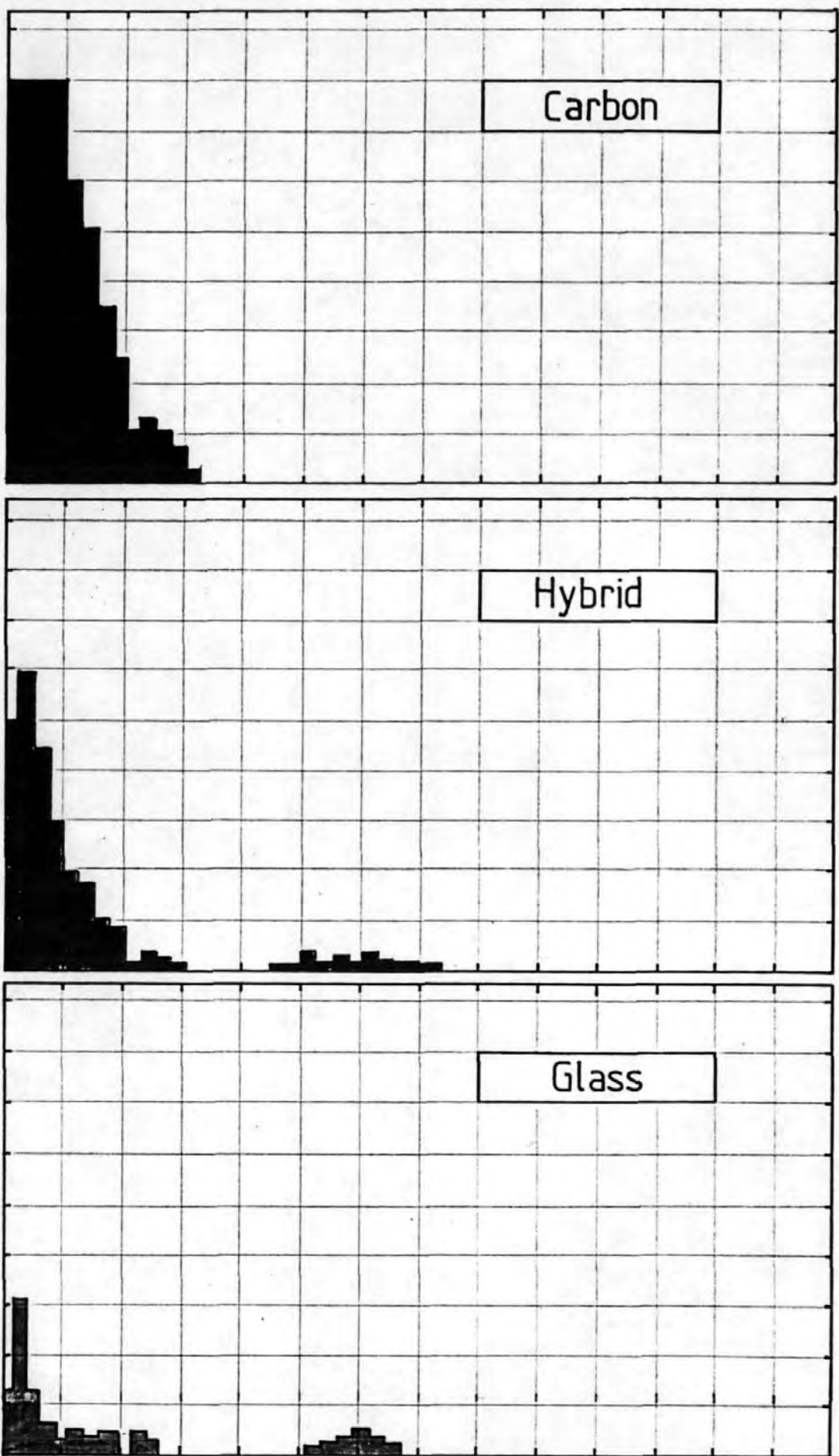


Figure 32: The classical amplitude distribution histograms from three composites during acoustic emission monitoring of flexural tests.

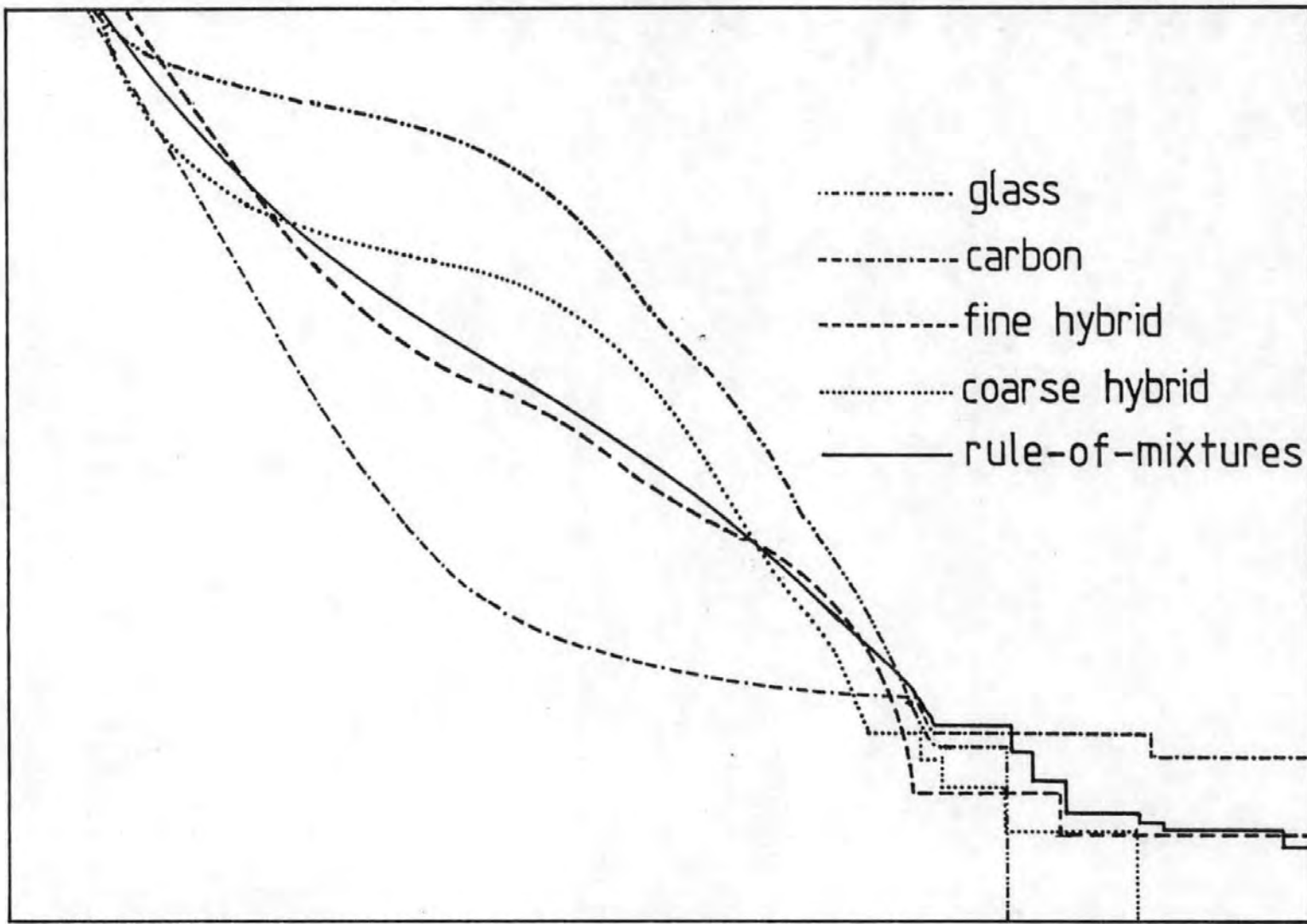


Figure 33: The cumulative amplitude distributions from acoustic emission signals during flexural tests on the indicated composites.

If the moduli of the composites are nominally the same, then the fibre fracture energy might sensibly be expected to be related to the square of the failure strain. This would suggest, as shown in the amplitude signatures, that the glass fibre composite would exhibit higher energy acoustic emissions.

In conclusion of this section it should be stressed that these results are based on a limited number of experiments and the conclusions are therefore tentative. However there was reasonable reproducibility within each specific group of tests. It would appear that the amplitude distribution acoustic emission technique offers a promising technique for the further understanding of composite failure mechanisms.

5.4 Finite element analysis

5.4.1 Results from triangular anisotropic constant strain finite elements

These results have been presented elsewhere (=247), and although that paper is included in Appendix 1, the conclusions of that work follow:

Because of the use of nodal averaging of the stresses in creating the diagrammatic output, the discrete values of stress at any individual node were not absolute values. In considering the stresses around a discontinuity, modelling a crack tip, the node on the crack edge nearest the crack tip node would have a finite stress for example. This is because it shares a common element with the node at the singularity. Similarly the stress value at the crack tip node would be reduced because it is in an element containing the free (cracked) edge.

As expected there was no net increase in stress between different sections normal to the loading direction. This was ascertained by measurement of the area under each of the stress curves. The x (transverse) and xy (shear) stresses produced had a zero net stress when the sign (tension = +, compression = -) of the stresses on the section was taken into account.

The single edge notch (SEN) and rectangular cantilever (RC) specimens with grips free to pivot in the plane of the specimen produced a net bending because of the moment of the loading forces in respect of a line running perpendicular to the crack at the tip. This bending generated compressive forces on the edge of specimen away from the notch, which was more pronounced in the RC specimen than in the SEN specimen. To compensate for this, the stress concentration at the singularity was also greater in the RC, than in the SEN, analysis. All of the load applied in the RC specimen was applied on a line normal to, but running through, the crack. The same magnitude of load in the SEN specimen was applied to the specimen uniformly across the section. The net bending force was therefore greater in the RC specimen, with the results predicted above thus being an obvious consequence of the loading geometry.

In the double edge notch (DEN) and centre notch (CN) specimens there was no significant bending of the specimen because of the constraints imposed by the symmetry of the system. As a result of this the stress concentration at the singularity was appreciably reduced in both cases. Both DEN and CN analysis generated longitudinal stresses which were nominally the same at the crack tip for a given anisotropy of material properties.

Throughout the range of specimens and material anisotropies analysed, a reduction of the modulus normal to the notch caused a marked increase in the x-stress (parallel to the notch), and hence tended to propagate the crack in its own direction. It is worth pointing out that this is a homogeneous analysis, but even so what is effectively an addition of fibres parallel to the crack will still tend to "funnel" the stress at the crack along the line of that crack, and effectively along the weak plane (all-resin or fibre-matrix interface) of a reinforced material.

Similarly an increase in the modulus normal to the notch will lead to a resultant increase in the y-stress (normal to the notch), and hence the crack will tend to turn. In a practical composite with a heterogeneous structure this will again be equivalent to the crack running in the weak (matrix or interface) direction.

Photoelastic tests with an isotropic Araldite CR39 model showed that the stress patterns generated by the finite element analysis were at least in qualitative agreement with those obtained using the photoelastic material.

5.4.2 Isoparametric finite element analysis

The isoparametric finite element analysis was carried out essentially in three stages:

- a) element R36510 from PAFEC 70+ on the ICL 1904,
- b) element R36510 from PAFEC 70+ on the dual PRIME 550, and
- c) element R44215 from PAFEC 75 on the dual PRIME 550,

because the computer system was first replaced, and level 3.1 of the new PAFEC software was subsequently made available. Details of the software changes which were necessary to run these numerical analyses are contained in section 3.4.2 (pages 99-102). In all cases it was necessary to use the nodal averaging and stress contours computer programs specially written in stage (a) for ease of comprehension of the output. (The versions of this software for stage (c) above are included at Appendix Seven, sections v-ix.)

Once system (c) was running successfully a series of 36-element finite element meshes were analysed. These are described in detail in section 4.4, with a summary of the results in table 35, page 135. Three sets of material properties were used for single fibre composites, and a carbon-shell glass-core hybrid was also analysed. Because of symmetry it was possible to obtain a reasonable model by analysis of one-half of the four-point bend beam by constraining the line of symmetry.

The CPU time required to run these problems was found to be reasonably independent of the numerical values in the input data for elastic constants, and the sandwich model did not take significantly longer. The major aim was to analyse problems with stress singularities, and this is discussed further in the following section. However it was evident that 36 elements was inadequate to represent the complex stress pattern in the problem. An attempt was thus undertaken to set up a larger finite element mesh.

An 810-element, 3439-node finite element mesh (90 X 9 elements) was set up to model a similar four-point bend problem to that in the 36-element analysis. (NOTE: for comparison, the finite element analysis of the Ford Sierra body structure used 11574

elements, with the rear suspension cross member accounting for one-fifth of the total elements (=248)). Several attempts were made to run this program, but because of system failures the run regularly stopped in phase 6 (setting-up the element and global stiffness matrices – over half of the total run time). It was eventually realised that there was a barrier within the PRIME system to prevent programs running beyond 7200 CPU-seconds (2 hours of dedicated computer time) and that this fell part way through phase 6, so that the trap for programs stuck-in-a-loop was catching a program which had not run its normal course. The program was eventually run overnight by special arrangement, with the trap removed. The total run time was 9 hours 49 minutes, with 25416 seconds (7 hours 4 minutes) of CPU-time used. Because of the impracticability of running programs of this size on a regular basis on a multi-user system this aspect of the work was abandoned.

The displaced shape of the 810-element problem is shown in figure 24 (page 138) with the original mesh and loading condition superimposed. In reality the intended problem was not analysed, as the loads were in practice applied on the wrong sides of the beam and at 90° to the intended direction. The problem solved was thus one in which the left-hand load was applied to the lower surface pulling to the right and the right-hand load was applied at the top surface pulling to the left, hence the distorted shape.

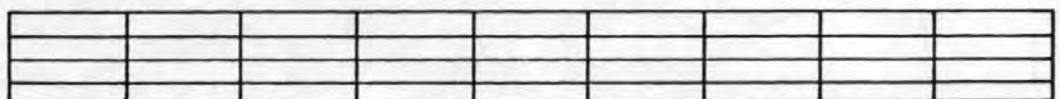
5.4.3 Isoparametric quarter-point finite elements for stress singularity modelling

Several authors have shown that isotropic materials with an appropriate \sqrt{r} singularity can be modelled using standard finite elements with isoparametric quarter-point mapping. The approach is now capable of very accurate fracture mechanical computations using standard computer programs. The technique has often been satisfactorily demonstrated with two-dimensional examples. It has recently been concluded by Peano and Pasini (=249) that the quarter-point technique should be applied with caution to three-dimensional problems involving curved crack fronts modelled with standard polynomial elements.

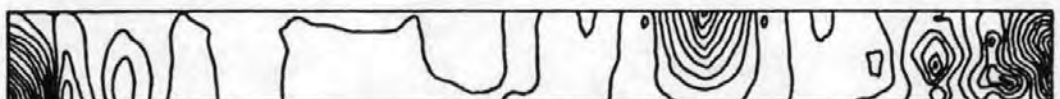
One of the original aspects of this work was an attempt to modify a standard finite element system to allow the modelling of a stress singularity in a two-dimensional representation of an anisotropic material.

In the PAFEC 70+ representations, this could be achieved by resetting the position of those midside-nodes adjacent to the crack tip node to the quarter-point positions, and by the use of a dummy subroutine R25101. The latter subroutine checks the node positions and resets any “misplaced” nodes to the midside position, thus by replacing the subroutine it was possible to use quarter-point nodes. It was of course essential to ensure that the remainder of the finite element grid was correct when using this misplaced nodes scheme. The statement to warn that the midside nodes were to be replaced occurred in the calling subroutine (R25100), and was therefore removed.

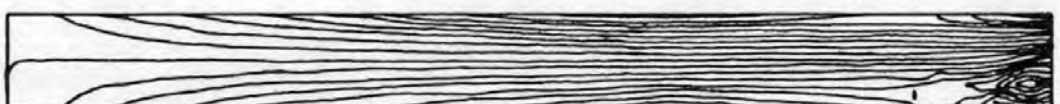
In the PAFEC 75 representations, suppression of the replacement of midside nodes could be achieved by specifying the crack tip node in the CRACK.TIP module. The stress solution software for the R44215 anisotropic element calls different matrix divide subroutines to those called for isotropic solutions. It was thus necessary to use a dummy



36 element mesh



x-stress contours
from 22 to -34 in steps of 2



y-stress contours
from 189 to -210 in steps of 21



xy-stress contours
from 21 to -10 in steps of 1

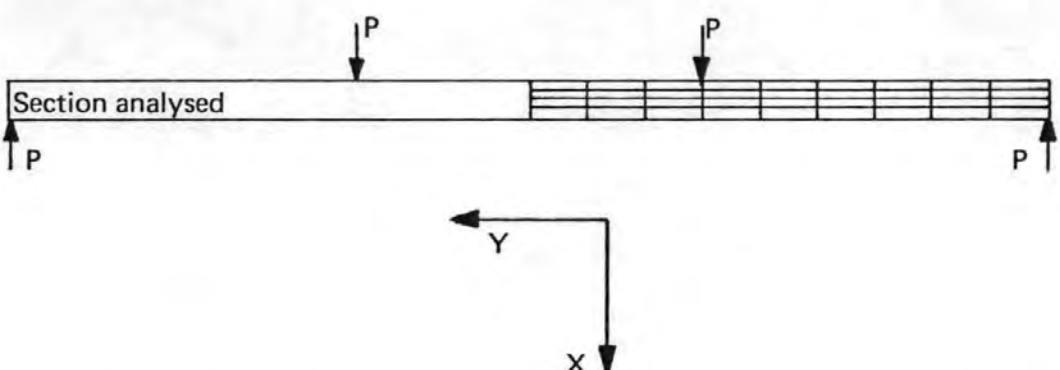


Figure 34: Typical stress contours from the finite element analysis of a notched anisotropic beam in four-point flexure ($a/w = 1/4$).

double-precision matrix divide subroutine (DMATDI), and the listing for this is contained on sectors D7-D9 of microfiche 1 in Appendix 7.

The stresses for the cracktip (node 129) in the 36-element PAFEC 75 analysis are summarised in table 36. The stress at the cracktip node was found to increase according to the model employed, in the sequence: unnotched, notched and then singularity. In the unnotched model the cracktip node was contained in the depth of the material, in the notched model the cracktip node was positioned at the cracktip but all midside nodes remained in their normal positions, and in the singularity model the midside nodes were shifted to the quarter points.

The physical significance of the \sqrt{r} singularity has not been fully investigated. It seems likely that the circular/spherical form of the singularity will become ellipsoidal in an anisotropic material, because of the heterogeneity of the stress field and the material properties. The form of the singularity will be more complex at the interface between two regions of different material properties. It did not prove possible to test this possibility because of the size of the mesh required and the consequent high computer processing time.

5.5 Cryogenic testing

An annular chamber to allow the testing of composites at approximately 77K was designed, built and shown to be capable of achieving the required temperature. However because of unexplained corrosion of adjacent metalwork, and the difficulty of obtaining alumina to fabricate the mechanical linkage/thermal insulator to attach and isolate the loading rig and the testing machine, the testing at 77K was abandoned.

There was however some testing of composites which had been immersed in liquid nitrogen. Three basic groups of these composites were examined: those immersed in liquid nitrogen and allowed to remain there until the liquid had boiled off, then allowed at least 24 hours to recover; those immersed in liquid nitrogen immediately prior to testing; and those control samples which remained at ambient temperature throughout. The results for the first group of EAS carbon-glass hybrids are presented in figure 35. These are also typical of the results for both HMS and XAS carbon hybrids.

It can be seen from the figure that each group (carbon 50:50, hybrid, and glass) lies approximately on a straight line from the origin, as is expected from the equation for elastic strength ($\sigma' = E\epsilon'$), with some slight scatter around the ideal. The experimental deviation within each group of composite-type/temperature-history is of the same order of magnitude as the scatter within each composite group, with no clear trends indicated.

It must therefore be concluded that no significant damage accumulates from the thermal stressing cycle resulting from the exposure to liquid nitrogen. This confirms the prediction in section 2.5 (page 79) that no significant damage would occur after this exposure. Additional problems may arise in real tests at 77K, especially the freezing-out of segmental motion in the resin, and the conversion of moisture in the material to ice-crystals.

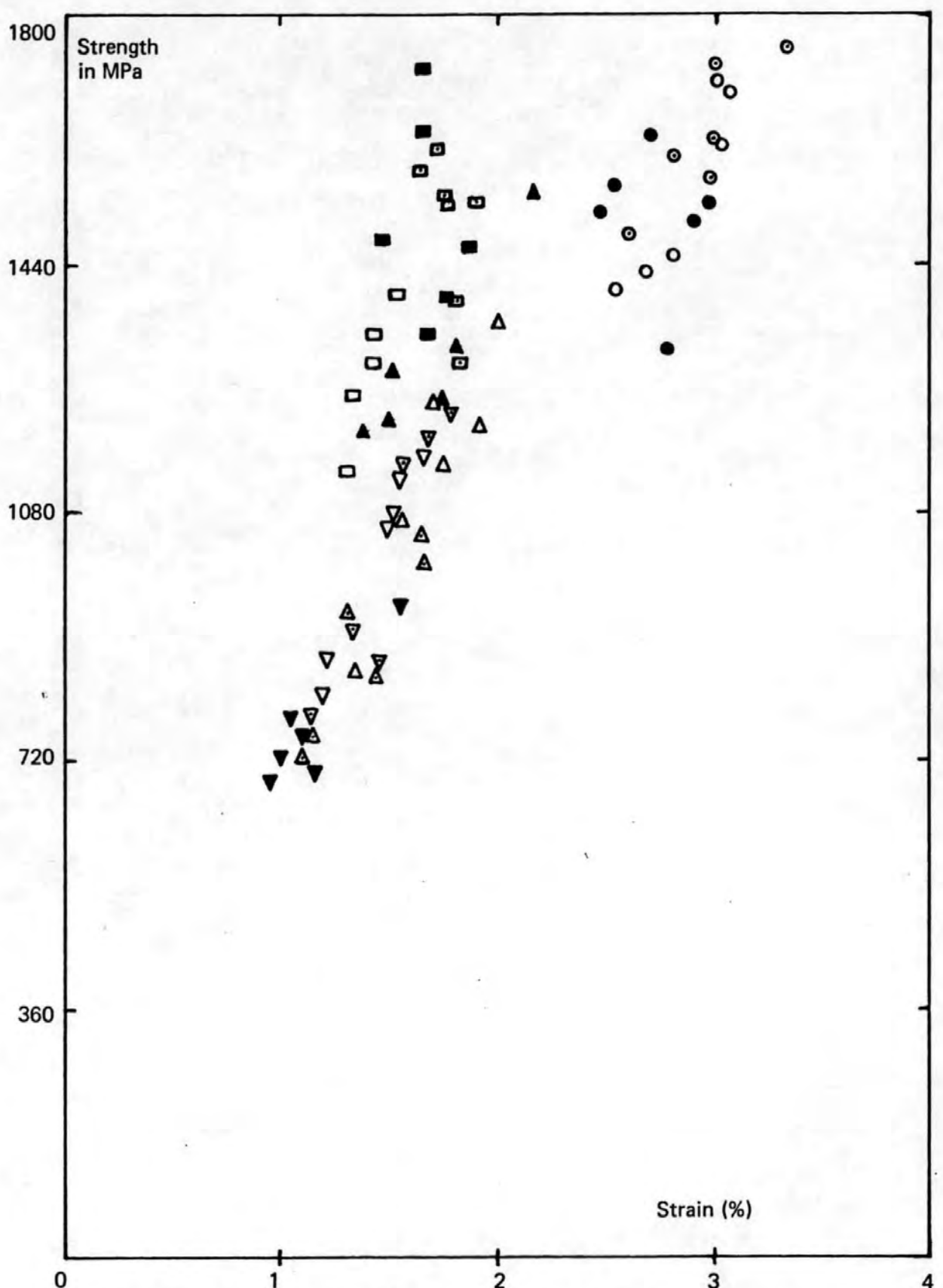


Figure 35: Typical plot of initial failure strength against calculated elastic failure strain, for EAS-carbon hybrids. Composites: carbon (\square), fine hybrid (∇), coarse hybrid (Δ), glass (\circ). Liquid nitrogen exposure: none (open), 24 hours recovery (solid), immediately prior to test (dotted).

5.6 Scanning electron micrographs

In all the scanning electron micrographs the glass fibres have a nominal diameter of 30 µm and are smooth sided. The carbon fibres have a nominal diameter of 7 µm and have surface striations running parallel to the major axis of the fibre. In all cases the filament voltage was 25 kV. The 1.0/10.0/100.0 U-bar is an integral part of the image, the length of the bar being the indicated number of micrometres. This is preferable to a figure for magnification as it is independant of the image enlargement. The four digit number at the bottom centre of the image is the film exposure counter.

5.6.1 General views of hybrid fracture surfaces

Figure 36 (Plate 0001) shows an area of composite with a few glass fibres, or their pullout holes in the foreground, with an area of carbon fibres behind. There are large areas of pure resin between the glass and carbon sections, and also within the monofibre groups. The pullout lengths in the carbon fibres are generally rather small. It should be noted that because of the difference in the fibre radii, eighteen carbon fibres have a cross-sectional area approximately equal to one glass fibre, (ie this is the fibre ratio required for a 50/50 volume fraction hybrid, as illustrated).

Figure 37 (Plate 0002) is a general view of the corner of a specimen, with the edges in the foreground and to the right of the image. Once again there are large resin-rich areas. In this case the resin-rich area to the right is probably due to the method of manufacture – the base of the mould was filled with resin before fibres were added. One third of the distance from the left hand edge of the photograph is a single glass fibre entirely surrounded by carbon fibres – a very local realisation of the ideal intimate mixture being sought. The fracture surface of this single fibre appears in greater detail in figure 40 (Plate 0003).

Figure 38 (Plate 0006) is a close-up of a glass-rich area of the composite. The small fragment of resin is of the order of 4 fibre diameters long. This could have been caused either by two parallel cracks propagating into this segment simultaneously, or it may indicate that the critical length in this material is extremely small.

Figure 39 (Plate 0010) shows another corner of a specimen, which is primarily glass fibres, but in a resin-rich area. There is evidence of a pulled-out misaligned carbon fibre at a position about 100 µm diagonally from the corner.

5.6.2 Glass fibres

Figure 40 (Plate 0003) shows the glass fibre to the left of figure 37 (Plate 0002) in greater detail. On the assumption that the crack has run from the right towards the fibre, it can be seen that there are multiple crack fronts within the fracture surface, followed by catastrophic failure from the position at which the crack reached approximately one-third of the fibre diameter.

Figure 41 (Plate 0005) shows another glass fibre fracture surface. On this occasion it would appear that the crack ran catastrophically through the fibre.

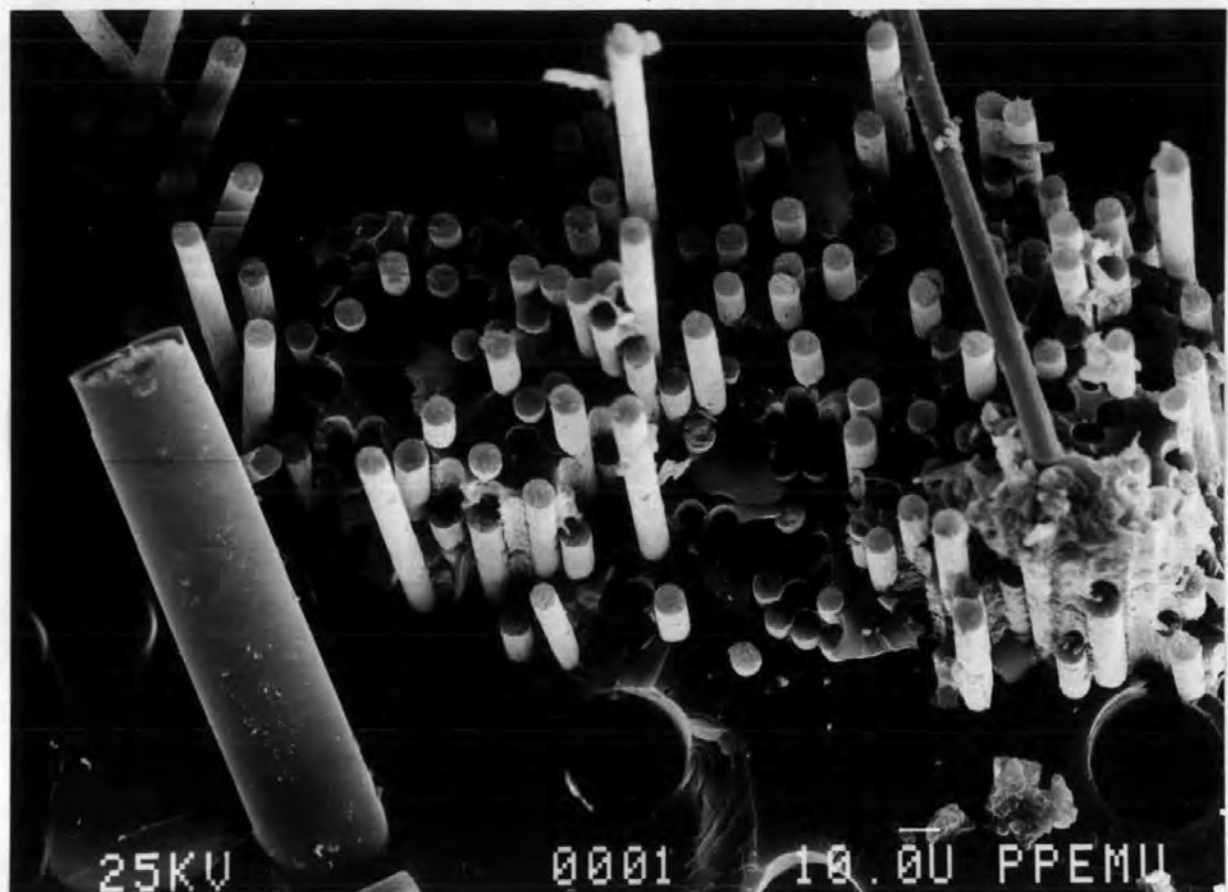


Figure 36: Electron micrograph of a hybrid fracture surface (Plate 0001)

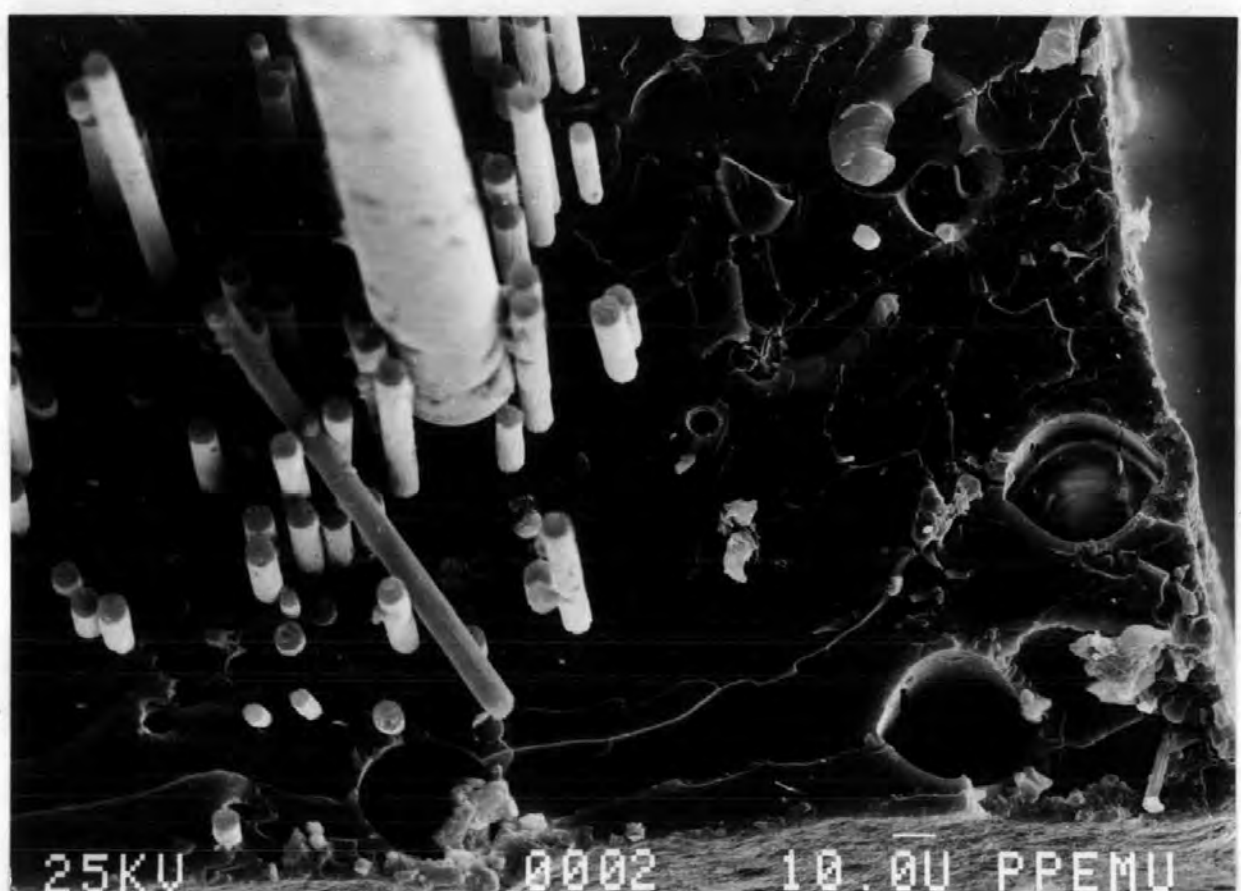
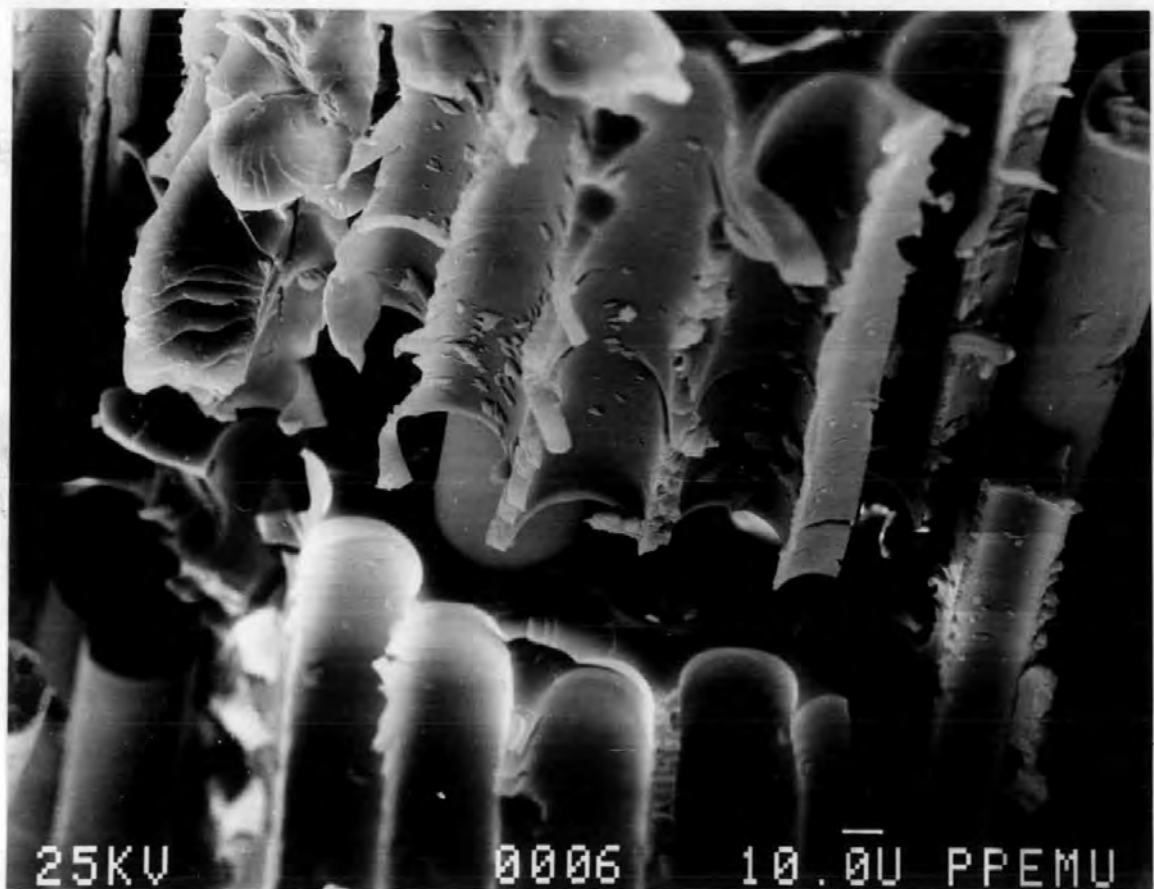


Figure 37: Electron micrograph of a hybrid fracture surface (Plate 0002)

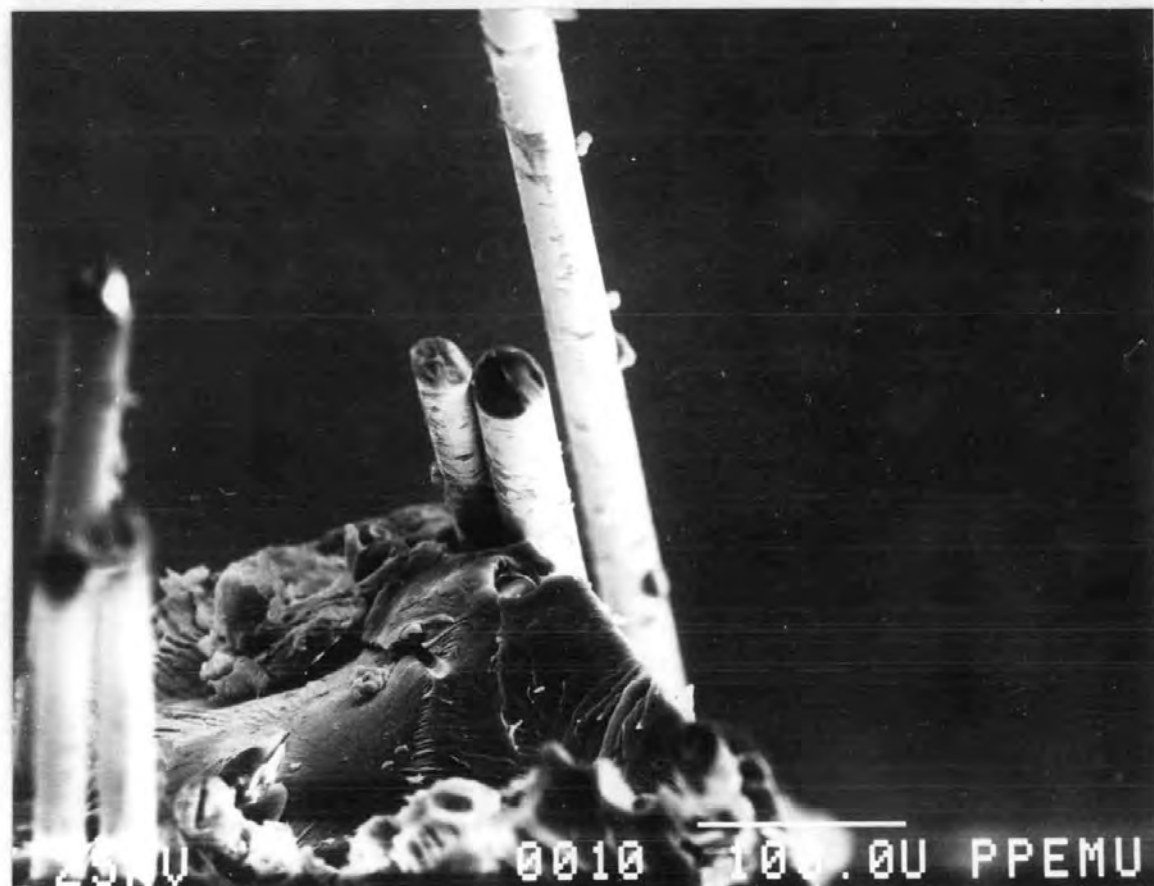


25KV

0006

10.0U PPemu

Figure 38: Electron micrograph of a hybrid fracture surface (Plate 0006)

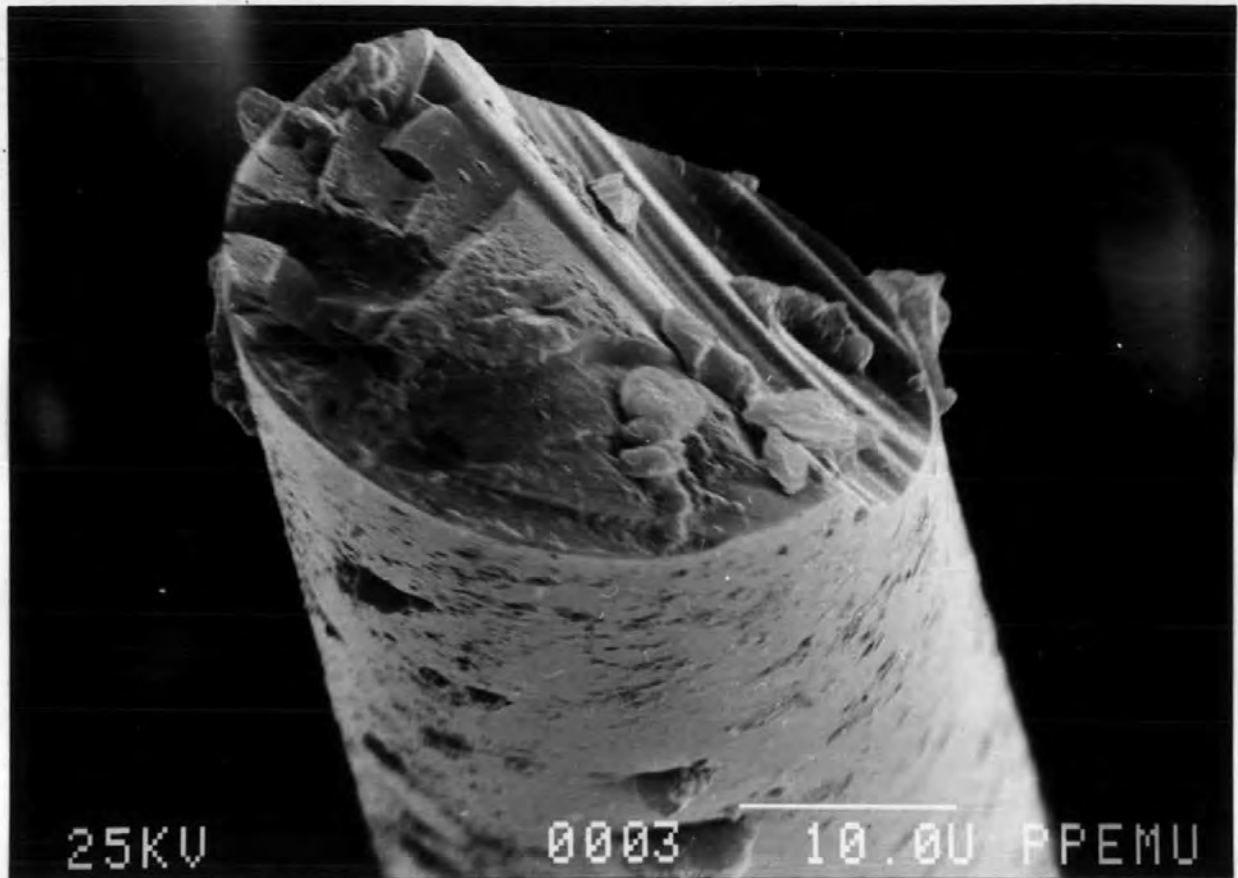


25KV

0010

10.0U PPemu

Figure 39: Electron micrograph of a hybrid fracture surface (Plate 0010)

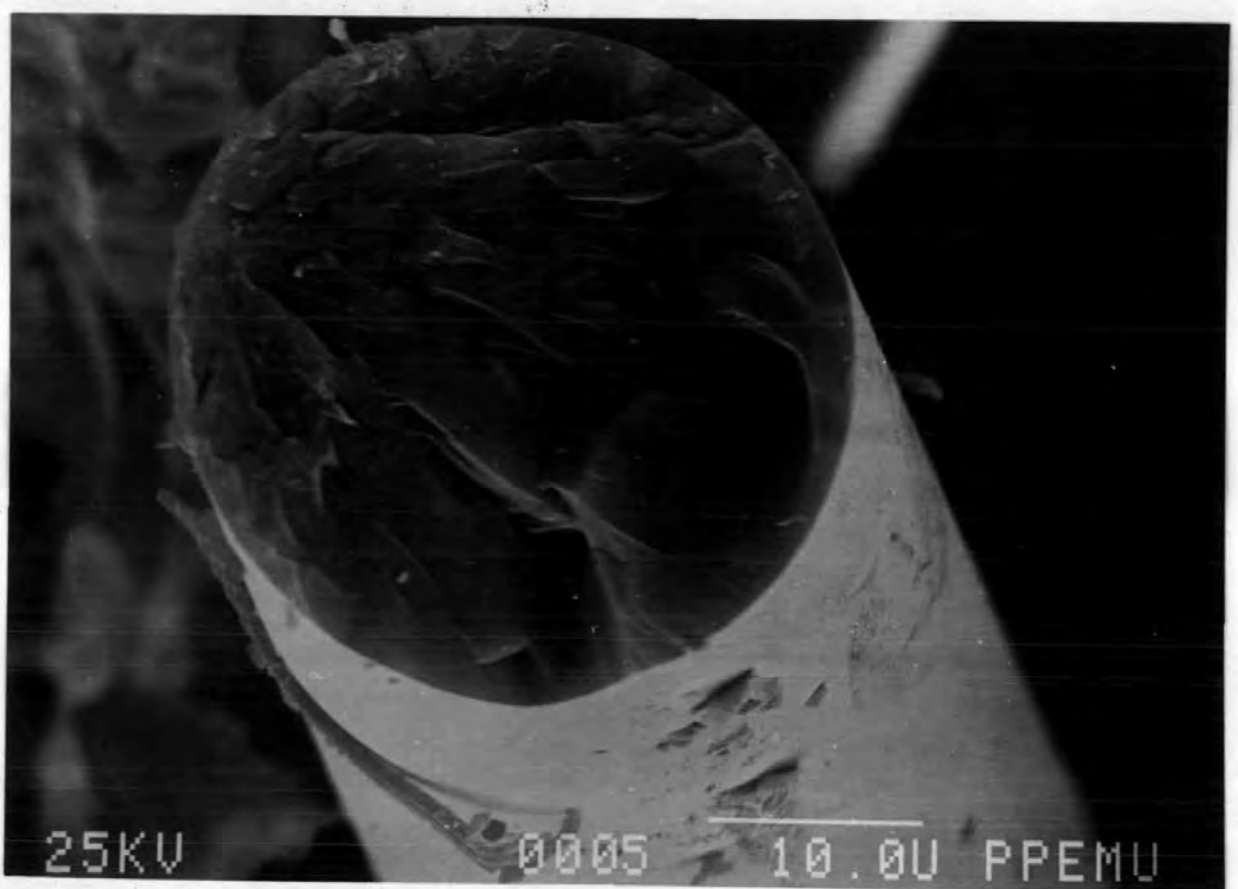


25KV

0003

10.0U PPemu

Figure 40: Electron micrograph of a glass fibre from plate 0002 (Plate 0003)



25KV

0005

10.0U PPemu

Figure 41: Electron micrograph of a fractured glass fibre (Plate 0005)

5.6.3 Carbon fibres

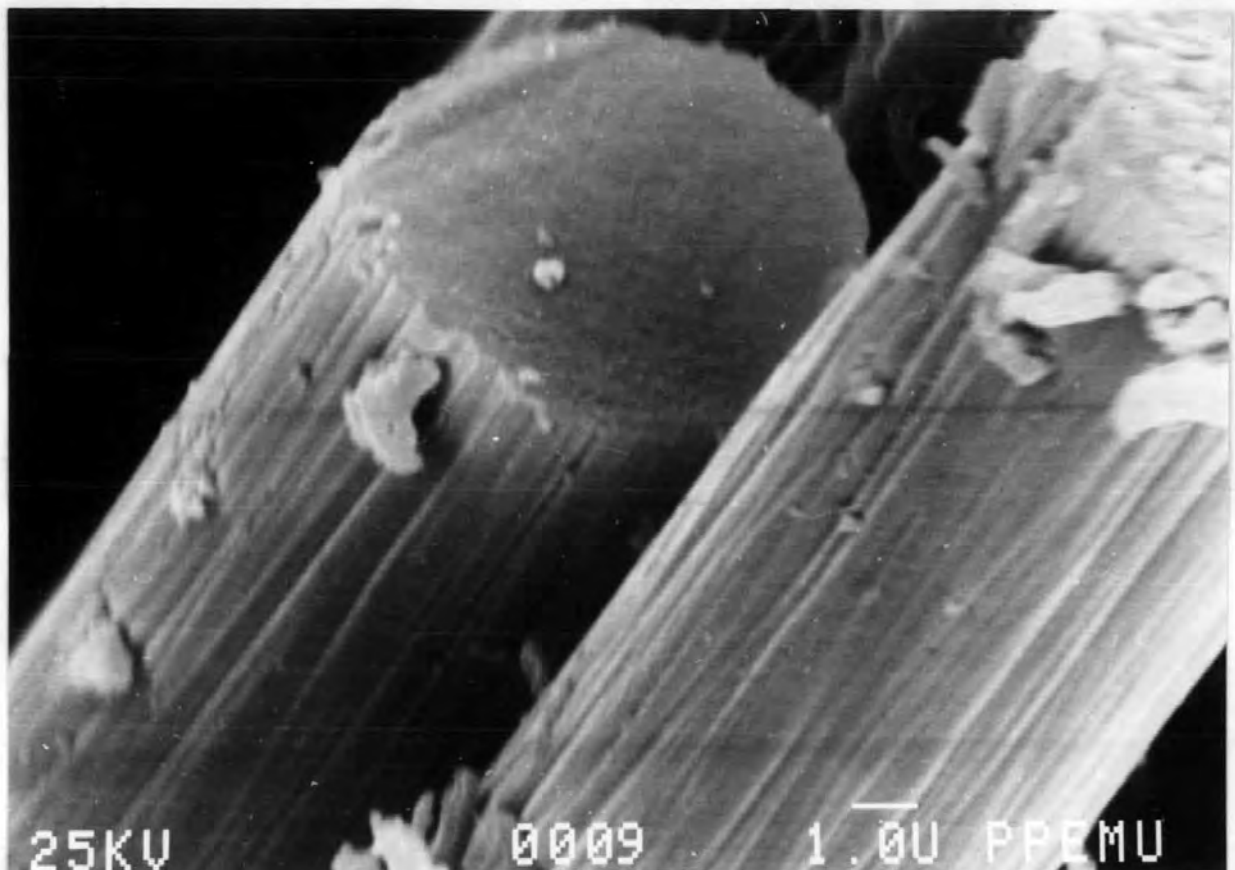
Figure 42 (Plate 0008) is a general view of a carbon-fibre rich area of a hybrid composite. The large aspect ratio of the pulled-out fibres is worthy of note. At bottom centre, immediately above the first zero of the plate number, there is a carbon fibre which has split parallel to the major axis of the fibre. A variety of fracture surfaces are evident with surface irregularity ranging from less than 1 μm up to slightly more than one fibre diameter in the case of the split fibre.

Figure 43 (Plate 0009) is a view of the left-hand edge of the central cluster of fibres in Plate 8 from the same angle. The longitudinal striations along the length of the fibre can be seen to taper as individual lamellae run to the surface. The fractured surface of a single fibre (magnified over 7000 times) can be seen to be extremely flat suggesting brittle catastrophic failure, except at the rear left corner which is possibly the entry point of the propagating crack.

Figure 44 (Plate 0004) shows two carbon fibres with an apparent site of crack initiation at the closest point to contact. In both fibres the radial markings are from this point (ie not radial in respect of the fibre). There is apparently either damage of the fibre or a surface defect on the left-hand fibre about one diameter from the fracture surface on the right-hand edge. It is impossible to say whether this arose from handling of the fibre in the Aircomb or in fabrication, or whether the damage occurred during mechanical loading either before, or as a result of, the local fibre fracture.

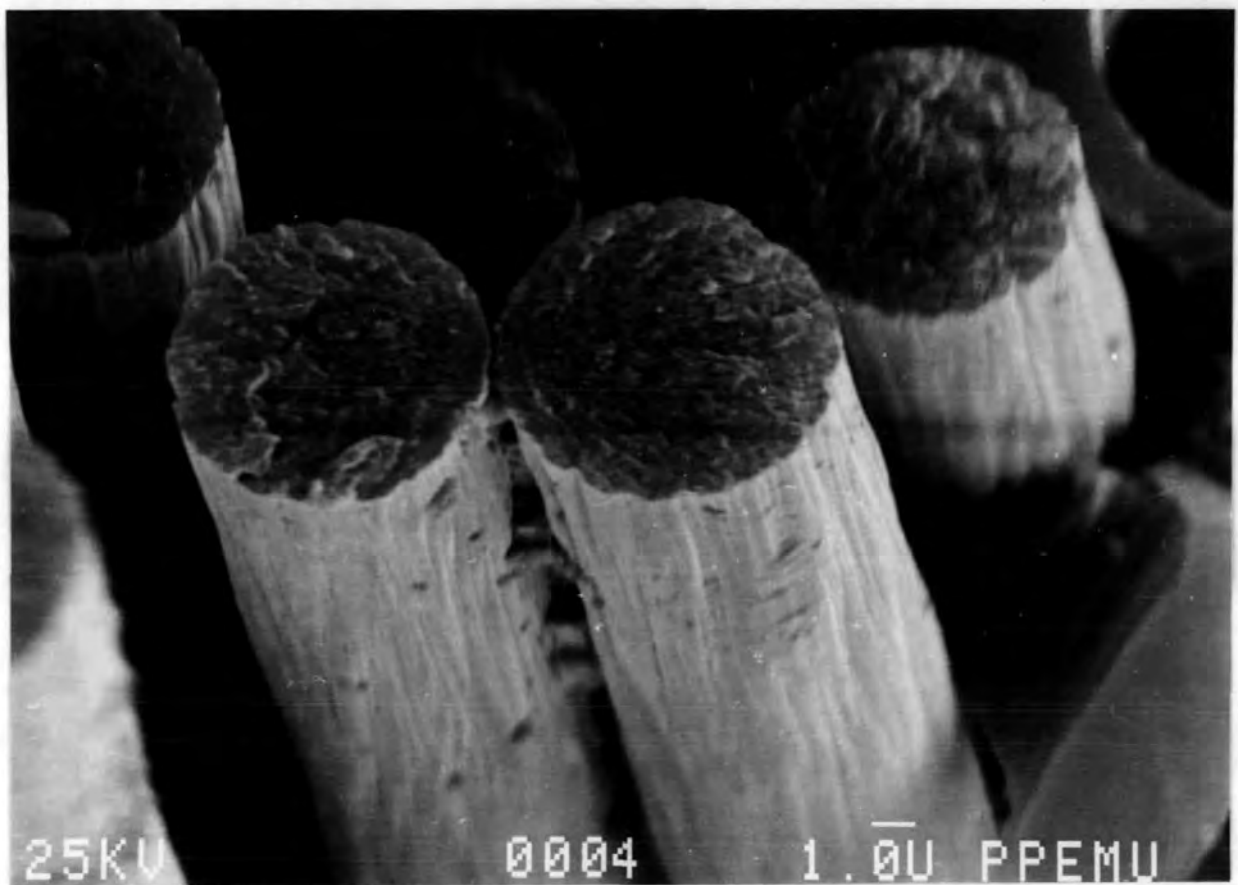


Figure 42: Electron micrograph of a carbon fibre rich fracture surface (Plate 0008)



25KV 0009 1.0U PPEMU

Figure 43: Electron micrograph of a cluster of carbon fibres in plate 0008 (Plate 0009)



25KV 0004 1.0U PPEMU

Figure 44: Electron micrograph of a possible crack initiation site (Plate 0004)

6 Summary

The intention of this thesis was to examine a variety of aspects of fibre composite hybrid materials utilising both carbon fibres and glass fibres. In order of presentation these aspects were:

- mixing techniques,
- description of hybrid microstructure,
- the strength of hybrid composites and the "hybrid effect",
- acoustic emissions arising from hybrids,
- finite element modelling of singularities in hybrid microstructures,
- properties at cryogenic temperatures, and
- scanning electron micrographs.

The Courtaulds air knife has been developed and extended into an aircomb which can form flat unidirectional ribbons of carbon or glass fibres from individual rovings of these materials. By passing one of each of these ribbons back through the device, now known as the Aircomb, they can be recombined to produce an intimately mixed tow of carbon and glass fibres.

A scheme for the classification of hybrid microstructures has been proposed, and was published in Composites (=19). Further to this scheme an attempt was made to classify the intimately mixed hybrids more thoroughly by the introduction of microstructure parameters. Three parameters were examined: nearest neighbour index, chi-squared index, and the contiguity index. However in the intimate composites fabricated for this work it was found that the scale of the microstructure was too large to be able to assign a single index to an individual composite.

A new equation to predict the extent of the "hybrid effect" (synergistic strengthening) has been proposed. This equation assumes that both the elastic modulus and the failure strain of the composite change with the volume fraction of each monofibre composite in a simple linear manner. In experiments to test this equation a large proportion of the composites failed prematurely by buckling. Those few composites which failed in a classical flexural testing mode were generally close to the value predicted by the new equation. An examination of data from the thesis by Gruber (=246), showed that all but one of the composites tested exceeded the value predicted by the new theory. In this case the composites were Kevlar 49 mixed with E-glass, a combination which more closely matches the assumptions for the equation than the carbon-glass system.

In the acoustic-emission-count monitoring of the carbon-glass composites, the hybrids were found to be noisier than either of the monofibre composites, and the noisiness increased with the intimacy of mixing of the two types of fibre. In the amplitude-distribution analysis of the acoustic emission signals, the fine mix hybrid was found to have a cumulative histogram at failure which closely matched that predicted by taking average values for each of the amplitude channels from the histograms of the two monofibre composites. The appearance of the hump corresponding to amplitudes associated with

glass fibres was found to occur immediately prior to failure.

In the constant strain triangular finite element analysis of anisotropic materials it was found that changing the major axis of the material caused the stress concentration to be funnelled along the weak direction of the material, that is parallel to the fibres, despite an homogeneous model being analysed. It was also found that the bending moment arising from the method of loading of fracture toughness specimens caused the stress concentration factor for equivalent loadings, specimen dimensions and a/w ratios to descend in the order: rectangular cantilever, then single edge notch, with both double edge notch and centre notch having the lowest stress concentration.

Isoparametric quadrilateral finite element analysis of anisotropic models was attempted using PAFEC finite element schemes. Subroutines were developed for singularity matrix division, nodal averaging of stresses, and the stress contour graphics presentation of the results. Models with a wide range of material anisotropies and a core-shell, two-material model were successfully analysed. A \sqrt{r} singularity was modelled in all of the above material systems. No significant results were obtained from this part of the work because large finite element models could not be run due to the overloaded schedule for the PRIME computer.

Both monofibre and hybrid composites which had been subjected to one thermal cycle down to liquid nitrogen temperature (77K) were subjected to mechanical testing at ambient temperature. There was no evidence to suggest that deterioration of the cycled composites had occurred. This was in line with predictions.

The microstructures of fractured composites were examined using the scanning electron microscope, both to look for changes of failure mode and to check the intimacy of mixing.

7: References

- 1 L.H. van VLACK
'Introduction: Ceramic Microstructures'
in: R.M. FULRATH and J.A. PASK
"Ceramic microstructures: their analysis, significance and production"
John Wiley, 1968
Proceedings of the 3rd Berkeley International Materials Conference, University of California,
Berkeley, 13-17 June 1966.
- 2 M.W. DARLINGTON, P.L. McGINLEY and G.R. SMITH
'Creep anisotropy and structure in short fibre reinforced thermoplastics, 1: prediction of 100-second creep modulus at small strains'
Plastics and Rubber: Materials and Applications, May 1977, 2(2), 51-58.
- 3 Y. BENVENISTE and J. ABOUTI
'A two dimensional mixture theory for biaxially fibre reinforced composites with application to dynamic crack problems'
International Journal of Engineering Science, September 1978, 16(9), 615-636.
- 4 H.L. COX
'The elasticity and strength of paper and other fibrous materials'
British Journal of Applied Physics, March 1952, 3, 72-79.
- 5 V.V. BOLOTIN
'Statistical theory of defect build up in composite materials and the scale factor effect in reliability'
Polymer Mechanics, March-April 1976, 12(2), 213-230.
- 6 M. HLAVACEK
'On waveguide type propagation in elastic fibre reinforced composites'
Archiwum Mekhaniki Stosowanej, 1978, 30(2), 189-201.
- 7 H. MURAKAMI, G. HEGEMEIER and A. MAEWAL
'A mixture theory for thermal diffusion in unidirectional composites with cylindrical fibres of arbitrary cross section'
International Journal of Solids and Structures, 1978, 14(9), 723-737.
- 8 G. VERCHERY
'Comportement des matériaux composites à fibres orientées'
Journées Elasticité anelastivité, 1971.
- 9 F.J. GUILD
'Property microstructure relationships in GFRP'
Ph.D. thesis, C.N.A.A., Plymouth Polytechnic, March 1978.
- 10 F.J. GUILD and B.W. SILVERMAN
'The microstructure of glass fibre reinforced polyester resin composites'
Journal of Microscopy, November 1978, 114(2), 131-141.
- 11 H. KRENCHEL
"Fibre Reinforcement"
Akademisk Forlag, Copenhagen, 1964.
- 12 H.P. ROSSMANITH
'A note on the random volume fractions of composite materials'
Acta Mechanica, 1977, 27(1), 269-273.
- 13 P. STROEVEN
'The analysis of fibre distributions in fibre reinforced materials'
Journal of Microscopy, December 1977, 111(3), 283-295.
- 14 J.V. MILEWSKI
'The combined packing of rods and spheres in reinforcing plastics'
Industrial and Engineering Chemistry, Product Research and Development, December 1978,
17(4), 363-366.

- 15 M.Z. KANOVICH, M.A. KOLTUNOV and S.L. ROGINSKII
'Investigation of the fibre packing density in a unidirectional composite'
Polymer Mechanics, 1976, 12(3), 493-495.
- 16 S.V. KULKARNI, B.W. ROSEN and H.C. BOEHM
'Cost performance evaluation of hybrid composite materials'
31st Annual Technical Conference, SPI, Washington DC, February 1976, Paper 17-A.
- 17 S.V. KULKARNI, B.W. ROSEN and H.C. BOEHM
'Evaluation of cost effectiveness of hybrid composite laminates'
Journal of Aircraft, December 1977, 14(12), 1153-1154.
- 18 J. SUMMERSCALES and D. SHORT
'Carbon fibre and glass fibre hybrid reinforced plastics'
Composites, July 1978, 9(3), 157-166.
- 19 D. SHORT and J. SUMMERSCALES
'Hybrids—a review: Part 1: Techniques, design and construction'
Composites, October 1979, 10(4), 215-221.
- 20 M.G. BADER and P.W. MANDERS
'Failure strain enhancement in carbon glass fibre hybrid composites'
Proceedings of the 2nd International Conference on Composite Materials,
Metallurgical Society of AIME, Toronto, April 1978, Paper 14.3, 1147-1165.
- 21 J. AVESTON and A. KELLY
'Tensile first cracking strain and strength of hybrid composites'
Philosophical Transactions of the Royal Society of London, 21 January 1980, A 294 (1411),
519-534.
- 22 D.A.G. MARSHALL
'The mechanical properties of carbon-glass composites manufactured by a vacuum box moulding technique'
M.Sc. thesis, Lancaster University, November 1974.
- 23 F.J. GUILD
Private communication.
- 24 E.E. EL-HINNAWI
'Methods in chemical and mineral microscopy'
Elsevier, Amsterdam, 1966, 25-31.
- 25 G.A. MOORE
'Application of computers to quantitative analysis of microstructures'
in FULRATH and PASK (see reference 1).
- 26 B.D. RIPLEY
'Modelling spatial patterns'
Read before the Research Section of the Royal Statistical Society, 16 March 1977, 172-212.
- 27 B.W. ROSEN, S.N. CHATTERJEE and J.J. KIBLER
'An analysis model for spatially oriented fibre composites'
ASTM STP 617, March 1977, 243-254.
- 28 P. DAVIS
'Data description and presentation', Chapter 3 of "Describing point patterns"
Oxford University Press Science in Geography Series, Oxford, 1974, 29-35.
- 29 P.E. LLOYD and P. DICKEN
"Location in space: a theoretical approach to economic geography"
Harper and Row, New York, 1977.
- 30 P.J. CLARK and F.C. EVANS
'Distance to the nearest neighbour as a measure of spatial relationships in population'
Ecology, October 1954, 35(4), 445-453.

- 31 H.R. THOMPSON
 'Distribution of distance to the nth. nearest neighbour in a population of randomly distributed individuals'
Ecology, April 1956, 37(2), 391-394.
- 32 L.L. EBERHARDT
 'Some developments in distance sampling'
Biometrics, 1967, 23, 207-216.
- 33 P. GREIG-SMITH
 'The use of random and contiguous quadrats in the study of the structure of plant communities'
Annals of Botany, London, 1952, NS16, 293-316.
- 34 K.A. KERSHAW
 'The use of cover and frequency in the detection of pattern in plant communities'
Ecology, April 1957, 38(2), 291-299.
- 35 M.B. USHER
 'The relation between mean square and block size in analysis of similar patterns'
Journal of Ecology, April 1969, 57(2), 505-514.
- 36 R.E. MILES
 'The sampling by quadrats of planar aggregates'
Journal of Microscopy, August 1978, 113(3), 257-267.
- 37 H.J.G. GUNDERSEN
 'Notes on the estimation of the numerical density of arbitrary profiles: the edge effect'
Journal of Microscopy, November 1977, 111(2), 219-223.
- 38 R.E. MILES and P.J. DAVY
 'On the choice of quadrats in stereology'
Journal of Microscopy, May 1977, 110(1), 27-44.
- 39 R. MEAD
 'A test for spatial pattern at different scales using data from a grid of contiguous quadrats'
Biometrics, June 1974, 30, 295-307.
- 40 A.R. CLAPHAM
 'Overdispersion in grassland communities and the use of statistical methods in plant ecology'
Journal of Ecology, 1936, 24, 232-251.
- 41 H. MORITSA
 'Measuring the dispersion of individuals and analysis of the distributional patterns'
Memoirs, Faculty of Science, Kyusha University, Series E, 2, 215-235.
- 42 P.G. MOORE
 'A test for non-randomness in plant populations'
Annals of Botany, London, 1953, NS17, 57-62.
- 43 STEVENS
 in an Appendix to E. ASHBY
 'The quantitative analysis of vegetation'
Annals of Botany, London, 1935, 45, 779-802.
- 44 G. MATHERON
 'Principles of geostatistics'
Economic Geology, 1963, 58, 1246-1266.
- 45 S.A.M. EARLE
 'Spatial presentation of data from regional geochemical stream surveys'
Transactions of the Institute of Mining and Metallurgy, Section B: Applied Earth Science, May 1978, 87(2), B61-B65.
- 46 W.R. CRIBB
 'Quantitative metallography of polyphase microstructures'
Scripta Metallurgica, October 1978, 12, 893-898.

- 47 K.S.M.A. MIRZA
 'A statistical study of the structure of mixtures of particulate solids'
 Ph.D. thesis, University of Exeter, April 1970.
- 48 R.E. BONNER
 'On some clustering techniques'
I.B.M. Journal of Research and Development, 1964, 8, 22-32.
- 49 H.H. McCARTY, J.C. HOOK and D.S. KNOS
 'The measurement of association in industrial geography'
 University of Iowa Department of Geography, 1956.
- 50 B.J. SCHACTER, A. ROSENFIELD and L.S. DAVIS
 'Random mosaic models for textures'
IEEE Transactions — Systems, Man and Cybernetics, September 1978, SMC8(9), 694-702.
- 51 J.I. CLARKE and D.W. RHIND
 'The relationship between the size of areal units and the characteristics of population structure'
 Durham University Census Research Unit Working Paper 5, September 1975.
- 52 C. GOLDSCHEIDER
 "Population, modernisation and social structure"
 Little and Brown, Boston, 1971, 39-40.
- 53 J.I. CLARKE
 'Population and scale'
 Durham University Census Research Unit Working Paper 1, May 1975.
- 54 D.W. RHIND
 'Geographical analysis and mapping of the 1971 U.K. census data'
 Durham University Census Research Unit Working Paper 3, June 1975.
- 55 N.B. RYDER
 'Notes on the concept of population'
American Journal of Sociology, March 1964, 69(5), 447-463.
- 56 S.W. TSAI
 'Structural behaviour of composite materials'
 NASA Report CR-71, 1964.
- 57 Z. HASHIN
 'The elastic moduli of heterogeneous materials'
Journal of Applied Mechanics, 1962, 29, 143-150.
- 58 Z. HASHIN and B.W. ROSEN
 'The elastic moduli of fibre reinforced materials'
 Winter Meeting, ASME, November 1963, Paper 63-WA-175.
- 59 J.C. HALPIN and S.W. TSAI
 'Environmental factors in composite materials design'
 AFML Technical Report TR67-423, 1967.
- 60 J.C. HALPIN and J.L. KARDOS
 'The Halpin-Tsai equations: a review'
Polymer Engineering and Science, May 1976, 16(5), 344-352.
- 61 D. SHORT and J. SUMMERSCALES
 'Elastic and thermal properties of composites'
 in N.L. HANCOX:
 "Fibre Composite Hybrid Materials"
 Applied Science Publishers, Barking, 1981, chapter 3, 69-117.
- 62 T. HAYASHI
 'On the improvement of mechanical properties of composites by hybrid composition'
 8th Reinforced Plastics Congress, BPF RPG, Brighton, October 1972, Paper 22, 149-152.

- 63 C.C. CHAMIS and R.F. LARK
 'Non-metallic hybrid composites: analysis, design, application and fabrication'
 in W.J. RENTON:
 "Hybrid and Select Metal Matrix Composites"
 AIAA, New York, 1977, chapter 2, 13-51.
- 64 G.M. GUNYAEV
 'Polycomponent high modulus composites'
Polymer Mechanics, September-October 1977, 13(5), 685-692.
- 65 A.M. SKUDRA, E.Z. PLUME, G.M. GUNYAEV, V.A. YARTSEV and N.H. BELYAEV
 'Properties of fibreglass plastics reinforced with high modulus fibres'
Polymer Mechanics, January-February 1972, 8(1), 57-62.
- 66 C.C. CHAMIS
 'Approximate design-analysis procedures for hybrid composites'
 34th Annual Technical Conference, SPI, New Orleans, January-February 1979.
- 67 C.C. CHAMIS and J.H. SINCLAIR
 'Prediction of properties of intraply hybrid composites'
 NASA Technical Memorandum TM 79087, 1979.
- 68 J. AVESTON and J.M. SILLWOOD
 'Synergistic fibre strengthening in hybrid composites'
Journal of Materials Science, October 1976, 11(10), 1877-1883.
- 69 A. KELLY
 'Fibre reinforcement of brittle matrices'
 in G. PIATTI:
 "Advances in Composite Materials"
 Applied Science Publishers, Barking, 1978, chapter 6, 113-129.
- 70 N. RAO and K.E. HOFER
 'Fatigue behaviour of graphite-glass-epoxy composites'
 Illinois Institute of Technology Research Institute Report IITRI-D6070, April 1973.
- 71 K.E. HOFER, N. RAO and M. STANDER
 'Fatigue behaviour of graphite glass epoxy hybrid composites'
 2nd International Conference on Carbon Fibres, Plastics Institute, London, February 1974,
 Paper 31, 201-212.
- 72 H.E. EDWARDS, N.J. PARRATT and K.D. POTTER
 'Synthesis and application of aligned discontinuous composites'
 2nd International Conference on Composite Materials, Metallurgical Society of AIME, Toronto,
 April 1978, 975-993 + 1300-1301.
- 73 A.R. BUNSELL and B. HARRIS
 'Hybrid carbon and glass fibre composites'
Composites, July 1974, 5(4), 157-164.
- 74 A.R. BUNSELL and B. HARRIS
 'Hybrid carbon-glass fibre composites'
 Proceedings of the 1st International Conference on Composite Materials, Metallurgical Society of
 AIME, Geneva and Boston, April 1975, 174-190.
- 75 I.R. MCCOLL and J.G. MORLEY
 'Crack growth in hybrid fibre composites'
Journal of Materials Science, June 1977, 12(6), 1165-1175.
- 76 S. FISCHER, G. MAROM and F.R. TULER
 'Hybrid effects in composites: a comparison between interlaminar and transplaminar configurations'
Journal of Materials Science, April 1979, 14(4), 863-868.
- 77 P.W.R. BEAUMONT
 'Fracture mechanisms in fibrous composites'
 in R.A. SMITH:
 "Fracture Mechanics: Current Status, Future Prospects"
 Pergamon Press, Ontario, 1979, 211-233.

- 78 P.W.R. BEAUMONT and P.D. ANSTICE
 'A failure analysis of micromechanisms of fracture of carbon fibre and glass fibre composites in monotonic loading'
Journal of Materials Science, October 1980, 15(10), 2619-2635.
- 79 P.W. MANDERS
 'The strength of mixed fibre composites'
Ph.D. thesis, University of Surrey, September 1979, BLL thesis D29013/79.
- 80 D.G. HARLOW and L.S. PHOENIX
 'The chain-of-bundles probability model for the strength of fibrous materials: Part 1 — analysis and conjectures'
Journal of Composite Materials, April 1978, 12(2), 195-214.
- 81 D.G. HARLOW and L.S. PHOENIX
 'The chain-of-bundles probability model for the strength of fibrous materials: Part 2 — a numerical study of convergence'
Journal of Composite Materials, July 1978, 12(3), 314-334.
- 82 J.W. HITCHON and D.C. PHILLIPS
 'An investigation of some carbon fibre and interfacial properties of carbon fibre-epoxy composites'
UKAEA Harwell Report AERE-G760, January 1977.
- 83 W.G.J. t'HART
 'Investigation of the length strength dependency of carbon fibres and the related unidirectional composite strength'
National Aerospace Laboratory Amsterdam Report NLR TR 78050, April 1978.
- 84 J.M. HEDGEPATH
 'Stress concentrations in filamentary structures'
NASA Technical Note TN D-882, 1961.
- 85 J.R. HOUGHTON and P.F. PACKMAN
 'Pulse analysis of acoustic emission signals'
NASA Contractor Report CR 2927, December 1977.
- 85a I.M. DANIEL and T. LIBER
 'Nondestructive evaluation techniques for composite materials'
12th Symposium on Nondestructive Evaluation, San Antonio, April 1979, 226-244.
- 86 T.F. DROUILLARD, edited F.J. LANER
 "Acoustic Emission — a bibliography with abstracts"
IFI/Plenum Data Co., New York, 1979.
- 87 F.J. GUILD, D. WALTON, R.D. ADAMS and D. SHORT
 'The application of acoustic emission to fibre reinforced composite materials'
Composites, July 1976, 7(3), 173-179.
- 88 J.H. WILLIAMS and S.S. LEE
 'Acoustic emission monitoring of fibre composite materials and structures'
Journal of Composite Materials, October 1978, 12(4), 348-370.
- 89 J. KAISER
 'Untersuchungen über das Auftreten von Geräuschen bei Zugversuch'
Ph.D. thesis, Technische Hochschule München, 1950.
- 90 T.J. FOWLER
 'Acoustic emission testing of fibre reinforced plastics'
Fall Convention, ASCE, San Francisco, October 1977, Paper 3092.
- 91 R. PRAKASH
 'Non-destructive testing of composites'
Composites, October 1980, 11(4), 217-224.
- 92 B.H. SCHOFIELD
 'Acoustic emission under applied stress'
USAF Laboratory Technical Report ASD-TDR-63-509, 1963/1964.

- 93 C.A. TATRO
 'Some techniques in the detection of crystal slip in metals'
 Michigan State University Division of Engineering Research, 1959.
- 94 R.L. BELL
 'Acoustic emission transducer calibration: transient pulse method'
 National Fall Conference, ASNT, Cleveland Ohio, 16-19 October 1972.
- 95 P.S. SHOEMAKER
 'Acoustic emission: an experimental method'
 M.S. thesis, Michigan State University, 1961.
- 96 R.G. LIPTAI
 'An investigation of the acoustic emission phenomenon'
 Ph.D. thesis, Michigan State University, 1963.
- 97 B.B. McCULLOUGH
 'An experimental method for the investigation of acoustic emission'
 M.S. thesis, Tulane University, 1965.
- 98 H.L. DUNEGAN and C.A. TATRO
 'Acoustic emission effects during mechanical deformation'
 in R.F. BUNSHAH:
 "Techniques of metals research, volume 5, part 2"
 Interscience Publishers, New York, 1971, Chapter 12, pages 273-312.
- 99 J.B. LEAN, J. PLATEAU, C. BACHET and C. CRUSSARD
 'On the formation of sound waves during tensile testing of metal specimens'
 Comptes Rendus Hebdomadaires des Seances de l'Academie des Sciences, 19 May 1958, 246, 2845-2848, in French.
- 100 H. BORCHERS and H.M. TENSI
 'Improved piezoelectric method for investigation of processes in metals during mechanical stressing and phase change'
 Zietschrift fur Metallkunde, April 1960, 51(4), 212-218.
- 101 J. EISENBLATTER, W. HEIDE, H. JOST and R. von KLOT
 'Research work on the continuous monitoring of crack extension in pressure vessels, Part 2: further investigations in respect to the acoustic waves emitted during crack extension'
 NLL translation RISLEY-TR-2161-909.1.9F, July 1971 of Battelle Institute (Frankfurt) Research Report 31/1, March 1971.
- 102 B.J. SHAW
 'On the use of piezoelectric films for ultrasensitive strain gauges, metal failure warning devices and for acoustic emission'
 Ultrasonics Symposium, IEEE, Monterey, 5-7 November 1973.
- 103 R.G. LIPTAI, H.L. DUNEGAN and C.A. TATRO
 'Acoustic emission generated during phase transformations in metals and alloys'
 International Journal of Non-destructive Testing, 1969, 1, 213-221.
- 104 R.H. CHAMBERS and S.A. HOENIG
 'New techniques in non-destructive testing by acoustical and exo-electron emission'
 University of Arizona Engineering Experiment Station Report to ARPA contract F33615-69-C1707, 31 August 1969, NTIS AD-720-357.
- 105 W.D. JOLLY
 'Evaluation of the acoustic emission system'
 South West Research Institute Project 17-2440, EEI Project RP-79 Progress report 2, 2 December 1969.
 in R.D. WYLIE:
 "In service inspection program for nuclear reactor vessels", 54-63.
 NTIS PB-188-347.
- 106 P. BUCHMAN
 'On acoustic emission from ferroelectric crystals'
 Solid State Electronics, January 1972, 15(1), 142-144.

- 107 S.L. HALVERSON, T.T. ANDERSON, A.P. GAVIN and T. GRATE
 'Radiation exposure of a lithium niobate crystal at high temperatures'
IEEE Transactions on Nuclear Science, December 1970, NS17(6), 335-340.
- 108 W. PRIMAK, T.T. ANDERSON and S.L. HALVERSON
 'Ionising radiation effects in lithium niobate'
Nuclear Technology, January 1971, 10, 76-84.
- 109 A.P. GAVIN and T.T. ANDERSON
 'High temperature acoustic sensors for boiling detection'
IEEE Transactions on Nuclear Science, February 1971, NS18(1), 340-344.
- 110 T.T. ANDERSON, A.P. GAVIN, J.R. KARVINEN, C.C. PRICE and K.J. REIMANN
 'Detecting acoustic emission in large liquid metal cooled fast breeder reactors'
ASTM STP 505, 1972, 250-269.
- 111 K.J. RIEMAN
 'Nondestructive testing: high temperature ultrasonic transducers'
Argonne National Laboratory (Illinois) Report:
 "Instrumentation and Control Activities at Argonne", December 1971, 57-58.
- 112 W.P. MASON, H.J. McSKIMIN and W. SHOCKLEY
 'Ultrasonic observation of twinning in tin'
Physical Review, May 1948, 73(10), 1213-1214.
- 113 R.H. CHAMBERS and S.A. HOENIG
 'New techniques in non-destructive testing by acoustical and exo-electron emission'
University of Arizona Engineering Experiment Station Report to ARPA Contract F33615-68-C-1707,
 28 February 1969, NTIS AD-691-230.
- 114 C.J. RENKEN
 'Method and means for measuring acoustic emissions'
United States patent 3 930 405, 6 January 1976.
- 115 L.C. LYNNWORTH, E.P. PAPADAKIS, D.R. PATCH, K.A. FOWLER and R.L. SHEPARD
 'Nuclear reactor applications of new ultrasonic transducers'
IEEE Transactions on Nuclear Science, February 1971, NS18(1), 351-362.
- 116 L.C. LYNNWORTH and J.E. BRADSHAW
 'Magnetostriction transducers for acoustic emission, impulse, vibration and noise analysis'
Materials Research and Standards, March 1971, 11(3), 33-35.
- 117 K.A. FOWLER
 'Acoustic emission simulation test set'
Materials Research and Standards, March 1971, 11(3), 35-36.
- 118 T. LAUHOFF
 'Electroacoustic transducer with a magnetostrictive element'
German patent 2 333 482, 16 January 1975.
- 119 H.E. ROMINE
 'The acoustics of straining and fracture in the notched sheet specimen'
Symposium "The Testing and Evaluation of Materials for Solid Propellant Rocket Motor Casings",
 US Materials Advisory Board, Washington, 2-3 February 1959, NTIS AD-230-340.
- 120 C.S. BARRETT and O.R. TRAUTZ
 'Low temperature transformations in lithium and lithium-magnesium alloys'
Transactions of the American Institute of Mining and Metallurgical Engineers, 1948, 175, 579-605.
- 121 J.R. MASTANDREA and M.V. SCHERB
 'Electret polymer transducer'
McDonnell Douglas NT Control Number LAR 11 239, 1972 to NASA Langley Research Centre.
- 122 G.J. CURTIS
 'Acoustic emission in stressed epoxy bonded structures'
UKAEA Harwell Report AERE-R7684, March 1974.

- 123 G. CURTIS
 'A broadband polymeric foil transducer'
Ultrasonics, July 1974, 12(4), 148-154.
- 124 B.W. MAXFIELD and R. COCHRAN
 'Electromagnetic detection of acoustic emission from a martensitic transformation'
Materials Evaluation, February 1973, 31(2), 17-20.
- 125 J.W. PHILLIPS
 'The stress pulses produced by brittle fracture of rods'
 Brown University Division of Applied Mathematics Technical Report No. 8 on National Science Foundation grant NSF-GK-749, December 1968.
- 126 A.K. SHOEMAKER
 'The embrittling effect of small elastic stress waves on crack toughness of a structural steel'
Journal of Materials Science, September 1967, 2(3), 597-624.
- 127 P.H. HUTTON, H.N. PEDERSEN and J.C. SPANNER
 'Crack detection in pressure piping by acoustic emission'
Battelle Northwest Report BNWL-433, July 1967, 4(1-4), 10.
 "Nuclear safety quarterly report: January, February, March 1967 for Nuclear Safety Branch of USAEC Division of Reactor Development and Technology"
- 127a J.C. WADE, P.S. ZEREWEKH and R.O. CLAUS
 'Detection of acoustic emission in composites by optical fibre interferometry'
 In "Optical Fibre Interferometer for the Study of Ultrasonic Waves in Composite Materials"
NTIS N82-11125, October 1981, 17-23.
- 128 a) A. NIELSEN
 'Acoustic emission detection during straining of steel'
Danish Atomic Energy Research Establishment RISO Report M-1290, September 1970.
- b) A. NIELSEN
 'Acoustic emission source based on pencil lead breaking'
Danish Welding Institute (Svejsecentralen Copenhagen) Report 80.15
 from: Park Allé 345, DK-2600 Glostrup, Denmark.
- c) H.J. RINDORF, J.C. HANSEN and T. LICHT
 'Appendix C: In-situ sensitivity calibration of acoustic emission systems'
Brüel & Kjaer Technical Review No. 2, 1981, 38-42.
- d) Anon
 'The Arved Nielsen pencil lead acoustic emission source'
Endevco product literature (undated!)
 from: Endevco UK Division, Melbourn, Royston, Hertfordshire, SG8 6AQ.
- e) Code Sub-group of the European Working Group on Acoustic Emission
 'Addendum: Acoustic Emission Reference Source'
NDT International, August 1981, 14(4), 184.
- 129 M.A. HAMSTAD and R.G. PATTERSON
 'Considerations for acoustic emission monitoring of spherical Kevlar-epoxy composite pressure vessels'
Lawrence Livermore Laboratory Report UCRL-79356, 16 May 1977.
- 130 F.R. BRECKENRIDGE, C.E. TSCHIEGG and M. GREENSPAN
 'Acoustic emission: some applications of Lambs problem'
Journal of the Acoustical Society of America, March 1975, 57(3), 626-631.
- 131 W.F. HARTMAN
 'Experiments with a portable acoustic emission simulator and calibration device'
 12th meeting, American Working Group on Acoustic Emission, New York, 5-7 December 1973.
- 132 D.O. HARRIS
 'The effect of gain and frequency bandpass on acoustic emission observed from growing fatigue cracks'
Dunegan Endevco Technical Report DE74-4, January 1974.

- 133 C.C. FENG
 'Acoustic emission transducer calibration: spark impulse calibration method'
 Endevco Engineering Report 74-7-C, 1974.
- 134 D.B. EGLE and A.E. BROWN
 'A note on pseudo-acoustic emission sources'
Journal of Testing and Evaluation, May 1976, 4(3), 196-199.
- 135 L.J. GRAHAM
 'Acoustic emission transducer characterisation'
North American Rockwell Corporation Report SCTR-71-19, December 1971.
- 136 P.H. HUTTON and H.N. PEDERSEN
 'Crack detection in pressure piping by acoustic emission'
Battelle Northwest Report, September 1969,
 "Nuclear Safety Quarterly Report: May, June, July 1969 for USAEC Division of Reactor Development and Technology"
- 137 S.L. McBRIDE and T.S. HUTCHISON
 'Helium gas jet spectral calibration of acoustic emission transducers and systems'
Canadian Journal of Physics, 1 September 1976, 54(17), 1824-1830.
- 138 G.A. GREEN
 'Simple method for the direct comparison of acoustic emission detection systems'
Nondestructive Testing International, April 1978, 11(2), 69-71.
- 139 A. KAMIO
 'On the relation of a recorded value of acoustic emission to the sizes of cracks'
Hi-Hakai Kensa (Japanese Journal of NDI), August 1971, 20(8), 368-369.
- 140 N.I. DREIMAN
 'Sound emission by metals and alloys'
Industrial Laboratory, January 1972, 38(1), 52-54.
- 141 A. KANNO, M. SAKAKI and K. KATSUMATA
 'Correlation between acoustic emission and crack size calibrated by standard AE source generated by dropped steel ball'
Hi-Hakai Kensa (Japanese Journal of NDI), July 1974, 23(7), 357-363.
- 142 A.E. BROWN and R.G. LIPTAI
 'Round-Robin testing of acoustic emission source'
ASTM STP 505, 1972, 318-331.
- 143 D. BIRCHON
 'The potential of acoustic emission in NDT'
British Journal of Nondestructive Testing, May 1976, 18(3), 66-71.
- 144 J. HOLT and D.J. GODDARD
 'Assessment of an acoustic emission transducer for waveguide application'
Central Electricity Research Laboratories (Leatherhead) Laboratory Note RD-L-N3-76, March 1976.
- 144a C.B. SCRUBY, H.N.G. WADLEY, R.J. DEWHURST, D.A. HUTCHINS and S.B. PALMER
 'A laser-generated standard acoustic emission source'
Materials Evaluation, December 1981, 39(13), 1250-1254.
- 145 A.G. EVANS and M. LINZER
 'Acoustic emission in brittle materials'
Annual Reviews in Materials Science, 1977, 7, 179-208.
- 146 A. ROTEM and J. BARUCH
 'Determining the load time history of fibre composite materials by acoustic emission'
Journal of Materials Science, November 1974, 9(11), 1789-1798.
- 147 E.C. JESSEN, H. SPANHEIMER and A.J. de HERRERA
 'Prediction of composite pressure vessel performance by application of the Kaiser effect in acoustic emission'
ASME Paper H 300-12-2-037, June 1975.

- 148 J. FITZRANDOLPH, D.C. PHILLIPS, P.W.R. BEAUMONT and A.S. TETELMAN
'The fracture energy and acoustic emission of a boron-epoxy composite'
Journal of Materials Science, March 1972, 7(3), 289-294.
- 149 D.K. RATHBUN, A.G. BEATTIE and L.A. HILES
'Filament wound materials — evaluation with acoustic emission'
Proceedings of the 8th Symposium on Nondestructive Evaluation in Aerospace, Weapons Systems and Nuclear Applications, Texas, 22 April 1971.
- 150 H.L. BALDERSTON
'The broad range detection of incipient failure using the acoustic emission phenomena'
ASTM STP 505, 1972, 297-317.
- 151 M. FUWA, A.R. BUNSELL and B. HARRIS
'Tensile failure mechanisms in carbon fibre reinforced plastics'
Journal of Materials Science, December 1975, 10(12), 2062-2070.
- 152 R.L. MEHAN and J.V. MULLIN
'Analysis of composite failure mechanisms using acoustic emissions'
Journal of Composite Materials, April 1971, 5(2), 266-269.
- 153 R. DUKES
'Materials requirement and validation for large marine structures in fibre reinforced plastics'
Proceedings of the Symposium "Reinforced Plastics — Recent Advances in the Marine Field"
PRI RPG, Southampton, September 1972, Paper 2.
- 154 R.G. LIPTAI
'Acoustic emission from composite materials'
ASTM STP 497, 1972, 285-298.
- 155 M. ARRINGTON and B. HARRIS
'Some properties of mixed fibre cfrp'
Composites, July 1978, 9(3), 149-152.
- 156 A.A. POLLOCK
'Acoustic emission 2: acoustic emission amplitudes'
Non-destructive Testing, October 1973, 6(5), 264-269.
- 157 Dunegan Endevco, 'Now Hear This', 1976, 4(1).
- 158 J. WADIN and A.A. POLLOCK
'Periodic proof testing of fibreglass booms through the use of non-Kaiser acoustic emission responses'
9th National Technical Conference, SAMPE, Atlanta, October 1977, 519-560.
- 159 L.J. GRAHAM and R.K. ELSLEY
'Characterisation of acoustic emission signals and application to composite structures monitoring'
Proceedings of the Review Meeting of Progress in Quantitative NDE, ARPA and AFML, Thousand Oaks CA, May 1978, 219-225.
AFML Technical Report TR 78 55, 40-45.
- 160 F.J. GUILD, M.G. PHILLIPS and B. HARRIS
'Acoustic emission studies of damage in GRP'
NDT International, October 1980, 13(5), 209-218.
- 161 A.A. POLLOCK
'Acoustic emission'
Engineering, 19 June 1970, 209(5433), 639-642.
- 162 A.T. GREEN, C.S. LOCKMAN and R.K. STEELE
'Acoustic verification of structural integrity of Polaris chambers'
Modern Plastics, July 1964, 41(11), 137-139 + 178 + 180.
- 163 J.V. MULLIN and R.L. MEHAN
'Evaluation of composite failures through fracture signal analysis'
Journal of Testing and Evaluation, May 1973, 1(3), 215-219.

- 164 J.H. SPEAKE and G.J. CURTIS
 'Characterisation of the fracture processes in cfrp using spectral analysis of the acoustic emissions arising from the amplification of stress'
 Proceedings of the 2nd International Conference on Carbon Fibres, Plastics Institute, London, February 1974, Paper 29, 186-193.
- 165 D.M. EGAN
 'Acoustic emission analysis of fibre composite failure mechanisms'
 M.S. thesis in Mechanical Engineering and in Ocean Engineering, Massachusetts Institute of Technology, May 1977, BLL thesis 79/31845.
- 166 D.M. EGAN and J.H. WILLIAMS
 'Acoustic emission spectral analysis of fibre composite failure mechanisms'
 Massachusetts Institute of Technology NASA Contractor Report CR 2938, January 1978.
- 167 J.H. WILLIAMS and D.M. EGAN
 'Acoustic emission spectral analysis of fibre composite failure mechanisms'
 Materials Evaluation, January 1979, 37(1), 43-47.
- 168 C.R. MORAIS and A.T. GREEN
 'Establishing structural integrity using acoustic emission'
 ASTM STP 571, 1975, 184-199.
- 169 M. TAKEHANA and I. KIMPARA
 'Internal fracture and acoustic emission of fibreglass reinforced plastics'
 Proceedings of the International Conference on the Mechanical Behaviour of Materials, SMSJ, Kyoto Japan, August 1971, 157-167.
- 170 E. HINTON and D.R.J. OWEN
 "An introduction to finite element computations"
 Pineridge Press Ltd, Swansea, 1979.
- 171 R. COURANT
 'Variational methods for the solution of problems of equilibrium and vibration'
 Bulletin of the American Mathematics Society, 1943, 49, 1-43.
- 172 R.W. CLOUGH
 'The finite element method in plane stress analysis'
 Proceedings of the 2nd Electronic Computation Conference, American Society of Civil Engineers, Pittsburgh PA., 8-9 September 1960, 345-378.
- 173 M.D. MATHERS and K.N. MORMAN
 'Theoretical and computational methods for composite structures — a survey of computer programs'
 Society of Automotive Engineers, Paper 790983, 1979.
- 174 D. BUSHNELL and B.O. ALMROTH
 'Finite-difference energy method for non-linear shell analysis'
 Proceedings of the Shell Conference, LMSC + AFFDL, Palo Alto CA, August 1970.
- 175a K.J. BATHE
 'ADINA — a finite element program for automatic dynamic incremental nonlinear analysis'
 Massachusetts Institute of Technology Report 82448-1, September 1975.
- 175b K.J. BATHE, S. BOLOURCHI, S. RAMASWAMY and M.D. SYNDER
 'Some computational capabilities for nonlinear finite element analysis'
 Nuclear Engineering and Design, 1978, 46, 429-455.
- 176 C.A. BREBBIA (Editor)
 "A Handbook of Finite Element Systems"
 CML Publications, Southampton, 1981.
- *** *Useful reference received too late for inclusion in text.*
- B. FREDRIKSSON and J. MACKERLE
 'Structural Mechanics Finite Element Computer Programs — Surveys and Availability'
 Linköping Institute of Technology (Sweden) Report LiTH-IKP-R-054, September 1975.

- 177a 'ASAS User Manual, Version G, First Edition'
ASAS, Surrey, January 1977.
- 177b J.H. ARGYRIS
'The TRIAX-6 element for axisymmetric analysis by the matrix displacement method'
Journal of the Royal Aeronautical Society, December 1966, 70(3), 1102-1106.
- 178 T.K. HELLEN and S.E. PROTHEROE
'BERSAFE finite element system'
Computer Aided Design, January 1974, 6(1), 15-24.
- 179a T.K. HELLEN
'BERSAFE (Phase 1) Users Guide'
CEGB Report RD/B/N1761, 1970.
- 179b T.K. HELLEN
'BERSAFE (Phase 1) Advice and Sample Problems'
CEGB Report RD/B/N1813, 1971.
- 179c K. FULLARD
'FLHE Users Guide'
CEGB Report RD/B/N1849, 1971.
- 179d K. FULLARD
'FLHE Advice and Sample Problems'
CEGB Report RD/B/N2304, 1972.
- 180 NASTRAN:
 a) SP221(xx) : Theoretical manual
 b) SP222(xx) : Users manual
 c) SP223(xx) : Programmers manual
 d) SP224(xx) : Demonstration problems
 where xx : 00 is level 15.0, September 1970.
 xx = 01 is level 15.5, June 1972.
 xx = 02 (unknown)
 xx = 03 is level 16.0, March 1976.
 xx = 04 is level 17.0, December 1977.
 xx = 05 is level 17.5, December 1978.
 e) NASTRAN: user's experiences,
 Proceedings of the NASTRAN Users Colloquia:
 i) TM-X-2378 : 1st meeting : September 1971.
 ii) TM-X-2637 : 2nd meeting : September 1972, Hampton VA.
 iii) TM-X-2893 : 3rd meeting : September 1973.
 iv) TM-X-3278 : 4th meeting : September 1975, Hampton VA.
 v) TM-X-3428 : 5th meeting : October 1976, Ames Research Centre, Moffett Field, N77-20485
 vi) CP-2018 : 6th meeting : October 1977, Cleveland OH., N78-12443.
 vii) CP-2062 : 7th meeting : October 1978, Marshall SFC, Huntsville ALA, N78-32466.
 viii) CP-2131 : 8th meeting : October 1979, Goddard SFC, Green Belt MA, N80-24648.
 ix) CP-2151 : 9th meeting : October 1980, Kennedy SC, Cocoa Beach FL, N80-33782.
 x) CP-2249 : 10th meeting: May 1982, New Orleans. N83-12452.
 f) Navy – NASTRAN Users Colloquia : Naval Ship Research & Development Centre, Bethesda, Md.
 i) AD 764 298 : 1st meeting : January 1970.
 ii) AD 764 507 : 2nd meeting : December 1970.
 iii) AD 764 299 : 3rd meeting : March 1972.
 iv) AD 764 508 : 4th meeting : March 1973.
 v) AD A004 604 : 5th meeting : September 1974.
 g) E.I. FIELD, D.N. HERTING and M.J. MORGAN
'NASTRAN Users Guide (Level 17.5)'
NASA CR-3146, June 1979.
 h) C.C. CHAMIS, J.H. SINCLAIR and T.L. SULLIVAN
'NASTRAN as an analytical research tool for composite mechanics and composite structures'
NASA Technical Memorandum TM-X-3428, 1976, 381-417.
 i) C.C. CHAMIS and J.H. SINCLAIR
'The effects of eccentricities on the fracture of off-axis fibre composites'
33rd Annual Technical Conference, SPI, Washington DC, February 1978, Paper 22-A.

- 181 PAFEC 75 Handbooks, PAFEC Limited, Nottingham
 a) Theory, results : December 1975
 b) Get started : September 1977
 c) Easidata, 2nd edition : December 1977
 d) Data Preparation : November 1978
 e) Data Preparation 3.1 Supplement : 1980
 f). Systems: continuously updated looseleaf file.
- 182a C.A.P. CASTIGLIANO
 "Théorie de l'équilibre des Systèmes élastiques et ses applications"
 Auguste Frédéric Negro, Turin, 1879.
 Translation by E.S. ANDREWS:
 "The theory of equilibrium of elastic systems and its applications"
 Dover Publications, New York, 1966.
- 182b M.A. EISENBERG
 "Introduction to the mechanics of solids"
 Addison-Wesley, Philippines, 1980.
- 183 J.L. SWEDLOW
 'Crack tip finite element analysis'
 10th Symposium on Naval Structural Mechanics — Fracture Mechanics
 September 1978, 529-540.
- 184 A.J. FAWKES, D.R.J. OWEN and A.R. LUXMOORE
 'An assessment of crack tip singularity models for use with isoparametric elements'
 Engineering Fracture Mechanics, 1979, 11(1), 143-159.
- 185 J.E. AKIN
 'Computational methods for local singularities'
 in J.T. ODEN:
 "Computational methods in non linear fracture mechanics"
 North Holland Publishing Company, 1980, chapter 1, 1-2.
- 186 J.E. AKIN and S. SWANY
 'Analysis of material interface cracks by singularity elements'
 in A.R. LUXMOORE and D.R.J. OWEN:
 "Numerical Methods in Fracture Mechanics"
 University of Wales, Swansea, January 1978, 747-754.
- 187 I.W. YU and W.K. WILSON
 'Generation of singular elements for the analysis of cracked bodies'
 in J.E. AKIN and W.H. GRAY:
 "Computer Technology in Fusion Energy Research"
 ASME, New York, 1978, 99-114.
- 188 M.B. KASEN
 'Mechanical and thermal properties of filamentary reinforced structural composites at cryogenic temperatures, 1: glass reinforced composites'
 Cryogenics, June 1975, 15, 327-349.
- 189 M.B. KASEN
 'Mechanical and thermal properties of filamentary reinforced structural composites at cryogenic temperatures, 2: advanced composites'
 Cryogenics, December 1975, 15, 701-722.
- 190 Conference "Non-metallic materials and composites at low temperatures"
 Munich, 10-11 July 1978; Plenum Press, New York, 1979.
- 191 Conference "Non-metallic materials and composites at low temperatures"
 Geneva, 4-5 August 1980; Plenum Press, New York, 1982.
- 192 J.R. KASTELIC, A. HILTNER and E. BAER
 'Crazing, yielding and fracture in polycarbonate and polyethylene terephthalate at low temperatures'
 Journal of Macromolecular Science — Physics, 1973, B7(4), 679.
- 193 Seminar: "Relationships between structure and mechanical behaviour in polymeric solids",
 American Society for Metals, Chicago Ill, 1973.

- 194 K. KADOTANI
 'Mechanical properties of plastic composites under low temperature conditions'
Composites, April 1980, 11(2), 87-93.
- 195 R.E. SCHRAMM and M.B. KASEN
 'Cryogenic mechanical properties of boron-, graphite- and glass-reinforced composites'
Materials Science and Engineering, November 1977, 30(3), 197-204.
- 196 M.B. KASEN
 'Letters: Mechanical properties of plastic composites under low temperature conditions'
Cryogenics, April 1981, 12(2), 107.
- 197 J.V. LARSEN and R.A. SIMON
 'Carbon fibre composites for cryogenic filament wound vessels'
NASA Centre Report CR120 889, 1972.
NOL Technical Report TR 71-201.
- 198 J. HERTZ, J.L. CHRISTIAN and M. VARLAS
 'Advanced composite applications for spacecraft and missiles'
AFML Technical Report AFML-TR-71-186-VOL-2, 1972.
- 199 L.L. VASILIEV, L.S. DOMOROD and S.A. TANAEVA
 'A study of the thermophysical properties of composite high-molecular compound-based materials with a fibrous filler from 10-400K'
 Pages 309-315 of reference 190.
- 200 P.R. NELSON and M.H. KRIM
 'A thermally inert cylindrical truss concept'
NASA Technical Memorandum TM-X-3377-PT-1, April 1976, 275-304.
- 201 N.J. PARRATT and K.D. POTTER
 'Behaviour and benefits of hybrid reinforced composites'
PERME Technical Report TR 81, November 1978.
- 202 N.J. PARRATT and K.D. POTTER
 'Mechanical behaviour of intimately-mixed hybrid composites'
 3rd. International Conference on Composite Materials,
 Metallurgical Society of AIME, Paris, August 1980, 313-326.
- 203 R.D. HENSHELL and K.G. SHAW
 'Crack tip finite elements are unnecessary'
International Journal of Numerical Methods in Engineering, 1975, 9(3), 495-507.
- 204 W.F. BROWN and J.E. SRAWLEY
 'Plane strain crack toughness testing of high strength metallic materials'
ASTM STP 410, 1967.
- 205 W.K. WILSON
 'Combined mode fracture'
Ph.D. thesis, University of Pittsburgh, 1969.
- 206 W.S. BLACKBURN
 'Calculation of stress intensity factors at crack tips using special finite elements'
 Conference on Mathematics of Finite Elements and Applications,
 Brunel University, April 1972, 327.
- 207 N.L. HANCOX
 'Introduction to Fibre Composite Hybrids'
 in N.L. HANCOX (editor):
 "Fibre Composite Hybrid Materials"
Applied Science Publishers, Barking, 1981, chapter 1, 1-22.
- 208 E.M. TREWIN, Courtaulds Carbon Fibre Unit
 Personal communication.
- 209 J.B STURGEON
 'Specimens and test methods for carbon fibre reinforced plastics'
Royal Aircraft Establishment Technical Report 71026, February 1971.

- 210 H. WELLS, W.J. COLCLOUGH and P.R. GOGGIN
 'Some mechanical properties of carbon fibre composites'
 AERE Harwell Report R6149, July 1969
 24th Annual Reinforced Plastics/Composites Conference, SPI, Washington DC, February 1969,
 Paper 2-C.
- 211 'Grafil (R) test methods', Courtaulds Carbon Fibre Unit, March 1980
 a) Section 4 – unidirectional composite properties: flexural strength : test reference 404.14
 b) " flexural modulus " 405.22
 c) " flexural modulus " 405.14
 d) " interlaminar shear strength " 406.13
- 212 S. TIMOSHENKO
 "Strength of Materials", John Wiley, 1955.
- 213 T.A. COLLINGS and R.G. FINBOW
 'Variation of Young's modulus with fibre volume fraction on unidirectional carbon fibre reinforced plastic'
 Royal Aircraft Establishment Technical Report 70006, January 1970.
- 214 D.F. ADAMS and R.L. THOMAS
 'Test methods for the determination of unidirectional composite shear properties'
 12th National Symposium, SAMPE, Anaheim, October 1967, Section AC-5.
- 215 N.J. WADSWORTH and J. HUTCHINGS
 'The measurement of adhesion between fibres and resin in composites'
 Royal Aircraft Establishment Technical Memorandum MAT14, December 1967.
- 216 K.T. KEDWARD
 'The short beam test method of estimating shear strengths'
 "Testing Fibrous Composites for Mechanical Properties" Conference, Institute of Physics and Physical Society, National Physical Laboratory, Teddington, 15-17 July 1970.
- 217 S.A. SATTAR and D.H. KELLOG
 'The effect of geometry on the mode of failure of composites in short-beam shear tests'
 ASTM STP 460, December 1969, 62-71.
- 218 M.G. BADER, J.E. BAILEY and I. BELL
 'The fracture behaviour of carbon fibre reinforced composites'
 in W.W. KRIESEL and H. PALMOUR III (editors):
 "Ceramics in severe environments: Volume 5 of Materials Science Research", Plenum Press, New York, 1971, ISBN 306-38505-8.
- 219 W.W. STINCHCOMB, E.G. HENNEKE and H.L. PRICE
 'Use of the short beam shear test for quality control of graphite-polyimide laminates'
 ASTM STP 626, May 1976, 96-109.
- 220 'ASTM test for apparent horizontal shear strength of reinforced plastics by short beam method (D2344-76)'
- 221 J.J. WHITNEY, D.L. STANSBARGER and H.B. HOWELL
 'Analysis of the rail-shear test: applications and limitations'
 Journal of Composite Materials, January 1971, 5(1), 24-34.
- 222 'ASTM Standard Methods of Test for interlaminar shear strength of structural reinforced plastics at elevated temperatures (D2733-70)'
- 223 H.S. LOVELESS and J.H. ELLIS
 'A comparison of methods for determining the shear properties of glass/resin unidirectional composites'
 Journal of Testing and Evaluation, September 1977, 5(5), 369-374.
- 224 P.E. BALL and J.A. RAYMOND
 'The materials/design interface in reinforced plastics'
 Conference: Designing to avoid mechanical failure, Plastics Institute, Cranfield, 8-10 January 1973,
 Paper 2.

- 225 'Best test for fibre composites'
Materials Engineering, February 1981, 93(2), 64.
- 226 C.C. CHAMIS and J.H. SINCLAIR
'10° off-axis tensile test for interlaminar shear characterisation of fibre composites'
NASA TN D 8215; N76-22314/NSP.
- 227 P. BABB
'Fracture characteristics of glass-fibre-polyester composites'
M. Phil thesis, Plymouth Polytechnic, September 1979.
- 228 Y.K. CHEUNG and I.P. KING
'Computer methods and computer programs'
in O.C. ZIENKIEWICZ:
"The Finite Element Method in Engineering Science"
McGraw-Hill, London, 1971, chapter 20, 435-499.
- 229 P.J. HEWSON
'Two dimensional stress analysis'
Plymouth Polytechnic Composite Materials Research Group
Report 101/PJH, 12 November 1973.
- 230 R.D. HENSELL
'A survey of the use of finite element method in stress analysis'
in P. STANLEY (editor):
"Computing developments in experimental and numerical stress analysis"
Applied Science, Barking, 1976, 1-19.
- 231 C.A. FARNFIELD and P.J. ALVEY (editors)
"Textile terms and definitions, seventh edition"
Textile Institute, Manchester, 1975.
- 232 L.M. SOFFER and R. MOLHO
'Cryogenic resins for glass filament-wound composites'
Aerojet General Report 3343: NASA CR 72114: NASA N67-25076, January 1967.
- 233 N.P. CHEREMISINOFF and P.N. CHEREMISINOFF
"Fibreglass-reinforced plastics deskbook"
Ann Arbor Science Publishers, Michigan, 1978.
- 234 'Yarn designation systems for plastic reinforcement fabrics'
Fothergill and Harvey publication no. 112, 1980.
- 235 H.S. KATZ and J.V. MILEWSKI
"Handbook of fillers and reinforcements for plastics"
Van Nostrand Reinhold, New York, 1978.
- 236 A.J. ROBERTS, Courtaulds Carbon Fibre Unit
Personal communication
- 237 C.E. KNOX
'Advances in glass fibre fabrics for plastics reinforcements'
6th. Reinforced Plastics Congress, BPF RPG, London, November 1968, Paper 13.
- 238 J.O. OUTWATER
'Fibre-reinforced polymer composites: a general review'
in J.W. WEETON and E. SCALA (editors):
Proceedings of the Fall Meeting "Composites — State of the Art",
The Metallurgical Society of AIME, Detroit, 18-21 October 1971, 11-21.
- 239 M. LANGLEY
"Carbon fibres in engineering"
McGraw-Hill, Maidenhead, 1973.
- 240 J. THEBERGE
'Glass and carbon fibre thermoplastic composites'
Conference on Advanced Composite Technology,
Technology Conference Associates, El Segundo CA., 14-16 March 1978, Paper 6, 52-90.

- 241 P. FAZIO and D. FELDMAN
'Polymers in sandwich panels'
Plastics and Rubber International, April 1980, 5(2), 67-72.
- 242 D.R. LOVELL
'Reinforcements'
in N.L. HANCOX (editor):
"Fibre Composite Hybrid Materials"
Applied Science Publishers, Barking, 1981, chapter 2A, 23-35.
- 243 'Launching a new era in composite materials technology'
RK Textile Composite Fibres Ltd., Brighton Road, Heaton Norris, Stockport, SK4 2BE, 1982.
- 244 'Hercules Product Data' Sheets 840-1/851/847-3/838-1
Hercules Inc., Graphite Fibres Business Centre, P.O. Box 98, Magna UT84044, August 1981.
- 245 T.E. PRITCHARD, J.E. BATEMAN and A.C. FLESHER
'An Apple II based image digitising system for use with immunoelectrophoresis plates'
SERC Rutherford Appleton Laboratory Report RL-82-040, May 1982.
- 246 M.B. GRUBER
'Mechanical properties of hybrid composites'
Master of Mechanical and Aerospace Engineering thesis, University of Delaware, June 1981.
- 247 J. SUMMERSCALES and D. SHORT
'Finite element analysis of stress concentrations at crack tips in anisotropic materials'
Research Meeting VII: Fracture Mechanics, PRI PPG, London, 16 March 1978.
Plymouth Polytechnic Composite Materials Research Group Report 118, March 1978.
- 248 'Sierra: Compute-a-crash saving'
The Engineer, 23 September 1982, 255(6600), 46-51.
- 249 A. PEANO and A. PASINI
'A warning against misuse of quarter-point elements'
International Journal for Numerical Methods in Engineering (Short Communications), February 1982, 18(2), 314-320.

APPENDIX INDEX

	<u>Appendix</u>	<u>Pages</u>
Index		1
Publications, papers and special lectures during the research	1	2-3
Research Meeting VII: Fracture Mechanics, March 1978		fiche F1: A1-C10
Composites, July 1978		fiche F1: D1-D10
Composites, October 1979		fiche F1: E1-E7
Composites, January 1980		fiche F2: A1-A6
36th Reinforced Plastics Conference, February 1981		fiche F2: B1-B4
Chapter 3 of 'Fibre Composite Hybrid Materials', March 1981		fiche F3: A1-E1
Courses, conferences and other training during the research	2	4
Publication contracts and permission for microfiches	3	5-15
Major sources of relevant publications	4	16
Research laboratory reports		fiche A: A1-C7
Conferences		fiche A: D1-E10
Bibliographies	5	16-17
Carbon fibre with glass fibre hybrid reinforced plastics		fiche B: A1-D3
Textbooks on composite materials		fiche B: D4-D8
Theses on reinforced polymeric materials		fiche B: D9-E12
Acoustic emission in fibre composites		fiche C: A1-C6
Cryogenic properties of fibre composites		fiche C: D1-E5
Electron microscopy of fibre composites		fiche C: E8-E12
Suppliers of anisotropic/orthotropic finite element software	6	18-19
Computer software listings	7	20-21
Q definition of system subroutines		fiche MF1: A1-A6
L-PICTURE computer generated random microstructure		fiche MF1: A7-A10
L-ANALYSIS calculation of microstructure parameters		fiche MF1: B1-B4
L-SYPRGM prediction of extent of hybrid effect		fiche MF1: B5-C5
XAA1 command file to submit PAFEC 75 job		fiche MF1: D1-D2
AA1 command file to run PAFEC job with plotting		fiche MF1: D3-D6
L-DIVIDE dummy subroutine for singularity in PAFEC		fiche MF1: D7-D9
L-SCA nodal averaging and output graphics (PAFEC)		fiche MF1: E1-E8
L-CONB stress contour plotting for PAFEC		fiche MF2: A1-A10
L-GRAPH plotting program for graphs on linear axes		fiche MF2: B1-D3
L-CROI reference database program		fiche MF3: A1-C4
L-SLCT specific selections from database		fiche MF3: D1-D11
Definitions and specifications for fibrous reinforcement	8	22-26
Derivation of the equations for flexural properties	9	27-30
Scott Bader Crystic 272 polyester resin data sheets	10	31-36
Description of Courtaulds Air Knife	11	37

NOTE: The microfiches included in these appendices are organised in rows (A-E) and columns (1-12), such that top centre will be A6 or A7, and midside right will be C12.

APPENDIX ONE: Publications, papers and special lectures during the research

- @ FINITE ELEMENT ANALYSIS OF THE STRESS CONCENTRATIONS AT CRACK TIPS IN ANISOTROPIC MATERIALS: verbal presentation and abstract
Research Meeting VII: Fracture Mechanics
Plastics and Rubber Institute Polymer Properties Group
LONDON, 16 March 1978.
- @ CARBONFIBRE AND GLASSFIBRE HYBRID REINFORCED PLASTICS
Composites 9(3), July 1978, pp. 157-166.
- @ HYBRIDS – A REVIEW, PART 1: TECHNIQUES, DESIGN AND CONSTRUCTION
Composites 10(4), October 1979, pp. 215-221.
- @ HYBRIDS – A REVIEW, PART 2: PHYSICAL PROPERTIES
Composites 11(1), January 1980, pp. 33-38.

THE HYBRID CONCEPT: verbal presentation only
Discussion Meeting: Effective use of fibrous reinforcements for performance
Plastics and Rubber Institute Reinforced Plastics Group
HIGH WYCOMBE, 8 October 1980.
- @ THE USE OF CGHRP IN TRANSPORT
36th Annual Reinforced Plastics/Composites Conference
The Society of the Plastics Industry
WASHINGTON DC, 19 February 1981, Paper 11-D.

THE USE OF CARBON FIBRE AND GLASS FIBRE HYBRID REINFORCED PLASTICS IN TRANSPORTATION: verbal presentation only
NRC/UBC Joint Seminars on Composite Materials
National Research Council of Canada Department of Mechanical Engineering
VANCOUVER BC, 23 February 1981.

THE SIGNIFICANCE OF FAILURE STRAIN IN CALCULATING THE STRENGTH OF HYBRID COMPOSITES: verbal presentation only
NRC/UBC Joint Seminars on Composite Materials
University of British Columbia Department of Metallurgy
VANCOUVER BC, 24 February 1981.
- @ THE ELASTIC AND THERMAL PROPERTIES OF COMPOSITES, pp. 69-117.
Chapter 3 of N.L. Hancock (editor):
"Fibre Composite Hybrid Materials", pp. x + 290.
(Applied Science Publishers Limited, Barking Essex, March 1981)
(Distributed by Macmillan Inc., New York in the USA and Canada.)
- A NEW THEORETICAL APPROACH TO THE STRENGTH OF FIBRE COMPOSITE HYBRID MATERIALS
13th BPF Reinforced Plastics Group Congress
BRIGHTON, 11 November 1982, Paper 53, pp. 225-229.
- AMPLITUDE DISTRIBUTION ACOUSTIC EMISSION ANALYSIS OF UNIDIRECTIONAL FIBRE COMPOSITE HYBRID MATERIALS: verbal presentation only
Institution of Metallurgists meeting: High Performance Composite Materials
LONDON, 2 December 1982.

@ These items included as microfiche copies enclosed on the following page.

APPENDIX TWO: Courses, conferences and other training undertaken during research

	<u>Course Title</u>	<u>Venue</u>	<u>Duration</u>	<u>Organiser</u>
1977:				
Autumn	Fortran IV Computing	Plymouth	10 hours	PP Mathematical Sciences
1978:				
March	Fracture Mechanics	London	1 day	PRI Polymer Properties Group
May	New Fibres and their Composites	London	2 days	The Royal Society
November	Manufacturing for Quality	Brighton	3 days	BPF Reinforced Plastics Group
1979:				
April	Polymer Engineering	Loughborough	2 days	SRC PED
1980:				
January	Operation of the JSM-35 S.E.M.	Plymouth	1 week	PP Electron Microscopy Unit
April	Microprocessors for Engineers	Plymouth	2 hours	PP Mechanical Engineering
June	Future of Reinforced Plastics	London	2 days	PRI & Reinforced Plastics
September	Engineering Properties of Polymers	London	1 day	PRI Polymer Properties Group
October	Effective Use of Fibrous Reinforcements	High Wycombe	½ day	PRI Reinforced Plastics Group
November	Plastics in an Energy Intensive World	London	1 evening	PRI Business Studies Group
1981:				
February	Reinforced Plastics/Composites	Washington	5 days	Soc. Plastics Industry
Spring	Apple II Pascal Language	Plymouth	3 hours	PP Mathematical Sciences
April	Polymer Engineering	Loughborough	2 days	SRC PED
April	Acoustic Emission	London	1 day	SERC PED
November	Advanced Composites	London	1 day	Institute of Physics and PRI
1982:				
November	Reinforced Plastics	Brighton	3 days	BPF Reinforced Plastics Group
December	Measurement of Polymeric Solids	Teddington	2 days	NPL
December	High Performance Composite Materials	London	1 day	Inst. Metallurgists

APPENDIX THREE: Publication contracts and permission for microfiches

	<i>Page</i>
Copyright transfer re. Composites, July 1978.	6
Copyright transfer re. Composites, October 1979.	7
Copyright transfer re. Composites, January 1980.	8
Agreement re. Fibre Composite Hybrid Materials.	9
Letter to the Society of the Plastics Industry.	10
Reply from the Society of the Plastics Industry.	11
Letter to Applied Science Publishers Ltd.	12
Reply from Applied Science Publishers Ltd.	13
Letter to Composites.	14
Reply from Composites.	15

COPYRIGHT TRANSFER AGREEMENT

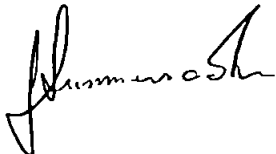
Copyright to the article entitled Carbon fibre and glass fibre hybrid reinforced plastics

by J. Summerscales and D. Short

is hereby transferred to IPC Business Press Limited. However, the author* reserves the following Rights:

1. All proprietary Rights other than Copyright
2. The Right to grant or refuse permission to third parties to republish all or part of the article or translations thereof; such third parties must also obtain the permission of IPC. However, IPC may grant rights to reprint complete Issues or Volumes of the journal
3. The Right to use all or part of this article in future works of their own, such as lectures, reviews or textbooks

(Signature)



(title, if not author)

(date) 5/5/78

The signed statement must be returned to the Managing Editor of:

COMPOSITES

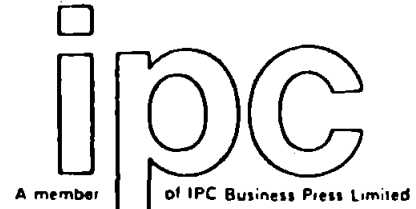
IPC House, 32 High Street, Guildford, Surrey, GU1 3EW, England.

*To be signed by at least one of the authors (who agrees to inform the others, if any) or, in the case of a 'work made for hire', by the employer

IPC Science and Technology Press Ltd

IPC House, 32 High Street, Guildford, Surrey, England GU1 3EW
Telephone: Guildford 0483 71661

IPC Science and Technology Press Ltd
Westbury House, Bury Street,
Guildford, Surrey GU2 5BH, UK
Telex: 859556 SCITEC G
Tele: 0433 31261 Telex: 859556 Scitec G



COPYRIGHT TRANSFER AGREEMENT

Copyright to the article entitled 'Hybrids - a review. Part 1. Techniques, design and construction'

by D Short and J Summerscales

is hereby transferred to IPC Business Press Limited. However, the author* reserves the following Rights:

1. All proprietary Rights other than Copyright
2. The Right to grant or refuse permission to third parties to republish all or part of the article or translations thereof; such third parties must also obtain the permission of IPC. However, IPC may grant rights to reprint complete Issues or Volumes of the journal
3. The Right to use all or part of this article in future works of their own, such as lectures, reviews or textbooks

(Signature) 

(title, if not author) —

(date) 17 August 1979

The signed statement must be returned to the Managing Editor of:

Composites, Mr Tim Feest

IPC House, 32 High Street, Guildford, Surrey, GU1 3EW, England

P O Box 63, Westbury House, Bury Street, Guildford, Surrey, GU2 5BH

*To be signed by at least one of the authors (who agrees to inform the others, if any) or, in the case of a 'work made for hire', by the employer

IFC Science and Technology Press Ltd

IPC House, 32 High Street, Guildford, Surrey, England GU1 3EW

Telephone: Guildford 01233 71661

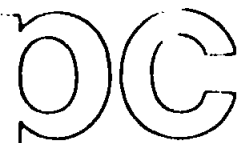
IFC Science and Technology Press Ltd

P.O. Box 63, Westbury House, Bury Street,

Guildford, Surrey GU2 5BW, UK

Telex: 859556 SCITEC G.

Tele: 0992 31261 Telex: 859556 Scitec G



of IPC Business Press Limited

A member

COPYRIGHT TRANSFER AGREEMENT

Copyright to the article entitled 'Hybrids - a review. Part 2. Physical properties'.

by D Short and J Summerscales

is hereby transferred to IPC Business Press Limited. However, the author* reserves the following Rights:

1. All proprietary Rights other than Copyright
2. The Right to grant or refuse permission to third parties to republish all or part of the article or translations thereof; such third parties must also obtain the permission of IPC. However, IPC may grant rights to reprint complete Issues or Volumes of the journal
3. The Right to use all or part of this article in future works of their own, such as lectures, reviews or textbooks

(Signature)


John Summerscales.

(title, if not author)

(date) 25th October 1979

The signed statement must be returned to the Managing Editor of:

"Composites, Mr Tim Feest

~~IPC House, 32 High Street, Guildford, Surrey, GU1 3EW, England,~~

P O Box 63, Westbury House, Bury Street, Guildford, Surrey, GU2 5BH.

*To be signed by at least one of the authors (who agrees to inform the others, if any) or, in the case of a 'work made for hire', by the employer

AGREEMENT

An AGREEMENT made this 31st day of October 1978 between

Dr. D. Short and Dr. J. Summerscales

(Name)

School of Engineering Science, Plymouth Polytechnic,
Drake Circus, Plymouth PL4 8AA

(Address)

(hereinafter called the AUTHOR) of the one part, and APPLIED SCIENCE PUBLISHERS LIMITED, 22 Rippleside Commercial Estate, Barking, Essex, England (hereinafter called APPLIED SCIENCE) of the other part, whereby it is mutually agreed as follows:

Book Title: Hybrid-Fibre Composite Materials

Editor: Dr. N.L. Hancock

1. Applied Science have invited the Author to write a manuscript to be included as part of the above publication relating to Prediction of short term elastic, strength and thermal properties, failure criteria, and design optimisation of about 30 printed pages (approximately 12,000 words) including formulae, tables and illustrations (each illustration is equivalent to 200 words). The manuscript and drawings will be sent to the Editor in the English language and typewritten in double spacing by September 1979
2. The Author agrees to take care that: (a) diagrams and photographs are supplied in a form ready for the blockmaker (b) literature references, including authors' names and initials, volume numbers of periodicals, years of publication, patent numbers and the like, are carefully checked before delivery of the manuscript.
3. The Author agrees to approve the proofs without delay as agreed.
4. If the Author introduces changes into the proofs which constitute departure from the original manuscript he agrees to bear the cost of such changes unless otherwise agreed, such costs to be deducted from royalties.
5. Applied Science acquires the sole and exclusive copyright and will use its endeavours to prevent illegal reproduction and re-sale in such form.
6. Applied Science will pay to the Author a royalty of 1 per cent of the sales receipts of the English edition of the book. By "sales receipts" is meant the total amount of receipts encashed by Applied Science on account of all copies of the English edition sold throughout the world, except those sales made to the Author in accordance with paragraph 9. The royalties will be calculated yearly and payment made within four months after 31st December of each calendar year.
7. Applied Science will divide the royalty equally amongst authors if there is more than one, unless otherwise stated. Applied Science will also present to the Author one free copy of the book.
8. Illustrations, tables and diagrams, will be supplied to Applied Science free of any copyright charges. The Author warrants to the Editor of the book and Applied Science that his manuscript will in no way whatever violate any existing copyright and that it contains nothing of a libellous or scandalous character. The Author is to obtain written permission from author and publisher to quote passages from books or journals and to reproduce illustrations, tables and diagrams for which a copyright exists.
9. The Author may purchase copies of the book for his own use at a discount of 30% off the retail price.

The Author: D Short

Applied Science Publishers Limited: J.J. Shelley

A9



PLYMOUTH POLYTECHNIC

Director: R.F.M. Robbins, B.Sc., Ph.D., C.Chem., F.R.I.C.

Drake Circus Plymouth Devon PL4 8AA
Phone: 0752 21312 Telex: 454

Our ref. JS/GMF

Your ref.

Ms. Catherine A. Randazzo
Assistant Manager
Reinforced Plastics/Composites Institute
The Society of the Plastics Industry
355 Lexington Avenue
New York 10017
USA

Reply to:

Dept. Mechanical Engineering
Tele. No. (0752) 264656

Date: 24th March 1981

Dear Ms. Randazzo

I am hoping to submit a thesis to the Council for National Academic Awards in pursuance of the degree of Ph.D., and within the regulations there exists a requirement that the thesis contains a copy of all papers published in my name during the research.

After consulting the correspondence relating to this paper I am unsure about the legal position. I would therefore be most grateful if you could give me permission to make a microfiche of the paper(s) published in the proceedings of the 36th Reinforced Plastics/Composites Conference. This would be specifically for inclusion in the thesis, in order to minimise the thickness thereof.

Thank you in anticipation of your reply.

Yours sincerely

JOHN SUMMERSCALES
Research Assistant

**The Society of the
Plastics Industry, Inc.**

355 Lexington Avenue
New York, New York 10017
(212) 573-9400

April 14, 1981

Mr. John Summerscales
Research Assistant
Plymouth Polytechnic
Dept. Mechanical Engineering
Drake Circus
Plymouth
Devon
England PL4 8AA

Dear Mr. Summerscales,

In reply to your March 24th letter, you may certainly make a microfiche of your paper that was published in the 36th RP/C Preprint book.

I wish you good luck in your present undertaking.

Sincerely yours,

Catherine A. Randazzo
Catherine A. Randazzo
Assistant Manager,
Reinforced Plastics/
Composites Institute

CAR/st



PLYMOUTH POLYTECHNIC

Director: R.F.M. Robbins, B.Sc., Ph.D., C.Chem., F.R.I.C.

Drake Circus Plymouth Devon PL4 8AA
Phone: 0752 21312 Telex: 4542

Our ref. JS/GMF

Your ref.

Dr. Ian Shelley
Applied Science Publishers Ltd
22 Rippleside Commercial Estate
Ripple Road
Barking
ESSEX

Reply to:

Dept. Mechanical Engineering

Tele. No. (0752) 264656

Date: 24th March 1981

Dear Dr. Shelley

I am hoping to submit a thesis to the C.N.A.A. in pursuance of the degree of Ph.D., and within the regulations there exists a requirement that the thesis contains a copy of all papers published in my name during the research.

After consulting the correspondence relating to this paper I am unsure about the legal position. I would therefore be most grateful if you could give me permission to make a microfiche of the paper(s) published in Dr. Hancox's book "Fibre Composite Hybrid Materials". This would be specifically for inclusion in the thesis, in order to minimise the thickness thereof.

Also we will be involved in the research display section of the Polymer Engineering Directorate Review Meeting/Exhibition, so if you could supply publicity material for the book we would be able to include these!

Thank you in anticipation of your reply.

Yours sincerely

JOHN SUMMERSCALES
Research Assistant



APPLIED SCIENCE PUBLISHERS LTD

A Company within Elsevier Science Publishers

RIPPLESIDE COMMERCIAL ESTATE
BARKING ESSEX IG11 0SA ENGLAND

Telephone No: 01-595 2121
Telegrams: Elsbark, Barking

Mr. J. Summerscales,
Mechanical Engineering Dept.,
Plymouth Polytechnic,
Drake Circus,
Plymouth,
Devon PL4 8AA

31st March, 1981

IJS/BC

Dear Mr. Summerscales,

Thank you for your letter of 24th March. The situation surrounding the copyright of your chapter published in Fibre Composite Hybrid Materials, edited by Dr. Hancox, is contained within the Agreement signed by you and Dr. Short. Strictly, Applied Science is the owner of the copyright of your chapter and you are, therefore, correct to seek our permission to make a microfiche of your chapter for inclusion in your thesis. On behalf of Applied Science, I grant you permission to make a microfiche copy of your chapter for inclusion in your thesis.

Your request for publicity material for the book has been passed to our Promotions Dept. and I expect they will send you the information you require in the near future. How many copies of the leaflet do you require?

Yours sincerely,

IAN J. SHELLEY

cc: Mr. R. Young (ASP)



PLYMOUTH POLYTECHNIC

Director: R.F.M. Robbins, B.Sc., PhD, C.Chem, FR.I.C.

Drake Circus Plymouth Devon PL4 8AA
Phone: 0752 21312 Telex: 4542

Our ref. JS/GMF

Your ref.

Mr. Tim Feest
The Editor
Composites
PO Box 63
Westbury House
Bury Street
Guildford
SURREY GU2 5BH

Reply to.

Dept. Mechanical Engineering
Tele. No. (0752) 264656

Date: 24th March 1981

Dear Mr. Feest

I am hoping to submit a thesis to the C.N.A.A. in pursuance of the degree of Ph.D., and within the regulations there exists a requirement that the thesis contains a copy of all papers published in my name during the research.

After consulting the correspondence relating to this paper I am unsure about the legal position. I would therefore be most grateful if you could give me permission to make a microfiche of the paper(s) published in the journal "Composites" dated July 1978, October 1979 and January 1980. This would be specifically for inclusion in the thesis, in order to minimise the thickness thereof.

Thank you in anticipation of your reply.

Yours sincerely

JOHN SUMMERSCALES
Research Assistant

composites

IPC Science and Technology Press Limited

P.O. Box 63 Westbury House

Bury Street Guildford Surrey

England GU2 5BH

Telephone: 0483 34261 Telex: 859556 Scitec G

Our Reference: TF/DH/COMP

9th April 1981

Mr John Summerscales
Research Assistant
Plymouth Polytechnic
Drake Circus
Plymouth
Devon
PL4 8AA

cc A. A. Smailes
C. Evans

Dear Mr Summerscales

Thank you for your letter of the 24th March.

Regarding your request to make microfiche copies of the papers listed in your letter, I am happy to grant permission for this on behalf of IPC Science and Technology Press, on the understanding that the microfiche copies will be used solely to meet the CNAA regulations regarding submission of your PhD thesis.

Yours sincerely

Tim Feest

Tim Feest
Managing Editor

APPENDIX FOUR: Major sources of relevant publications (microfiche A)

Microfiche A included on the following page contains details of the reports and conferences from which much of the background information to this project was obtained. The reports are listed in an alphanumeric sequence according to the report number allocated by the issuing establishment. The conferences are listed in an alphanumeric sequence according to an arbitrary code of up to five characters, formed from some of the initial letters of the meeting title.

APPENDIX FIVE: Bibliographies (microfiche B and microfiche C)

The bibliographies in this appendix, and the literature surveys contained in Appendix One, are intended to be comprehensive. However, the interdisciplinary nature of the subjects makes it unavoidable that some works worthy of inclusion have been omitted. This will of course apply especially to references published in the few months immediately prior to the compilation of the lists. It should be noted that some items have been included unchecked, based entirely on the knowledge that the author is, or has previously been, working in the relevant research area.

The individual items are arranged in alphabetical order by the surname of the principal author. Where an author has published more than one paper these are arranged in chronological order. Where a paper has more than one author, the item is cross-referenced to the principal author. Anonymous items are included at the end of the bibliography. Some of the publication details have been considerably condensed, these can be interpreted by reference to Appendix Four.

Key to microfiches (rows are denoted A-E, columns by 1-12)

<i>Subject</i>	<i>Fiche</i>	<i>Start</i>	<i>End</i>	<i>No. Pages</i>
a) Report sequences from UK laboratories	A	A1	C7	31
b) Conferences and other regular publications	A	D1	E10	22
c) Carbon Glass Hybrid Reinforced Plastics	B	A1	D3	39
d) Textbooks on composite materials	B	D4	D8	5
e) Theses on reinforced polymeric materials	B	D9	E12	16
f) Acoustic emission in fibre composites	C	A1	C6	30
g) Cryogenic properties of fibre composites	C	D1	E5	17
h) Electron microscopy of fibre composites	C	E8	E12	5

JOHN SUMMERSCALES Ph.D Thesis: Appendix Four: microfiche A

JOHN SUMMERSCALES Ph.D. Thesis: Appendix Five: Microfiche B

JOHN SUMMERSCALES Ph.D. Thesis: Appendix Five: Microfiche C

APPENDIX SIX: Suppliers of orthotropic/anisotropic finite element schemes

- i) ADINA :
(Europe) : Mr. G. Larsson,
ADINA Engineering AB, Stangjarnsgatan 227, S72473 Vasteras, Sweden.
Tel: 021-30 22 33
- (America) : K.-J. Bathe,
Department of Mechanical Engineering, Massachusetts Institute of Technology,
Cambridge, Massachusetts 02139, USA.
- ii) ANSYS : Mr. P. Kohnke,
Swanson Analysis Systems Inc, Johnson Road, PO Box 65, Houston, PA 15342, USA.
Tel: (412) 746 3304
Tx : 510 690 8655
- iii) APPLE-SAP:
ITALIMPIANTI SpA, CAD Systems Dept., P. zza Piccapietra 9, 16121 Genova, Italy.
Tel: Genoa 5998
Tx : 27238-27262-28390 italimp
- iv) ARGUS:
Merlin Technologies Inc., 977 Town and Country Village, San Jose, CA 95218, USA
Tel: (408) 247 4003
- v) ASAS:
Atkins Research and Development,
Woodcote Grove, Ashley Road, Epsom, Surrey KT18 5BW, England
Tel: 03737-26140/29678
Tx : 23497 Atkins G
- vi) ASKA:
Iko Software Service GmbH, Albstadtweg 10, D7000 Stuttgart 80, Germany
Tel: (07 11) 78 21 31
Tx : 7 255 490 ikos
- vii) BERSAFE: Mr. G. Marshall,
BERSAFE Advisory Group, CEGB, Berkeley Nuclear Laboratories,
Berkeley, Gloucestershire GL13 9PB
Tel: 0453-810451
Tx : 43227
- viii) CASTOR:
CETIM, 52 Avenue Felix Louat, 60300 Senlis, France
Tel: (4) 453 32 66
Tx : 140006 CETIM SENLI
- ix) COMET-PR:
(Europe) Instituto Sperimentale Modelli e Strutture SpA,
Viale Giulio Cesare 29, 24100 Bergamo, Italy
Tel: (035) 24 30 43
Tx : 301249 ISMES I
- (America) McDonnell Douglas Automation Company, St. Louis, Missouri, USA
- x) DIAL: Mr. Don Wong,
Structures, Department 81-12, Building 154, Lockheed Missiles and Space Company,
P.O. Box 504, Sunnyvale, CA 94086, USA
(see also NEPSAP)
- xi) FLASH 2: Dr. U. Walder and Partners,
Weltistr. 48, 3006 Bern, Switzerland
- xii) MARC:
Marc Analysis Research Corp., Verrijn Stuartlaan 29,
2288 EK Rijswijk, The Netherlands
Tel: 070 907786

xiii) NASTRAN:

(Europe) MacNeal-Schwendler GmbH, 8000 Munchen 80,
Prinzregentenstrasse 78, West Germany
Tel: (089) 4702 068
Tx : (841) 523 784 msg d

(America) Science and Technology Information Division, Office of Technology Utilisation,
National Aeronautical and Space Administration, Washington DC, USA

MacNeal-Schwendler Corporation, 7442 North Figueroa Street,
Los Angeles, California 90041, USA
Tel: (213) 254 3456
Tx : (910) 321 2492 macn schw lsa

xiv) NEPSAP: Lockheed Missiles and Space Co. Inc., Sunnyvale CA

Tel: (408) 742 4321 xtn 21397
(see also DIAL)

xv) NISA: Engineering Mechanics Research Corp, Suite 308,
25900 Greenfield Road, Oak Park, MI 48237, USA
Tel: (313) 968 1606

xvi) PAFEC 75:

PAFEC Limited,
Strelley Hall, Main Street, Strelley, Nottingham NG8 6PE
Tel: (0602) 292291

xvii) PATCHES/PATRAN:

Prototype Development Associates Inc, 1740 Garry Avenue,
Santa Ana, CA 92705
Tel: (714) 556 2800

(Europe: PATRAN only)

Kins Development Limited, Woodcote Grove, Ashley Road, Epsom, Surrey KT18 5BW
Tel: (03727) 40121
Tx : 266701

xviii) SAP 7: Structural Mechanics, Computer Laboratory DRC 394, University of Southern California,
Los Angeles, CA 90007, USA

xix) SCIA: Eclipse Computer Services, 4 Parklands, Great Linford, Milton Keynes, MK14 5DZ
Tel: (0908) 612425

(Europe) SCIA Scientific Application Group, Attenrodestraat 6,
B3385 Meensel-Kiezegem, Belgium
Tel: 016 63 20 44
Tx : 64277 scia b

xx) SPAR/EAL:

Engineering Info Systems Inc., 5120 Campbell Avenue, Suite 240,
San Jose, CA 95130
Tel: (408) 379 0730

xxi) STAGS: Structures Laboratory, Department 52-33, Building 205,
Lockheed Research Laboratories, 3251 Hanover Street, Palo Alto, CA 94304
Tel: (415) 493 4411 xtn 45527/45195

xxii) SUSAN:

Genesys Limited, Lisle Street, Loughborough LE11 OAY, England
Tel: (0509) 39185/8
Tx : 341747

xxiii) TITUS:

FRAMATOME, Centre de Calcul, BP13, 71380 Saint Marcel, France
Tel: (85) 46 80 74
Tx : FRAMCHA CHALN 800668

APPENDIX SEVEN: Computer software listings

The listings of computer programmes written for this project are included in this appendix on microfiches. A brief description of each follows.

- i) Q microfiche MF1, sectors A1-A6
descriptions of the PRIME system library subroutines used in the programmes here.
- ii) L-PICTURE microfiche MF1, sectors A7-A10
a programme which utilises a random number generator to produce drawings of random-mixed hybrid composite microstructures.
- iii) L-ANALYSIS microfiche MF1, sectors B1-B4
programme to analyse data from line transects of the microstructure and calculate the microstructure parameters.
- iv) L-SYPRGM microfiche MF1, sectors B5-C5
programme to predict the extent of any hybrid effect in a mixed fibre composite.
- v) XAA1 microfiche MF1, sectors D1 & D2
command file to submit the PAFEC job and the stress plotting job to the batch processor.
- vi) AA1 microfiche MF1, sectors D3-D6
command file to run a PAFEC job with plotting.
- vii) L-DIVIDE microfiche MF1, sectors D7-D9
dummy subroutine to model a crack tip singularity in PAFEC 75.
- viii) L-SCA microfiche MF1, sectors E1-E8
programme to calculate nodal stress averages for PAFEC and generate stress contour data files.
- ix) L-CONB microfiche MF2, sectors A1-A10
stress contour plotting of the data file from L-SCA.
- x) L-GRAPH microfiche MF2, sectors B1-D3
general plotting program for graphs on linear cartesian axes.
- xi) L-CROI microfiche MF3, sectors A1-C4
database software for manipulation of literature bibliographies and index.
- xii) L-SLCT microfiche MF3, sectors D1-D11
programme to generate specific bibliographies from L-CROI files.

John Supina's
Computer Systems

MF 1

John Supina's
Computer Systems

ROTATIONS

MF 3

APPENDIX EIGHT: Definitions and specifications for fibrous reinforcements

A8a: Definitions used for fibrous systems (=231)

Denier	: the weight in grams of 9 (nine) kilometres of fibre
End	: the smallest commercially available bundle of glass filaments; consists of 204 monofilaments in a single continuous strand (=232)
Fibre	: a unit of matter characterised by flexibility, fineness and high ratio of length to thickness
Filament	: a fibre of indefinite length
Roving	: a bundle of continuous, untwisted glass fibres (=233)
Strand	: one of the individual components, namely a single, a two-fold, or a multi-fold yarn, of a folded or cabled construction
Tex	: a unit in the ISO system for describing the linear density (mass/unit length) of fibres, filaments and yarns
	1 tex = 1 gram per kilometre 1 kilotex = 1 g/m or 1 kg/km 1 millitex = 1 mg/km
Tow	: a large number of filaments collected together into a loose strand or assemblage, substantially without twist
Warp	: the lengthways thread in a fabric as woven
Weft	: the widthways thread in a fabric as woven
Yarn	: a product of substantial length and relatively small cross section of fibres or filaments, with or without twist
Yield	: defined as the number of yards per pound of reinforcement

A8b: Designation of reinforcement yarns (=234)

The information contained in standard fabrics designation is illustrated by the following examples:

a) Fothergill and Harvey fabric Y093; designated 11 x 2 x 3 EC5:

- 11 tex singles yarn
- 2 of which are first twisted together, and then
- 3 of the resulting folded yarns are twisted together (final tex = 66)
- E indicates E-glass
- C indicates continuous fibres
- 5 indicates five-micron filament diameter.

b) Fothergill and Harvey fabric Y652; designated 198 x 2 CS7:

- 198 tex yarn,
- 2 of which are twisted together (final tex = 396)
- C indicates C-glass
- S indicates staple: short lengths of fibre spun together for bulk,
- 7 indicates seven-micron filament diameter.

c) Carbon fibre, Courtaulds system designation XY(Z):

- X gives the fibre type, eg: EXA-S
- Y gives the number of filaments per yarn, eg: 3K ≡ 3000
- Z is included only if the yarn is twisted.

d) Carbon fibre, Toray system designation XYZ:

- X gives the fibre type, eg: T300
- Y gives the number of filaments per yarn, eg: 1000, 3000
(1000 yarn = 67 tex; 3000 yarn = 198 tex; 6000 yarn = 396 tex)
- Z is A (twisted), B (untwisted) or C (not twisted)
(twisted yarns have 15 turns per metre)

A8c: The grades of glass fibres (=235-242)

A : high alkali grade — originally made from standard window glass

C : chemical grade — acid resistant

D : low dielectric grade, good transparency to radar frequencies

E : electrical insulation grade (varies according to the availability of local raw materials, ease of production and fluorine emission restrictions: magnesia-free and fluorine-free compositions exist

M : high modulus grade (also known as YM31A)

R : European equivalent of 'S-glass' — easier to produce

S : high strength grade

For these fibreglass compositions and their comparative properties see table A2, which is based on a table in reference (=235). The functions of the most common glass-forming oxides are given in Table A1 below:

Table A1: The functions of the oxides in glasses

<u>Glass forming Oxide</u>	<u>Behaviour in Glassy Melted State</u>	<u>Contribution to Finished Glass Properties</u>
SiO ₂	Most desirable glass-forming oxide, but requires extremely high melting temperatures, has high viscosity, and slow rate of bubble release	Very low thermal expansion
Na ₂ O,K ₂ O,Li ₂ O	Low viscosity and good fluidity	High thermal expansion, easily attacked by moisture
CaO,MgO	Intermediate viscosity, easily devitrified	Improved chemical durability and resistance to attack by water, acids, alkali
B ₂ O ₃	Intermediate viscosity, acts as fluxing agent	Low thermal expansion
Al ₂ O ₃	Increases melt viscosity	Assists in improving chemical durability
Fe ₂ O ₃	Present as impurity unless used as colorant, lends some fluxing action, but absorbs infra-red and interferes with transfer of heat through melt	Discolors green in small quantities
ZnO	Slightly higher viscosity	Adds to chemical durability
PbO	Substantially reduces melt viscosity and acts as fluxing agent	Increases glass density and brilliance (light transmission), induces high thermal expansion
BaO	Intermediate glass viscosity	High density, some benefit in increasing chemical durability
TiO ₂	Slightly higher viscosity	Improves chemical durability, especially alkali resistance

Table A2: Fibre glass compositions and their comparative properties

Fibre Glass Composition	"A"	"C"	"D"	"E"	"M"	"S"
Description, definition, and characterisation	Typical soda-lime-silica glass, limited for reinforcement due to poor resistance to water	Chemical glass — possesses improved durability, making it preferred composition for applications requiring corrosion resistance	Glass with improved dielectric strength and low density, developed for improved electrical performance	Borosilicate type, used for major share of all reinforcement applications	Special composition developed for high modulus to impart greater rigidity to reinforced structures	Glass with high tensile strength and modulus, developed for aerospace applications
Chemical properties:						
Chemical composition % (by weight)						
SiO ₂	72.0	65.0	74.5	54.0	53.7	65.0
Al ₂ O ₃	0.6	4.0	0.3	14.0	25.0	
Fe ₂ O ₃	—	0.2	tr	0.2	0.5	tr
CaO	10.0	14.0	0.5	17.5	12.9	tr
MgO	2.5	3.0	—	4.5	9.0	10.0
B ₂ O ₃	—	6.0	22.0	8.0	(Li ₂ O-3.0)	tr
Na ₂ O	14.2	8.0	1.0	0.6	(BeO-8.0)	tr
K ₂ O	—	—	1.5	—	(TiO ₂ -8.0)	—
ZrO ₂	—	—	(Li ₂ O-0.5)	—	2.0	—
SO ₃	0.7	0.1	—	—	(CeO-3.0)	—
F ₂	—	—	—	0.1	—	—
Physical properties						
Specific gravity	2.5	2.49	2.16	2.54	2.89	2.49
Virgin tensile strength, GPa	2.4	2.8	2.4	3.5	3.5	4.6
Tensile modulus elasticity, GPa	68	69	52	72	110	86
Thermal properties						
Softening point, °C	700	750	770	850	devitrifies	860
Coefficient of thermal expansion mm/mm/°C X 10 ⁻⁷	162	72	31	50	—	29
Optical properties						
Index of refraction	1.512	1.541	1.47	1.547	1.635	1.523
Electrical properties						
Dielectric constant, 22°C, 10 ⁶ Hz	6.90	6.24	3.56	5.80	—	4.53
Loss tangent, 22°C, 10 ⁶ Hz	0.0085	0.0052	0.0005	0.0001	—	0.002
Chemical resistance—						
14 μ fibre						
% weight-loss—						
1 hr boil-in						
H ₂ O	11.1	0.13	—	1.7	—	—
1.0N H ₂ SO ₄	6.2	0.10	—	48.2	—	—
0.1N NaOH	15.0	2.28	—	9.7	—	—

A8d: The carbon fibres

Table A3: Carbon fibres and their comparative properties (=235, 236, 239, 242, 243, 244)

Manufacturer Trade designation	Tensile strength (MPa)	Elastic modulus (GPa)	Relative density	Elongation (%)	Fibre diameter (µm)
Courtaulds, Coventry					
Grafil A	2300	180-200	1.82	1.27	7
Grafil Super A	3000	225			
Grafil HTS	2400-2800	207	1.70		8
Grafil HMS	1700-2100	385-415	2.00		7.5
RK Textile, Stockport					
RK30	2900	230	1.78	1.25-1.5	
RK35	3500	230	1.78	1.5-1.8	
Celanese Corp					
Celion GY70	1724	530	1.96	0.38	8.4
Celion 3000	3033	248	1.76	1.2	7
Great Lakes Carbon					
Fortafil CG-3	1724	172	1.80		
Hercules Inc.					
Type AS	2827	207-234	1.80	1.3	7.8-8.1
Type HTS	2758	234-255	1.80	0.1	7.4-7.8
Type HMS	2344	344-379	1.88	0.5	7.2-7.5
Hercules Inc., 'Magnamite'					
Type HMS	2206	345	1.83	0.58	8
Type HMU	2758	379	1.84	0.70	8
Type AS1	3103	228	1.80	1.32	8
Type AS4	3587	235	1.80	1.53	8
Stackpole					
Panex 30	2758	206	1.74	1.3	8
Panex 30Y/800d	1551	262	1.75		
Union Carbide					
Thornel MAT VMA	1379	241	1.99		9
Thornel 300	2482	234	1.76	1.3	6.9
Thornel Type P	1379	379	1.99	0.5	11

A8e: Typical composite efficiencies attained in reinforced plastics (Table A4) (=238, 241)

Fibre configuration	Fibre length	Volume fraction (%)	Longitudinal tensile strength (MPa)	Efficiency (Exptl/Theor) (%)
			Theory	Experiment
Filament wound (unidirectional)	Continuous	77	2140	1240
Cross-laminated	Continuous	48	1360	500
Cloth-laminated	Continuous	48	1360	296
Mat-laminated	Continuous	48	1360	394
Chopped random fibre	Non-continuous	13	418	103
Glass flakes	Non-continuous	70	1141	138

A8f: The stages of resin cure (=233)

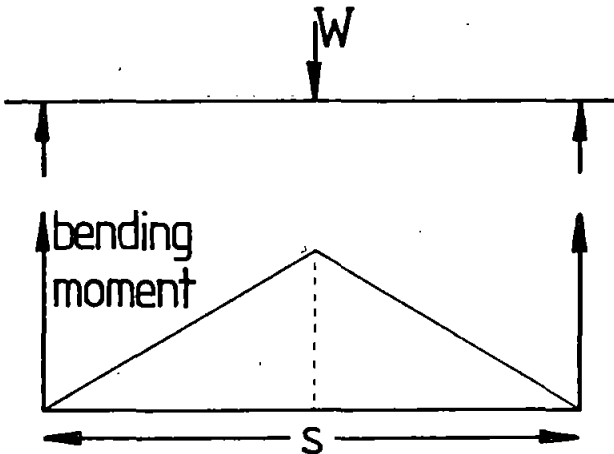
A-stage (resol): An initial or early stage in the reaction of some thermosetting resins, the material is still soluble in certain liquids and fusible.

B-stage (resitol): An intermediate stage reaction step during which the material swells when in contact with certain liquids and becomes soft when heat is applied. The material may not dissolve or fuse entirely.

C-stage (resite): Final reaction stage of various thermosetting resins, in which the material is insoluble and infusible. A fully cured thermosetting resin moulding is in this stage.

APPENDIX NINE: Derivations of the equations for flexural properties

A9a: Flexural modulus from three point bend



$$\frac{d^2y}{dx^2} = \frac{Wx}{2EI}$$

$$\frac{dy}{dx} = \frac{Wx^2}{4EI} + \text{const} \quad (\text{when } \frac{dy}{dx} = 0, x = \frac{s}{2}, \therefore \text{const} = \frac{-Ws^2}{16EI})$$

$$\frac{dy}{dx} = \frac{Wx^2}{4EI} - \frac{Ws^2}{16EI}$$

$$y = \frac{Wx^3}{12EI} - \frac{Ws^2x}{16EI} + \text{const} \quad (y = 0, x = 0, \text{const} = 0)$$

At central deflection, $x = \frac{s}{2}$

$$\therefore y = \frac{Ws^3}{96EI} - \frac{Ws^3}{32EI}$$

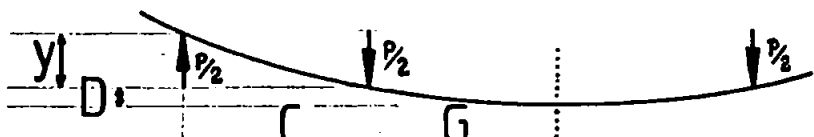
$$= \frac{Ws^3}{EI} \left(\frac{1}{96} - \frac{1}{32} \right) = \frac{Ws^3}{EI} \left(\frac{1-3}{96} \right) = \frac{1}{48} \frac{Ws^3}{EI}$$

$$E = \frac{Ws^3}{48I\delta} \quad \text{But } I = bd^3/12$$

$$\therefore E = \frac{Ws^3}{4bd^3\delta}$$

A9b: Elastic modulus from four point bending

Upper rollers to lower rollers:



$$\frac{d^2y}{dx^2} = \frac{Px}{2EI}$$

$$\frac{dy}{dx} = \frac{Px^2}{4EI} + \text{const}$$

$$\text{When } x = C, \frac{dy}{dx} = \frac{-PC(A - C)}{2EI}$$

$$\therefore \text{const} = -\frac{PC^2}{4EI} - \frac{PC(A - C)}{2EI} = \frac{-PC}{2EI} \left(A - \frac{C}{2} \right)$$

$$\frac{dy}{dx} = \frac{Px^2}{4EI} - \frac{PC}{2EI} \left(A - \frac{C}{2} \right)$$

$$y = \frac{Px^3}{12EI} - \frac{PC(A - C/2)x}{2EI} + \text{const}$$

$$\text{When } x = 0, y = 0, \text{const} = 0$$

$$\text{When } x = C$$

$$y = \frac{PC^3}{12EI} - \frac{PC^2(A - C/2)}{2EI}$$

Lower rollers to lowest point:

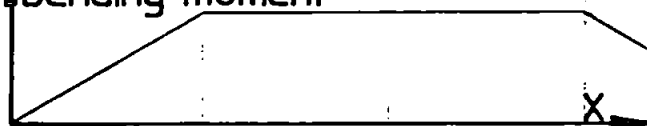
$$\frac{d^2y}{dx^2} = \frac{PC}{2EI}$$

$$\frac{dy}{dx} = \frac{PCx}{2EI} + \text{const}$$

$$\text{When } x = (A - C), \frac{dy}{dx} = 0$$

$$\therefore \text{const} = \frac{-PC(A - C)}{2EI}$$

bending moment



$$\frac{dy}{dx} = \frac{PCx}{2EI} - \frac{PC(A-C)}{2EI}$$

$$y = \frac{PCx^2}{4EI} - \frac{PC(A-C)x}{2EI} + \text{const}$$

When $y = 0, x = 0, \therefore \text{const} = 0$

$y = D$ = deflection at centre below mid-rollers

$$D = \frac{PC(A-C)^2}{4EI} - \frac{PC(A-C)^2}{2EI}$$

$$\therefore D = -\frac{PC(A-C)^2}{4EI}$$

Total deflection from upper supports:

$$Z = \frac{PC^3}{12EI} - \frac{PC^2}{2EI} \left(A - \frac{C}{2} \right) - \frac{PC(A-C)^2}{4EI}$$

$$\therefore Z = \frac{PC}{2EI} \left(\frac{C^2}{6} - \frac{C(2A-C)}{2} - \frac{(A^2 - 2AC + C^2)}{2} \right)$$

$$= \frac{PC}{4EI} \left(\frac{C^2 - 2AC + A^2 - A^2 + 2AC - C^2}{3} \right)$$

But $A = S/2$

$$\therefore Z = \frac{PC}{4EI} \left(\frac{C^2}{3} - \frac{S^2}{4} \right) = \frac{PC}{4EI} \left(\frac{4C^2 - 3S^2}{12} \right)$$

To obtain flexural modulus from load applied and deflection below centre rollers:

$$E = \frac{PC(A-C)^2}{4ID} \quad (I = BH^3/12)$$

$$= \frac{3PC(A-C)^2}{BH^3 D} \text{ kg m}^{-2}$$

Convert to Fortran IV and Newtons:

$$E = 3 * P * C * (A - C) ** 2 * 9.80665 / (1000000 * B * D * H ** 3) \text{ MPa}$$

E = flexural modulus

D = midspan deflection (in mm)

G = half-minor span = 0.02775 m

B = width of material = 0.0375 m

A = half major span = 0.091 m

S = total span

P = applied load

C = A - G

A9c: RAE Flexural strength rig: suitability for flexural modulus

Flexural strength = $\sigma_{1F} = 3WL/2bd^2$: shear and transverse stresses related to V_f and matrix properties.

Flexural modulus = $E_{1F} = WL^3/4bd^3\delta$: calculate at 20% failure load, errors occur unless moduli are equivalent in tension and compression.

Timoshenko & Gere eqn 6.46:

$$\delta = \frac{5qL^4}{384EI} \left[1 + \frac{48\alpha_s EI}{5GAL^2} \right]$$

From Kalnin when tensile modulus, $E = 27\text{Msi}$
the shear modulus, $G = 1\text{Msi}$

but $A = bd$ $I = bd^3/12$

$\therefore I/A = d^2/12$

$$\therefore \delta = \frac{5qL^4}{384EI} \left[1 + \frac{4\alpha_s Ed^2}{5GL^2} \right]$$

α_s = shear coefficient = 3/2 for rectangle.
 $d = 2\text{ (mm)}$

$$= \frac{5qL^4}{384EI} \left[1 + \frac{4 \times 3 \times 27 \times 4}{5 \times 2 \times L^2} \right]$$

\therefore contribution due to shear is $1:129.6/L^2$

L (mm):	10	20	40	60	80	100	200
shear factor:	1.296	0.324	0.081	0.036	0.020	0.013	0.003

CRYSTIC 272

Isophthalic resin for filament winding

APPENDIX TEN

Introduction

CRYSTIC 272 is an isophthalic polyester resin developed for high performance applications, using filament winding, extrusion, centrifugal moulding or contact moulding methods. The outstanding wetting characteristics of CRYSTIC 272 with glass fibre, make it particularly suitable for use with continuous roving. Fully cured mouldings made with CRYSTIC 272 have high mechanical strength and excellent strength retention in wet environments at medium temperatures up to 60°C. Laminates made with this resin are exceptionally consistent in both mechanical and chemical properties producing a very low scatter in test results.

Formulation

CRYSTIC 272 can be formulated for use in hot, heat-assisted, and cold-curing conditions.

Parts by weight	Formulation 1	Formulation 2	Formulation 3	Formulation 4	Formulation 5
CRYSTIC 272	100.	100	100	100	100
Catalyst Powder B	2	1	-	-	-
Catalyst Paste H	-	-	4	-	-
Catalyst M	-	-	-	2	-
Catalyst O	-	-	-	-	2
Cumene hydroperoxide (80%)	-	1	-	-	-
Accelerator E	-	1 to 4	1 to 4	1 to 4	1 to 4

Catalyst and accelerator should not be mixed directly together since they can react with explosive violence.

The resin must be allowed to attain workshop temperature before being formulated for use.

Hot curing: Formulation 1

The catalyst must be thoroughly dispersed in the resin. The catalysed resin will remain usable at workshop temperature (20°C) for approximately five days. Curing should be carried out at a temperature between 80°C and 140°C. For most applications 120°C will be found satisfactory. At this temperature 2 to 4 minutes curing time is usually sufficient but the exact time is largely dependent on the bulk or thickness of the moulding. The table below shows approximate setting times for Formulation 1, 100 pbw CRYSTIC 272 containing 2 pbw Catalyst Powder B.

	Formulation 1
Setting time in minutes of CRYSTIC 272 at 80°C	8
Setting time in minutes of CRYSTIC 272 at 100°C	4
Setting time in minutes of CRYSTIC 272 at 120°C	2

The Catalyst Powder B and cumene hydroperoxide must be thoroughly dispersed in the resin. Shortly before use the correct amount of Accelerator E should be added and stirred into the resins which will then remain usable at workshop temperature (20°C) for 6 to 24 hours. This formulation will gel at 60°C and above, and is particularly suitable for the filament winding of pipes, and in winding and drawing applications where a long pot life is required.

Catalysing: Formulations 3, 4 and 5

The catalyst must be thoroughly dispersed in the resin. The catalysed resin will remain usable at workshop temperature (20°C) for approximately eight hours. Shortly before use the correct amount of Accelerator E should be added and stirred into the catalysed resin.

When a liquid catalyst is used it may be easier to add the accelerator to the resin first, and then catalyse small amounts of accelerated resin as required. The accelerated resin without catalyst has a long storage life, and this method has many advantages in workshop conditions.

For most practical purposes there will be no difference in properties between laminates made with Formulation 3 using Catalyst Paste H, and those made with Formulations 4 and 5. However, laminates cured with Catalyst Paste H sometimes have marginally better performance when used in aggressive chemical environments at elevated temperatures.

Pot life

The amount of Accelerator E controls the pot life of the resin in cold-curing formulations, and can be approximately determined from the following table which shows the pot life of Formulation 3, 100 pbw CRYSTIC 272 containing 4 pbw Catalyst Paste H.

Parts of Accelerator E to 100 parts CRYSTIC 272 containing 4 pbw Catalyst Paste H	1.0	2.0	3.0	4.0
Pot life in minutes at 15°C	35	21	15	12
Pot life in minutes at 20°C	25	16	12	9
Pot life in minutes at 25°C	14	12	10	8

Cold-curing should not be carried out at temperatures below 15°C.

The pot life of Formulation 5 will be similar to Formulation 3 whilst that of Formulation 4 will be slightly shorter.

Post-curing

Satisfactory laminates for many applications can be made from CRYSTIC 272 by curing at workshop temperature (20°C). When optimum chemical, water and heat-resistant properties are required however, mouldings made using Formulations 2, 3, 4 and 5 should be post-cured. After release from the mould, laminates should be allowed to mature for 24 hours at workshop temperature (20°C). They should then be post-cured for three hours at 80°C or 15 hours at 50°C. The post-cure is most effective if it is carried out immediately after the 24 hour maturing period.

Post-curing is not normally necessary for hot-cured mouldings (Formulation 1) provided that the moulding cycle is adequate.

For all applications involving foodstuffs, it is essential to follow the recommendations detailed under 'Food containers'.

Food contact

Mouldings which are to be used with foodstuffs should be cured with Catalyst O (Formulation 5). After release from the mould, laminates should be allowed to mature for 24 hours at workshop temperature (20°C). They should then be post-cured for a minimum of three hours at 85°C. The post-cure is most effective if it is carried out immediately after the 24 hour maturing period. The mouldings must be thoroughly wet-steam cleaned for at least one hour before being put into use. If wet-steam cleaning is not practical, and the moulding is a vessel or of suitable shape, it should be filled with hot water (60 – 80°C) containing a non-perfumed detergent and left to stand for two hours. It should then be emptied and thoroughly washed in several batches of clean hot water.

These precautions are essential to avoid the tainting of foodstuffs. Fabricators are advised to ask Scott Bader for detailed recommendations for specific applications.

Pigmentation

CRYSTIC 272 may be pigmented by the addition of up to 10% of Crystic Pigment Pastes. Pigments should be chosen with care since they may adversely affect the chemical resistant properties of the laminate.

Caution:

Safe handling information for this material is contained in Scott Bader Material Safety Data Sheet – A Guide to the Safe Handling of Unsaturated Polyester Resin and Resin Systems – Technical Leaflet No. 957.

CRYSTIC 272 is subject to the Highly Flammable Liquids and Liquefied Petroleum Gases Regulations 1972 since it has a flash point below 32°C (90°F) when tested in accordance with Schedule No. 1 of these regulations.

Liquid CRYSTIC 272 must be kept away from naked flames and it is recommended that the storage temperature should not exceed 20°C (68°F).

Packaging

CRYSTIC 272 is supplied in 25 kg and 225 kg steel containers. Bulk supplies can be delivered by road tanker.

Typical properties of liquid CRYSTIC 272

Viscosity at 25°C	3.5 poise
Specific gravity at 25°C	1.10
Acid value	18 mgKOH/g
Volatile content	41%
Appearance	light straw
Stability in the dark at 20°C	6 months
Gel time at 25°C (determined under laboratory conditions using: CRYSTIC 272 100 pbw, Catalyst Paste H 4 pbw, Accelerator E 4 pbw)	8 minutes
Test methods as in BS 2782 : 1976	

Typical properties of a CRYSTIC 222 glass fabric

Barcol hardness (Model GYZJ-934-1)	45
Water absorption	16 mg
Deflection temperature under load (1.80 MPa)	75°C
Specific gravity at 25°C	1.20
Refractive index $n \frac{20}{D}$	1.570
Elongation at break*	3.8%
Tensile strength	75 MPa† (11,000 lbf/in²)
Tensile modulus	3.5 GPa (0.51 x 10⁶ lbf/in²)
Volumetric shrinkage	8.3%
Test methods as in BS 2782 : 1976	

* Filtered resin, void-free casting

† 1 MPa equals 1 MN/m² equals 1 N/mm² and is approximately 145 lbf/in².

Laminate properties – all test methods as in BS 2782 : 1976

Typical properties of a CRYSTIC 222 glass fabric laminate

Cure	24 hours at 20°C, 5 hours at 80°C and 3 hours at 120°C
Glass content	61 – 63%
Tensile strength Dry at 20°C After 2 hour boil in water At 70°C – dry	317 MPa (46,000 lbf/in²) 303 MPa (44,000 lbf/in²) 310 MPa (45,000 lbf/in²)
Flexural strength Dry at 20°C After 2 hour boil in water At 70°C after storage for 7 days at 70°C	503 MPa (73,000 lbf/in²) 483 MPa (70,000 lbf/in²) 441 MPa (64,000 lbf/in²)
Flexural modulus Dry at 20°C After 2 hour boil in water At 70°C after storage for 7 days at 70°C	19 GPa (2.75 x 10⁶ lbf/in²) 18 GPa (2.6 x 10⁶ lbf/in²) 15.9 GPa (2.3 x 10⁶ lbf/in²)
Compressive strength 6.3 mm (0.25 inch) thickness specimen supported Dry at 20°C	276 MPa (40,000 lbf/in²)
Elongation at break at 20°C	2.0%
Prepared according to Appendix N – BS 3532 : 1962	

Laminate prepared with CRYSTIC 272

Laminate as before, cured for 7 days at 20°C

Flexural strength	434 MPa (63,000 lbf/in ²)
Flexural modulus	18 GPa (2.6×10^6 lbf/in ²)

Typical properties of a CRYSTIC 272 conditioned coatings laminate

Cure	7 days at 20°C
Glass content	55 – 58%
Thickness	6 mm
Tensile strength Dry at 20°C	250 MPa (36,000 lbf/in ²)
Tensile modulus Dry at 20°C	16 GPa (2.3×10^6 lbf/in ²)
Flexural strength Dry at 20°C Wet**	324 MPa (47,000 lbf/in ²) 262 MPa (38,000 lbf/in ²)
Flexural modulus Dry at 20°C Wet**	13.8 GPa (2.0×10^6 lbf/in ²) 13.8 GPa (2.0×10^6 lbf/in ²)
Laminate prepared with Marglass 266 Araton 810 finish	
** After 7 days immersion in water at 70°C	

Typical properties of a CRYSTIC 272 conditioned coatings laminate

Measured in the direction of the reinforcement

Cure	7 days at 20°C
Glass content	75%
Tensile strength Dry at 20°C	827 MPa (120,000 lbf/in ²)
Tensile modulus Dry at 20°C	27.6 GPa (4.0×10^6 lbf/in ²)
Compressive strength 6.3 mm (0.25 inch) thickness specimen supported Dry at 20°C	345 MPa (50,000 lbf/in ²)

Typical properties of a CRYSTIC 1A/1B prepreg laminate cured at 80°C

Cure	24 hours at 20°C and 3 hours at 80°C
Glass content	42 - 46%
Thickness	6 mm
Tensile strength Dry at 20°C	180 MPa (26,000 lbf/in ²)
Tensile modulus Dry at 20°C	12.0 GPa (1.7 x 10 ⁶ lbf/in ²)
Flexural strength Dry at 20°C	280 MPa (40,500 lbf/in ²)
Flexural modulus Dry at 20°C	9.5 GPa (1.4 x 10 ⁶ lbf/in ²)
Interlaminar shear strength (single lap) Dry at 20°C	10 MPa (1450 lbf/in ²)
Short beam shear strength (span:depth ratio = 5:1) Dry at 20°C	21 MPa (3000 lbf/in ²)
Laminate prepared with alternate layers 300 g/m ² CSM/800 g/m ² WR	

Typical properties of a CRYSTIC 272 chopped strand mat laminate

Cure	24 hours at 20°C and 16 hours at 40°C	
Glass content	34%	After 2 hour boil in water (tested wet)
Tensile strength	132 MPa (19,000 lbf/in ²)	127 MPa (18,400 lbf/in ²)
Tensile modulus	8.2 GPa (1.2 x 10 ⁶ lbf/in ²)	8.3 GPa (1.2 x 10 ⁶ lbf/in ²)
Flexural strength	193 MPa (28,000 lbf/in ²)	194 MPa (28,100 lbf/in ²)
Flexural modulus	6.4 GPa (0.9 x 10 ⁶ lbf/in ²)	5.9 GPa (0.86 x 10 ⁶ lbf/in ²)
Elongation at break	2.0%	1.9%
Laminate prepared with 4 layers of 450 g/m ² mat.		

All information is given in good faith but without warranty. We cannot accept responsibility or liability for any damage, loss or patent infringement resulting from the use of this information.

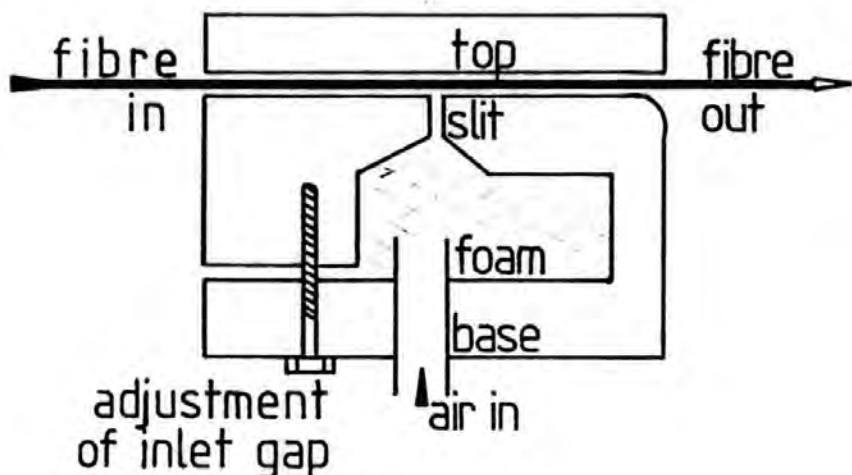
APPENDIX ELEVEN: Courtaulds Air Knife: fibre handling and spreading

Ideally fibre is handled as little as possible avoiding passage over sharp radii. Staple fibre has associated twist which gives rise to processing problems so continuous fibre is preferred as it is twist free.

Fibre wound onto packages is difficult to handle without some damage to the fibre so fibre in tubs or bucket containers is preferred.

Untreated fibre is more difficult to prepreg than treated fibre and in some instances it has been found desirable to wash and dry the untreated fibre prior to processing.

The preferred technique for spreading the continuous fibre is with a design of air knife. Air is fed to the base of the air knife at 0.14 to 0.35 kgf/cm² (2-5 lbf/in.²) and the air flow broken up with a packing of plastic foam material. From this inner chamber the air passes through a transverse slit about 0.114 mm (0.0045 in.) wide. The width of the air knife depends on the width the fibre is to be spread normally 51 to 76 mm (2 to 3 in.). The top of the air knife is made from transparent 'Perspex' (acrylic) to permit observation of the degree of spreading. The gap between the base of the air knife and the top on the fibre inlet side is adjustable to obtain the best spreading conditions normally set at 2.38 mm (3/32 in.).



John Summerscales

Ph.D thesis:

The mechanical properties of carbon fibre with glass fibre hybrid reinforced plastics.

ABSTRACT:

Fibre composite hybrid materials are generally plastics reinforced with two different fibre species. The combination of these three materials (in this thesis they are carbon fibres, glass fibres and polyester resin) allows a balance to be achieved between the properties of the two monofibre composites. Over the fifteen years since the introduction of continuous carbon fibre as a reinforcement, there has been considerable speculation about the "hybrid effect", a synergistic strengthening of reinforced plastics with two fibres when compared with the strength predicted from a weighted average from the component composites.

A new equation is presented which predicts the extent of the hybrid effect. Experiments with a variety of carbon-glass hybrids were undertaken to examine the validity of the theory and the effect of the degree of inter-mixing of the fibres. The classification and quantification of the hybrid microstructures was examined with a view to cross-correlation of the intimacy of mixing and the strength.

Mechanical tests were monitored with acoustic emission counting and acoustic emission amplitude distribution equipment. Some specimens were subjected to one thermal cycle to liquid nitrogen temperature prior to testing. Fracture surfaces were examined in the scanning electron microscope.

Numerical analysis by finite element methods was attempted. A constant strain triangular element was used initially, but in the later analyses the PAFEC anisotropic isoparametric quadrilateral elements were used. The system was adapted so that a \sqrt{r} singularity could be modelled, and post processor software was written to allow nodal averaging of the stresses and the presentation of this data graphically as stress contour maps.